**Title**
New constraints on water temperature at Lake Bonneville from carbonate clumped isotopes



**Author**
Mering, John Arthur

**Publication Date**
2015

Peer reviewed|Thesis/dissertation

UNIVERSITY OF CALIFORNIA

Los Angeles

# New constraints on water temperature at Lake Bonneville from carbonate clumped isotopes

A thesis submitted in partial satisfaction of

the requirements for the degree Master of Science

in Geochemistry

by

John Arthur Mering

2015

ABSTRACT OF THE THESIS

New constraints on water temperature at Lake Bonneville

from carbonate clumped isotopes

by

John Arthur Mering

Master of Science in Geochemistry

University of California, Los Angeles, 2015

Professor Aradhna Tripati, Chair

In the Great Basin, paleoshoreline reconstructions for closed basin lakes indicate that highstands correspond with Pleistocene glacial maxima. Lacustrine deposits at these sites are physically and chemically sensitive to changes in the balance between precipitation and evaporation, which drive lake level fluctuations. However, uncertainties remain regarding the magnitude of temperature change in the region between glacial and interglacial periods. In this thesis, carbonate clumped isotope thermometry is applied to define the parameters of temperature, evaporation, and precipitation at Lake Bonneville. Bonneville was the most expansive lake in the Great Basin during the Last Glacial Maximum (LGM).

Multiple phases of carbonate were evaluated, including aragonitic shells of two taxa of lacustrine gastropod, marls, and tufa. Carbonate clumped isotope results of ancient material were

calibrated by comparison to measurements of modern lacustrine carbonates at sites, where water temperatures are constrained. Summer water temperatures were estimated from gastropod and marl samples during the LGM, from 23 to 19 ka BP. Tufa and gastropod samples were also analyzed during the Stansbury Oscillation phase of lake history, from 25.8 to 24.5 ka, and the Bonneville Highstand and Provo phases of the lake, from 18 to 14.5 ka.

Reconstructed water paleotemperatures were applied to estimate summertime and mean annual air temperatures using lake-atmospheric transfer functions. Warm season (May through September) water temperatures are estimated to be 7.1±0.6ºC lower than present-day values of 18.1 to 19.0ºC in the Bonneville Basin, and 3.1±0.9ºC lower than present-day values of 19.7ºC in the Sevier Subbasin. Annual air temperatures are estimated to be 9.2±0.8ºC lower than present-day values of 8.7 to 9.5ºC in the Bonneville Basin, and 3.3±1.1ºC lower than present-day values of 10.1ºC in the Sevier Subbasin. Clumped isotope temperature reconstructions exceed the PMIP climate model ensemble mean in the Bonneville Basin, but suggest less cooling than the ensemble mean in the Sevier Subbasin.

Clumped isotope temperatures are also combined with carbonate oxygen isotope ($\delta^{18}O$) ratios to determine water $\delta^{18}O$ associated with mineral precipitation, which tracks evaporative enrichment in lakes. Results indicate that lake water $\delta^{18}O$ was above modern precipitation values, but that enrichment of water was less than at the modern Great Salt Lake. Reconstructed evaporation, derived from clumped isotope temperatures, varied from 60 to 83 percent of modern values, while precipitation over the lake was determined to be 75 percent of the modern rate. These results are lower than the PMIP3 ensemble mean, and suggest that Lake Bonneville transgressed, at least initially, as a result of lower evaporation, and not increased precipitation.

The thesis of John Arthur Mering is approved.

Jonathan Mitchell

David Jacobs

Aradhna Tripati, Committee Chair

University of California, Los Angeles

2015

## TABLE OF CONTENTS

## FIGURES

## TABLES

**ACKNOWLEDGMENTS**

I would like to thank Jack Oviatt for guiding me in the field and sharing his essential insight on the Pleistocene Great Basin. Steve Nelson contributed lacustrine tufa samples. Peter Hovingh contributed modern gastropods. Jonathan Mitchell and David Jacobs served as committee members, and provided feedback on drafts. Juan Lora provided guidance on interpretation of climate models. Will Defliese contributed insight on clumped isotope methodology and calibration. Given the ample page space provided it would be remiss of me not to extend thanks to the many other individuals who assisted with analyses and provided camaraderie throughout the research and writing process, including: Rob Eagle, Victoria Petryshyn, Antra Priyadarshi, Ben Elliot, Andrew Kowler, Jianwu Tang, John Wilson, Bryce Mitsunaga, Ryan Dill, Lilian Chou, Audrey Brown, Angel Fulgencio, Samantha Praskin, and Drew Henry. Most importantly, Aradhna Tripati encouraged me to pursue this work, and provided constant support from start to finish. I am truly grateful for having had this incredible research opportunity. Funding for this work was provided by an NSF Career Grant, and a Geological Society of America Graduate Research Grant.

## 1. INTRODUCTION

During the late Pleistocene, lakes were expanding throughout the Great Basin, from southern Oregon to Mexico, and established highstands between roughly 25 and 15 ka (Gilbert, 1890; Hostetler et al., 1994; Oviatt, 1997; Oviatt et al., 1999; Reheis et al., 2014; Ibarra et al., 2014). Although the positions and ages of lake shorelines are established (Fig. 1), the underlying hydrologic causes for lake transgressions and regressions have been debated for over a century. Yet the balance between precipitation and cooling requisite for deep lakes to form is relatively unconstrained.

Several hypotheses invoke enhanced winter precipitation as the dominant mechanism promoting lake highstands in the Great Basin. Antevs (1948) suggested the mean position of the Polar Jet Stream (PJS) was deflected further south during stadial intervals, enhancing winter precipitation across Western North America. However, this model did not account for offsets in timing of lake highstands across the region. Subsequent geochronological work indicates that during the Last Glacial Maximum (LGM), from 23-19 ka, lakes in the southern Great Basin were extensive, but many systems to the north continued to transgress after the LGM (Lyle et al., 2012; Munroe and Laabs, 2013; Reheis et al., 2014; Oster et al., 2015). An alternative hypothesis is the timing of lake level highstands reflects both the mean position of the PJS and the position of the PJS during temporary excursions (Munroe and Laabs, 2012).

Recent work suggests that storm tracking across Western North America may have also been forced by changes in the Aleutian Low and North Pacific High (Oster et al., 2015), in addition to conditions over the Laurentide Ice Sheet (Antevs, 1948; Clark and Bartlein, 1995). It has been hypothesized that the timing of lake highstands may have been dictated by the mean position of the jet stream, steered by a strengthened North Pacific High, with only narrow bands

of latitude receiving enhanced moisture at any given time (Oster et al., 2015). However, Lora et al. (submitted) demonstrate that the opposite state was more likely during the LGM, with a lowered North Pacific High and Aleutian Low. Lowering of these components likely increased the frequency of extreme winter precipitation events, delivered by atmospheric rivers to the west coast of North America. However, atmospheric rivers are unlikely to have been responsible for substantial moisture delivery into the Great Basin.

Not all studies identify winter storms as the most likely cause for regional lake advance. Lyle et al. (2012) observe that lakes in the Southern Great Basin expanded before, and during the LGM, while many lakes in the Northern Great Basin did not achieve highstands until after the LGM. They identify the Sierra Nevada and Cascade Mountains as strong barriers that would have inhibited transport of moisture inland from the coast into the central and northern Great Basin. They suggest that a strengthened summer monsoon from the tropical East Pacific could have penetrated further north at the LGM, providing moisture to facilitate the transgression of more northerly lakes. However, they do not provide a mechanism for increased northwards monsoon activity.

It has also not been unequivocally demonstrated that increased precipitation was responsible for lake transgressions. Diminished evaporative loss during cooler stadial summers is identified as a primary cause for the advance of many lake systems. Temperature decrease of 7 to 10ºC in the Northern Great Basin has been suggested as sufficient to transgress lakes without increase in precipitation (Kaufman et al., 2003; Ibarra et al., 2014).

As the climatic conditions required to generate large lakes in the Great Basin remain underdefined, the application of thermodynamically sensitive proxies provide valuable insight into the underlying causes of lake transgression. Here, new constraints on water temperature are

reported from carbonate clumped isotopes, in order to evaluate the paleohydrologic framework of Lake Bonneville (Figs. 1, 2). Lake Bonneville was the largest late Pleistocene lacustrine system in the Great Basin, reaching a maximum surface area of 47,800 $km^2$ by 18 ka (Currey, 1982; Oviatt et al., 1999, 1994a; Oviatt, 1997; Sack, 1999). Because the lake was extensive, and geomorphic features are well preserved, Bonneville has been a site of considerable climatic interest since the $19^{th}$ century (Gilbert, 1890). The transgressive phase coincides with the Northern Hemisphere LGM.

Carbonate clumped isotope thermometry provides a direct constraint on the temperature of mineral formation, which cannot accurately be assessed using conventional oxygen isotope techniques alone (Huntington et al., 2010; Tripati et al., 2010; Csank et al., 2011; Eagle et al., 2013). Here, accurate reconstructions of lake surface temperature, derived from clumped isotopes, are applied to generate more highly resolved estimates of annual air temperature, evaporation, and precipitation.

Despite promise as a terrestrial climate proxy, the application of clumped isotopes to lacustrine carbonates has been limited in scope to date (Huntington et al., 2010; Lechler et al., 2013; Huntington et al., 2014; Petryshyn et al., 2015), in part because of limited calibration datasets. In fact, previous clumped isotope studies of lake material, utilized calibration datasets developed from measurements of synthetic carbonate to determine paleotemperature (Huntington et al., 2010; Lechler et al., 2013; Huntington et al., 2014; Petryshyn et al., 2015). To address this issue, new clumped isotope measurements of modern lacustrine carbonate were carried out as part of this study in order to constrain the relationship between water temperature and clumped isotope signatures ($\Delta_{47}$) in lake carbonates (Appendix E).

Samples were collected in the field from sites in Western Utah and Eastern Nevada

(Table 1; Figs. 2-3). Clumped isotope measurements were made on gastropods at seven sites, and lacustrine marl at six sites (Tables 1-2). Clumped isotope measurements were also collected on a suite of tufa from the Pilot Valley Subbasin of Lake Bonneville (Table 3), encompassing transgressive-closed basin, and open-basin lake conditions (Figs. 2-3).

## 2. GEOLOGIC SETTING

### 2.1. Basin Setting

Lake Bonneville was comprised of two major basin units, and numerous smaller subbasins (Fig. 2). The largest unit is the Bonneville Basin, which includes the modern Great Salt Lake. The floor of the Bonneville Basin is characterized by shallow gradients. The Bear, Weber, and Jordan Rivers deliver the majority of water to the Bonneville Basin (Table 25). The smaller Sevier Subbasin is the southern component of the lake (Fig. 2). It is approximately 100 m higher in elevation than the Bonneville Basin, and its waters are geochemically distinct (Pedone. 2003; Hart et al., 2004). The Sevier and Beaver Rivers are the principal drainages in the Sevier Subbasin (Hart et al., 2004).

The modern climate at Bonneville is arid, and characterized by cool winters, and dry summers. For this study, climate data from the 1971 to 2000 period of record were evaluated (PRISM Climate Group, 2013). Figure 5 and Table 26 present modern climate normals at study sites. In general, sites in the Bonneville Basin are cooler and drier than sites in the Sevier Subbasin. Modern Mean Annual Air Temperatures (MAAT) at sites evaluated in this study range from 8.7 to 10.5°C. Average annual precipitation at study sites ranges from 205 to 380 mm. May is the wettest month at sites, accounting for 11 to 14 percent of annual precipitation.

## 2.2. Lake History

Prior to 32 ka, ephemeral saline lakes were present in the Bonneville Basin (Balch et al., 2005). Water levels began to rise circa 32 ka (Fig. 3). The Stansbury Shoreline (1,370 m elevation) was briefly established 1-2 times during the transgressive phase (Fig 3). A fall in lake level of 30-50 m, between 25.8 and 24.5 ka, defines the Stansbury Oscillatory period (Oviatt et al., 1992; Oviatt, 1997). The Stansbury Oscillation correlates with Heinrich Event 2, although it is not clear whether lake levels dropped synchronously with ice rafting in the North Atlantic, or slightly out of phase (Oviatt, 1997). The existence of a teleconnection with the North Atlantic is further supported regionally, where montane glaciers in the Wasatch and Uinta Mountains, east of the Bonneville Basin, also retreated and advanced contemporaneously with the Laurentide Ice Sheet (Clark and Bartlein, 1995).

Following the Stansbury period, the lake experienced a prolonged transgression up to the Bonneville shoreline at 1,550 m elevation (Oviatt, 1997; Oviatt et al., 1999). LGM marl and gastropods evaluated in this work (Fig. 4) correlate with the transgressive phase of the lake. Lake levels rose at approximately 60 m/ka during this interval (Oviatt et al., 1992). At 18 ka, shortly after the LGM, the lake began to overflow at an alluvial dam at the northern margin, near Red Rock Pass, in Southern Idaho (Oviatt, 2015). The development of an outlet prevented lake levels from rising above 1,550 meters. The highstand was shortlived, and terminated with the Bonneville Flood (O'Connor, 1993). The flood occurred over less than a year, and released over 4,700 cubic kilometers of water (O'Connor, 1993). Flood discharge is estimated to have been 1 million $m^3/s$ (O'Connor, 1993), which is nearly three times to historic peak flow of the Amazon River recorded in June 1953 (O'Connor and Costa, 2004).

Failure of the northern threshold resulted in a 100 m drop in lake levels to the Provo

Shoreline at 1,450 m (Godsey et al., 2011; Miller et al., 2013). The lake remained hydrologically open throughout the Provo phase (Godsey et al., 2011; Miller et al., 2013). Although there is some disagreement on the duration of the Provo shoreline, radiocarbon chronology indicates rapid regression by 14.5 ka (Sack, 1999; Godsey et al., 2011; Miller et al., 2013). Closed basin conditions were permanently established after lake levels dropped below the Provo threshold (Balch et al., 2005; Miller et al., 2013; Oviatt, 2015). The Post-Provo regression roughly correlates with the termination of H1 (Oviatt, 1997).

### 2.3. Age Control

Chronology at Lake Bonneville has been established from radiocarbon measurements at shoreline deposits (Table 2). Materials reported in papers include mollusk shells, tufa, bone, and terrestrial plant material (Oviatt et al., 1992; Godsey et al., 2005; Godsey et al., 2011; Oviatt, 2015). Most recent studies present calibrated data, adjusted to calendar years before present (Godsey et al., 2011; Oviatt, 2015). Interpretation of radiocarbon measurement on samples of lacustrine origin (e.g. mollusk shell, tufa) at Bonneville is complicated by reservoir effects, which arise when the $^{14}C$ concentration within the Dissolved Inorganic Carbon (DIC) reservoir of lake water mixes with $^{14}C$-deficient carbon (Yu et al., 2007; Oviatt, 2015). When dilution is significant, carbonates precipitating from lake water record apparent ages that are too old (Oviatt, 2015). A reservoir effect is inferred at a paleoshoreline when $^{14}C$ dates for lacustrine material are significantly older than dates of terrestrial materials (e.g. charcoal, wood) measured within the same stratigraphic interval (Oviatt, 2015). Conversely, postdepositional interaction with water may introduce additional $^{14}C$ into a sample, resulting in a radiocarbon age that is younger than the true sample age (Oviatt, 2015). Hydrograph reconstructions of the lake (Fig. 3) omit $^{14}C$

measurements that show obvious signs of reservoir effects, or diagenesis (Miller et al., 2013; Oviatt, 2015). Volcanic ash has also been used to supplement radiocarbon chronology at some localities (Appendix A).

### 2.4. Prior Paleoclimate Results

When Lake Bonneville was extensive, lake level was controlled by both climatic and basin scale processes (Fig. 3). Climate proxy studies provide a range of potential scenarios that would have led to a deep lake in the Bonneville Basin. Regional Climate Models RCMs (i.e. Hostetler et al., 1994), and surveys of vegetation data (Madsen et al., 2001) predict an enhanced North-South moisture gradient during the LGM. Evaluations of fossil remains of flora have been used to predict temperature and moisture availability. Madsen et al. (2001) utilized the detritus record of fossil woodrat middens and raptor nests to make interpretations on floral and faunal assemblages in the region. They suggest that LGM summer temperatures in the Northwest portion of the Bonneville Basin were 6-7° C below modern levels, and a continuously dry and cool regime was maintained from 28 to 14 ka. They infer that precipitation may have increased slightly during transgressive phase of Bonneville when more water-loving montane shrubs began to repopulate the northwest portion of the Bonneville Basin. The Mean Annual Air Temperature (MAAT) derived from the floral archive of packrat middens range from 1.3 to 4.3°C, during the interval of 28 – 14 ka (Madsen et al., 2001). The floral record indicates that the climate during the Provo Phase, after 18 ka, may have been wetter and warmer than the full glacial regime (Broughton et al., 2000; Madsen et al., 2001; Oviatt et al., 2003).

The results of some hydrologic budget analysis for the Bonneville Basin also indicate that depressed summer temperatures may exert a stronger forcing on transgressions than precipitation

change. Kaufman et al. (2003) utilized amino acid racemization in lacustrine ostracodes to propose that Bonneville temperatures were 10°C colder than late Holocene levels at circa 20 ka. They report Mean Annual Air Temperature (MAAT) of 1.1±2.5°C during the interval of 24 to 12 ka. Significantly cooler summers, without major changes in precipitation, may have been sufficient to promote deep water conditions at Bonneville (McCoy, 1981; Kaufman et al., 2003).

Climate model outputs from the Paleoclimate Modeling Intercomparison Project Phase 3 (PMIP3) provide a range of atmospheric parameters at Lake Bonneville during the LGM (Appendix C). The Mean Annual Air Temperature (MAAT) predicted from the PMIP3 multi-model ensemble mean is –2.3±3.5°C in the Bonneville Basin, and –1.6±2.7°C in the Sevier Subbasin (Appendix C). Ensemble mean warm season (May through September) air temperatures are 6.5±4.6 °C in the Bonneville Basin and 7.6±4.0°C in the Sevier Subbasin. The MAAT temperature depression exhibited in the PMIP3 Ensemble Mean, relative to pre-Industrial control values is -7.9±2.6 °C in the Bonneville Basin, and -7.6±2.2°C in the Sevier Subbasin. May through September temperature depression of the PMIP3 ensemble mean is -8.6±3.4°C in the Bonneville Basin and -8.1±2.9°C in the Sevier Subbasin.

It should be noted that the PMIP3 model boundary conditions for pre-Industrial climate do not accurately represent late Holocene values at the sites evaluated (Appendix C). PMIP3 model controls are 3-4°C lower than modern climate records. The accuracy of the model control data can be interpreted by comparison of PMIP boundary conditions with the modern climate record. Modern Mean Annual Air Temperature (MAAT) at the Great Salt Lake is 11.3°C, and the average temperature at Bonneville Basin sites sampled in this study is 9.1°C, while the average air temperature at study sites in the Sevier Subbasin is 10.1°C (USGS Station 10010100 near Saline; Hren and Sheldon, 2012: PRISM Climate Group, 2014). Approximately 1°C of

temperature discrepancy between modern climate and PMIP controls can be attributed to anthropogenic emissions since the industrial revolution (IPCC, 2013). Because the boundary conditions are not well matched with modern climate observations at Lake Bonneville, temperature depression is the most suitable parameter for comparison of proxy data against model data. In the case of PMIP3 models, the difference between LGM and pre-Industrial control values is calculated, while paleotemperatures from clumped isotopes are compared to modern air temperatures.

## 3. LACUSTRINE CARBONATES

In lakes, as in the ocean, carbonates are an important repository of paleoenvironmental information (Epstein et al., 1953; Kelts and Hsü, 1978; Anadon et al., 2009; Solari et al., 2010). Carbonates precipitate in most lacustrine settings and can form at the lake surface, in the bottom waters, and at lake margins. However, the manifestation of carbonate in a paleoclimate record will depend upon a complex relationship between climate, geochemical setting, and basin morphology (Platt and Wright, 1991). Seasonal bias in carbonate formation is also likely, and may also differ subtly between different types of carbonates. However, in most cases the season of growth for a carbonate can be discerned with reasonable certainty.

At Lake Bonneville, extensive marl beds are present across virtually all subbasins (Fig. 4). Mollusk shells are common in littoral deposits (Fig. 4). Lacustrine tufa and beach rock is common in the swash zone at established shorelines. Carbon and oxygen stable isotope measurements have previously been carried out on marl (Oviatt et al., 1994; Oviatt, 1997), tufa (Nelson et al., 2005), and dense cave carbonates (McGee et al., 2012). Samples evaluated using clumped isotopes in this work include 2 species of gastropod, endogenic carbonate from the

Bonneville White Marl, and lacustrine tufa.

### 3.1. Gastropods

Two species of gastropods are well represented in Bonneville deposits (Fig. 4). *Stagnicola bonnevillensis* is an aquatic pulmonate gastropod from the Lymnaeidae family. Living *Stagnicola bonnevillensis* are restricted to three sites in Utah (Clarke, 1991). Water at these sites was between 16 and 18°C in June 1990 (Clarke, 1991). *Pyrgulopsis bonnevillensis* are gill breathing members of the Hydrobiidae family, which are widespread throughout the Great Basin (Hershler et al., 2007). Fossil specimens of Pyrgulopsis were observed in the field to often co-occur with Stagnicola in sand and gravel paleoshoreline deposits. In modern springs, Pyrgulopsis are abundant in waters between 12 and 19°C, although some variants have colonized hot springs and may be present in waters greater than 30°C (Hershler and Liu, 2009). In this work, fossil Pyrgulopsis gastropods are described as a single taxa, as has previously been done (Sack, 1999; Godsey et al., 2005).

Both Stagnicola and Pyrgulopsis species exclusively occupy the photic zone, and prefer shallow, well-oxygenated intervals near shore (Hershler and Sada, 2002; Shanahan et al., 2005). Shell growth occurs as a function of water temperature and food availability (Platt and Wright, 1991; Hershler and Sada, 2002; Shanahan et al., 2005; Hren and Sheldon, 2012). Studies of modern Pyrgulopsis and Stagnicola populations indicate that shell growth correlates positively with water temperature up to approximately 30°C (Hershler et al., 2007; Lysne et al., 2007). Neither species precipitates shell at temperatures below 9-10°C (Vaughn, 1953; Lysne and Koetsier, 2006). In the modern day Bonneville Basin, water and air temperatures are above 9°C from mid-April though October. However, with cooler annual temperatures, the probable interval

conducive to gastropod growth is reduced. Figures 6-7 provide modern water and air temperature curves for the Bonneville Basin with the timeframe of gastropod growth highlighted. In Figures 6 and 7, it is demonstrated that with moderate, 3-5°C annual temperature depression, the window of time during which water temperatures would have been above 9-10°C is shortened, which in turn reduces the window of time that Pyrgulopsis and Stagnicola are able to precipitate shell (Figs. 6 and 7). Temperature depression exceeding 3-5°C, would have likely caused gastropods in Lake Bonneville to calcify from May-September.

### 3.2. Lacustrine Marl

Marl was deposited across virtually all basins of the lake (Fig. 4) during the transgressive phase and highstand (Oviatt et al., 1994). Although marl deposition continued during the deglacial Provo Phase, sand increases upsequence in deposits (Oviatt et al., 1994a; Godsey et al., 2011). This is likely due to shallowing, as the basin floor began to rebound, following the Bonneville Flood. Provo aged (18-14.5 ka) marl outcrops are less suitable for hydroclimate analyses as these units often contain reworked marl from the pre-flood highstand (Sack, 1999). Marl varies greatly in character throughout the Bonneville and Sevier Basins. It is thinly bedded to massive (Oviatt et al., 1994), and contains variable amounts of carbonate, siliciclastic material, and diatoms. Previous work on lacustrine marl indicates that this phase of carbonate precipitates in equilibrium with lake surface waters (Talbot, 1990).

The mechanisms governing calcification in marl differ from those responsible for shell growth in gastropods. In modern lakes, endogenic carbonate precipitation is observed to occur during the warmer intervals of the year. Evaporation increases carbonate saturation, and higher temperatures lower $pCO_2$ in water. During the spring and summer, photosynthetic uptake also

lowers $pCO_2$ in the upper water column (Platt and Wright, 1991; Oviatt et al., 1994; Hren and Sheldon, 2012). Although endogenic precipitation of carbonate occurs largely in the upper water column, marl predominantly accumulates in pelagic and lagoonal settings, where bottom waters are less disturbed. Depending upon water depth and distance from shore, detrital grains of silt and sand may be present.

### 3.3. Tufa and Cements

Tufa and carbonate cements occur extensively at the shorelines of Lake Bonneville. Tufa varies in texture, from smooth calcite, to porous units with significant infilling of micrite and spar (Nelson et al., 2005; Felton et al., 2006). Tufa precipitation in energetic shallow energetic environments is driven by $CO_2$ outgassing, and is often enhanced by evaporation and photosynthetic uptake of $CO_2$ (Platt and Wright, 1991). The following reaction describes tufa formation (Felton et al., 2006):

(1) $$Ca^{2+} + 2HCO_3^- = H_2O + CO_2 + CaCO_3$$

At Bonneville, photosynthetic uptake of $CO_2$, and wave action, are thought to have both positively influenced pH, driving tufa formation (Felton et al., 2006). In the Canadian Rockies, carbonate precipitation in microbialites is largely tied to photosynthesis (Petryshyn et al., 2015). Measurements of microbialite and tufa at the Great Salt Lake, and Walker Lake, indicate that carbonate cements in Great Basin lakes also typically form during summer months (Anderson et al., 2013; Petryshyn et al., 2015). In this work, a June through August calcification interval is inferred for tufa samples from Lake Bonneville.

### 3.4 Clumped Isotope Analysis of Lacustrine Carbonates

Lakes provide important archives of terrestrial climate variability. Paleoenvironmental reconstructions from lake sediments can be used to enhance understanding of ecosystem change both within the lake and its surrounding environment (Street-Perrott and Harrison, 1984; Smol, 1992). Lake levels are sensitive to changes in both precipitation and evaporation. However it is difficult to estimate hydrologic variables individually without additional proxies (Olander et al., 1999; Schleser et al., 1999; Powers et al., 2010). Isotopic analysis of lacustrine sediments provides one such tool for constraining air temperature and hydrology.

Carbonate clumped isotope thermometry overcomes some of the limitations posed by traditional oxygen isotope measurements in the study of paleohydrologic conditions by providing a thermodynamically-based means for reconstructing water temperature (Huntington et al., 2010; Tripati et al., 2010; Csank et al., 2011; Eagle et al., 2013). Although, the influence of temperature upon $\delta^{18}O_{water}$ and $\delta^{18}O_{carbonate}$ has been understood for over 60 years (Urey et al., 1951; Epstein et al., 1953), this relationship cannot be used with confidence to determine the temperature of carbonate precipitation in terrestrial settings, such as ancient lakes, where $\delta^{18}O_{carbonate}$ can be measured, but the $\delta^{18}O$ composition for lake water must estimated. Meteoric waters exhibit large amounts variability in $\delta^{18}O$, with latitude, moisture source, and elevation influencing the isotopic composition of lake water (Horton et al., in press). Additionally, lake water often undergoes large seasonal swings in $\delta^{18}O$ forced by evaporation (Henderson and Shurman, 2010; Horton et al., in press). The influx of groundwater of unique $\delta^{18}O$ composition will also influence the isotopic value of lake water (Henderson and Shurman, 2010; Horton et al., in press). Because of these uncertainties, it is difficult to reliably predict the $\delta^{18}O$ composition of mineral precipitating fluid in a lake with confidence.

The clumped isotope method is based on the exchange of isotopes between isotopologues of carbonate-containing groups (Ghosh et al., 2006; Schauble et al., 2006; Csank et al., 2011; Eagle et al., 2013; Tripati et al., 2010, 2014). The clumped isotope value ($\Delta_{47}$) can be related to the temperature of ambient waters at the time of mineralization, where lower temperatures are associated with a greater abundance of $^{13}C$-$^{18}O$ bonds. In Equation 2, cooler temperatures favor the forward reaction:

(2) $$Ca^{12}C^{18}O^{16}O_2 + Ca^{13}C^{16}O_3 = Ca^{13}C^{18}O^{16}O_2 + Ca^{12}C^{16}O_3$$

The abundance of multiply-substituted isotopologues (e.g. $^{13}C^{18}O^{16}O$) in carbon dioxide liberated from carbonate via digestion in anhydrous phosphoric acid reflects the original clumped isotope abundance of the carbonate mineral (Hill et al., 2014). Recent advances in gas source isotope ratio mass spectrometry, allow for accurate measurements to be made of clumped isotopes in $CO_2$. The measurement of clumped isotopes is discussed using the $\Delta_{47}$ term (See Section 4.6 for information on stable isotope notation). During analysis of clumped isotopes, carbonate oxygen isotope ($^{18}O/^{16}O$) ratios are simultaneously measured and can be combined with temperature data to calculate $^{18}O/^{16}O$ values of lake water at the time of carbonate precipitation (Urey et al., 1951; Epstein et al., 1953; Vasconcelos et al., 2005). A complete description of analytical procedure and notation is provided in the methods section of this paper.

### 3.5. Constraining Air Temperature Using Clumped Isotopes

There is generally some level of bias associated with the season of growth recorded by different types of lacustrine carbonates. Defining the relationship between air temperature and water temperature during intervals of mineral growth is essential towards interpretation of data in a paleoclimate context (Schleser et al., 1999; Hren and Sheldon, 2012). Study at modern lakes indicates that summer epilimnion temperature will typically shift by 0.5-1.0°C for every 1°C change in air temperature (Robertson and Ragotzkie, 1990). Thus, if the season of carbonate growth is known, or can be inferred, the associated air temperature may be reconstructed. In northern hemisphere mid-latitude closed basin lakes it has been demonstrated that carbonate is precipitated during warmer months (Hren and Sheldon, 2012). However, open lakes may precipitate carbonate earlier in the year. Hren and Sheldon (2012) identified linearity for heat exchange between the atmosphere and lake waters at 88 modern lakes, across a broad range of latitude and elevation. They demonstrate that seasonal water temperatures (e.g. April-June, June-August, April-October) can be correlated with mean annual air temperatures (MAATs).

## 4. MATERIALS AND METHODS

### 4.1 Lake Calibration

The body of literature for clumped isotope measurements of modern lacustrine samples is limited (Huntington et al., 2010; Lechler et al., 2013; Huntington et al., 2014; Petryshyn et al., 2015). In order to define paleotemperature at Lake Bonneville, new linear calibration relationships are reported for clumped isotopes in lacustrine samples (Appendix E). Samples in the lake-specific clumped isotope calibration include aragonitic shells of gastropods, biologically mediated lake carbonates (e.g. microbialites), and inorganic phases (e.g. tufa, cement, micrite).

Calibration samples encompass a wide range of latitude, elevation, and lake types. Table 28 includes a list of modern lake sites analyzed for calibration purposes.

The most notable result of the calibration experiment (Tables 28-29) is that the temperature of calcification in lakes fits regressions that are of intermediate slope and intercept relative to previously reported clumped isotope calibrations (Appendix E). In this study, the reported slope for gastropod calibration is 0.053, while the micrite line used to calibrate marl is 0.052, and the microbialite / tufa line is 0.048. The steepest clumped isotope calibration that these results are compared to is that of Ghosh et al. (2006) with a slope of 0.064, while the calibration with the shallowest slope is presented by Defliese et al. (2014), with a value of 0.037.

**4.2. Field Work**

Field sample collection was carried out at sites within the Bonneville Basin and Sevier Subbasin in October 2012 (Figs. 2 and 4; Tables 1 and 2). Gastropods were collected from sand and gravel strata that correspond with littoral conditions (Fig. 4). The two gastropod taxa represented in samples are *Pyrgulopsis bonnevillensis* and *Stagnicola bonnevillensis.* Based on radiocarbon ages (Table 2), and sequence stratigraphic interpretations (Fig. 4), the localities sampled record the initial transgression of the lake to a given shorezone. Lacustrine marl was collected from above the sandy gastropod-bearing beds (Fig. 4).

Samples of lacustrine tufa representing the Stansbury, Bonneville, and Provo shorezones were selected from the collection of Steve Nelson at Brigham Young University (Table 3). These samples are from sites at the Pilot Valley Subbasin at the west end of the lake. Oxygen and carbon stable isotope values were previously reported for these samples (Nelson et al., 2005), but clumped isotope abundances were not measured. Tufa samples varied in texture.

Some materials were porous, and contained micrite and spar. Others were dense, and lacked void spaces. The latter were prepared for clumped isotope analyses.

### 4.3. Elevation and Age Control at Sites

#### 4.3.1. Isostatic Rebound Correction

Differential post-lacustrine isostatic rebound has caused the modern elevation of contemporaneous paleoshorelines to be non-uniform across the Bonneville Basin (Oviatt et al., 1992). Rebound is greatest in basin centers, but generally more limited near basin margins. Highstand shorelines, at islands near center of the basin, are reported to have experienced up to 74 m greater rebound than contemporaneous shorelines at the basin margin (Currey, 1982). Provo shorelines experienced up to 59 m greater rebound near basin center points. Rebound likely occurred in two phases. The first episode, which occurred in response to the Bonneville Flood (18 ka), would have been completed by the end of the Provo lake phase (14.5 ka). Post-Provo rebound likely was complete prior to the Gilbert lake episode, at 11.5 ka (Oviatt, 2014).

It is possible to compare samples from shorelines that experienced dissimilar degrees of isostatic rebound, as reported in Table 1, utilizing the following relationship (Currey, 1982; Oviatt et al., 1992):

(3) $$Z_a = Z_r - [(Z_r - 1200)/(Z_b - 1200)] * [Z_b - 1552]$$

($Z_a$) = rebound-free adjusted altitude

($Z_r$) = modern mapped altitude of the sample. This level has been rebounded.

($Z_b$) = local altitude of the Bonneville shoreline

(1552) = average unrebounded altitude of Bonneville shoreline

(1200) = basin floor altitude at the beginning of the Bonneville lake cycle

**Altitudes are presented in meters

### 4.3.2. Age Control

Chronologic control was provided by radiocarbon ages (Tables 1-2), and comparison of site elevation to up-to-date lake hydrographs (Fig. 3). The Bonneville hydrograph represents a compilation of radiocarbon dates from lacustrine carbonate (gastropod, tufa, ostrocode valves), charcoal, wood, and bone from shorezones. It is comprehensive, and is useful for screening for lake reservoir effects in samples. Reservoir effects arise when carbonates record ages that are "too old," due to dilution of $^{14}C$ within the Bonneville DIC reservoir with radiocarbon deficient water.

The paleoshoreline age for a sample may also be determined by interpolation along the lake hydrograph (Fig. 3) with moderate certainty, once the rebound-adjusted altitude is determined. When reconstructing lake chronology, the following assumptions are permissible:

1. Charcoal ages represent the maximum age for a given shoreline
2. Lacustrine carbonate, including shell, tufa, and marl may be subject to $^{14}C$ reservoir effects. If a lacustrine carbonate at a given point along the time/altitude curve records an age older than charcoal at that altitude, the age is rejected.
3. Gastropods collected within lacustrine gravel at the base of the Bonneville White Marl correlate with the earliest transgression of the lake to that paleoshoreline.
4. Gastropod samples that occur in littoral deposits represent a narrow segment of time. The

lake rose quickly during the transgressive interval. The habitable environment for gastropods at a given site would have been preserved for a relatively period, as the lake continued to rise to its highstand.

5. Marl accumulated at rates of roughly 0.1 to 1 m/ka. Only marl collected directly above and adjacent to transgressive shoreline deposits is paired with these deposits, although it is recognized marl will reflect a slightly younger age at a given site.
6. Geochemical signals derived from gastropods reflect up to several years of growth. A 1-2 cm sample across marl laminae may reflect larger intervals of lake history.

### 4.4. Sample Preparation

#### 4.4.1. Biogenic Hard Parts

Aragonitic gastropod shells were separated by taxa. Shells were broken into pieces, sonicated in Milli-Q deionized water until clean, dried overnight at 50°C, and powdered using a mortar and pestle. Powdered shell was weighed out in amounts between 5 and 10 mg. The amount of sample required to yield sufficient $CO_2$ via acid digestion varied over the course of the study due to changes in tuning and sensitivity of "Chewbacca," the Thermo 253 IRMS in the Tripati Lab at UCLA. For a given study site, 4-10 individual gastropod shells were analyzed 1-4 times each. Analyses consisted of either 8 or 9 acquisition cycles consisting of 10 measurements of sample and reference $CO_2$ gas. Replicate analyses of individual shells served to test the reproducibility of isotope results. Individual gastropod shells represent short time scales. Analyses of multiple shells at a given site allowed for compilation of a statistically significant climatic signal.

Modern gastropod samples were evaluated for calibration (Appendix E). In many cases,

these required additional cleaning. Samples containing organic material, including soft tissue, were cleaned by scraping and reaction with dilute hydrogen peroxide (3%) for 20-30 minutes as has been done for other organic-rich carbonates (Eagle et al., 2013). For smaller modern gastropod shells with mean diameters less than 5 mm, tissue was separated by lightly crushing the shell with a mortar and pestle, soaking in ethanol for 20 minutes, and agitating lightly. Dense shell carbonate would typically accumulate at the bottom of the cleaning vessel, while soft tissue would float to the top of the column of ethanol. Shell carbonate was then collected, and washed in Milli-Q deionized water 2-3 times. Thorough removal of organics was ensured by a subsequent treatment of shell in 3% hydrogen peroxide for 20-30 minutes. Following peroxide treatment, modern gastropod shells were rinsed in Milli-Q deionized water, dried at 50 C, and powdered using a mortar and pestle. Analytical weights of modern carbonate also ranged from 5 to 10 mg.

#### 4.4.2. Carbonate Muds

In the field, marl was selected at sites overlying transgressive shorezone locations that contained gastropods. For a given study site, 2-6 individual blocks of marl were selected for clumped isotope analysis. Preparing multiple selections of marl ensured that reconstructed water temperatures encompassed the broadest interval of lake history possible. Preparing multiple samples of marl also eliminated bias in the cleaning procedure. Sample blocks, weighing 5-50 g, were disaggregated in Milli-Q water, and poured through a 212 μm steel mesh filter to exclude particles coarser than fine sand, including detrital clasts, charcoal, root, and biogenic shell fragments. Following sieving at 212 μm, the resultant slurry was allowed to settle for 5-10 minutes. The residue coming out of suspension was isolated by pouring the slurry into a second

beaker. This process was repeated until virtually no settling occurred. The final suspension was treated with dilute hydrogen peroxide (1.5-3%) for 20-60 minutes to remove residual organic material (Eagle et al., 2013). Carbonate was collected on 0.45 μm cellulose nitrate filter membranes, and dried over night at 50° C. Depending on instrument sensitivity and carbonate content of the processed sample, the amount of material reacted in phosphoric acid to generate $CO_2$ for analysis varied between 10 and 50 mg for individual experimental runs. Marl samples were analyzed 1-4 times each. Analyses consisted of either 8 or 9 acquisition cycles consisting of 10 measurements of sample and reference $CO_2$ gas. Replicate analyses of cleaned marl samples served to test the reproducibility of isotope results.

### 4.4.3. Tufas and Cements

Tufa samples from the Nelson et al. (2005) archive were selected from sites encompassing the Stansbury, Bonneville, and Provo lake stages. Tufas and cements were cut perpendicular to laminae. Areas containing spar, or evidence of regrowth, were selected against. Powders were extracted by crushing rock chips to fine sand grain size, following methodology in Nelson et al. (2005). Powdered tufa samples were reacted in 3% $H_2O_2$ for 60 minutes to remove organic materials. Following peroxide treatment, samples were rinsed in Milli-Q deionized water and dried for 12 hours at 50°C. Cleaned powders were weighed out in 5 to 15 mg increments, depending on carbonate content and instrument sensitivity at the time of analysis. Analyses of tufa were replicated 2-4 times each. Table 3 contains a list of tufa samples run in this study.

### 4.5. Stable Isotope Notation

The value for enrichment or depletion of a given isotope is reported in delta (δ) notation, where:

(4) $\delta = (R_{sample}/R_{standard} - 1) * 1000$

The R term is the ratio between the rare isotope (e.g. $^{18}O$, $^{13}C$) and common isotope (e.g. $^{16}O$, $^{12}C$). For $\delta^{18}O_{water}$, the internationally agreed upon reference value ($R_{standard}$) is Vienna Standard Mean Ocean Water (V-SMOW), while for $\delta^{18}O_{carbonate}$ and $\delta^{13}C_{carbonate}$, the international reference material is based on a Jurassic-aged belemnite fossil from the Pee Dee formation (V-PDB). Oxygen isotope values reported relative to the V-SMOW standard can be related to V-PDB, using the following relationship:

(5) $\delta^{18}O_{V\text{-}SMOW} = 1.0392 * \delta^{18}O_{V\text{-}PDB} + 30.92$

The relationship between mineralization temperature, $\delta^{18}O_{water}$, and $\delta^{18}O_{carbonate}$ values are given below for calcite and aragonite:

(6) Aragonite (Kim et al., 2007): $1000 \times \ln\alpha_{Aragonite\text{-}H2O} = (17.88 \times 10^3)/T - 31.14$

(7) Calcite (Kim and O'Neil, 1997): $1000 \times \ln\alpha_{Calcite\text{-}H2O} = (18.03 \times 10^3)/T - 32.42$

In order to account for digestion in a common acid bath, a fractionation factor of 1.007954 was

applied, following equation 6 in Swart et al. (1991).

$\delta^{18}O$ and $\delta^{13}C$ have long been utilized (Urey et al., 1951; Epstein et al., 1953; Smol, 1992) to infer trends in precipitation, evaporation, and primary productivity in ancient aqueous environments. Evaporation preferentially removes water molecules containing $^{16}O$, enriching the $\delta^{18}O$ signature of remaining water (Horton et al., in press). Globally, $\delta^{18}O$ in precipitation varies as a function of latitude, distance from the ocean, and with respect to topography (Bowen and Ravenaugh, 2003). In non-biogenic lake carbonates, the $\delta^{18}O$ and $\delta^{13}C$ values can be interpreted concurrently (Talbot, 1990). Carbonates precipitating over similar intervals will display uniform covariance with respect to carbon and oxygen isotopes (Horton et al., in press). A detailed overview of oxygen isotopes in modern meteoric waters in the Bonneville Basin is provided in Appendix B.

### 4.6. $CO_2$ Clumped Isotope Notation

In contrast to conventional carbon and oxygen isotopes, clumped isotope values are presented relative to a stochastic distribution. The $\Delta_{47}$ value is defined by the following relationship, where $R_{45}$*, $R_{46}$*, $R_{47}$* are values for a stochastic distribution of carbon and oxygen isotopes in a given sample gas:

$$\Delta_{47} = [(R_{47}/R_{47}^{*} - 1) - (R_{46}/R_{46}^{*} - 1) - (R_{45}/R_{45}^{*} - 1)] \times 1000 \quad (8)$$

$$R_{45}^{*} = R_{13} + 2 \times R_{17}$$

$$R_{46}^{*} = 2 \times R_{18} + 2 \times R_{13} \times R_{17} + (R_{17})^2$$

$$R_{47}^{*} = 2 \times R_{13} \times R_{18} + 2 \times R_{17} \times R_{18} + R_{13} \times (R_{17})^2$$

Interlab comparison of clumped isotope results is accomplished by utilization of the Absolute Reference Frame, ARF (Dennis et al., 2011). Variable degrees of fragmentation of $CO_2^+$ ions in the sources of different IRMS units, necessitates a universal thermodynamically based reconstruction of these effects. The ARF is established through routine analysis of gases that differ in clumped isotope composition, due to equilibration at different temperatures, but retain comparable bulk isotope values.

In the Carbon Cycle and Climate Change Lab at UCLA, gases of two end member bulk isotope values were utilized. Bonedry tank $CO_2$ is isotopically depleted with respect to $\delta^{13}C$ and $\delta^{18}O$, while Evap Di + CM is enriched. Evap DI + CM gas was produced by equilibration of Carrera Marble $CO_2$ with evaporated dionized water. Aliquots of bonedry $CO_2$ and Evap DI+CM were equilibrated at 25°C and 1000°C. 1000°C gas samples result in stochastic clumped isotope distributions.

In this study, all clumped isotope temperatures were calculated via application of lake sample specific clumped isotope calibration regressions (Appendix E). Modern lake carbonates were analyzed for $\Delta_{47}$ and compared to local water and air temperature (Tables 28-29). Calibration equations were developed for lacustrine gastropods, microbialite and tufa, as well as micrite. Calibration results and calculations are presented in Appendix E.

### 4.7. Analytical Procedure for Clumped Isotopes

Samples were reacted for 20 minutes on a 90°C common phosphoric acid bath system in the Tripati Lab at UCLA. $CO_2$ was cryogenically purified using an automated vacuum line that was modeled on a system at the California Institute of Technology (Passey et al., 2010).

Organic compounds were removed with a Porapak column installed on a Thermo Trace GC Ultra gas chromatograph. $\delta^{13}C$, $\delta^{18}O$, $\Delta_{47}$, and $\Delta_{48}$ were determined using a Thermo 253 Gas Source isotope ratio mass spectrometer. For samples containing greater than 90% carbonate (i.e. gastropod shell), sufficient $CO_2$ gas was obtained from acid digestion of 5-10 mg of material. In the case of samples with lower carbonate content (e.g. carbonate muds), 10-50 mg samples were reacted to generate sufficient $CO_2$ gas. During 2013 and the first half of 2014, samples were run for 8 acquisition cycles consisting of 10 measurements of sample and reference gas. During the latter half of 2014, and through 2015, samples were run for 9 acquisition cycles consisting of 10 measurements of sample and reference gas. During each acquisition, sample gas voltages were compared to high purity Oztech brand $CO_2$ reference gas ($\delta^{18}O$ = 25.03‰ V-SMOW, $\delta^{13}C$ = -3.60‰ V-PDB). $CO_2$ gas standards, and carbonate standards of known isotopic compositions, were run every 4-5 analyses. Isotope values of carbonate standards run are presented in Table 4. The Digital Appendix contains set of raw data for sample and standard runs for the entire duration of the project.

### 4.7.1. $\Delta_{47}$ Absolute Reference Frame and Carbonate Standard Correction

Results were normalized following the Absolute Reference Frame correction and standardization process (Dennis, 2011). Signal interference due to electron backscattering in the source of the mass spectrometer was quantified and corrected for. During instrument operation, $CO_2$ gas standards of four compositions were measured routinely (Table 4), and used to evaluate the relationship of $\delta_{47}$ (bulk isotope composition) relative to $\Delta_{47}$ (clumped isotope). Aliquots of gas were cryogenically purified on a manual vacuum line system and collected in borosilicate breakseal tubes. Changes in slope of $\delta_{47}$ vs. $\Delta_{47}$ were attributed to shifting conditions in the

source of the mass spectrometer, and occasionally to the presence of organic contaminants. Samples were strictly run during periods of time in which the calculated slopes of regressions, relating $\delta_{47}$ vs. $\Delta_{47}$, did not change. All data are reported on the absolute reference frame (Dennis et al., 2011).

Residual values were also calculated from carbonate standards, and used to generate a secondary transfer function to correct sample runs. The secondary transfer function addresses variations in the acid digestion process, which although typically small, can introduce error into analyses. $\Delta_{47}$ values for sample and standard runs are presented in the Digital Appendix to this manuscript.

### 4.7.2. Background Correction

Background correction was carried out using two methods. Background Method 1 required off-peak measurements of the background state of the mass spectrometer following each acquisition cycle of sample gas vs. reference gas. This was conducted prior to 2014. Method 2 requires daily determination of peak shapes, and associated background values, in order to correct results. In Method 2, regressions are generated for masses 44-49 by measuring reference gas at several pressures (i.e. voltages) (Bernasconi et al., 2013).

### 4.7.3. Acid Digestion Correction

An acid digestion correction value of 0.092‰ was added to $\Delta_{47}$ values for samples reacted at 90°C (Henkes and Passey, 2013). There is some discussion over the quantification of the acid digestion fractionation factor, with published values for 90°C digestion ranging between 0.069 (Wacker et al., 2013) and 0.092‰ (Ghosh et al., 2006; Henkes et al., 2013). The acid bath

was maintained at constant temperature through use of a cylindrical heating block with a thermocouple feedback system. On two occasions during this study the temperature of the acid bath was physically measured with a glass thermometer and found to be at 90°C.

### 4.8. Climate parameter reconstruction

#### 4.8.1. Water to air transfer functions

Evaluation of seasonal relationships between air and water temperature in modern lakes indicate that lake surface temperature will closely match air temperature (Hren and Sheldon, 2012). In order to reconstruct air temperature at study sites, transfer functions relating lake surface temperature and annual air temperature were applied. In addition, new seasonal transfer functions were developed from the 88 lake dataset of air and water temperature presented in Hren and Sheldon (2012). Table 5 outlines the transfer functions considered in this study. It should be noted that JJA, MJJAS, and Warmest Month water temperatures slightly lag air temperature in the mid-latitude Northern Hemisphere lake dataset presented in Hren and Sheldon (2012). During fall, winter, and early spring, water is warmer than air. Given that lake carbonates largely precipitate during the warm months of the year, winter water temperature to air temperature transfer functions were not considered in this study.

#### 4.8.2. Evaporation reconstruction

Annual and seasonal evaporation rates were calculated using two unique approaches. Method 1 (Equation 9) is presented in Matsubara and Howard (2009). They develop an evaporation equation for the Great Basin, which relates elevation and mean air temperature, and is calibrated against pan evaporation rates at 24 sites:

(9) $E_{Lake} = 0.15T + 0.0004H – 0.54$

$E_{Lake}$ = annual evaporation over lake (m/yr)

T = Mean Annual Air Temperature

H = elevation (m AMSL)

This linear relationship preforms poorly when considering lower annual temperatures, that are near 0°C. At annual temperatures near, or below, freezing, the calculated evaporation is near zero. Thus, evaporation during the warm season is not fully accounted for in the Matsubara and Howard (2009) relationship.

Method 2, presented in Linacre (1993), is an approximation of the Penman equation. Linacre (1993) is better constrained than the Matsubara and Howard (2009) equation. In addition to temperature and elevation, dew point, wind speed, and latitude are also incorporated. Method 2 has previously been applied with success at other lake sites in the Great Basin (Ibarra et al., 2014), and Turkey (Jones et al., 2007):

(10) $E_{Lake}=[0.015 + (4\times10^{-4})T + 10^{-6}z]\times[480(T + 0.006z)/(84 - L) – 40 + 2.3\times u(T-T_d)]$

$E_{Lake}$ = monthly evaporation rate over lake (mm/day)

T = Mean Annual Air Temperature (°C)

z = Elevation (m AMSL)

u = wind speed (m/s)

L = Latitude

$T_d$ = dew point temperature (°C)

Dewpoint ($T_d$) temperature was estimated by compiling ranges of modern values at study sites. $T_d$ values for the LGM were assumed to change by magnitudes equal to shifts in air temperature from present (Jones et al., 2007; Ibarra et al., 2014). A mean windspeed of 3 m/s was also applied at all localities (Jewell et al., 2010). Evaporation was reconstructed at 1,350 m and 1,450 m AMSL. 1,350 m is the approximate elevation of the Stansbury Lake Level, corresponding with sites between 25.8 and 24.5 ka. 1,450 m is the elevation the lake attained by the middle of the LGM. In most cases, Evaporation Method 2 (Linacre, 1993) results in slightly higher evaporation estimates, relative to the Matsubara and Howard (2009) technique, but both are within error of each other. Results converge at air temperature inputs of approximately 10 °C. Modern pan evaporation rates in the Great Basin typically exceed the PMIP3 pre-Industrial control values by a factor of 2 to 4 times.

### 4.8.3. Precipitation reconstruction

To constrain precipitation, clumped isotope temperatures were also applied to two simple hydrologic models for the Great Basin presented in Matsubara and Howard (2009). These models are calibrated with modern evaporation, and runoff coefficients. A "multiplicative" model (Equation 11), and an "additive" model (Equation 12) were considered:

(11) $P/P_m = 2.2 + 0.2(T - T_m)$

(12) $(P - P_m) = 0.44 + 0.068(T - T_m)$

P = LGM precipitation (m/yr)

$P_m$ = Modern precipitation (m/yr)

T = LGM annual air temperature (°C)

$T_m$ = Modern annual air temperature (°C)

The multiplicative approach considers regional change in precipitation as a fraction of the modern value. The additive approach instead considers precipitation change over time by addition or subtraction of a fixed amount of precipitation, relative to the modern value. Application of the proportional "multiplicative" approach to describe changes in regional precipitation results in larger magnitude estimates for change in higher elevation areas, relative to the additive approach. The multiplicative approach may in some cases underestimate precipitation change in lowland areas, relative to the additive approach. Although both approaches yield similar values, the multiplicative approach may be slightly more suitable at Lake Bonneville. Applying the multiplicative model to reconstruct water inputs at Bonneville over a range of temperatures, Matsubara and Howard (2009) were able to generate a result for lake area that was smaller than the mapped lake paleoshoreline by a margin of 10 percent. The additive model resulted in a lake area value that was 26 percent smaller than the full extent of Lake Bonneville.

## 5. RESULTS

Analytical results are reported in Table 6. Clumped isotope values were applied to reconstruct the water temperature of calcification and the corresponding $\delta^{18}O$ value of lake water. Results are presented for specific sites and averages are calculated for the Bonneville Basin and the Sevier Subbasin. Gastropod shell clumped isotope temperatures are reported from six LGM-transgressive lake shoreline sites and one Stansbury Oscillation site (~25.8 to 24.5 ka). Results are reported for six LGM marl sites. Tufa results are reported at the Pilot Valley, and represent the Stansbury (25.8 to 24.5 ka), and Bonneville through Provo (18 to 14.5 ka) intervals. Gastropod temperatures are calibrated using a modern gastropod calibration line (Appendix E). Marl temperatures are reported along the modern micrite calibration line (Appendix E). Tufa samples are calibrated on the modern microbialite/ tufa calibration line (Appendix E).

### 5.1. Water Temperature Reconstructions

Clumped isotope measurements were carried out utilizing both Stagnicola and Pyrgulopsis gastropods (Figs. 7, 11 and 15). Measurements of co-occurring samples of both taxa at the Ferber Wash site are within error of one another (Table 6), with reconstructed temperatures of 11.6±1.0°C for Stagnicola, and 12.0±1.8°C for Pyrgulopsis. As such, these taxa are reported interchangeably. The mean gastropod shell clumped isotope temperature in the Bonneville Basin is 11.7±0.6°C, while the mean growth temperature in the Sevier Subbasin is 16.9±0.7 °C (Figs. 8, 12, and 16). Marl temperatures also differed across Bonneville and Sevier sites (Figs. 10, 13, and 16). In the Bonneville Basin, the temperature of endogenic carbonate precipitation recorded by marl is 21.7±2.9°C. Average marl temperature in the Sevier Subbasin is 24.4±0.6°C.

Tufa growth temperatures from the Stansbury, Bonneville, and Provo lake phases are reported from the Pilot Valley, near Wendover, NV at the western margin of Bonneville Basin (Fig. 16). On average tufa from the Stansbury Oscillation Shorezone is 14.0±2.7°C. Tufa from the Bonneville level is 13.1±3.9 °C, while tufa that formed at the Provo lake level records a temperature of 13.4±1.9°C.

**5.2. Water isotope reconstructions**

The reconstructed oxygen isotope composition of lake water (Table 6; Figs. 9 and 11) provides insight into evaporation trends in the lake at the time of carbonate precipitation. Water isotope reconstructions in this work are reported with a 1.2‰ correction applied to account for enrichment of $^{18}O$ in the glacial ocean (Eagle et al., 2013). All $\delta^{18}O_{water}$ values are reported relative to the V-SMOW standard. The reconstructed $\delta^{18}O$ value for lake water associated with gastropod shell growth shows slight enrichment in the Sevier Subbasin, relative to the Bonneville Basin (Figs. 14 and 15). Mean water $\delta^{18}O$ for Bonneville Basin gastropods is -6.0±0.2‰. Mean $\delta^{18}O$ for Sevier Subbasin gastropods is -5.3±0.4‰ .

Reconstructed water $\delta^{18}O$ from marl correlates inversely with latitude (Fig. 15). There is a 3.0‰ difference in values between the most northerly site (30GP), and the most southerly site (LRSW3). Mean $\delta^{18}O$ reconstructed from marl samples in the Bonneville Basin is -6.4±0.9‰, while the mean value of Sevier sites is -3.8±0.3‰.

The Pilot Valley tufa samples exhibit a negative trend across the Stansbury through Provo time series evaluated in this study (Fig. 17). Mean $\delta^{18}O$ for tufa precipitated during the Stansbury Oscillation is -4.4±0.7‰, while Bonneville aged tufa is -4.8±1.1‰ and Provo tufa is -5.3±0.7‰. The existence of an outlet at the northern margin of the lake during the Bonneville

and Provo phases would have decreased the residence time of water in the lake, and may account for the slight depletion in isotope values over the time series.

Reconstructed water isotopes were compared to modern regional values for the Great Salt Lake, local precipitation, and rivers, and an isotope enabled climate model (Figs. 14, 15, 20, Appendix B). All samples were significantly enriched, relative to modern precipitation oxygen isotope values. Gastropod reconstructed $\delta^{18}O_{water}$ exceeds modern precipitation by 7.5±0.4‰ in the Bonneville Basin and by 7.7±0.5‰ in the Sevier Subbasin. Marl reconstructed $\delta^{18}O_{water}$ exceeds modern precipitation values by 7.1±1.3‰ in the Bonneville Basin and by 9.2±0.8‰ in the Sevier Subbasin. Reconstructed $\delta^{18}O_{water}$ from tufa in the Pilot Valley exceeds modern precipitation values by 9.1±1.0‰ during the Stansbury Lake Phase, by 8.7±1.4‰ at the Bonneville level, and by 8.2±1.0‰ at the Provo level.

## 6. DISCUSSION

Here, clumped isotope-derived estimates of calcification temperatures for gastropods, marl, and tufa are reported for Lake Bonneville for the first time using three material-specific calibrations. In the following discussion, the climatological significance of these results is discussed for the different archives. Calibrated clumped isotope estimates of water temperature are applied to predict air temperature (Tables 10-18), evaporation rates (Tables 19-22), and precipitation rates (Table 35) at Bonneville. Results are discussed in the context of other regional proxy studies and model predictions (Table 23).

### 6.1. Season of Carbonate Growth and Selection of Transfer Functions

Air temperature was reconstructed at study sites using transfer functions that relate lake

surface temperature to air temperature (Table 5). Based upon modern lake data (Appendix E), seasons of growth were assigned to gastropod (Figs. 6 and 7), marl and tufa samples evaluated in this study. The water temperature reconstructed from gastropods is inferred to represent May through September conditions (Tables 7-10). Endogenic carbonate precipitation in marl is restricted to high lake surface temperatures (above 20°C), and is interpreted to occur in association with peak air temperature (Tables 11-14). Tufa growth temperatures are intermediate to marl and gastropod values, and are assessed using a June-August transfer function (Tables 15-18). Reconstructed gastropod temperature (Fig. 12) and marl temperature (Fig. 13) vary more greatly across the lake than during present day. Although questions may arise regarding the sensitivity of the lake specific clumped isotope calibrations, it should be noted that regardless of calibration applied, N-S trends of similar magnitude are calculated. The implications of this are further discussed in Section 6.2.

### 6.1.1. Gastropod Transfer Function and Temperature Reconstruction

The mean annual air temperature reconstructed for gastropods in the Bonneville Basin is -0.1±0.7°C, which is 9.2°C below modern values (Fig. 5; Tables 7-8). Mean annual air temperature reconstructed for gastropods in the Sevier Subbasin is 6.8±1.0°C, which is 3.3°C below modern values (Fig. 5). A 6.9°C temperature difference between the basins exceeds the modern air temperature vs. latitude gradient which is 1-2°C.

Gastropods were assigned a May-September transfer function (Figs. 6-7), based upon assessment of calcification in modern specimens. Lymnaeid snails are not active below 10°C (Vaughn, 1953). Similarly, Pyrgulopsis genus snails in the Snake River system have not been observed to calcify at water temperatures below 9.2°C±3.7°C (Lysne and Koetsier, 2006). The

assignment of an April-October growth season, as has been suggested for other mid-latitude lakes (Hren and Sheldon, 2012), would not be appropriate at Bonneville, where the modern average air temperature is slightly below 10°C, during both April and October (Figs. 6-7). Moderate-to-severe cooling would have reduced water temperatures significantly below 10°C during April and October, limiting shell growth to the May-September interval LGM (Figs. 6-7).

### 6.1.2. Marl Transfer Function and Temperature Reconstruction

Marl reconstructed air temperatures (Tables 11-14) were significantly warmer than gastropod and tufa archives. The calibration line used to calculate marl temperatures was generated from measurements of lacustrine micrite at 8 modern sites (Appendix E). For the calibration, summer time mean temperatures for the June-August interval were selected. At most lakes used in the calibration, it was not possible to determine the window of carbonate precipitation with greater certainty. However, application of other clumped isotope calibrations (e.g. Ghosh et al., 2006 or Defliese et al., 2015) to the Bonneville marl dataset also result in elevated reconstructed water temperatures, well above the gastropod and tufa results presented this study. This indicates that marl precipitated at warmer temperatures than the other phases of carbonate evaluated in this study.

The window of endogenic carbonate precipitation associated with marl appears to have been very narrow, driven by evaporation and carbonate saturation. The assignment of an annual warm month calcification interval may over-represent the timeframe of endogenic carbonate growth in the Bonneville record. Historically, deposition of endogenic calcium carbonate in lakes has been attributed to two mechanisms: evaporation, and biologically mediated precipitation (Duston et al., 1986; Kelts and Hsu, 1978). In mid-latitude marl lakes, photosynthesis promotes

carbonate precipitation beginning in spring, when algal blooms lower $pCO_2$ in the upper water column (Schultze-Lam et al., 1997). However, in larger lakes, such as Lake Ontario, Hodell et al. (2003) observe correlation of endogenic carbonate precipitation with increases in both primary productivity and temperature, with maximum calcification occurring during hot El Niño years.

If carbonate saturation at Lake Bonneville were largely correlated with maximum lake temperature, the clumped isotope signal would be accordingly biased towards the warmest intervals of the depositional record. Air temperature reconstructed by application of the "warmest month-MAAT" transfer function to Bonneville marl is at, or above, modern average air temperature. This would indicate that deposition of endogenic carbonate in marl is primarily occurring on warm days.

### 6.1.3. Tufa Transfer Function and Temperature Reconstruction

Reconstructed temperatures for tufa do not reflect the extreme high values of marl. Calcification appears to have occurred over a significantly larger season of growth (Felton et al., 2006). Wave action, evaporation, and photosynthetic uptake of $CO_2$ have previously been identified as important factors in the precipitation of tufa at Lake Bonneville (Nelson et al., 2005; Felton et al., 2006).

The reconstructed tufa air temperatures in the Pilot Valley are 9.5 to 10.8°C below the modern value of 10.2°C (Tables 15-18). Annual air temperatures associated with tufa growth are -0.7±3.6°C during the Stansbury Phase, prior to the LGM. Tufa samples record a small decrease in water temperature during the Bonneville and Provo phases, when the lake was hydrologically open (Fig. 16). Open lake conditions may have slightly diminished the role of evaporation in the formation of tufa. Tufa reconstructions indicate that annual air temperature was -0.6±5.2°C at the

Bonneville highstand and -0.1±2.5°C during the Provo lake stages (Table 15).

Lacustrine tufa clumped isotope temperatures are intermediate to gastropods and marl, and were assigned a June-August (JJA) transfer function. The effectiveness of this approach can be assessed by comparison with contemporaneous gastropod temperature reconstructions (Table 7) during the Stansbury period of the lake history (25.8 to 24.5 ka). Reconstructed air temperature from Pilot Valley tufa (Table 15) closely matches gastropod-reconstructed values at Stansbury Gulch, to which a MJJAS growth interval was assigned. These sites are situated less than 0.5° latitude apart from one another, and would have likely been subject to similar water temperature conditions.

Previously, concerns have been voiced that kinetic effects associated with the formation of tufa may influence clumped isotope signatures. Although rapid outgassing in the swash zone may promote conditions in which precipitation of carbonate is not in equilibrium with the DIC reservoir, recent work indicates that any kinetic effect from such processes should be minor (Kele et al., 2014). Clumped isotope measurements of modern tufa and microbialites at the Great Salt Lake, Walker Lake, Lago Sarmiento, and Lake Bacalar produced results that correlate with seasonal or mean annual water temperature (Appendix E). The results collected in this work on ancient tufa at Lake Bonneville should reflect near, or complete, equilibration between water and carbonate.

### 6.2. Comparison of Bonneville Basin and Sevier Subbasin Reconstructed Temperatures

Clumped isotope calcification temperatures are higher in the Sevier Subbasin for both gastropods and marl, relative to the Bonneville Basin, during the LGM. The PMIP3 ensemble mean, and several other proxy or model studies (Hostetler et al., 1994; Madsen et al., 2001;

Jewell et al., 2006), also predict warmer, or wetter, conditions in the Sevier Subbasin. However, the reconstructed magnitude of difference in water temperature from clumped isotopes across the two basins of the lake exceeds these predications, and modern variations in air temperature (Figs. 11 and 12). Modern summer air temperature varies by 1.0-1.5°C between Bonneville and Sevier localities (Fig. 5). Different levels of response to summer heating in each basin may partially account for variation in temperature recorded by clumped isotopes in each basin.

If lake water in the smaller, and shallower, Sevier Subbasin were more responsive to changes in air temperature, summer water temperatures may have been higher. This would imprint a warmer clumped isotope signature in gastropod shells and in marl. Modern thermal trends across the North and South Arms of the Great Salt Lake provide context to evaluate this hypothesis. The North Arm is smaller in area and shallower than the South Arm, and exhibits higher annual and summer water temperatures. Although air temperature does not vary appreciably over the Great Salt Lake, surface water in the North Arm is 2-3°C warmer than the South Arm in the summer (Crosman and Horel, 2009; Horel, 2015). Annually, surface water in the North Arm is 1-2°C warmer (Horel, 2015). This discernable difference across the modern Great Salt Lake raises the possibility that annual water temperature response to heating may have not been uniform throughout Lake Bonneville. The elevation of Sevier Dry Lake, the low point of the Sevier Subbasin, is approximately 1376 m AMSL, while the Bonneville Basin floor is 1280 m AMSL (Oviatt, 1988). During the early LGM, maximum water depth in the Sevier Subbasin would have been in the range of 40 to 60 m, while water depth in the center of the Bonneville Basin would have been nearly 100 m greater. Water in the smaller and shallower Sevier Subbasin could have heated more quickly, and attained a higher peak temperature, during summer.

### 6.3. Proxy and Model Temperature Comparison

The paleotemperatures reported from gastropods and tufa in this study match, or slightly exceed, model and proxy predictions for cooling in the Bonneville Basin, during the last glacial interval (Table 24, Figs. 12 and 13). Amino acid racemization estimates indicate a temperature decrease of 10°C (Light 1996; Kaufman, 2003), and possibly up to 12°C (McCoy, 1981) in the Bonneville Basin during the late Pleistocene. Lemons et al. (1996) suggests temperature depression of 13°C may have been necessary to advance the lake. Annual air temperature reconstructed from gastropods in the Bonneville Basin during the LGM is 9.2±0.8°C below modern (Fig. 21), and air temperatures would have been 7.1±0.6°C lower than modern during the May through September interval (Fig. 22; Tables 7-10). Tufa clumped isotope estimates for air temperature during the Stansbury, Bonneville, and Provo lake phases are below modern temperatures by magnitudes of 9.5±3.6°C, 10.7±5.2°C, and 10.3±2.5°C, respectively (Tables 15-18). Gastropod derived air temperatures during the Stansbury Oscillation interval (25.8 to 24.5 ka) were 10.4±1.2°C below modern (Table 8). Together, these results indicate that temperatures were consistently below modern values during both the closed basin and post-LGM open basin phases of the lake (Figs. 12 and 16). The clumped isotope based reconstructions are lower than vegetation-based reconstructions (Madsen et al., 2001), which suggest temperature depression of 6-7°C during the last glacial (Table 24).

A clumped isotope based estimate of 9-11°C of cooling exceeds the PMIP3 climate model ensemble mean temperature depression of 7.9±2.6°C (Fig. 21). However, the PMIP model boundary conditions for pre-Industrial climate do not accurately represent late Holocene values at the sites evaluated (Appendix C). PMIP model controls are approximately 3-4°C lower than

modern climate records. The accuracy of the model control data can be interpreted by comparison of PMIP boundary conditions with the modern climate record. PMIP models were compared to gridded modern climate data extracted from the PRISM dataset, which has 800 m cell resolution, and 30-year climate averages downloaded from the NCDC (Appendix C). Approximately 0.9°C of temperature discrepancy between modern climate and PMIP controls can be attributed to anthropogenic emissions since the industrial revolution (IPCC, 2013). Because the boundary conditions are not well matched in the Bonneville Basin, the most suitable method for evaluation of clumped isotope temperature data against the PMIP archive is through comparison of differences between late Pleistocene and modern states.

### 6.4. Evaporation Reconstruction

Air temperature estimates were applied to constrain evaporation values for the carbonates investigated in this study (Tables 19-21). Although evaporation during the LGM may have been extremely low from autumn through early spring, clumped isotope results suggest that temperatures over the lake would have been sufficiently high from May through September to facilitate evaporation at approximately 62 percent of modern levels in the Bonneville Basin (Fig. 25), and 78 percent of modern levels in the Sevier Subbasin (Fig. 28). PMIP3 multi-model ensemble mean values for the Bonneville Basin and Sevier Subbasin indicate that daily evaporation rates were 74-75 percent of pre-industrial control values during the LGM (Figs. 25 and 28). Evaporation reconstructions were considered using the Linacre (1993) approximation of the Penman equation for evaporation over open water, and the Matsubara and Howard (2009) derivation for the Great Basin. Reconstructed evaporation rates were below modern values for the tufa and gastropod archives.

### 6.4.1. Potential Evaporation Scenarios

The seasonally calculated evaporation rate from the Linacre (1993) equation provides the most robust estimate (Tables 19-20). The Linacre (1993) equation considers latitude, windspeed, elevation, mean temperature, and dew point temperature, while the Matsubara and Howard (2009) formula accounts only for elevation and air temperature. Assessment of modern records indicates that the majority (70 to 80 percent) of annual evaporation occurs during May-September (Digital Appendix). Thus, the gastropod-based seasonal temperature estimate can be utilized to reconstruct evaporation over a calendar year. Multiplication of the MJJAS cumulative evaporation by a coefficient of 1.4 accounts for evaporation during October-April. The coefficient of 1.4 was determined by evaluation of modern evaporation rates at study sites. Modern rates were assessed by application of weather data to the Linacre (1993) equation, and by evaluation of historical pan evaporation rates in Utah.

Calculating annual evaporation from mean annual air temperature estimates (Digital Appendix) also influences the final result. If annual air temperature derived from gastropod and tufa lake temperatures (<1°C) are applied to the Matsubara and Howard (2009) formula, the calculated evaporation rate is less than 0.2 mm/day over the course of the year. Annual rates calculated using the Linacre formula are ~1 mm/day, less than 25 percent of modern annual rates (Digital Appendix).

When comparing evaporation estimates from clumped isotope temperatures to PMIP3 model outputs it is important to note differences in magnitude for each archive. In all cases, the PMIP3 evaporation rates are considerably lower for both the LGM and pre-Industrial control runs, relative to the clumped isotope based estimates presented here. Modern measured

evaporation rates are also 2-4 times greater than the pre-Industrial control values applied in models. Estimates calculated using the two equations cited in this thesis (Matsubara and Howard, 2009; Linacre, 1993) from modern air temperature data, are similar in magnitude to reported modern rates. The most important point for comparing data in this thesis to models is the magnitude (or percentage) change, relative to control values. Other work (e.g. Ibarra et al., 2014) followed a similar approach.

### 6.4.2. Evaporation in Marl

For all marl temperatures, the calculated annual evaporation rate exceeds modern values. Although marl clumped isotope results were applied to develop estimates of evaporation, these results are not considered to reflect the mean state at Lake Bonneville during LGM. As has been suggested in Section 6.1.2, the temperature record of the marl is near modern summer water temperatures at the Great Salt Lake. At modern summer evaporation rates, the amount of precipitation and runoff required to generate a lake at 1450 m would be 4 to 6 times modern values. For marl-based reconstructions, the requisite precipitation increase necessary to balance evaporation is improbable, when viewed in the context of the vegetation record (Madsen et al., 2001). Pollen and vegetative remains from the late Pleistocene indicate that pine and sagebrush populations would have been prevalent in the Bonneville Basin. These taxa prefer cool, relatively dry, conditions, and would not have tolerated substantial increases in annual precipitation during the LGM.

### 6.5. Oxygen Isotope Composition of Lake Water

The oxygen stable isotope records (Table 6; Figs. 9, 11, 14-15, 17-20) presented in this study indicate that waters were modified by evaporation. An isotope enabled climate model (Fig. 20) indicates that $\delta^{18}O_{water}$ in precipitation falling over the eastern Great Basin during the LGM would have not been enriched, or depleted, by more than 0.5‰ V-SMOW, relative to modern values. The oxygen isotope values of gastropod (Fig. 14), marl (Fig. 15), and tufa reported in this study, exhibit evaporative enrichment, of 7.1 to 9.2‰ above probable precipitation values at sites (-13 to -15‰). $\delta^{18}O$ values of lake water, reconstructed from tufa, decrease slightly from the Stansbury Phase (-4.4±0.7‰) to the open basin, Bonneville and Provo, phases (-4.8±1.1 to -5.3±0.7‰) of the lake (Fig. 17). Bonneville was sufficiently large during the open basin phase such that evaporative enrichment was only slightly less than during the closed basin, transgressive interval.

The reconstructed values of $\delta^{18}O_{water}$ indicate that evaporation rates differed between the Bonneville Basin and Sevier Subbasin (Figs. 14-15). Oviatt et al. (1994) previously attributed North–South increases in $\delta^{18}O_{carbonate}$ in marl to latitudinal gradients in temperature and evaporation. Solving for $\delta^{18}O_{water}$, by application of clumped isotope temperatures, allows for a more thorough evaluation of this hypothesis. With both marl and gastropods, the difference between meteoric precipitation and reconstructed $\delta^{18}O_{water}$ was greater in the Sevier Subbasin than in the Bonneville Basin. The greatest differentiation in oxygen isotope values between the basins is exhibited in marl (Fig. 15). The oxygen isotope record of water associated with marl formation reconstructed in this study exhibits a 3.0‰ difference from north to south. Although gastropods were sensitive to changes in lake temperature, the $\delta^{18}O$ signature recorded in shell would have likely encompassed a wider time frame than endogenic carbonate precipitation, and

would have been less responsive to lakewide differences in peak evaporation.

### 6.5.1. Oxygen Isotope Response to Changes in Lake Volume

Oxygen isotope results from this study were compared to the archive of deep water carbonate reported from Cathedral Cave and Craners Cave (Fig. 18) in McGee et al. (2012). Carbonate at these sites precipitated during intervals of inundation. Precisely constrained geochronology allowed McGee et al. (2012) to assess changes in the isotope record during individual lake phases. Figure 18 presentS reconstruction of lake water $\delta^{18}O$ for the McGee et al. (2012) series of $\delta^{18}O_{carbonate}$ measurements, based upon the assumption that bottom water temperatures at Cathedral and Craners Caves were 4°C, which is the level at which freshwater attains maximum density (Livingstone, 2003). Following the mineralogy reported in McGee et al. (2012), these deep water cave carbonates are classified as aragonite until 18.8 ka, while younger samples are calcite. $\delta^{18}O_{water}$ for aragonite was calculated using the relationship presented in Kim et al. (2007), while $\delta^{18}O_{water}$ in calcitic samples was determined using the Kim and O'Neil (1997) calibration.

The majority of gastropod, marl, and tufa samples reflect greater enrichment of $^{18}O$ relative to the cave deep water record. Lacustrine cave carbonate, was likely subject to cooler, and more consistent, temperatures throughout the year, and so $\delta^{18}O$ associated with that record may not be as strongly biased towards summer months as the lake surface carbonates targeted in this study. A slight decrease in $\delta^{18}O$ from the highstand (18 ka) through the early Provo Phase is recorded in both the surface water (i.e. tufa) and bottom water 'cave' carbonate samples. A steeply positive oxygen isotope trend in the McGee et al. (2012) samples at the end of the Provo Phase corresponds with regression of the lake, and indicates that shallowing, associated with

regression, may have led to more frequent mixing between surface and bottom waters.

### 6.5.2. Covariant Trends of $\delta^{18}O$ and $\delta^{13}C$ Imply Differentiated Lake Water Across Basins

Covariance of $\delta^{18}O$ and $\delta^{13}C$ in marl indicates that both basins were modified by evaporation, but that the rate of evaporation, and/or the composition of carbon and oxygen isotope reservoirs, in each basin may have been different. Positive $\delta^{18}O_{carbonate}$ and $\delta^{13}C_{carbonate}$ covariance occurs in lake basins that are characterized by negative effective precipitation (P minus E) conditions (Talbot and Kelts, 1990; Horton et al., in press). The slope of covariance is much greater in the Sevier Subbasin. The slope of the regression generated for Sevier Subbasin carbonates is steeper than that of the Bonneville Basin slope by a factor of six (Fig. 20). Significant chemical differentiation between these basins has been hypothesized in other work (Pedone, 2003; Hart et al., 2004).

## 6.6. Precipitation Reconstruction

Application of clumped isotope constrained air temperatures to the precipitation models developed by Matsubara and Howard (2009) indicate that Bonneville was drier than modern, during the LGM (Table 23). PMIP3 models predict slightly drier than modern conditions over the Bonneville Basin, and slightly wetter conditions over the Sevier Subbasin during the LGM (Figs. 31-33). Following the multiplicative approach, precipitation across the lake would have been 23 percent below modern levels during the LGM. Application of clumped isotope derived air temperatures to the additive model indicates that precipitation may have been 25 percent lower than modern (Table 23). The multiplicative approach outlined by Matsubara and Howard (2009) reflects elevation forcing on net runoff and evaporation. The additive approach assumes

an aerially uniform increase or decrease in precipitation with greatest change over topographically flat desert areas. Although both approaches yield similar values, the multiplicative approach is more suitable at Bonneville, where the Wasatch and Uinta mountains comprise part of the watershed, and exert strong forcing on precipitation.

### 6.6.1. Evaporation Balance Model

Simple water budget calculations were also considered (Appendix D), where evaporative losses were balanced with precipitation and river discharge into the lake. This approach oversimplifies the hydrologic balance and does not address uncertainties in groundwater input, overland flow into the lake, and river discharge. Results of these analyses indicate that precipitation and runoff would have increased by a factor of 2.7 to 3.7 to maintain the LGM lake level. The results of this approach are presented in Appendix D, accompanied by a discussion of error. A fully constrained water budget model for the Bonneville Basin that addresses heterogeneous topography, watershed responses to glaciation, and lake effect does not exist at this time, but may be available for evaluation in the future.

## 6.7. Climatic Implications

Here, Lake Bonneville clumped isotope results are evaluated in the context of regional evaporation and precipitation trends. Results presented here suggest that reduced evaporation rates, up to 40 percent below modern, may have played a large role in the development of lakes in the Northern Great Basin during the Late Pleistocene. Application of the air temperatures reconstructed in this study to the Matsubara and Howard (2009) hydrologic models indicate that Lake Bonneville could have advanced with precipitation over the lake at 23 to 25 percent below

modern values. These observations are consistent with prior studies, which have hypothesized the presence of a moisture dipole across the Great Basin, where lakes in the south reached highstands during, or before, the LGM, while lakes in the north, including Bonneville and Lahontan, did not reach maximum extent until after the LGM (Lyle et al., 2012; Ibarra et al., 2014; Oster et al., 2015; Lora et al., submitted). During the LGM, precipitation from three major sources may have affected Western North America, and contributed varying amounts of moisture to lakes. These sources, which are discussed in the following, include: the North Pacific (Antevs, 1948; Oster et al., 2015), the Central Pacific (Lora et al., submitted), and the tropical East Pacific (Lyle et al., 2012).

### 6.7.1. Decreased Evaporation

Based upon some model and proxy reconstructions, it has been hypothesized that fluctuations in lake level were due to evaporative changes (Lemons, 1996; Kaufman, 2003; Ibarra et al., 2014; PMIP3), and that late Pleistocene precipitation was at, or below, modern levels in the northern Great Basin. The results presented here (Figs. 25-27) support this hypothesis and indicate that large lakes in the northern Great Basin, including Bonneville, may not have initially expanded as a result of increased precipitation. Reconstructed temperature depression in the Bonneville Basin of 9-11°C, indicates that lake level rise may have been largely correlated with reduced evaporation. Clumped isotope data support LGM evaporation rates that were below modern values, by up to 40 percent. The oxygen isotope record also indicates that evaporative enrichment of lake water is less pronounced relative to modern values. Furthermore, investigation of Stansbury, Bonneville, and Provo tufa in the Pilot Valley suggests that lake temperatures were consistently depressed across much of the Bonneville lake cycle,

both before and after the LGM. As the lake rose, a strengthened lake effect would have moderated the local climate (Hostetler et al., 1994). Evaporation leaving the lake would have fallen back to the lake as direct precipitation, and would have been sequestered by high mountains within the larger catchment area, which would have made Bonneville self-sustaining to a certain extent.

### 6.7.2. The Role of Precipitation

Although precipitation and runoff input were necessary for the transgression of Lake Bonneville, lower evaporative loss identified in this study may have exerted even stronger influence in generating less negative effective precipitation, (P minus E). Based upon application of the Matsubara and Howard (2009) models (Figs. 31-33), precipitation over Lake Bonneville was reconstructed to be 23 to 25 percent below modern during the LGM. Although net precipitation over lake basins was from exogenous sources, lake-effect snowstorms may have also been common. A small lake effect has been observed at the modern Great Salt Lake, during winter, when land-water temperatures contrast by the greatest magnitude (Steenburgh et al., 2000).

Evaluation of historic transgressions of the Great Salt Lake provides insight into the effect of cooling, and precipitation, upon lake levels. During the winter of 1982-1983, Strong El Niño conditions delivered heavy precipitation to the Great Salt Lake. From 1984-1987, 1-2°C cooler air temperatures diminished evaporation over the lake (Bedford, 2005; PRISM Climate Group, 2014). The result was a rise in lake level of 6 m, relative to the historic lowstand period during the early 1960s. The more recent 1996-1997 El Niño event was not followed by cooler temperatures, and resulted in a smaller 2 m rise in lake levels. In the modern, at least, lake

transgressions require that evaporation rates be lower.

### 6.7.3. Precipitation Variation Across the Great Basin During the LGM

During the LGM, PMIP3 models predict higher annual temperatures and evaporation in the southern Great Basin, relative to Bonneville. Yet, lakes rose earlier in the south. Greater effective precipitation (P minus E) in the Mojave may have been more strongly driven by precipitation than reduced evaporation, in contrast with Lake Bonneville. Recent findings presented in Lora et al. (submitted) suggest that winter precipitation from atmospheric rivers was a major contributor of moisture to the southern Great Basin. The strongest expression of atmospheric rivers would have been in central and southern California, and could have promoted the rapid expansion of lakes in the Mojave. Lowering of the North Pacific High and strengthening of the Aleutian Low, would have generated trends similar to the positive phase of the Pacific Decadal Oscillation (Lora et al., submitted). This would have increased the frequency of extreme winter precipitation events delivered to the west coast of North America up to latitudes of 36 to 38 degrees north. The Sierra Nevada Mountains largely impeded penetration of atmospheric river storms far into the central and northern Great Basin. It should be noted that the mean conditions over the Pacific Ocean requisite for steering of the polar jet, observed by Oster et al. (2014), are not identified in recent model and proxy syntheses (Lora et al., submitted).

### 6.7.4. Monsoonal Delivery of Precipitation

Lyle et al. (2012) identify the Sierra Nevada and Cascade Mountains as strong barriers that would have inhibited transport of moisture inland from the coast into the central and northern Great Basin, and suggest a monsoon that penetrated further northwards from the Gulf of

California as an alternative to explain large lakes. Although monsoons may have delivered moisture to the southern Great Basin, Lyle et al. (2012) do not provide a valid mechanism to explain further northward migration of storms along this route. Global heat budget models demonstrate a southward shift of the ITCZ during the LGM, which has been shown to weaken the monsoon (Broccoli et al., 2006). In the modern era, the North American monsoon is strongest over Northern Mexico, and areas of Southern California, Arizona, and New Mexico, but periodically delivers moisture further north. The Sevier Subbasin is situated at the extreme northern margin for monsoonal precipitation delivery in the Great Basin, but the region receives less than 20 percent of annual water during the summer (Denniston et al., 2007). With a southward shift of the ITCZ, the probability of Gulf of California moisture reaching the Sevier Subbasin watershed during the LGM would be even lower.

### 6.8. Future Work

In this thesis it is demonstrated that water temperatures in the Bonneville Basin were significantly cooler than modern, and moderately cooler in the Sevier Subbasin. However, uncertainties regarding different annual heating trends of water in each basin (Section 6.2) complicate interpretation of results in the context of air temperature and evaporation. Future work on the thermal response of waters to summer heating in each basin may address this ambiguity.

The hydrologic interpretations of the results presented in this study vary depending on the specific estimation technique applied. As better constraints upon groundwater, runoff, and lake effect become available, these components should figure prominently in more advanced water budget assessments. Recent interpretations of Bonneville Basin and Sevier Subbasin hydrology

indicate that groundwater may have played a larger role during the time of Lake Bonneville than has been previously been documented (Oviatt, 2015). Current work to constrain the influence of lake effect upon snow and ice accumulation in the Wasatch and Uinta Mountains (e.g. Galewsky, 2013) will further resolve uncertainty.

## 7. CONCLUSIONS

In this thesis, carbonate clumped isotopes are applied for the first time to define the hydrologic parameters of temperature, evaporation, and precipitation at Lake Bonneville. Although this work should be considered preliminary, significant contributions are made in several areas. This thesis provides new insight on calcification temperature in three phases of lake carbonate. Biogenic aragonite in mollusk shells at Bonneville largely precipitated during the May through September interval, when water temperatures were most conducive to organismal development. High reconstructed clumped isotope temperatures in marl, irrespective of calibration, suggest that evaporation-driven carbonate saturation played a stronger role than photosynthetic uptake of $CO_2$ in the calcification of this phase. Tufa and beach rock from shorezones grew during warm summer months, but over a wider timeframe than marl.

During the LGM, climate at Lake Bonneville was determined to be cooler, and hence less evaporated, than the modern regime. Warm season (May through September) temperatures were estimated to be 7.1±0.6ºC lower than present-day values in the Bonneville Basin. Annual air temperatures are estimated to be 9.2±0.8ºC lower than present-day values in the Bonneville Basin. Clumped isotope temperature reconstructions are below the PMIP3 climate model ensemble mean in the Bonneville Basin. Calcification temperatures in the Sevier Subbasin are elevated, relative to the Bonneville Basin, but are also lower than the PMIP3 mean.

Clumped isotope temperatures were also combined with carbonate oxygen isotope ($\delta^{18}O$) ratios to determine values for $\delta^{18}O_{water}$ associated with mineral growth, a parameter that tracks evaporative enrichment in lakes. Results indicate that $\delta^{18}O_{water}$ at Lake Bonneville was enriched 7.1 to 9.2‰ above modern precipitation values, which is less than at the modern Great Salt Lake, where $\delta^{18}O_{water}$ is often greater than 9 to 11‰ above modern precipitation. Water $\delta^{18}O$ reconstructions were applied to reconstruct evaporation values across the lake. Lake water associated with marl precipitation in the Bonneville basin is enriched 7.1±1.3‰ above modern rain and snow, while lake water reconstructed from marl in the Sevier Subbasin is enriched 9.2±0.8‰ above modern precipitation. Covariation of $\delta^{18}O$ and $\delta^{13}C$ in marls suggests that isotopic pools for waters in each basin were unique. Broadly, these results suggest that the small southern Sevier Subbasin was subject to different climatic, and geochemical, parameters from the main body of the lake.

The oxygen isotope results in this work are also compared to bottom water reconstructions for $\delta^{18}O_{water}$. The majority of gastropod, marl, and tufa samples reflect greater enrichment of $^{18}O$ relative to the bottom water record. Isotopic differences between deep water carbonate and the shallow water phases evaluated in this study suggest that the timing of carbonate precipitation in the deep lake may have been subject to different controls than in surface waters. A slight decrease in $\delta^{18}O$ from the highstand (18 ka) through the early Provo phase is recorded in both the surface water (i.e. tufa from this study) and bottom water 'cave' carbonate samples, reported in McGee et al. (2012). Increasing $\delta^{18}O$ in bottom water samples at 15 ka, near the end of the Provo phase, indicates that shallowing, associated with regression, may have led to more frequent mixing between surface and bottom waters.

Although the results presented in this thesis do not permit direct evaluation of the sources

of precipitation feeding Bonneville during the LGM, simple water budget analyses suggest that the lake may have been able to transgress even with precipitation at 23 to 25 percent below modern values. Reconstructed evaporation rates, derived from clumped isotope temperatures, suggest that evaporation was at 37 percent below modern values in the Bonneville Basin, and 21 percent below modern in the Sevier Subbasin. Evaporation results for the Bonneville Basin, which comprises 70 percent of the lake catchment, are significantly below the PMIP3 ensemble mean prediction of 25 percent lower than modern values during the LGM. While lakes in the southern Great Basin may have been fed by atmospheric river precipitation during the LGM (Lora et al., submitted), moisture retention was enhanced at Lake Bonneville by diminished evaporation, likely coupled with a strengthened lake effect (Hostetler et al., 1994). Broadly, these results suggest that Lake Bonneville transgressed, at least initially, as a result of lower evaporation.

## 8. FIGURES

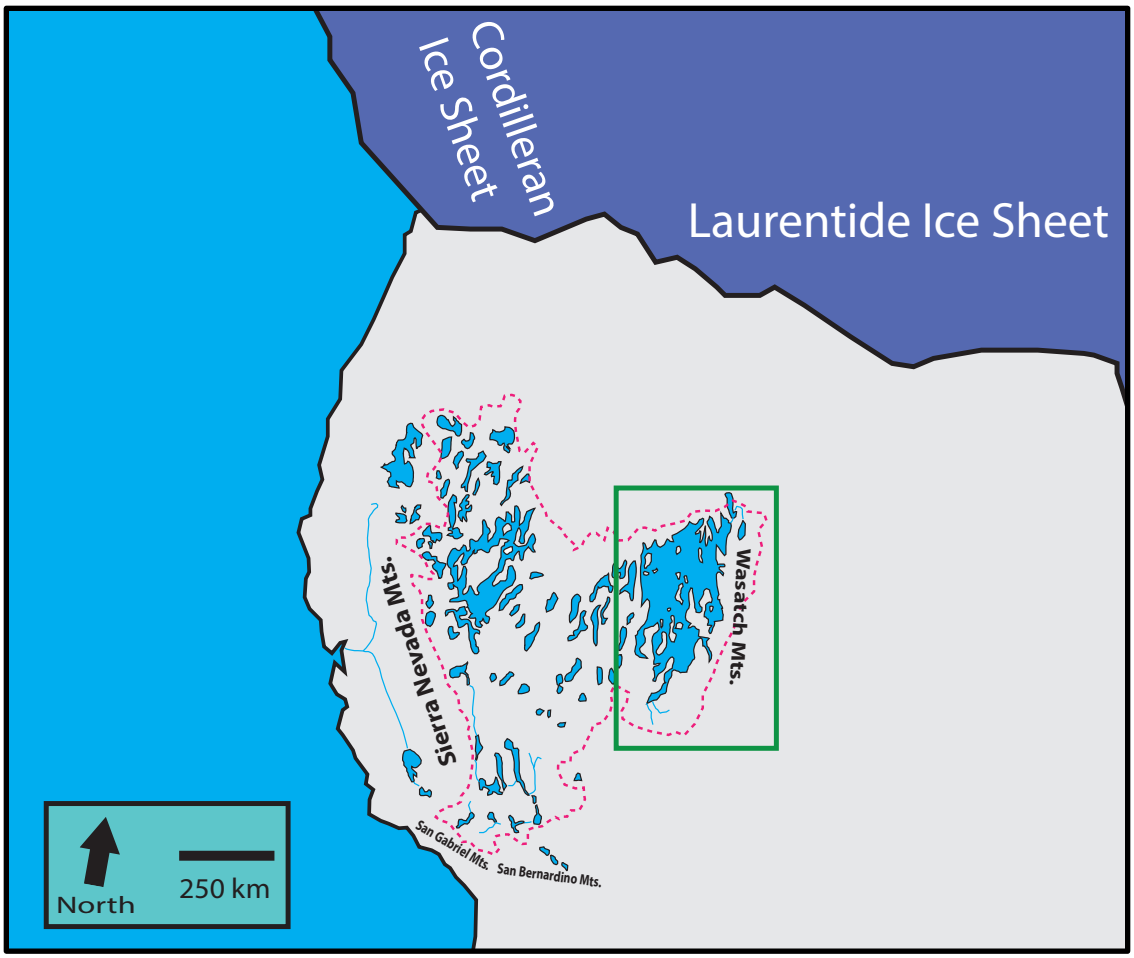


**Figure 1:** ***Lake shorelines reconstructed for the last ice age (21 ka), when atmospheric $CO_2$ levels were significantly (~100 ppm) lower than pre-industrial levels.*** The largest systems advancing at the time of the Last Glacial Maximum (LGM), 23 to 19 ka, were lakes Bonneville (green box) and Lahontan, which reached areas of approximately 52,000 and 22,000 square kilometers at their respective high stands. Numerous smaller lake systems were expanding from southern Oregon to Mexico at this time (Hostetler et al., 1994; Oviatt, 1997; Reheis et al., 2014; Ibarra et al., 2014). Over a century of scientific work at paleolakes across the intermontane west has enabled researchers to identify oscillations in lake levels during the late Pleistocene. Enhanced precipitation and diminished evaporation have been invoked as factors leading to the development of lakes. It has been suggested that lakes in the southern Great Basin expanded primarily as a function of precipitation delivery, while lowering of summer evaporation may have driven lake transgressions to the north (Kaufman, 2003; Ibarra et al., 2014; Lora et al., submitted). The Great Basin (red dashed boundary) is the largest endorheic region in North America, covering an area slightly less than $500{,}000^2$ km. It largely overlaps the Basin and Range physiographic province, bounded on the East by the Wasatch and Uinta Mountains, and the Sierra Nevada Range to the west. Regional extension has been ongoing across the Basin and Range, resulting in North-South trending graben valleys, bounded by ridges with reach elevations in excess of 3000 m. During glacial intervals, fresh and semifresh lakes expand in valleys. During interstadials, lakes retreat, become hypersaline, and often disappear altogether.

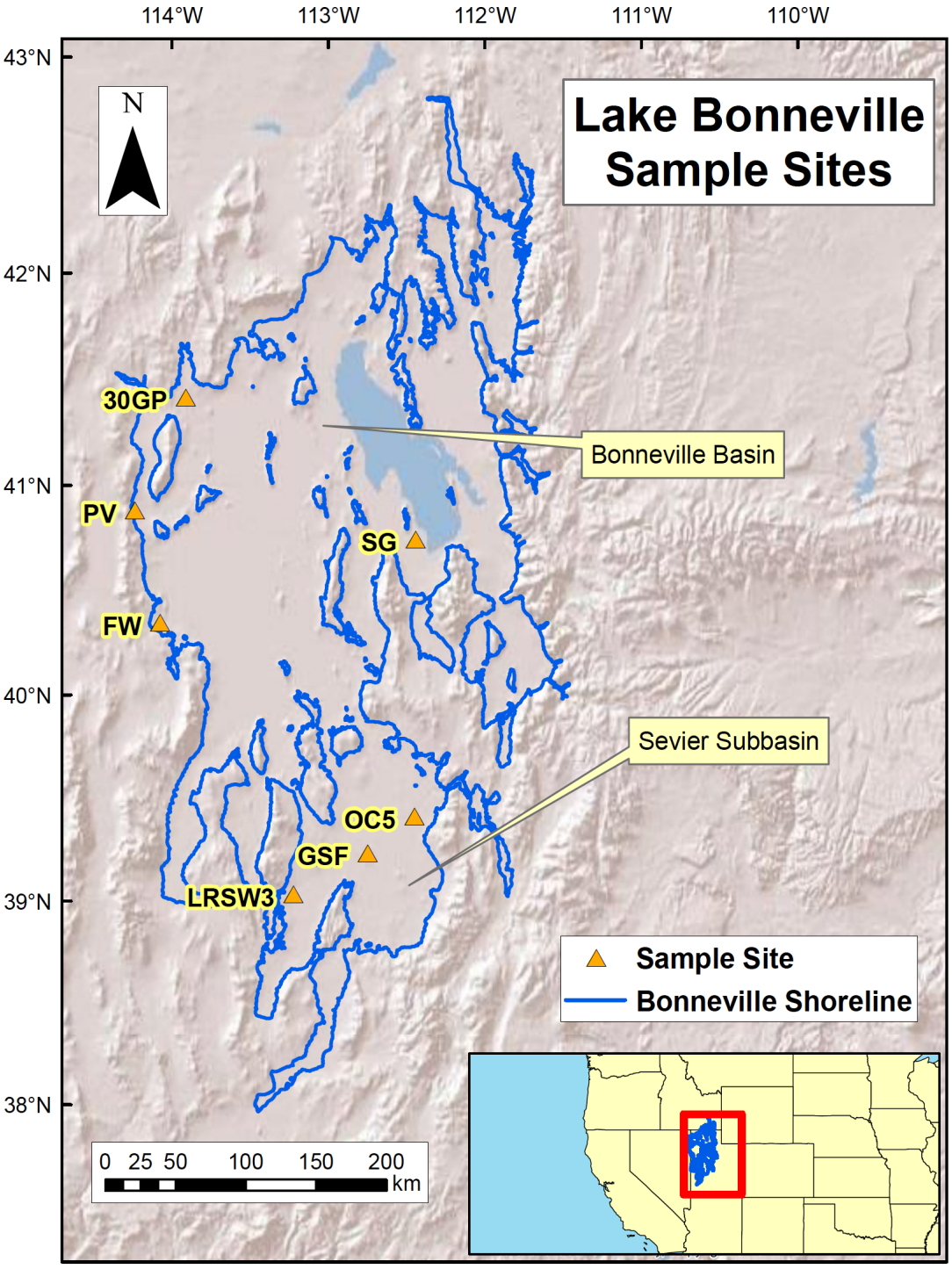


**Figure 2:** ***Lake Bonneville shoreline and sample localities. LGM samples were collected from both the Bonneville Basin and Sevier Subbasin.*** The Bonneville Basin comprises the main body of the lake. The smaller Sevier Subbasin is geochemically distinct from the Bonneville Basin (Hart et al., 2004). 30GP = Lucin Gravel Pit; PV = Pilot Valley; FW = Ferber Wash; SG = Stansbury Gulch; OC5 = DMAD Reservoir; GSF = Great Stone Face; LRSW3 = Long Ridge SW 3.

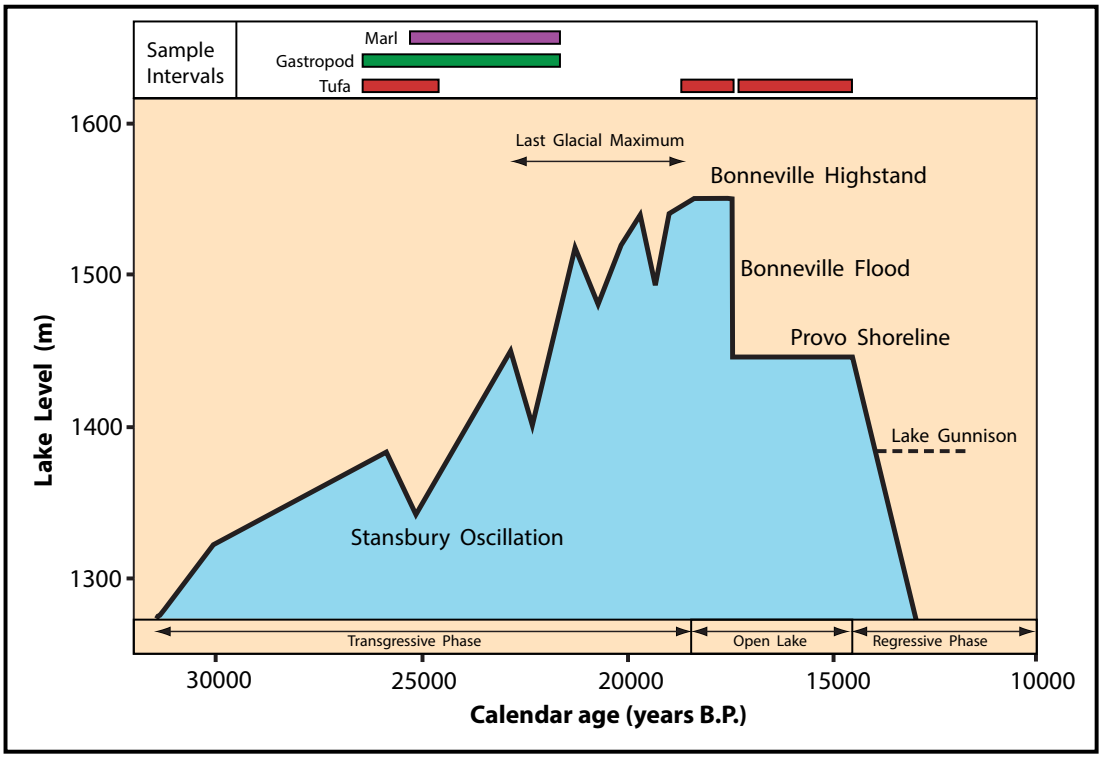


**Figure 3:** ***Timeline of the most recent transgressive lake cycle in the Bonneville Basin, with sample collection intervals shown at the top of the figure.*** Lake level is adjusted for post-lacustrine isostatic rebound. In this study, clumped isotope temperatures are reconstructed in both the Bonneville and Sevier Subbasins. Temperatures during the Bonneville and Provo intervals are assessed for lacustrine tufa deposits at localities in the Pilot Valley. Figure after Miller et al., 2013.

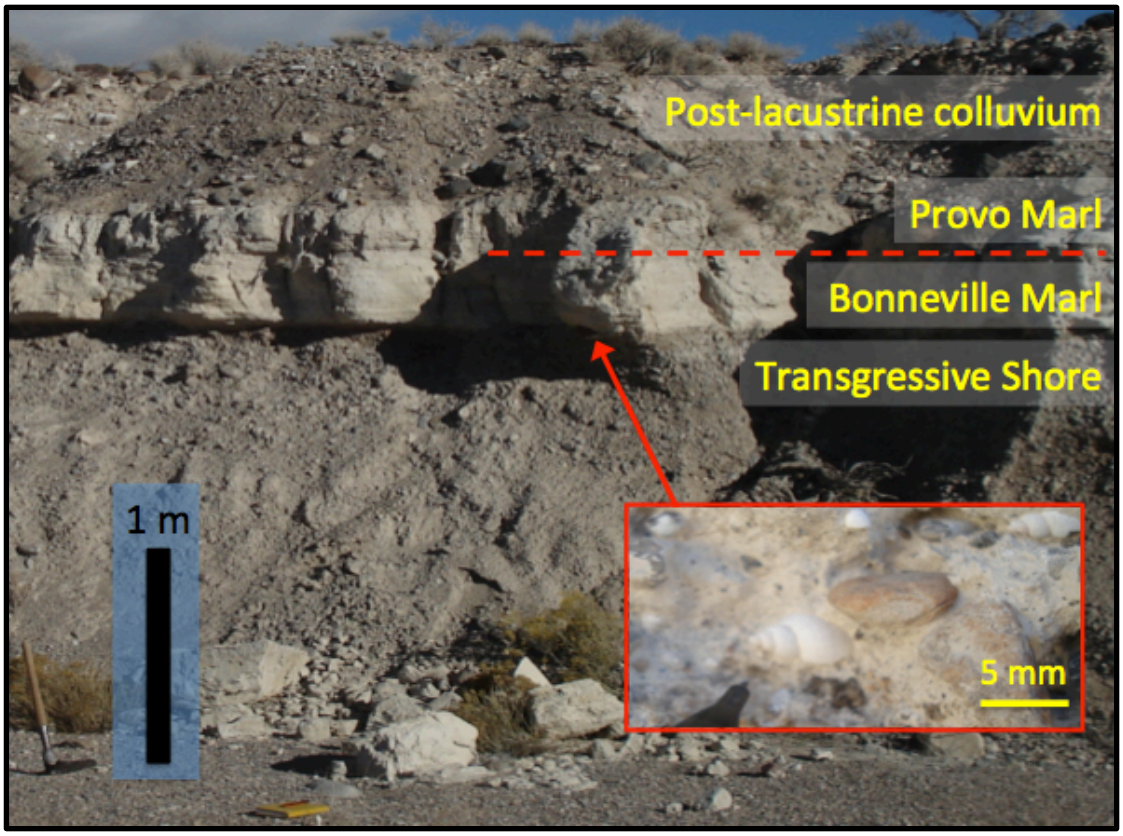


**Figure 4**: ***Typical transgressive shoreline exposure at the Ferber Wash field site, West-Central Bonneville.*** A unit of sand and gravel is overlain by transgressive marl. Gastropod shells were collected from the basal sand unit. Lacustrine marl is ubiquitous above sandy gastropod-bearing shorezone beds. Bulk samples of marl were collected immediately above the shell-bearing unit. Within the marl, a fine sand layer (dotted red line) denotes energetic shallowing associated with the Bonneville Flood at ~18 ka. Post-flood marl from the Provo phase is extensive, but less useful towards developing a comprehensive understanding of Lake Bonneville, as it contains large amounts of reworked transgressive and highstand marl. Provo-age marl is truncated by an erosional unconformity, and overlain by Holocene colluvium.

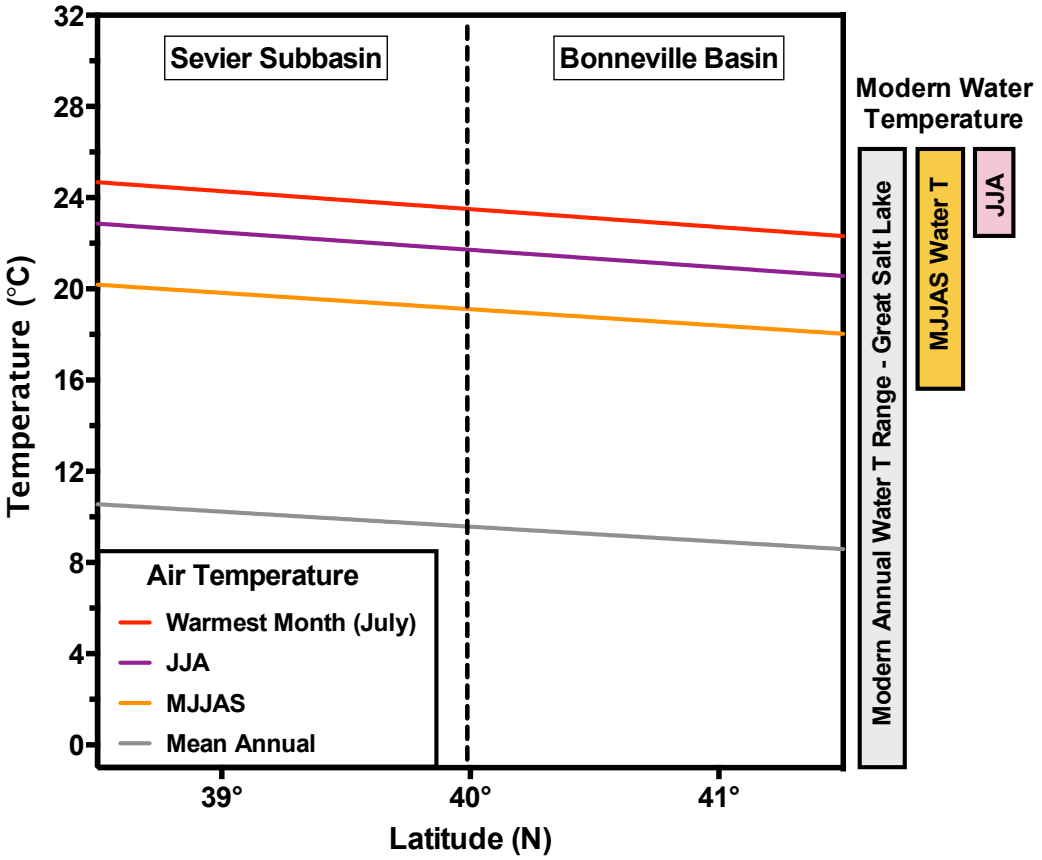


**Figure 5**: ***Modern air and water temperatures at Lake Bonneville study sites.*** The modern mean annual air temperature at sites ranges from 8.7 to 10.5°C, while mean summer (June-August) air temperatures range from 20.6 to 22.7°C. May-September air temperatures range from 18.1 to 20.1°C. July is the warmest month. Peak summer daytime water temperature at the modern Great Salt Lake is 26.1°C. Modern air temperature data is from the PRISM Climate Group. The modern surface water temperatures presented here are average monthly values at the Great Salt Lake, derived from Moderate Resolution Imaging Spectroradiometer (MODIS) data, and are comparable to USGS bucket samples (Alcott et al., 2012; NCAR Applications Laboratory 2013 Annual Report).

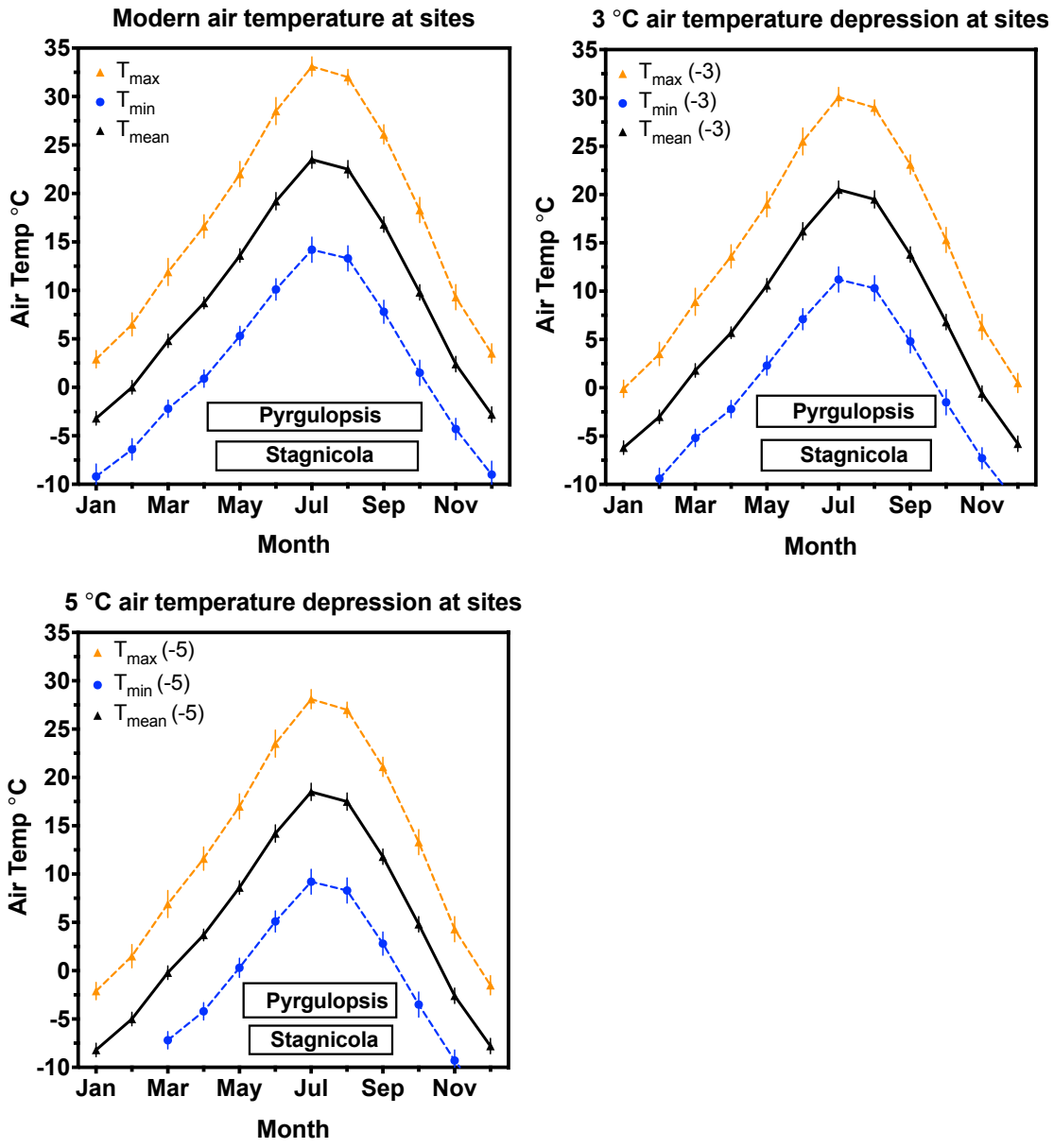


**Figure 6**: ***Modern air temperature at sample sites in the Bonneville Basin. 3 to 5°C depression of temperature reduces the annual interval during which air, and lake water, is above the minimum threshold for gastropod shell calcification.*** When interpreting clumped isotope results from Lake Bonneville, gastropod shell growth is inferred to occur between May and September. Temperature depression in excess of 5°C would confine shell growth to a more narrow period, relative to the modern. The air temperatures presented here are the average monthly values at sample collection sites in this study (PRISM Climate Group). **Upper left**: growth interval of Pyrgulopsis and Stagnicola at modern temperature. **Upper right**: growth interval with 3°C temperature depression. **Lower left**: growth interval with 5°C temperature depression. Growth window for Pyrgulopsis = 9.2°C±3.7°C (Lysne and Koetsier, 2006). Growth window for Stagnicola = 10°C (Vaughn, 1953).

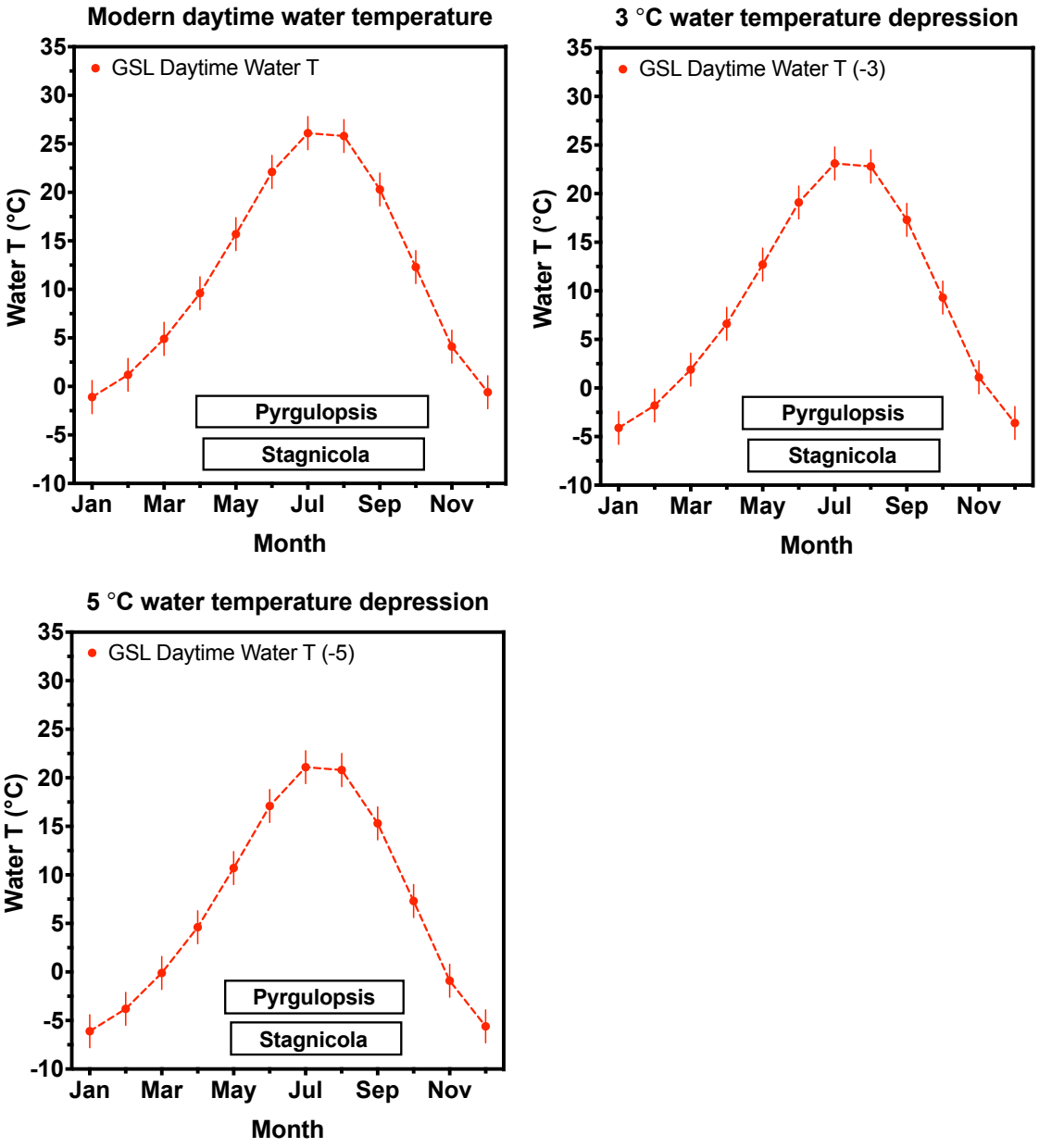


**Figure 7**: ***Modern daytime water surface temperature at the Great Salt Lake. 3 to 5°C depression of temperature reduces the interval during which lake water is above the minimum threshold for gastropod shell calcification.*** When interpreting clumped isotope results from Lake Bonneville, gastropod shell growth is inferred to occur between May and September. Average monthly water temperature values at the Great Salt Lake are derived from Moderate Resolution Imaging Spectroradiometer (MODIS) data, and are comparable to USGS bucket samples (Alcott et al., 2012; NCAR Applications Laboratory 2013 Annual Report). **Upper left**: growth interval of Pyrgulopsis and Stagnicola at modern temperature. **Upper right**: growth interval with 3°C temperature depression. **Lower left**: growth interval with 5°C temperature depression. Growth window for Pyrgulopsis = 9.2°C±3.7°C (Lysne and Koetsier, 2006). Growth window for Stagnicola = 10°C (Vaughn, 1953).

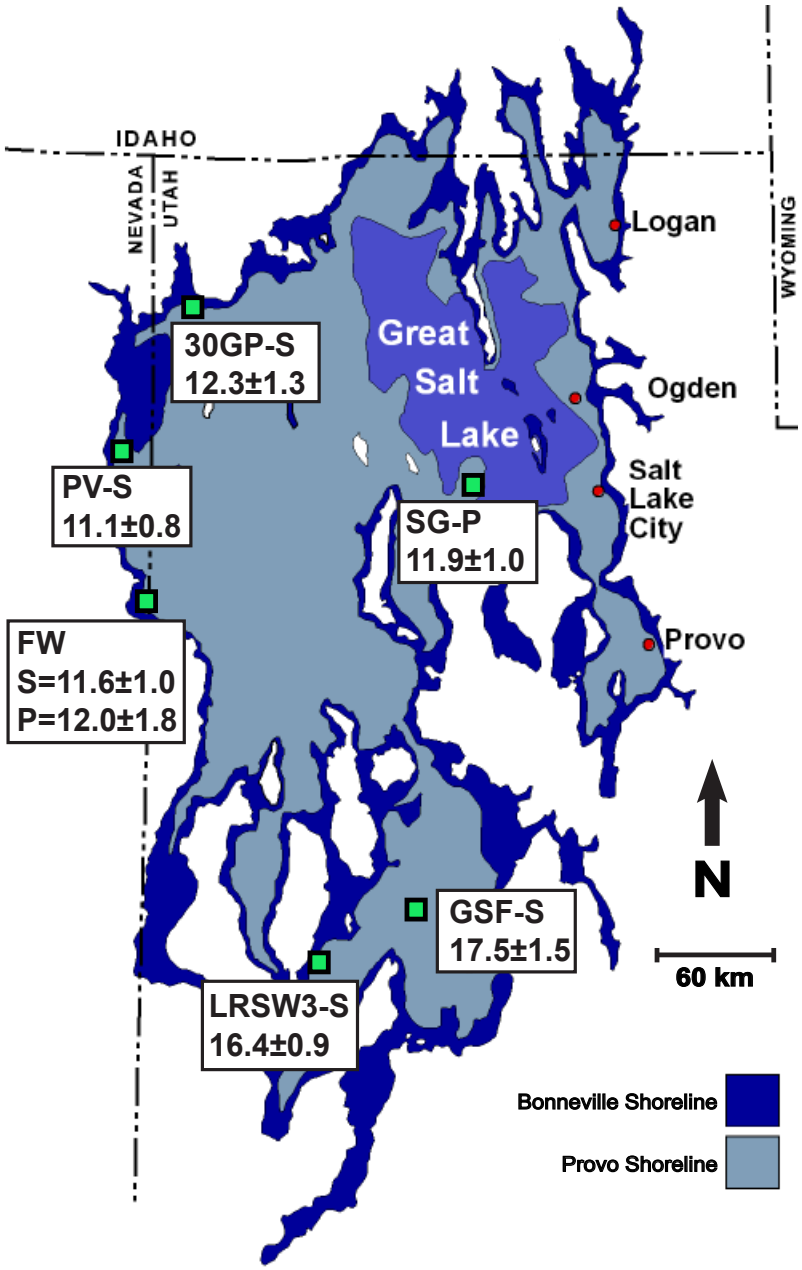


**Figure 8**: ***Reconstructed clumped isotope temperatures of gastropod shell at lake Bonneville. Collectively 66 gastropod shells were analyzed at 7 sites.*** Uncertainties in temperature are reported at 1 s.e. of the mean of analyses at a given site. For context, the Bonneville, Provo, and Great Salt Lake shorelines are included. Modern mean annual air temperature at study sites ranges from 8.7 to 10.5°C, while summer (June-August) air temperatures range from 20.6 to 22.7°C. May-September air temperatures range from 18.1 to 20.1°C. Modern climate data is from the PRISM Climate Group. Basemap: DeGrey et al., 2000.

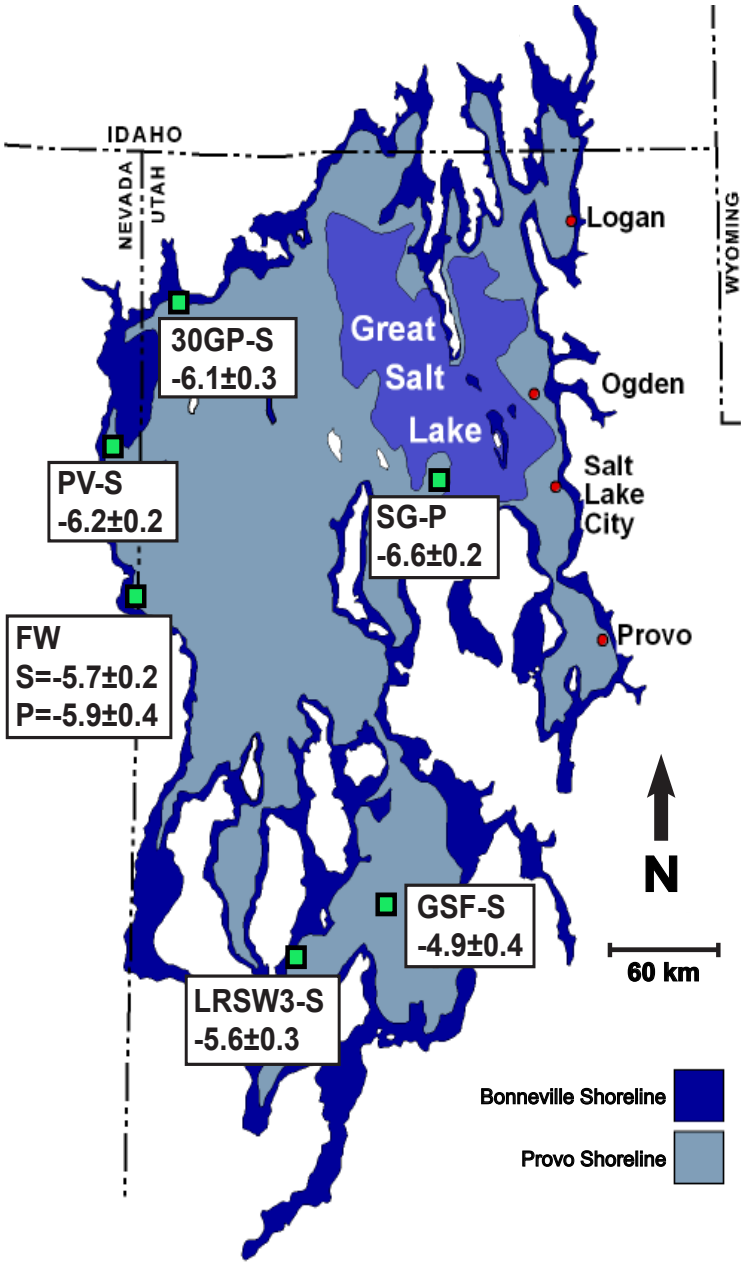


**Figure 9**: ***The oxygen isotope composition of lake water, reconstructed from gastropod shell at lake Bonneville. Collectively 66 gastropod shells were analyzed at 7 sites.*** Uncertainties in $\delta^{18}O$ are reported at 1 s.e. of the mean of analyses at a given site. A correction of 1.2‰ was subtracted from all results to account for global enrichment of surface waters during the LGM (Eagle et al., 2013). For context, the Bonneville, Provo, and Great Salt Lake shorelines are included. Modern precipitation $\delta^{18}O_{water}$ ranges from -12.6 to -13.5‰ V-SMOW (Bowen et al., 2014). The modern oxygen isotope composition of river water at Lake Bonneville ranges from -11 to -17‰ V-SMOW (Coplen and Kendall, 2000). Basemap: DeGrey et al., 2000.

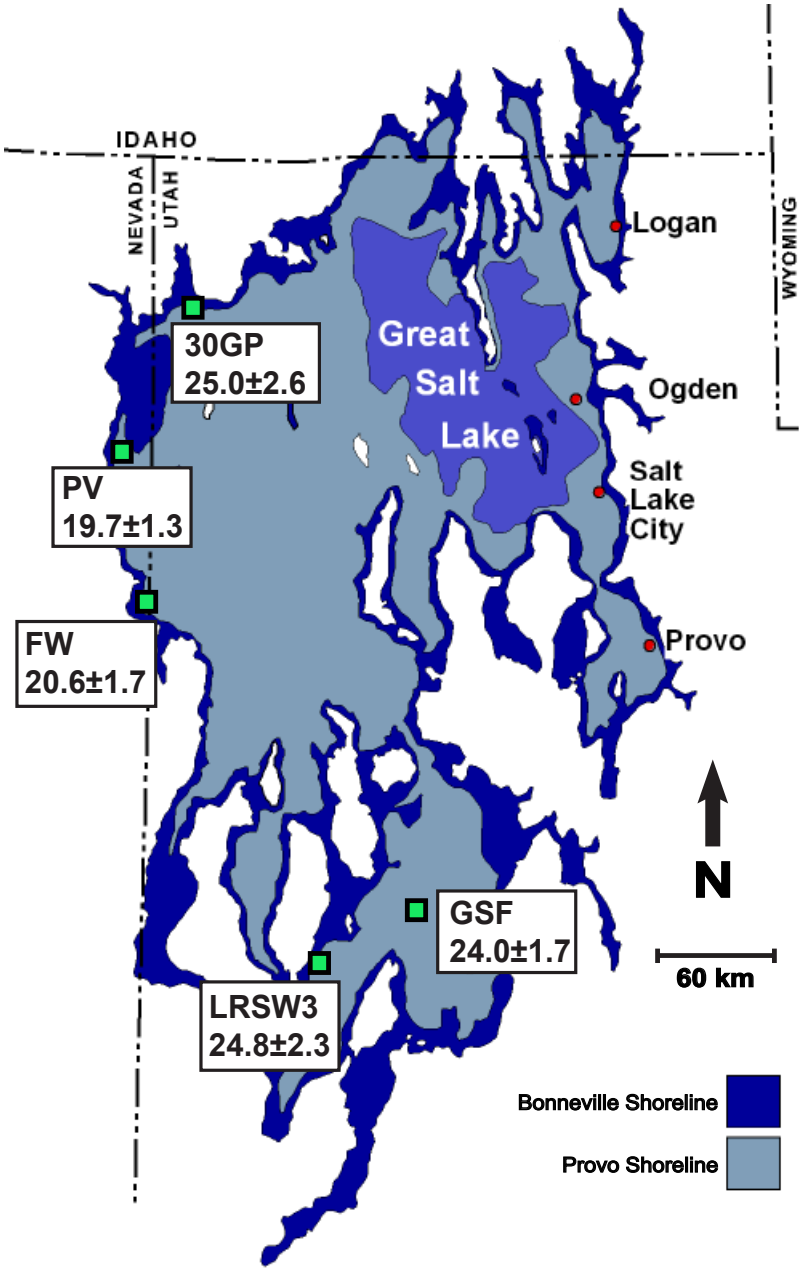


**Figure 10**: ***Reconstructed clumped isotope temperature from marl at lake Bonneville. Collectively, 24 marl measurement are reported 5 sites.*** Uncertainties in temperature are reported at 1 s.e. of the mean at sites. For context, the Bonneville, Provo, and Great Salt Lake shorelines are included. The Provo shoreline approximately corresponds to lake level for the time interval sampled. Report modern values here. Modern mean annual air temperature at study sites ranges from 8.7 to 10.5°C, while summer (June-August) air temperatures range from 20.6 to 22.7°C. May-September air temperatures range from 18.1 to 20.1°C. Modern climate data is from the PRISM Climate Group. Basemap: DeGrey et al., 2000.

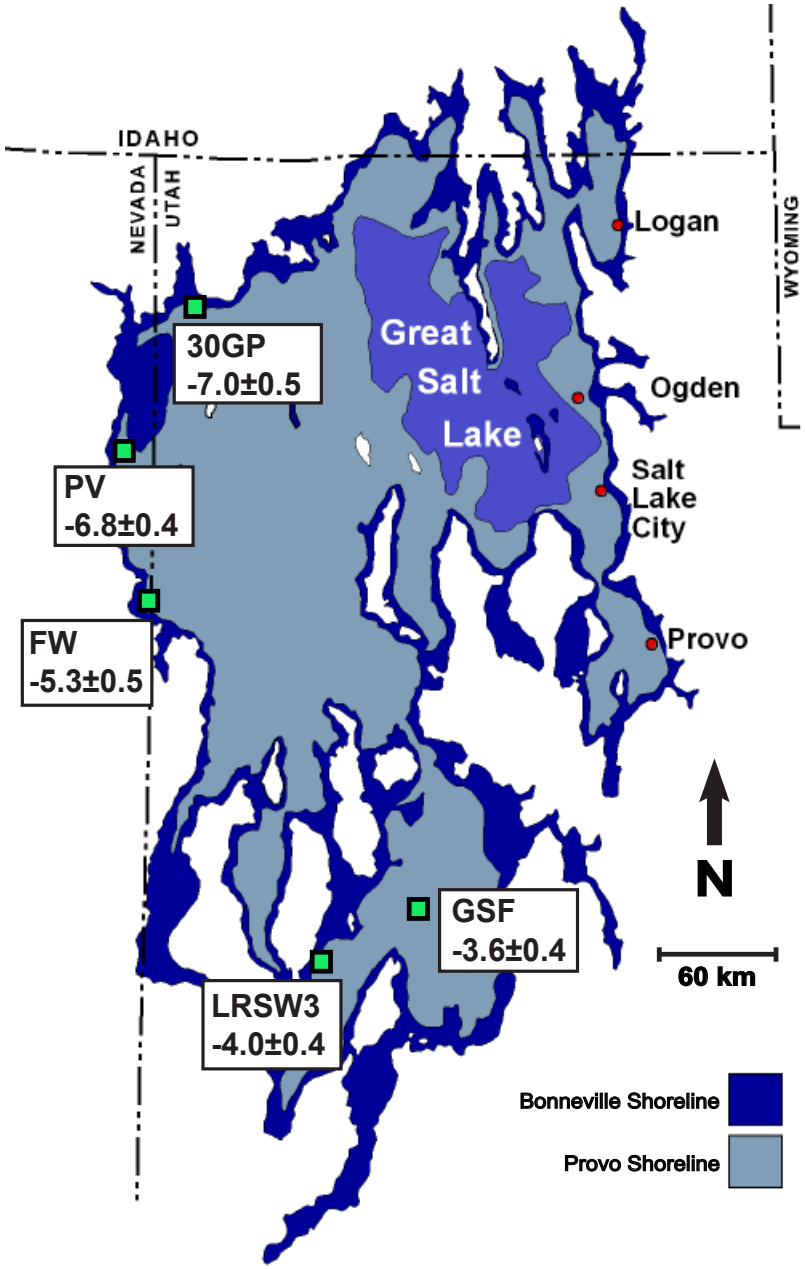


**Figure 11**: ***The oxygen isotope composition of lake water, reconstructed from marl at lake Bonneville. Collectively, 24 marl samples were analyzed at 5 sites.*** Uncertainties in $\delta^{18}O$ are reported at 1 s.e. of the mean of analyses at a given site. A correction of 1.2‰ was subtracted from all results to account for global enrichment of surface waters during the LGM (Eagle et al., 2013). For context, the Bonneville, Provo, and Great Salt Lake shorelines are included. Modern precipitation $\delta^{18}O_{water}$ ranges from -12.6 to -13.5‰ V-SMOW (Bowen et al., 2014). The modern oxygen isotope composition of river water at Lake Bonneville ranges from -11 to -17‰ V-SMOW (Coplen and Kendall, 2000). Basemap: DeGrey et al., 2000.

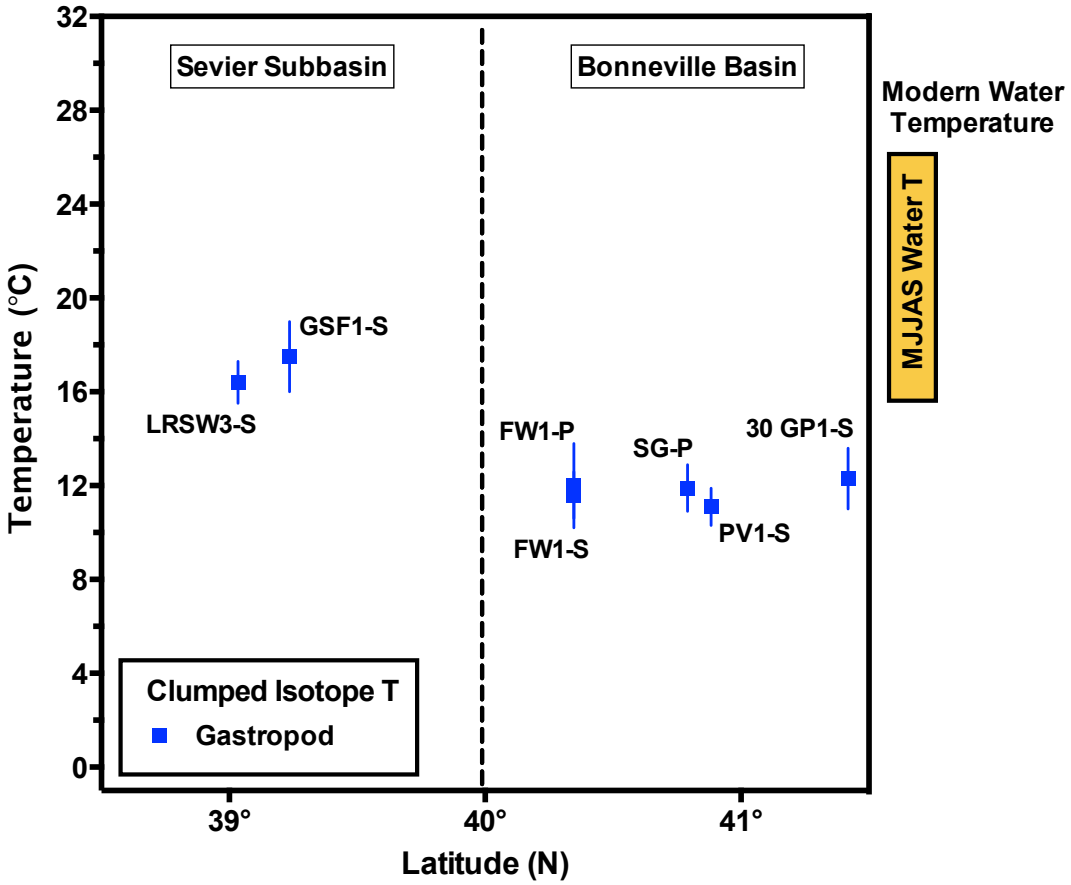


**Figure 12:** ***Temperature results for gastropods at study sites indicate that shell growth conditions were cooler in the Bonneville Basin, relative to the smaller Sevier Subbasin.*** The mean Bonneville Basin gastropod clumped isotope temperature for LGM (SG excluded) is 11.7±0.3 °C, while mean Sevier Subbasin gastropod clumped isotope temperature is 16.9±0.5°C. At all sites, gastropods record lower clumped isotope temperatures relative to corresponding marl. All uncertainties are reported at 1 stdev of the mean. Modern air temperatures are reported from the PRISM Climate Group gridded 1971-2000 dataset. The modern surface water temperatures presented here are average monthly values at the Great Salt Lake, derived from Moderate Resolution Imaging Spectroradiometer (MODIS) data, and are comparable to USGS bucket samples (Alcott et al., 2012; NCAR Applications Laboratory 2013 Annual Report).

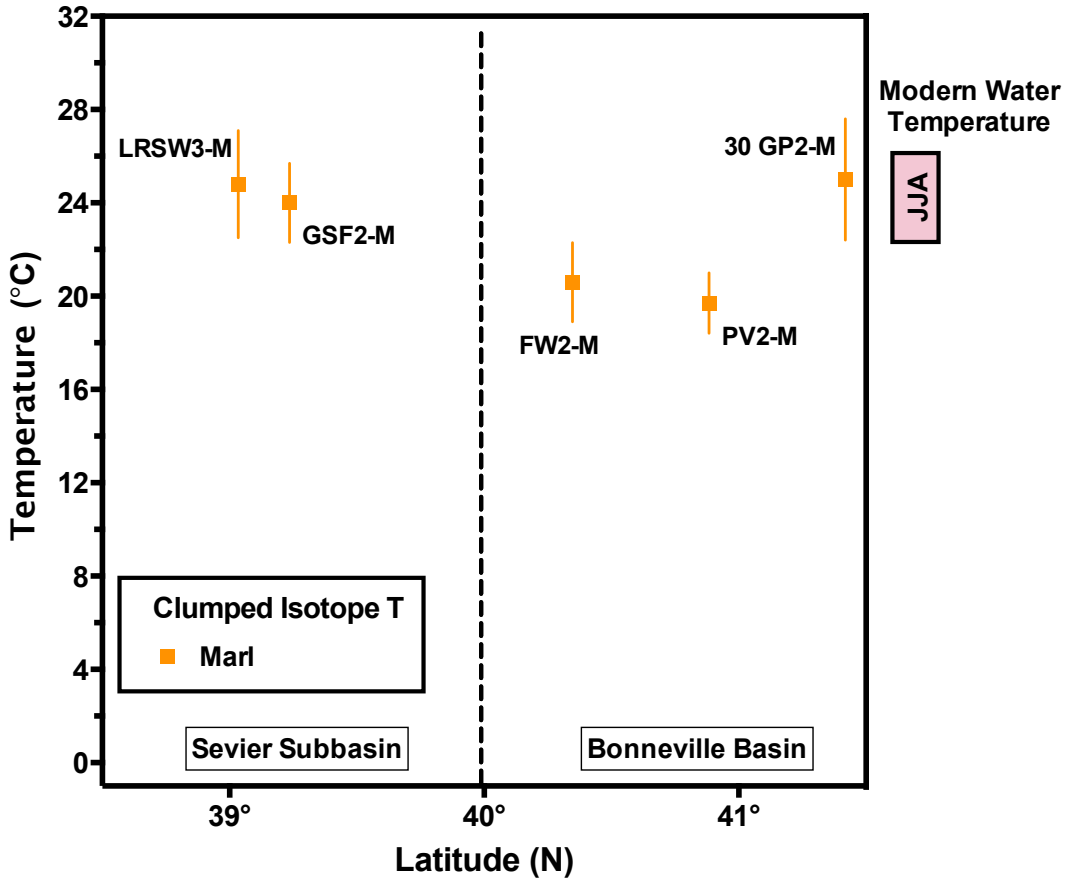


**Figure 13:** ***Temperature results for marl at study sites indicate that endogenic carbonate precipitation occurred when surface waters were near annual maxima.*** At all sites, marl records higher clumped isotope temperatures relative to corresponding gastropods. Bonneville Basin marl temperatures are lower than Sevier Subbasin values. The mean Bonneville Basin marl clumped isotope temperature for the LGM is 21.7±1.6°C, while the mean Sevier Subbasin gastropod clumped isotope temperature is 24.4±0.4°C. All uncertainties are reported at 1 stdev of the mean. Modern air temperatures are reported from the PRISM Climate Group gridded 1971-2000 dataset. The modern surface water temperatures presented here are average monthly values at the Great Salt Lake, derived from Moderate Resolution Imaging Spectroradiometer (MODIS) data, and are comparable to USGS bucket samples (Alcott et al., 2012; NCAR Applications Laboratory 2013 Annual Report).

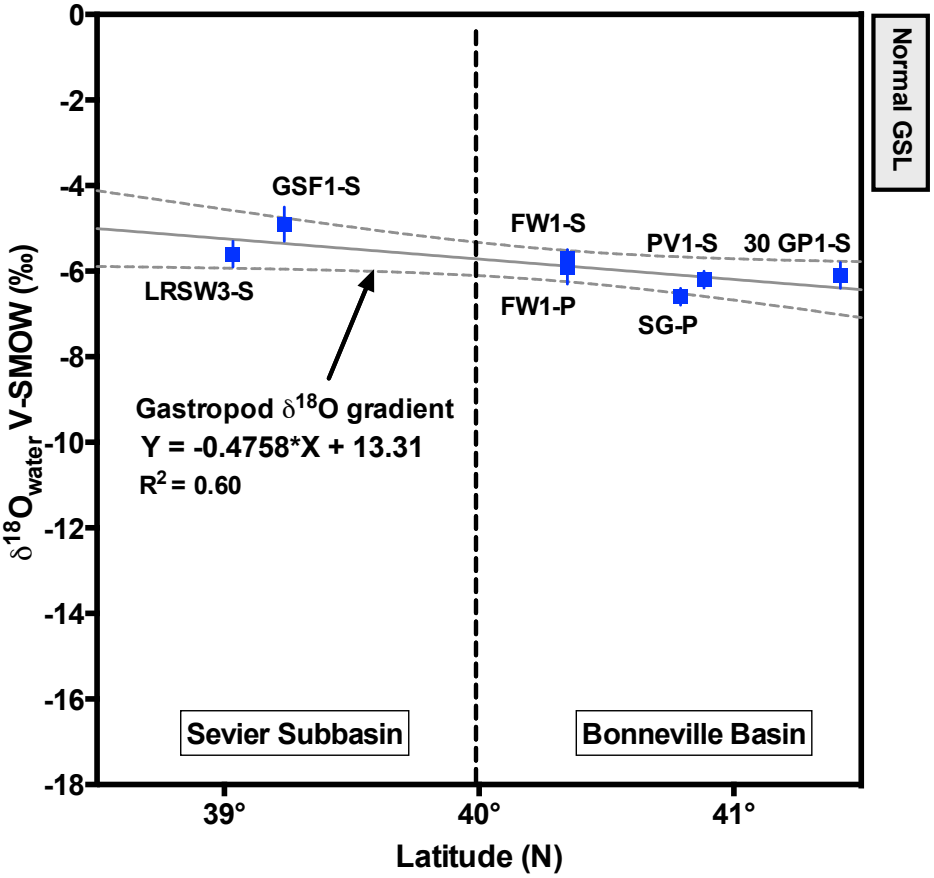


**Figure 14:** ***Gastropod derived lake water oxygen isotope values indicate that during intervals of shell growth lake water was more enriched than modern precipitation, but more negative than the typical range for the modern Great Salt Lake. The mean reconstructed value for Bonneville Basin gastropod shell (excluding SG) is -6.0 ± 0.1‰, while mean*** $\delta^{18}O_{water}$ ***reconstructed from Sevier Subbasin gastropod shell is 5.3 ± 0.3‰.*** $\delta^{18}O_{water}$ for modern rivers draining into the Great Salt Lake ranges from -11 to -17‰ (Coplen and Kendall, 2000). Modern precipitation over the Great Salt Lake, and surrounding basins, ranges from -12.6 to -13.5‰ (Bowen, 2014). The large historic range of Great Salt Lake oxygen isotope values include wet years during the 1980s when the lake underwent a minor transgression. Typical values in the South Arm of the Great Salt Lake range from 0 to -4‰ (Pedone, 2002). A correction of 1.2‰ was subtracted from all results to account for enrichment of surface waters during the LGM (Eagle et al., 2013).

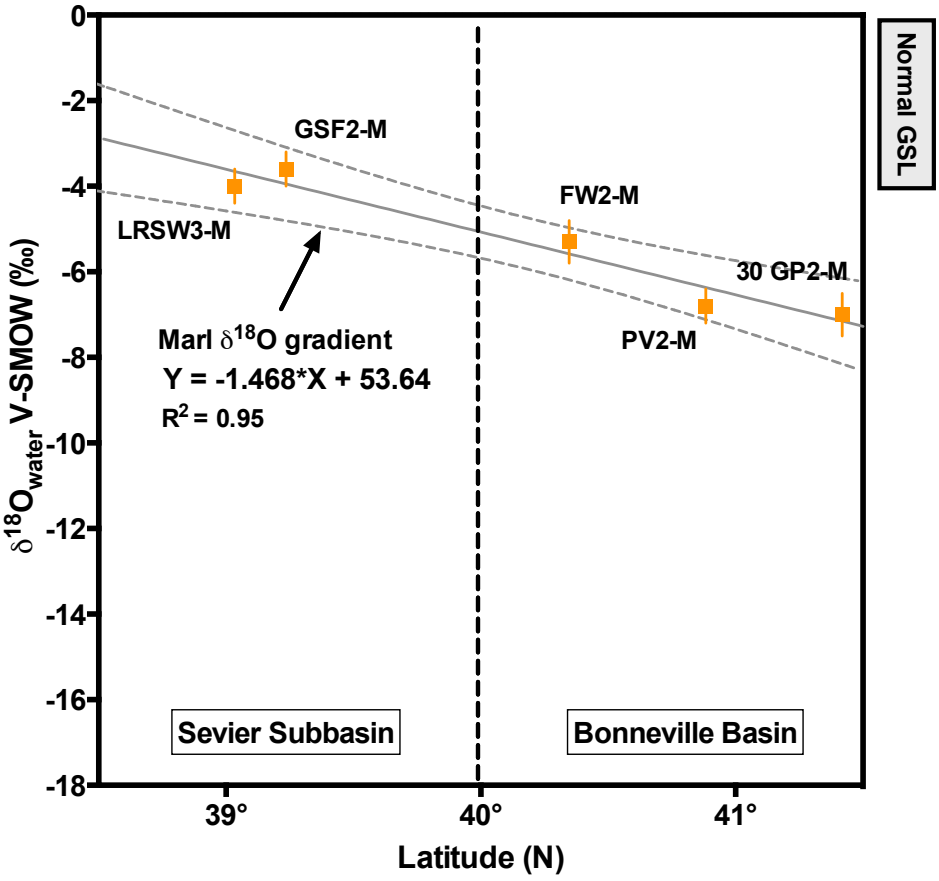


**Figure 15:** ***The lake water oxygen isotope record reconstructed from marl indicates that the lake was differentiated with respect to*** $\delta^{18}O$ ***across the Bonneville and Sevier regions during intervals of endogenic carbonate precipitation. The reconstructed*** $\delta^{18}O$ ***trend is shown with a 95% confidence band, and indicates a shift of 1.5‰ in lake water oxygen isotope values, inversely correlated with latitude.*** The regression p value is 0.006. Modern precipitation over the Great Salt Lake and surrounding basins ranges from -12.6 to -13.5‰ (Bowen, 2014). The large historic range of oxygen isotope values for the Great Salt Lake include wet years during the 1980s when the lake underwent a minor transgression. Typical values in the South Arm of the Great Salt Lake range from 0 to -4‰ (Pedone, 2002). A correction of 1.2***‰*** was subtracted from all results to account for enrichment the ocean during the LGM (Eagle et al., 2013).

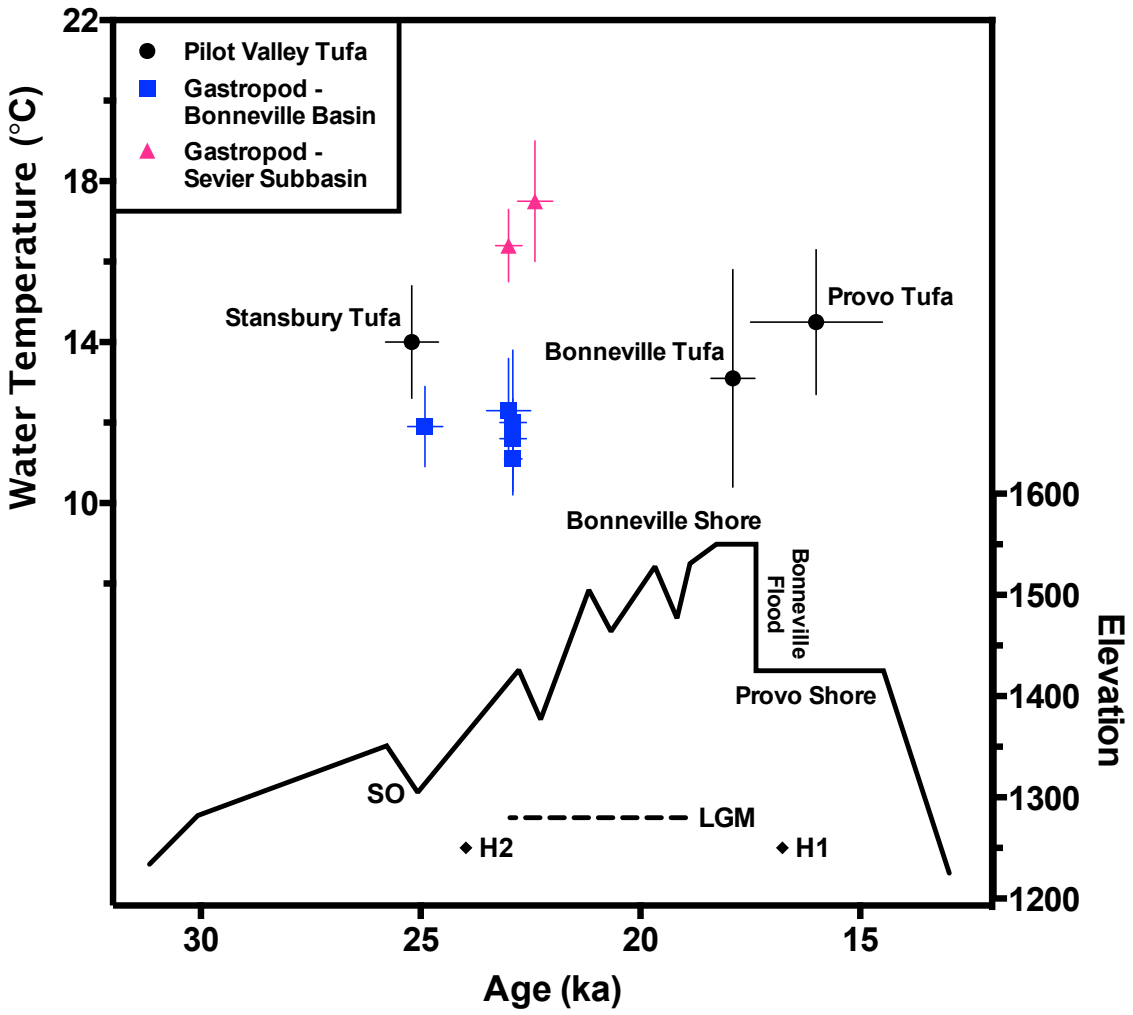


**Figure 16:** ***Bonneville clumped isotope water temperature reconstructions plotted with respect to probable sample age. Tufa temperatures are relatively static from the Stansbury Oscillation (SO) through the Provo phase, but may have decreased slightly during the Bonneville high stand. Offsets in temperature between phases reflect different intervals of mineral growth over the course of the year.*** Gastropods largely grew shell during late spring through early fall (May-September), while tufa grew over a shorter interval (assumed June-August). SO = Stansbury Oscillation; H2 = Heinrich Event 2 (Hemming, 2004); H1 = Heinrich Event 1 (Hemming, 2004); LGM = Last Glacial Maximum.

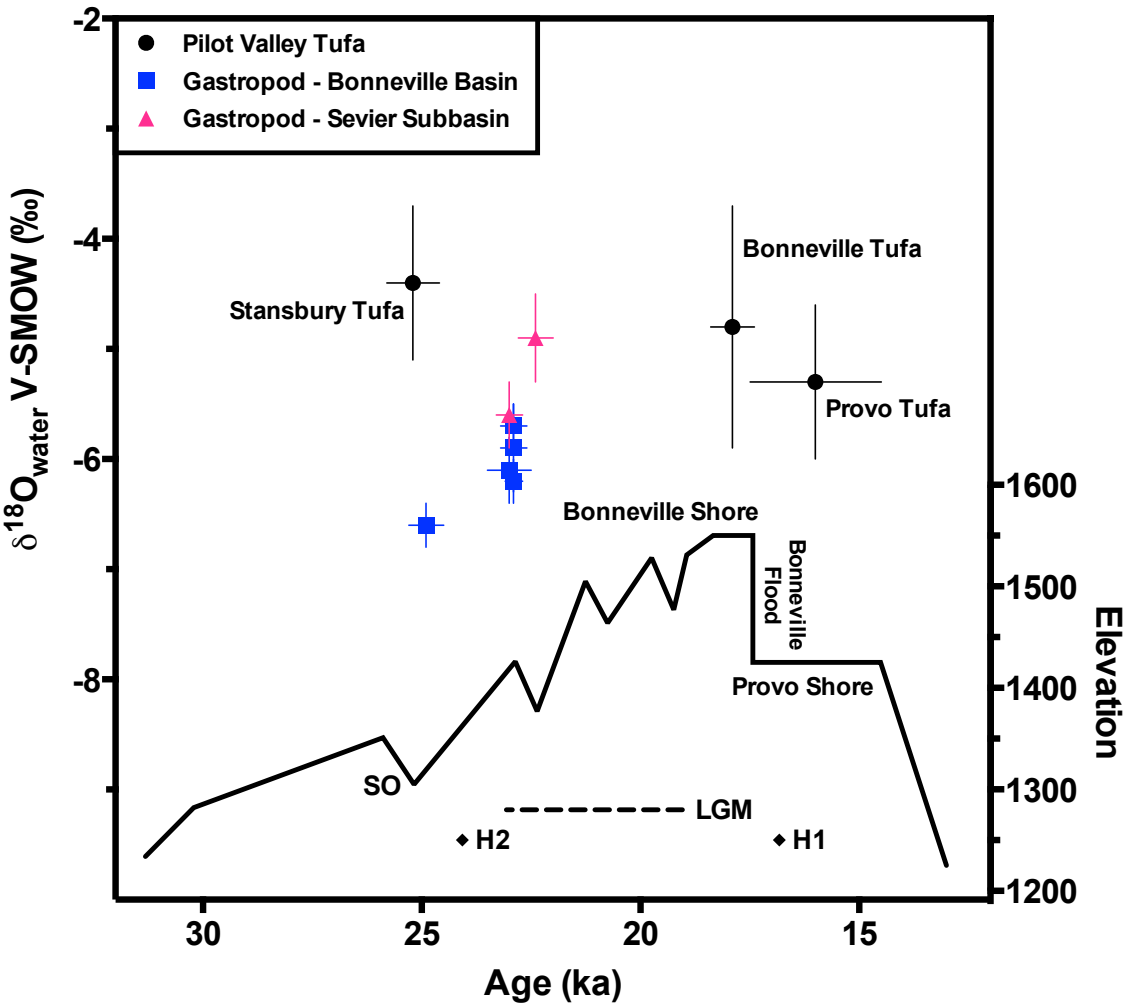


**Figure 17:** ***Reconstructed $\delta^{18}O_{water}$ at sites assessed in this thesis. Oxygen isotope values reflect summer lake conditions. In tufa from the Pilot Valley, $\delta^{18}O_{water}$ decreases between the Stansbury and Provo phases.*** The establishment of an outlet at the northern margin of the lake during the Bonneville-Provo interval may account for the depletion observed in tufa samples. SO = Stansbury Oscillation; H2 = Heinrich Event 2 (Hemming, 2004); H1 = Heinrich Event 1 (Hemming, 2004); LGM = Last Glacial Maximum. All isotope values are reported in parts per mil (‰), relative to V-SMOW. A 1.2‰ correction was applied to all samples in order to account for ice volume induced enrichment of waters during the LGM (Eagle et al., 2013).

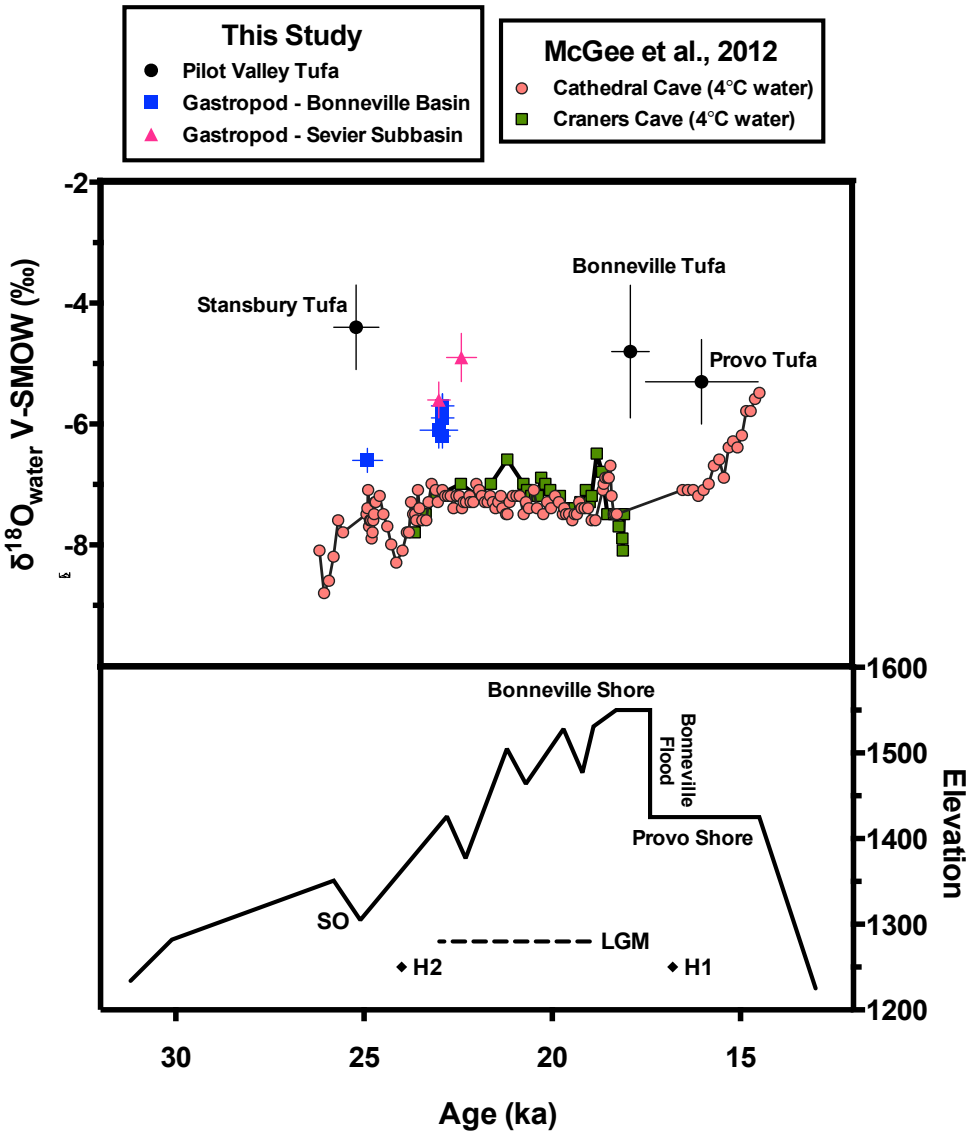


**Figure 18:** ***Reconstructed surface water δ $^{18}$O (this study) compared to δ $^{18}$O from lacustrine cave carbonates investigated in McGee et al. (2012). Here, hypolimnion temperatures of 4°C were applied to reconstruct oxygen isotope values in cave carbonates.*** The oxygen isotope values of reported in this study exhibit considerable evaporative enrichment, relative to probable LGM precipitation values (-13 to -15 ‰). The majority of gastropod and tufa samples reflect greater enrichment of $^{18}$O relative to the cave carbonate record. The timing of carbonate precipitation in the deep lake may have been subject to different controls than in surface waters. A slight decrease in $\delta^{18}$O from the Bonneville highstand (18 ka) through the early Provo phase is recorded in both the surface water (i.e. tufa) and cave carbonate samples. Increasing $\delta^{18}$O in the McGee et al. (2012) samples at 15 ka, near the end of the Provo phase, indicates that shallowing, associated with regression, may have led to more frequent mixing between surface and bottom waters. A water temperature of 4°C applied to cave carbonates, which formed in the deep lake, reflects the temperature at which fresh water attains maximum density. A 1.2‰ correction was applied to all samples in order to account ice volume induced enrichment of waters during the LGM (Eagle et al., 2013).

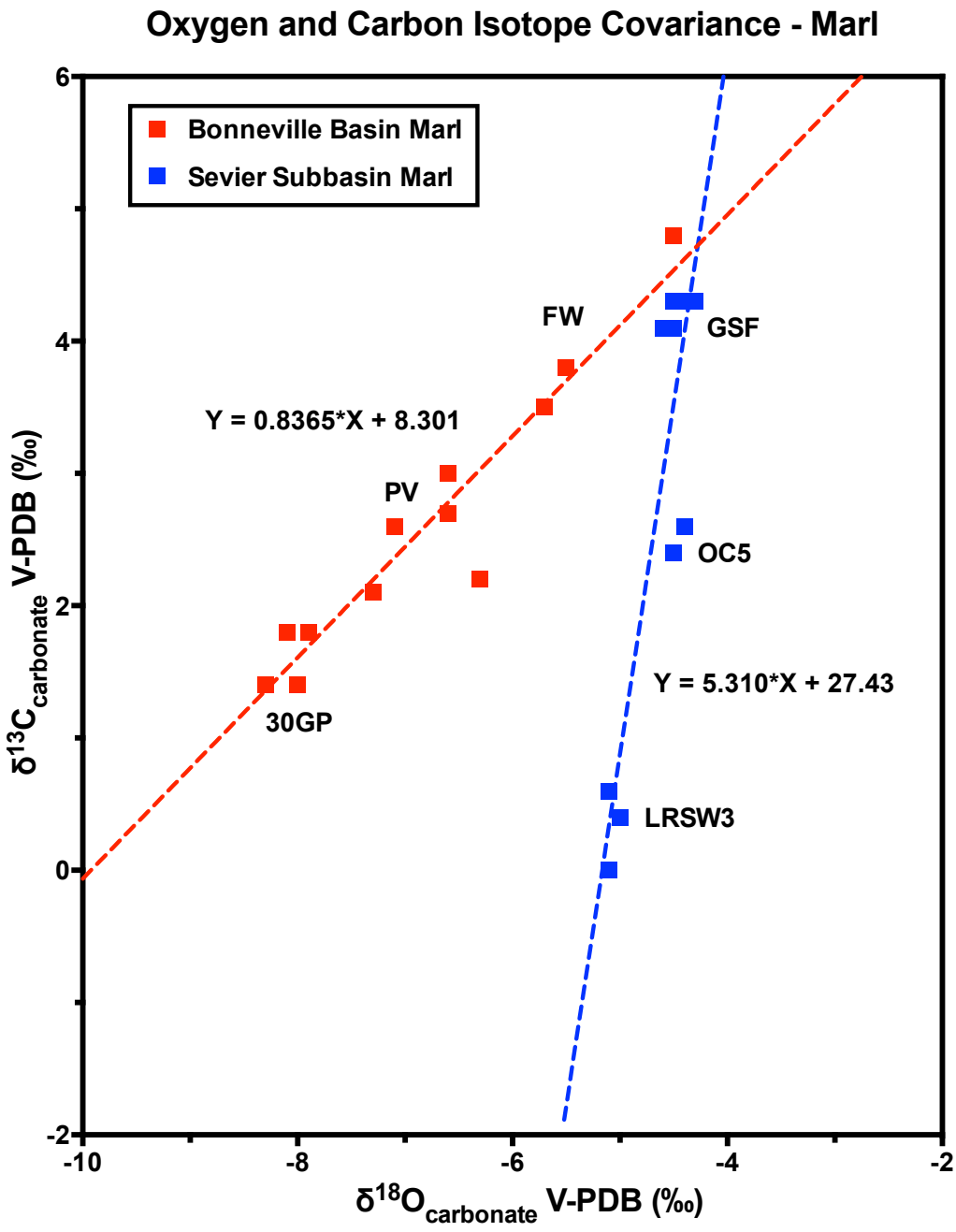


**Figure 19:** ***Unique trends for oxygen and carbon isotopic covariance indicate different evaporative histories in each basin.*** The regression for the Sevier Subbasin is steeper than that of the Bonneville Basin by approximately a factor of 6. Strongly differentiated isotopic covariance trends indicates that mixing of surface waters may have been relatively minimal between basins. Groundwater input of unique isotopic composition may have also comprised a significant component of the hydrologic budget in the Sevier Subbasin (Oviatt, 2015). Regression statistics: Bonneville Basin R-squared = 0.91, p-value < 0.0001; Sevier Subbasin R-squared = 0.78, p-value = 0.0003.

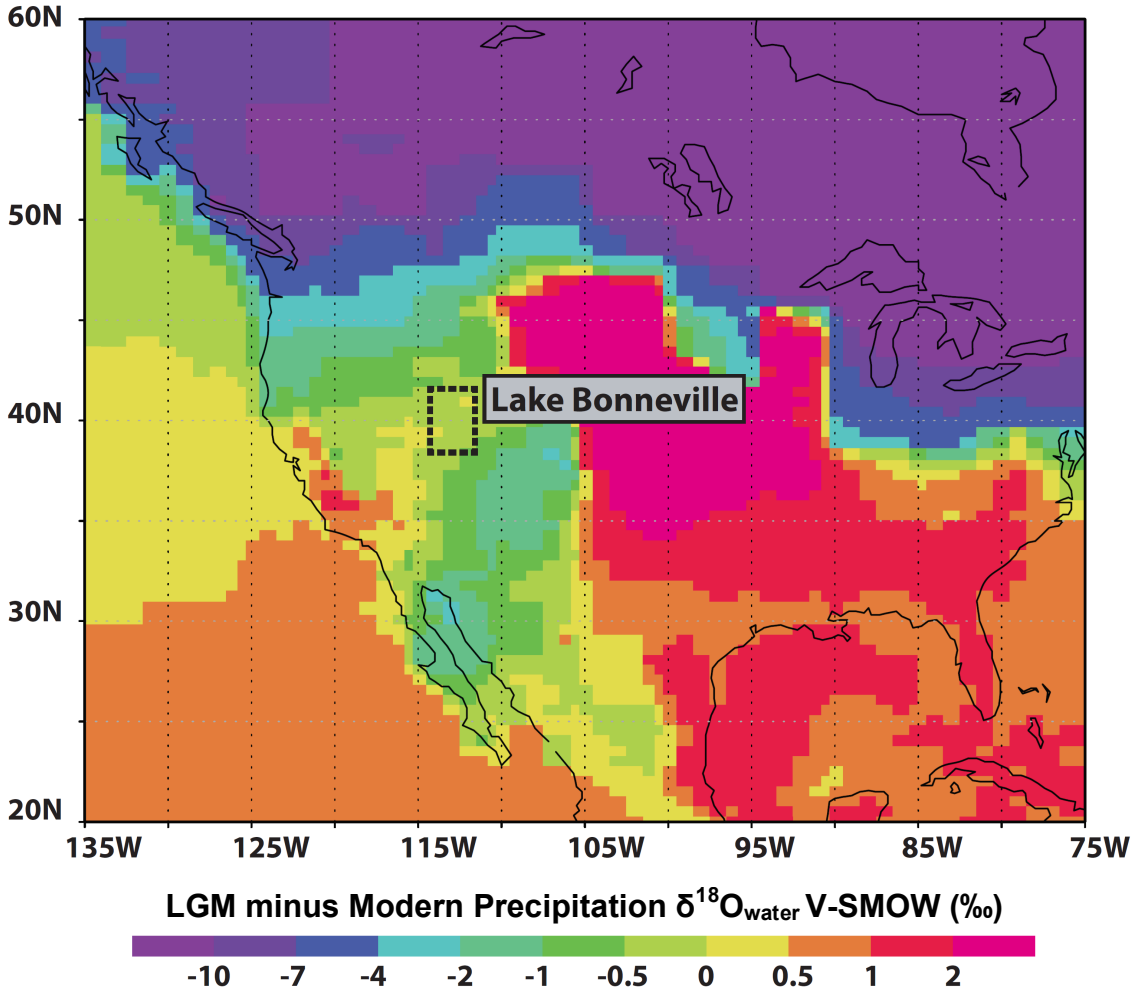


**Figure 20**: ***The LMDZ oxygen isotope enabled climate model indicates that $\delta^{18}O_{water}$ in precipitation may not have been appreciably enriched, or depleted, relative to modern values at Lake Bonneville during the LGM. Model predictions for enrichment or depletion are less than 0.5‰ in grid cells that correspond with Lake Bonneville.*** Lake water oxygen isotope values reconstructed from clumped isotope temperatures in this study suggest that surface water at Bonneville was enriched by 7.1 to 9.2‰ above modern precipitation values. Enrichment of lake water is attributed to evaporation (Horton et al., submitted). $\delta^{18}O_{water}$ of modern precipitation at sites evaluated in this study ranges from -12.6 to -13.5‰ V-SMOW (Bowen et al., 2014). With the exception of anomalously wet years, $\delta^{18}O_{water}$ in the modern Great Salt Lake is typically enriched by 9 to 14‰, above precipitation values. The model output shown here is considered preliminary at this time (Risi, 2014).

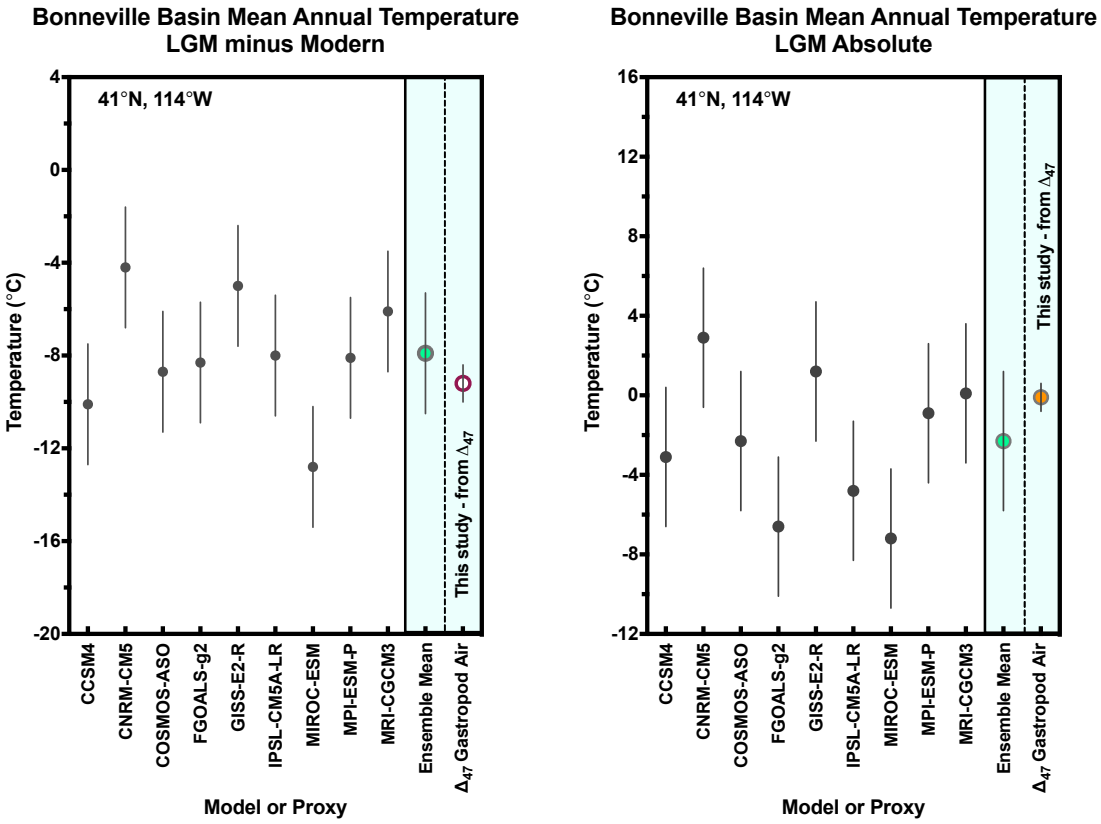


**Figure 21**: ***Clumped isotope temperature reconstruction for the Bonneville Basin during the LGM indicates higher absolute annual air temperature than the PMIP3 multi-model ensemble mean, but greater temperature depression.*** This trend can be attributed to application of different methods for reconstructing temperature depression. The pre-Industrial control values applied to PMIP3 data are lower than modern air temperatures, which were applied to gastropod data.

**Left**: LGM reconstructed mean annual air temperatures minus control values. The models COSMOS-ASO, FGOALS-g2, IPSL-CM5A-LR, and MPI-ESM-P predict a temperature depression of 8.1 to 8.7°C below pre-Industrial control values, which is similar to the gastropod clumped isotope prediction of 9.2±0.8°C cooling below modern values.

**Right**: LGM reconstructed absolute mean annual air temperatures. The MRI-CGCM3 model predicts an absolute annual air temperature of 0.1°C, which is comparable to the gastropod clumped isotope value of -0.1±0.7°C.

*$\Delta_{47}$ Gastropod Air* = Mean Annual Air Temperature (MAAT) estimated from Bonneville Basin gastropod clumped isotope temperatures, with a MJJAS water temperature to MAAT transfer function applied. Sites included in analyses: 30GP, PV, FW. For PMIP3 models, pre-Industrial control temperatures were subtracted from LGM model runs. For clumped isotope temperature comparisons, modern (1971-2000) annual data from the PRISM Climate Group database were applied as a control.

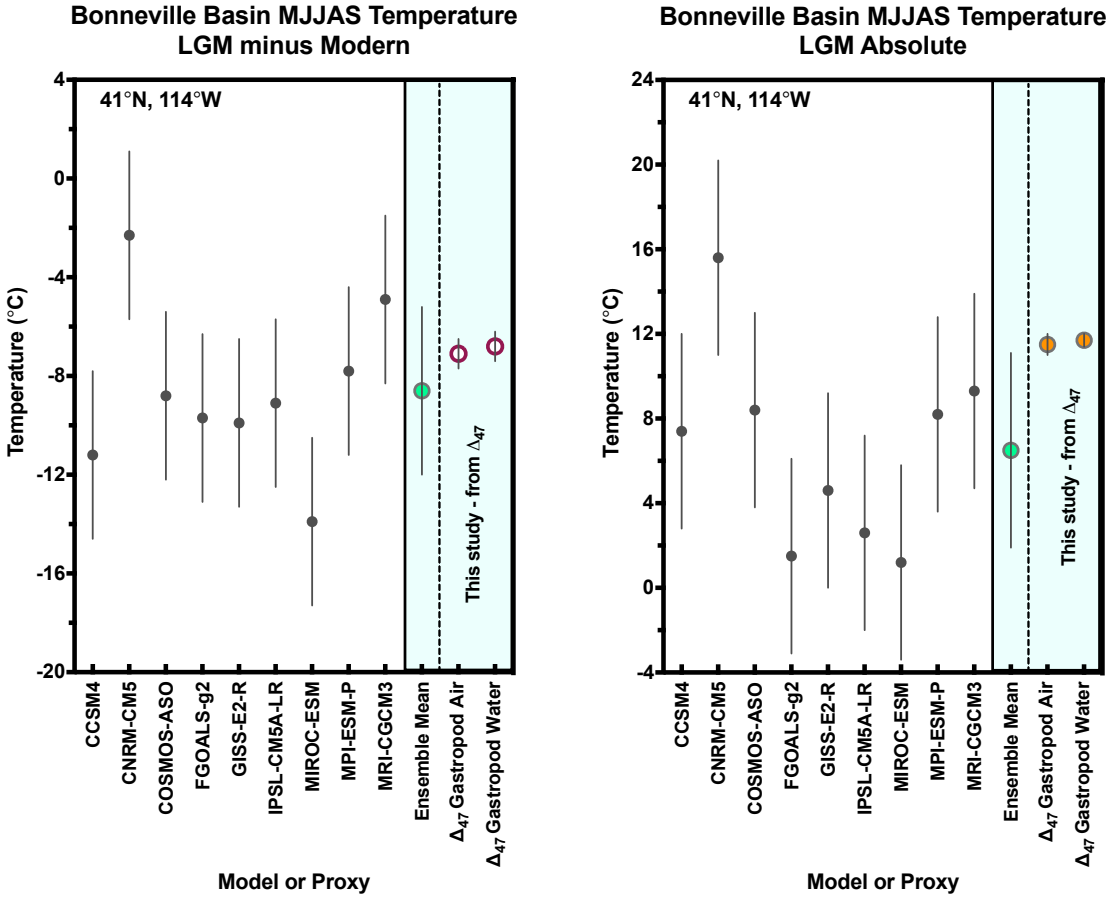


**Figure 22**: ***Clumped isotope temperature reconstructions for the Bonneville Basin during the LGM indicate higher absolute summer (MJJAS) temperature than the PMIP3 multi-model ensemble mean, and less temperature depression.***

**Left**: LGM reconstructed mean annual air temperatures minus control values, and clumped isotope water temperature estimates shown for comparison. The model MPI-ESM-P predicts a MJJAS air temperature depression of 7.8°C below pre-industrial control runs, which is similar to the gastropod clumped isotope prediction of 7.1±0.6°C cooling. **Right**: LGM reconstructed absolute MJJAS temperatures. With the exception of the CNRM-CM5 model (15.6°C), models predict absolute summer air temperatures that are lower than the MJJAS clumped isotope water temperature of. 11.7±0.3°C, and the air temperature calculation 11.5±0.5°C.

*$\Delta_{47}$ Gastropod Air* = May-September (MJJAS) air temperature estimated from Bonneville Basin gastropod clumped isotope temperatures, with a MJJAS water temperature to MJJAS air temperature transfer function applied. Sites included in analyses: 30GP, PV, FW. For PMIP3 models, pre-Industrial control temperatures were subtracted from LGM model runs. For clumped isotope temperature comparisons, modern (1971-2000) MJJAS data from the PRISM Climate Group database were applied as a control.

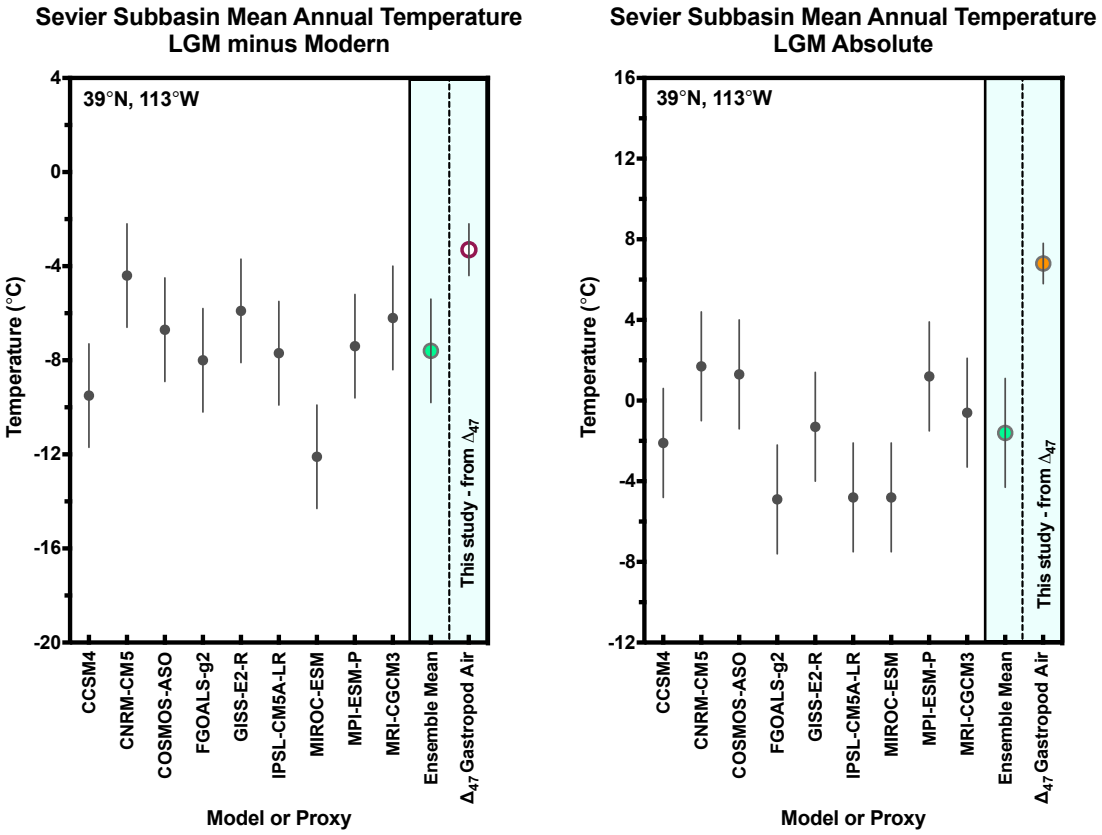


**Figure 23**: ***In the Sevier Subbasin, clumped isotope temperature reconstructions identify a higher absolute annual air temperature than the PMIP3 multi-model ensemble mean, and less temperature depression during the LGM.*** This trend can be attributed to differences in the methods used to reconstruct temperature depression. The pre-Industrial control temperatures applied to PMIP3 are lower than modern air temperatures, which were applied to gastropod data. Peak summer surface water temperature may have been higher in the Sevier Subbasin, which is smaller and shallower than the Bonneville Basin. Surface water could have responded more quickly to annual heating and cooling cycles, reaching a higher summer peak, in a manner analogous to the North Arm of the modern Great Salt Lake.

**Left**: LGM reconstructed mean annual air temperatures minus control values. The Sevier Subbasin annual air temperature depression reconstructed from clumped isotopes indicates LGM conditions that were 3.3±1.1°C cooler than modern, while the multi-model ensemble mean suggests 7.6±2.2°C of cooling below pre-Industrial control values. **Right**: LGM reconstructed absolute mean annual air temperatures. The gastropod clumped isotope value of 6.8±0.7°C is significantly greater than the multi-model ensemble mean (-1.6±2.7°C), and individual model results.

$\Delta_{47}$ *Gastropod Air* = Mean Annual Air Temperature (MAAT) estimated from Sevier Subbasin gastropod clumped isotope temperatures with a MJJAS water temperature to MAAT transfer function applied. Sites included in analyses: GSF, LRSW3. For PMIP3 models, pre-Industrial control temperatures were subtracted from LGM model runs. For clumped isotope temperature comparisons, modern (1971-2000) annual data from the PRISM Climate Group database were applied as a control.

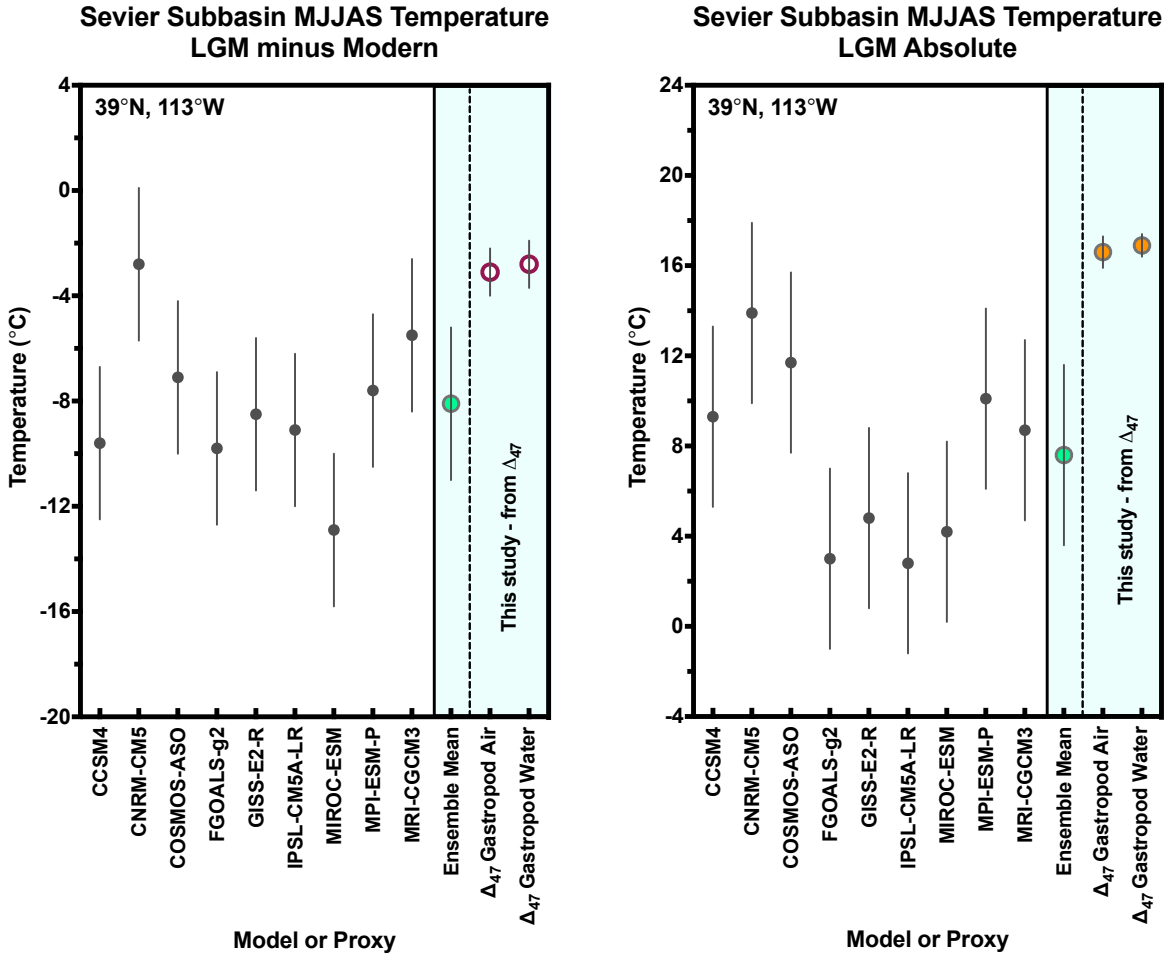


**Figure 24**: ***Clumped isotope temperature reconstructions for the Sevier Subbasin indicate higher absolute summer (MJJAS) temperature than the PMIP3 multi-model ensemble mean, and less temperature depression, during the LGM***.

**Left**: LGM reconstructed mean annual air temperatures minus control values, and clumped isotope water temperature estimates shown for comparison. The model CNRM-CM5 predicts a MJJAS air temperature depression of 2.8°C below pre-industrial control runs, which is similar to the gastropod clumped isotope prediction of 3.1±0.9°C cooling below modern values.

**Right**: LGM reconstructed absolute MJJAS temperatures. The gastropod based clumped isotope temperature (16.9±0.5°C) and reconstructed air temperature (17.3±0.7°C) significantly exceed individual model predictions as well as the multi-model ensemble mean value of 7.6±2.7°C.

*$\Delta_{47}$ Gastropod Air* = Mean Annual Air Temperature (MAAT) estimated from Sevier Subbasin gastropod clumped isotope temperatures, with a MJJAS water temperature to MAAT transfer function applied. Sites included in analyses: GSF, LRSW3. For PMIP3 models, pre-Industrial control temperatures were subtracted from LGM model runs. For clumped isotope temperature comparisons, modern (1971-2000) MJJAS data from the PRISM Climate Group database were applied as a control.

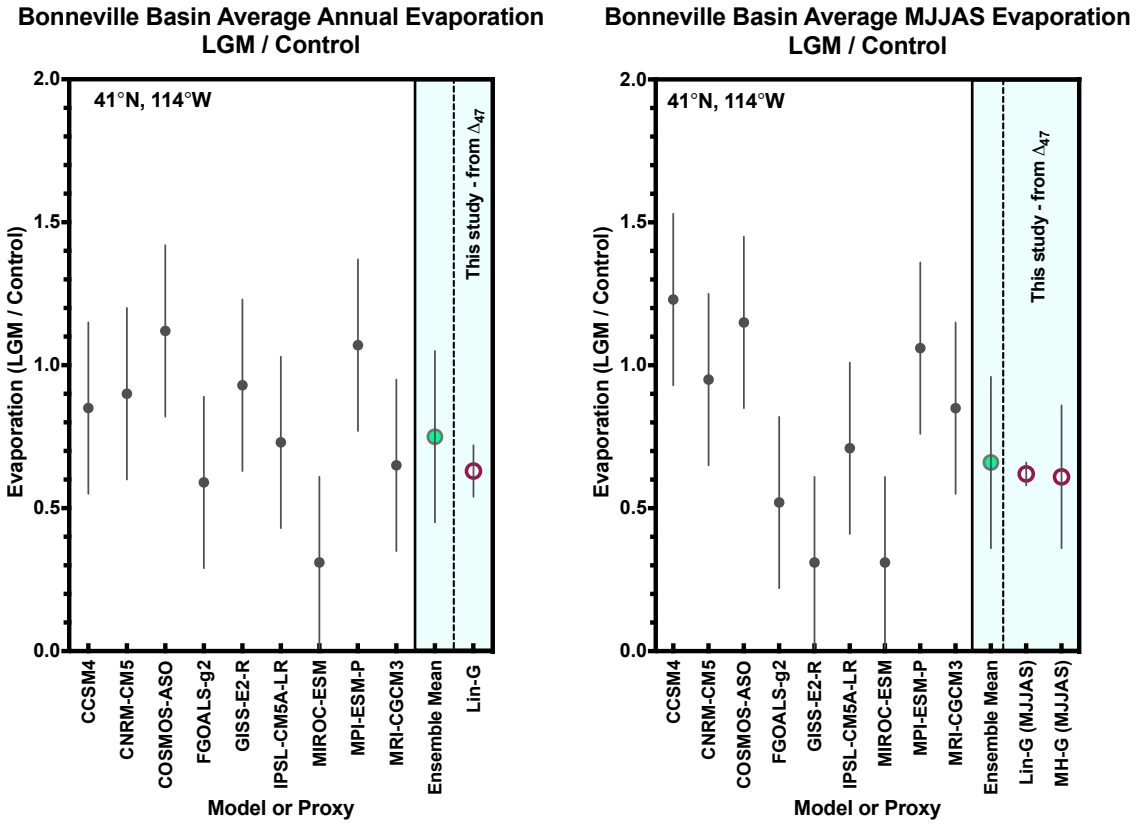


**Figure 25**: ***Clumped isotope based reconstructions of evaporation indicate that annual evaporation was 37 percent lower than modern, and summer evaporation was 38 to 39 percent below modern. The PMIP3 multi-model ensemble mean predicts annual evaporation 25 percent below modern, and summer evaporation at 34 percent below modern.***

**Left**: Reconstructed annual evaporation presented as a fraction of control value. Models FGOALS-g2 (41 percent decrease) and MRI-GCM3 (35 percent decrease) predict change in annual evaporation from modern that is similar to clumped isotope derived results. *Lin-G* = Annual evaporation from MJJAS gastropod temperature applied to the Linacre (1993) approximation of the Penman equation for evaporation over open water.

**Right**: Reconstructed May-September (MJJAS) evaporation presented as a fraction of control value. *Lin-G (MJJAS)* = evaporation from MJJAS gastropod temperature applied to Linacre (1993). *MH-G (MJJAS)* = evaporation from MJJAS gastropod temperature applied to the Great Basin hydrologic model presented in Matsubara and Howard (2009).

Sites included in analyses: 30GP, PV, FW. For PMIP3 models, LGM model runs are presented as a fraction of pre-Industrial control rates. Modern rates for clumped isotope data were calculated by application of the PRISM Climate Group database to the Linacre (1993) and Matsubara and Howard (2009) equations.

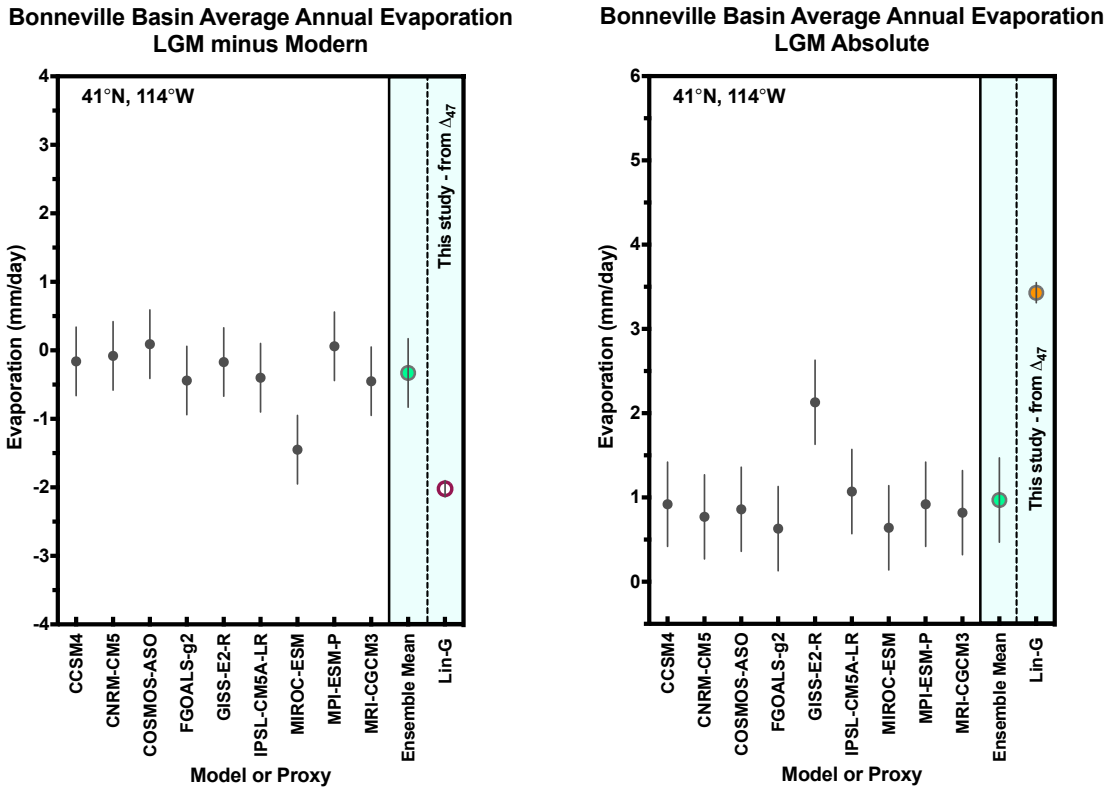


**Figure 26**: ***Clumped isotope based reconstructions of annual evaporation indicate that annual evaporation was lower than modern. Predicted evaporation from clumped isotopes is greater than PMIP3 models, but the magnitude of decrease below modern controls is also greater.*** Although most evaporation rates calculated for the Bonneville Basin during the LGM exceed PMIP3 model outputs, the magnitude of decrease relative to modern, or pre-industrial values, is the more relevant statistic. The rates calculated in this study are not directly intercomparable with model runs, which present evaporation rates over land, as has been noted elsewhere (Ibarra et al., 2014).

**Left**: Reconstructed annual evaporation minus control values. **Right**: Reconstructed absolute evaporation.

*Lin-G* = Annual evaporation from MJJAS gastropod temperature applied to Linacre (1993), and multiplied by a correction term to account for evaporation during October-April. Sites included in analyses: 30GP, PV, FW. For PMIP3 models, pre-Industrial control temperatures were subtracted from LGM model runs. Evaporation results were calculated using the Linacre (1993) approximation of the Penman equation for evaporation over open water. For clumped isotope based evaporation control, modern rates were calculated by application of temperatures from PRISM Climate Group database to the Linacre (1993) equation.

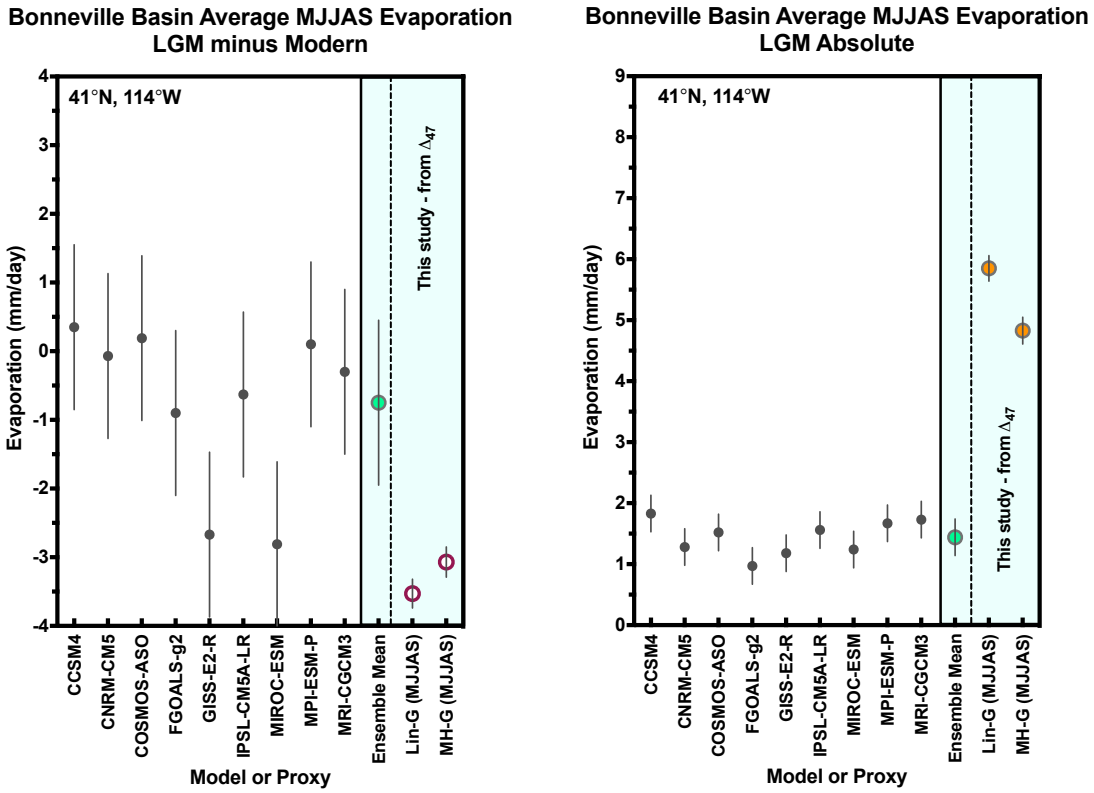


**Figure 27**: ***Clumped isotope based reconstructions of May-September (MJJAS) evaporation indicate that rates were lower than modern. Predicted MJJAS lake evaporation from clumped isotopes is greater than PMIP3 models, but the magnitude of decrease below modern controls is also greater.*** Although most evaporation rates calculated for the Bonneville Basin during the LGM exceed PMIP3 model outputs, the magnitude of decrease relative to modern, or pre-industrial values, is the more relevant statistic. The rates calculated in this study are not directly intercomparable with model runs, which present evaporation rates over land, as has been noted elsewhere (Ibarra et al., 2014).

**Left**: Reconstructed annual evaporation minus control values during May-September. **Right**: Reconstructed absolute evaporation during May-September.

*Lin-G (MJJAS)* = evaporation from MJJAS gastropod temperature applied to Linacre (1993), and multiplied by a correction term to account for evaporation during October-April. *MH-G (MJJAS)* = evaporation from MJJAS gastropod temperature applied to the Great Basin hydrologic model presented in Matsubara and Howard (2009). Sites included in analyses: 30GP, PV, FW. For PMIP3 models, pre-Industrial control temperatures were subtracted from LGM model runs. For clumped isotope based evaporation control, modern rates were evaluated by application of temperatures from PRISM Climate Group database to the Linacre (1993) and Matsubara and Howard (2009) equations, and by comparison to modern pan evaporation rates for the Bonneville Basin.

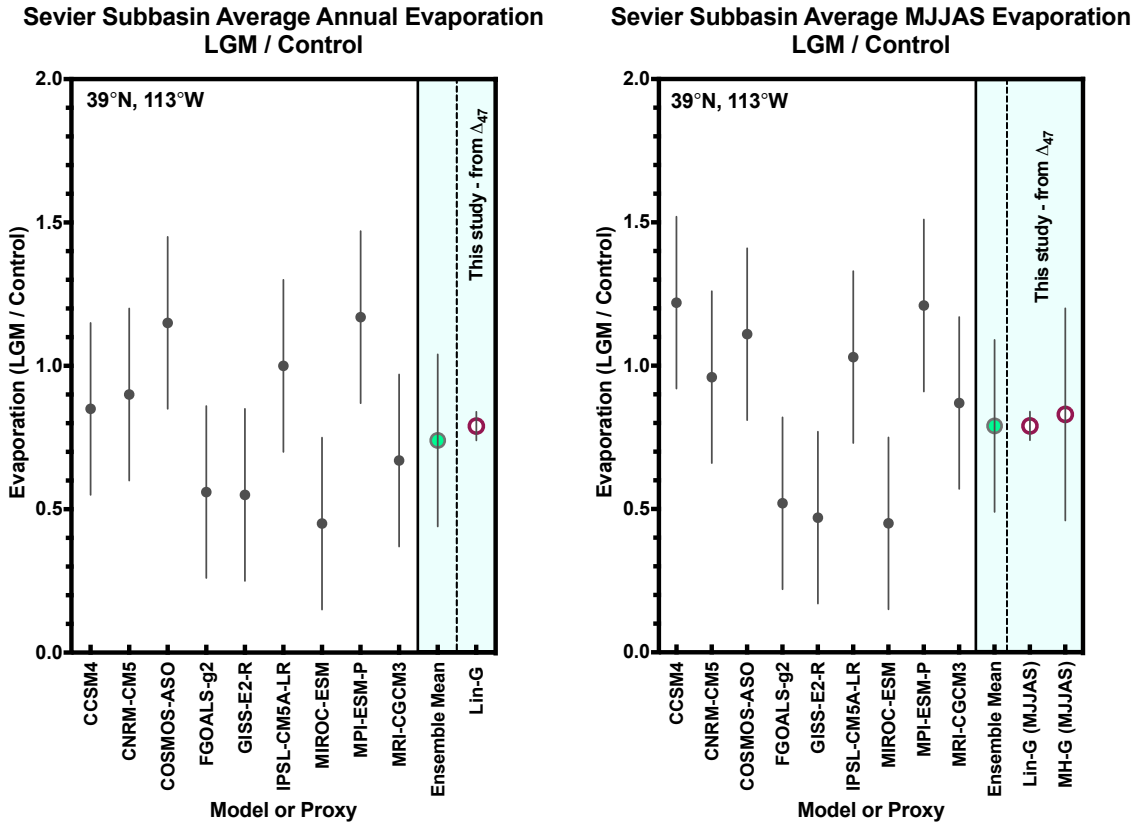


**Figure 28**: ***Clumped isotope based reconstructions of evaporation for the Sevier Subbasin indicate that annual evaporation was 21 percent lower than modern, and May-September evaporation was 17-21 percent below modern. The PMIP3 multi-model ensemble mean predicts annual evaporation 26 percent below modern, and summer evaporation 21 percent below modern.***

**Left**: Reconstructed annual evaporation presented as a fraction of control value. Models FGOALS-g2 (41 percent decrease) and MRI-GCM3 (35 percent decrease) predict change in annual evaporation from modern that is similar to clumped isotope derived results. *Lin-G* = Annual evaporation from MJJAS gastropod temperature applied to the Linacre (1993) approximation of the Penman equation for evaporation over open water.

**Right**: Reconstructed May-September (MJJAS) evaporation presented as a fraction of control value. Seasonal (MJJAS) evaporation was calculated using two methods. *Lin-G (MJJAS)* = evaporation from MJJAS gastropod temperature applied to Linacre (1993). *MH-G (MJJAS)* = evaporation from MJJAS gastropod temperature applied to the Great Basin hydrologic model presented in Matsubara and Howard (2009).

For PMIP3 models, LGM model runs are presented as a fraction of pre-Industrial control rates. For clumped isotope based evaporation control, modern rates were calculated by application of the PRISM Climate Group database to the Linacre (1993) and Matsubara and Howard (2009) equations. Sites included in analyses: GSF, LRSW3.

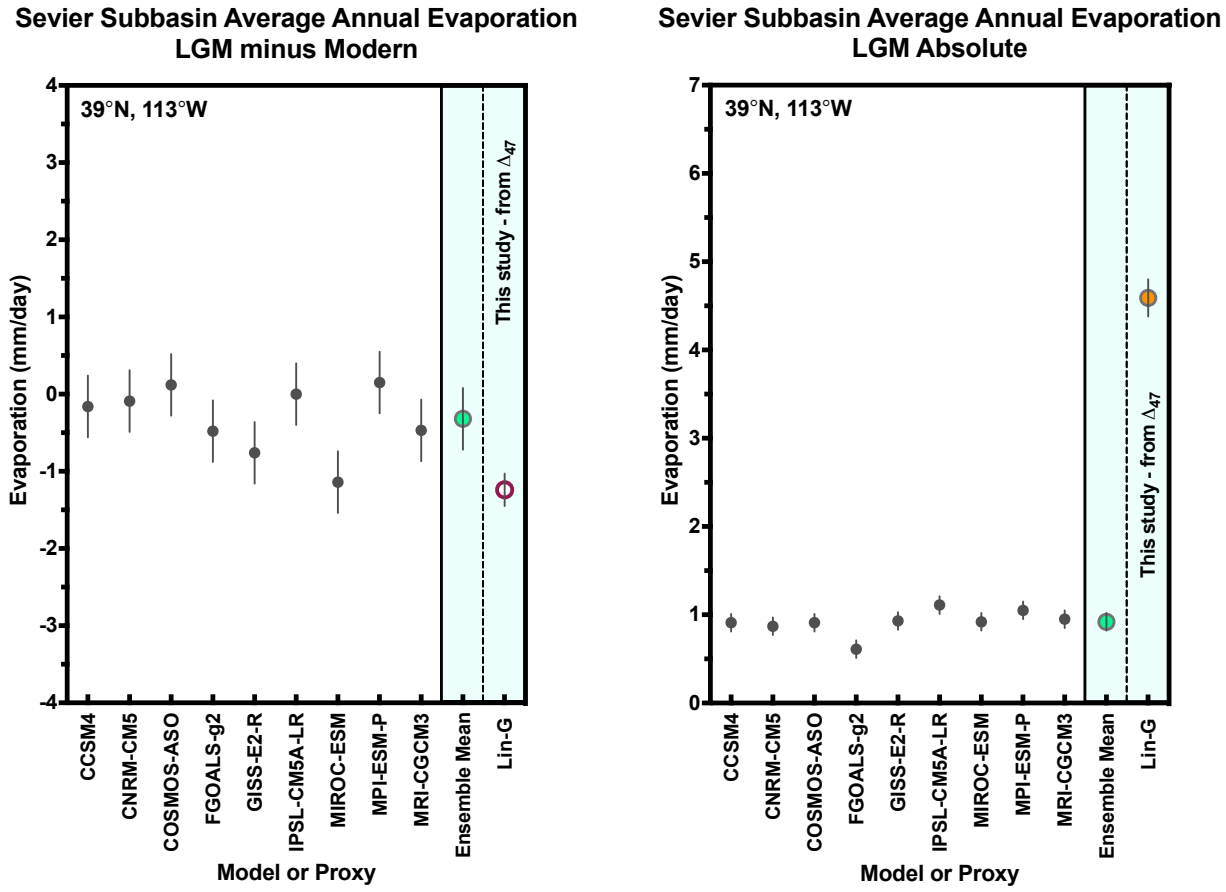


**Figure 29**: ***Clumped isotope based reconstructions of annual evaporation indicate that annual evaporation was lower than modern in the Sevier Subbasin. Predicted evaporation from clumped isotopes is greater than PMIP3 models, but the magnitude of decrease below modern controls is also greater.*** Although evaporation rates calculated for the Sevier Subbasin during the LGM exceed PMIP3 model outputs, the magnitude of decrease relative to modern, or pre-industrial values, is the more relevant statistic. The rates calculated in this study are not directly intercomparable with model runs, which present evaporation rates over land, as has been noted elsewhere (Ibarra et al., 2014).

**Left**: Reconstructed annual evaporation minus control values.
**Right**: Reconstructed absolute evaporation.

*Lin-G* = Annual evaporation from MJJAS gastropod temperature applied to the Linacre (1993) approximation of the Penman equation for evaporation over open water, and multiplied by a correction term to account for evaporation during October-April. Sites included in analyses: GSF, LRSW3. For PMIP3 models, pre-Industrial control temperatures were subtracted from LGM model runs. Modern control values applied to clumped isotope data were calculated by application of temperatures from the PRISM Climate Group database to the Linacre (1993) equation.

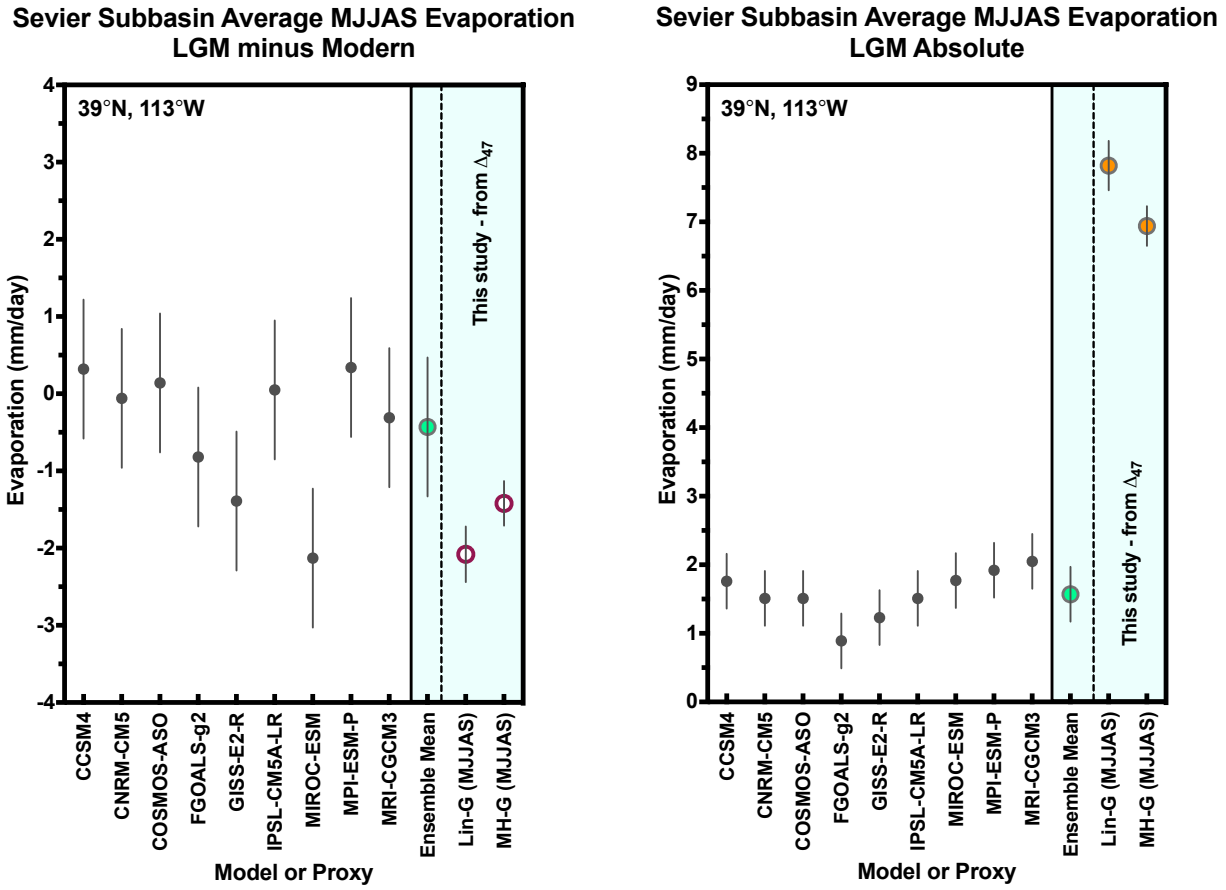


**Figure 30**: ***Reconstructed May-September (MJJAS) lake evaporation from clumped isotopes is greater than PMIP3 models, but the magnitude of decrease below modern controls is also more extreme than most model results.*** Although evaporation rates calculated for the Sevier Subbasin during the LGM exceed PMIP3 model estimates, the magnitude of decrease relative to modern, or pre-industrial values, is the more relevant statistic. The rates calculated in this study are not directly intercomparable with model runs, which present evaporation rates over land, as has been noted elsewhere (Ibarra et al., 2014).

**Left**: Reconstructed MJJAS evaporation minus control values. The MIROC-ESM model predicts a similar magnitude decrease in evaporation to the Linacre (1993), *Lin-G (MJJAS)*, clumped isotope based evaporation result.

**Right**: Reconstructed absolute MJJAS evaporation in the Sevier Subbasin.

*Lin-G (MJJAS)* = evaporation from MJJAS gastropod temperature applied to Linacre (1993), and multiplied by a correction term to account for evaporation during October-April. *MH-G (MJJAS)* = evaporation from MJJAS gastropod temperature applied to the Great Basin hydrologic model presented in Matsubara and Howard (2009). Sites included in analyses: GSF, LRSW3. For PMIP3 models, pre-Industrial control temperatures were subtracted from LGM model runs. For clumped isotope based evaporation control, modern rates were evaluated by application of temperatures from the PRISM Climate Group database to the Linacre (1993) and Matsubara and Howard (2009) equations, and by comparison to modern pan evaporation rates for the Sevier Subbasin.

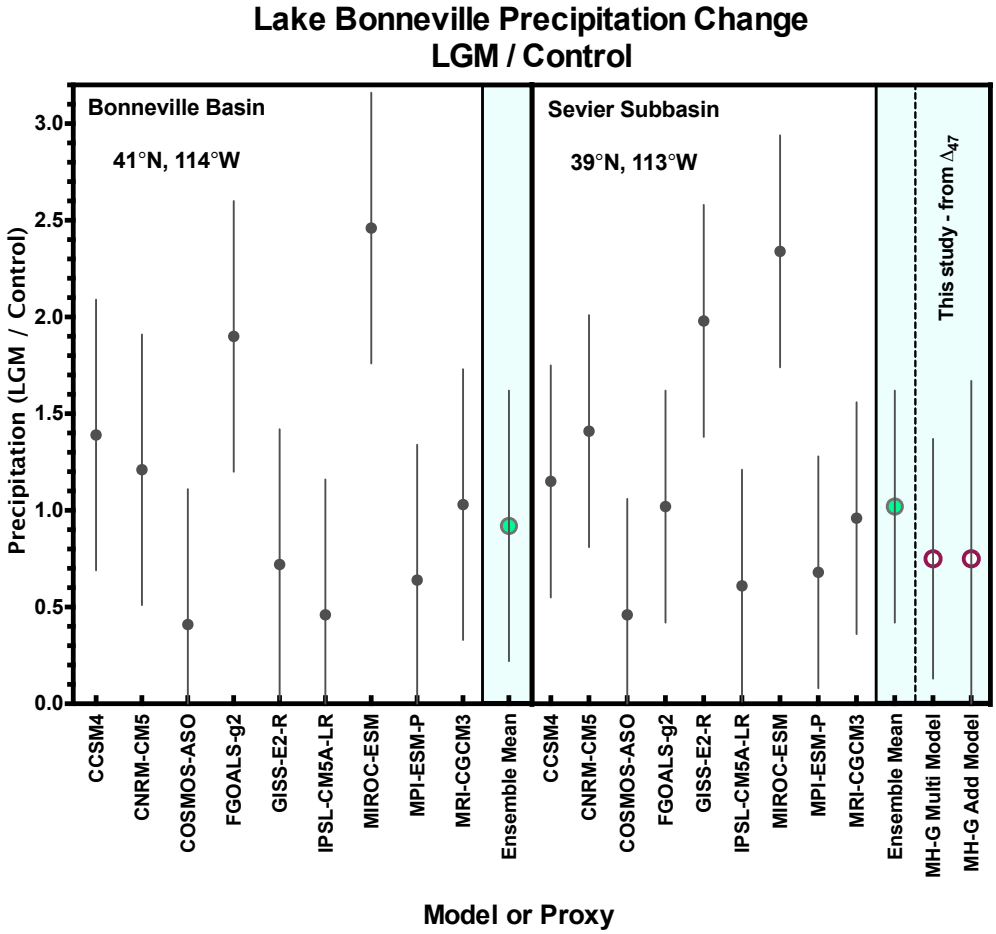


**Figure 31**: ***Clumped isotope based reconstructions of precipitation indicate a 25 percent decrease from modern values across the lake. The PMIP3 multi-model ensemble mean predicts annual precipitation at 8 percent below modern in the Bonneville Basin, and near modern values in the Sevier Subbasin.*** In this figure, the reconstructed annual precipitation over Lake Bonneville is presented as a fraction of control values. Precipitation values are presented for the entire lake, with values from the Bonneville Basin, and Sevier Subbasin, weighted by the area of each basin unit. The model GISS-E2-R (28 percent decrease) predicts change in annual precipitation from modern that is similar to the clumped isotope based result.

*MH-G Multi Model* = Annual precipitation from the Matsubara and Howard (2009) multiplicative model for the Great Basin. *MH-G Add Model* = Annual precipitation from the Matsubara and Howard (2009) additive model for the Great Basin. Modern precipitation values were extracted from the PRISM Climate Group database. Sites included in analyses: 30GP, PV, FW, GSF, LRSW3. For PMIP3 models, LGM model runs are presented as a fraction of pre-Industrial control rates.

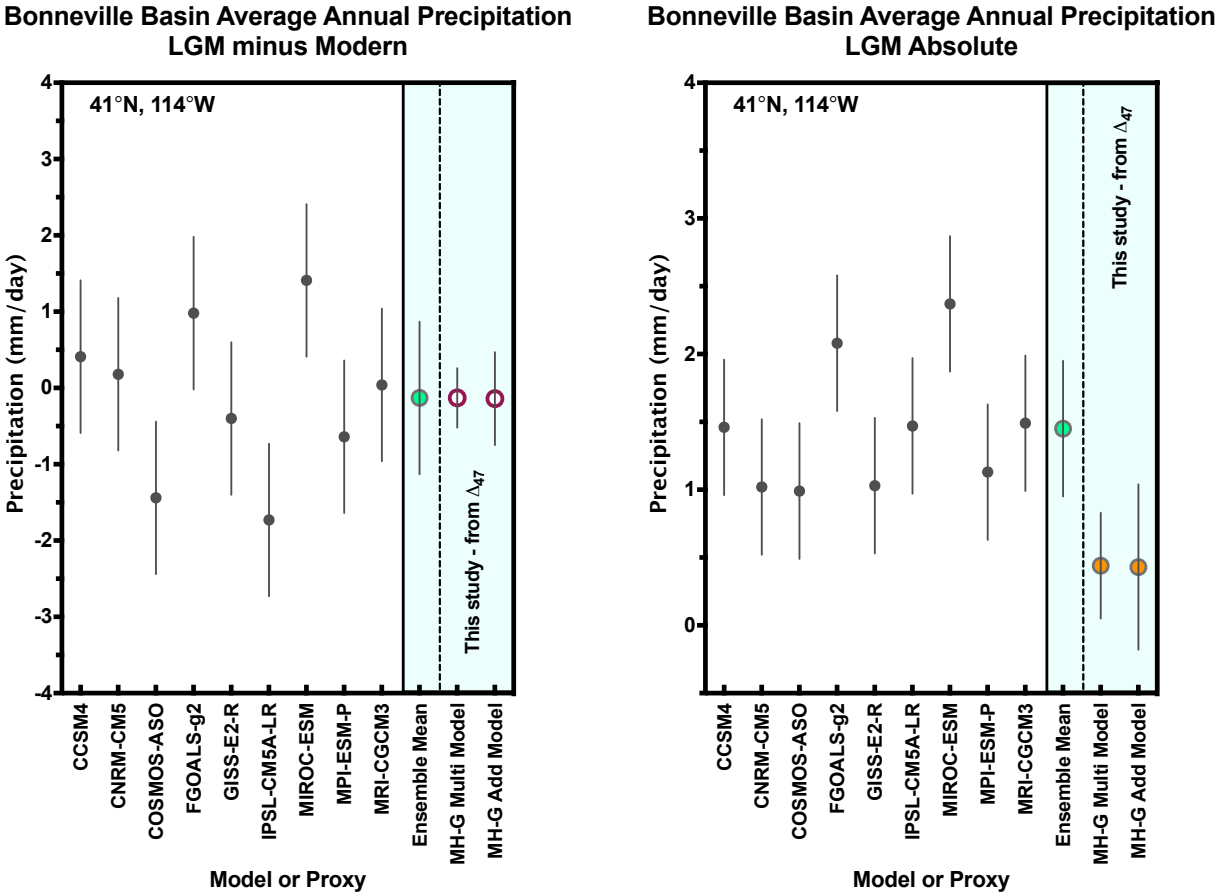


**Figure 32**: ***Comparison of precipitation estimates during the LGM for PMIP3 results in the Bonneville Basin and clumped isotope estimates for the entire lake system (this study).***

**Left**: Reconstructed annual precipitation minus control values.

**Right**: Reconstructed absolute precipitation. Estimated precipitation from clumped isotopes is significantly lower than PMIP3 model predictions. This can partially be attributed to offsets between PMIP3 pre-Industrial control values and the modern climate regime in the Bonneville Basin. For PMIP3 models, pre-Industrial control values were subtracted from LGM model runs. For clumped isotope based precipitation control values, modern (1971-2000) averages from the PRISM Climate Group database were applied.

Precipitation panel abbreviations: *MH-G Multi Model* = Matsubara and Howard (2009) Multiplicative Model for precipitation from gastropod clumped isotope results; *MH-G Add Model* = Matsubara and Howard (2009) Additive Model for precipitation from gastropod clumped isotope results.

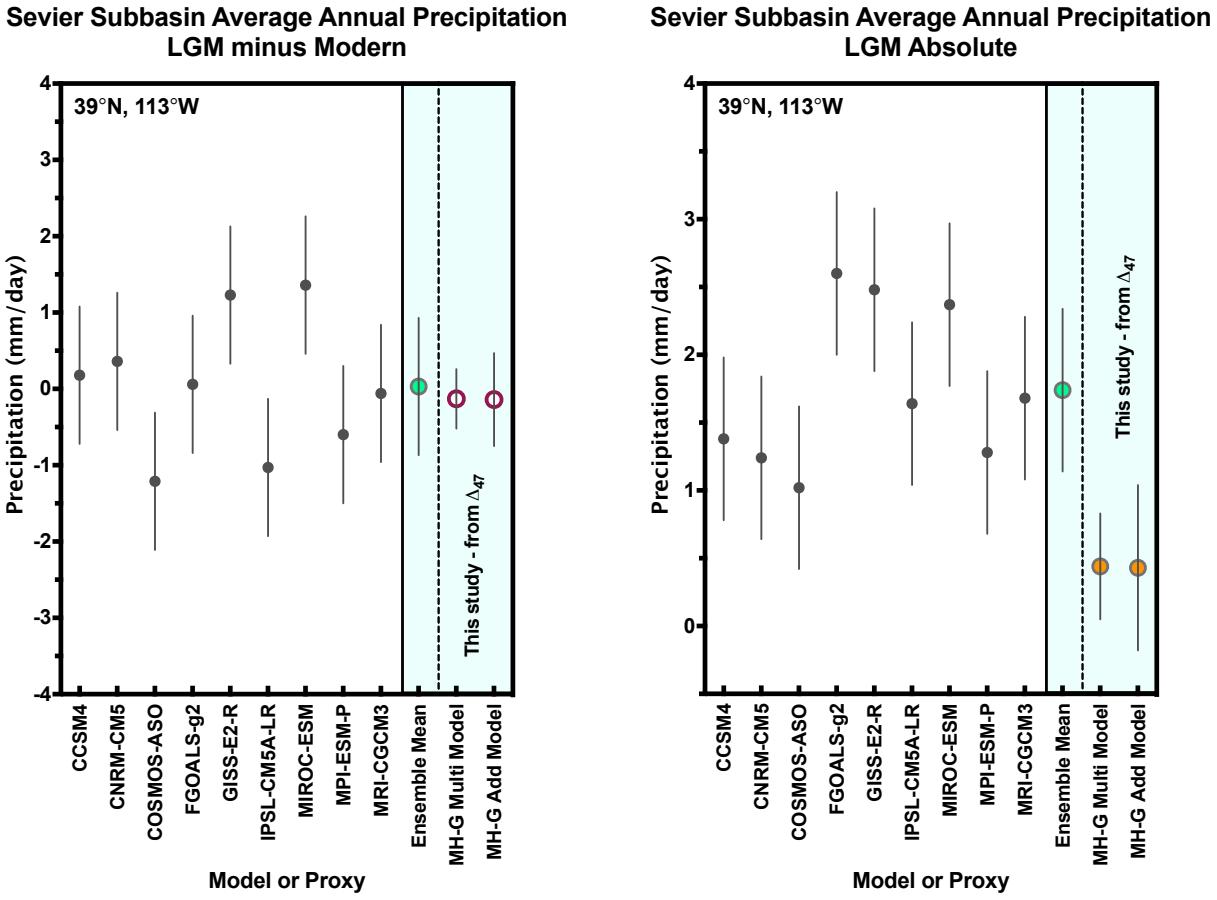


**Figure 33**: ***Comparison of precipitation estimates during the LGM for PMIP3 results in the Sevier Subbasin and clumped isotope estimates for the entire lake (this study).***

**Left**: reconstructed annual precipitation minus control values.

**Right**: reconstructed absolute precipitation. Estimated precipitation from clumped isotopes is significantly lower than PMIP3 model predictions. This can partially be attributed to offsets between PMIP3 pre-Industrial control values and the modern climate regime in the Sevier Subbasin.

For PMIP3 models, pre-Industrial control values were subtracted from LGM model runs. For clumped isotope based precipitation control values, modern (1971-2000) climate normals from the PRISM Climate Group database were applied. Precipitation panel abbreviations: MH-G Multi Model = Matsubara and Howard (2009) Multiplicative Model for precipitation from gastropod clumped isotope results; MH-G Add Model = Matsubara and Howard (2009) Additive Model for precipitation from gastropod clumped isotope results.

## 9.0 TABLES

## Table 1: Field Localities Visited

| Site | Material | Locality | Basin | Lat. | Long. | Elevation (m AMSL)[1] |
|---|---|---|---|---|---|---|
| **SG-1** | Gastropod: Pyrgulopsis | **Stansbury Gulch**: sand and gravel wedge with shells downslope from Stansbury shoreline. | Bonneville | 40.79 | -112.52 | 1337 |
| **PV-1** | Gastropod: Stagnicola | **Pilot Valley**: gastropod-bearing fine sand unit at base of marl. Early LGM. | Bonneville (Pilot Valley) | 40.88 | -114.23 | 1445 |
| **PV-2** | Marl | **Pilot Valley:** Marl directly above PV-1. | Bonneville (Pilot Valley) | 40.88 | -114.23 | 1445 |
| **30GP-1** | Gastropod: Stagnicola | **Gravel Pit on Hwy 30, N of Lucin**: shells from a sand bed above cobble line exposed in a gravel pit. Post-Stansbury, pre-LGM. | Bonneville | 41.42 | -113.91 | 1421 |
| **30GP-2** | Marl | **Gravel Pit on Hwy 30, N of Lucin**: Transgressive marl directly above 30GP-1 shells. Post Stansbury, pre-LGM. | Bonneville | 41.42 | -113.91 | 1421 |
| **FW-1** | Gastropod: Pyrgulopsis Stagnicola | **Ferber Wash**: gravel with shells at base of transgressive marl from the early LGM. | Bonneville | 40.35 | -114.07 | 1433 |
| **FW-2** | Marl | **Ferber Wash**: Marl 0-10 cm above FW-1. Marl is laminated. | Bonneville | 40.35 | -114.07 | 1433 |
| **LRSW-3** | Stagnicola within Marl | **Long Ridge SW:** near Sevier Dry Lake. Marl below Provo shoreline containing gastropods | Sevier | 39.03 | -113.22 | 1392 |
| **GSF-1** | Gastropod - Stagnicola | **Great Stone Face:** Shells in transgressive sand unit below marl. Sample from ~25 cm below marl base. | Sevier | 39.24 | -112.75 | 1448 |
| **GSF-2** | Marl | **Great Stone Face:** Sample marl 0-25 cm above Great Stone Face gastropod (GSF-1). | Sevier | 39.24 | -112.75 | 1453 |
| **OC-5A** | Gastropod - Pyrgulopsis | **DMAD Reservoir**: Shells from lens of fine sand, at base of transgressive marl. | Sevier | 39.41 | -112.45 | 1424 |
| **OC-5B** | Marl | **DMAD Reservoir:** Marl directly above OC-5A. | Sevier | 39.41 | -112.45 | 1424 |

**1. Shoreline elevation was corrected for post-lacustrine rebound (Oviatt et al., 1992).**

**Table 2: Ages of localities visited 2012**

| Site | Elevation (m AMSL)[1,2] | Age from Shoreline Elevation | $^{14}C$ Age | Calendar Age[3] | Calendar Age Range 1σ | References |
|---|---|---|---|---|---|---|
| **SG-1** | 1337.4 | 25,100 | 20710±310 | 24927 | 24516 - 25313 | Currey et al., 1983 |
| **PV-1** | 1445.5 | 22,900-22,800 | 19100±160 | 23007 | 22772 - 23241 | Sack, 1999 |
| **30GP-1** | 1421.0 | 23,400-22,500 | 20160±80 | 24227 | 24104 - 24347 | Oviatt, unpublished |
| **FW-1** | 1432.5 | 23,200-22,600 | 19260±140 | 23204 | 23009 - 23400 | Sack, 1999 |
| **LRSW-3** | 1391.7 | Marl with gastropods. No shorezone. | - | 23000 | - | Oviatt, unpublished |
| **GSF-1** | 1448.3 | 22,800-21,900 | 19195±145 | 23130 | 22931 - 23344 | Light, 1996 |
| **OC-5** | 1423.8 | 23,400-22,500 | 20100±400 | 24204 | 23643 - 24676 | Oviatt, unpublished |

**Table 3: Tufa samples from Nelson et al. (2005) archive**

| Sample | Locality | Lake Phase | Lat. | Long. | Collection Elevation (m) |
|---|---|---|---|---|---|
| **CIS 3** | Crater Island | Stansbury (25.8-24.3 ka) | 41.07 | -113.81 | 1320 |
| **CIS 7** | Crater Island | Stansbury (25.8-24.3 ka) | 41.11 | -113.78 | 1366 |
| **CIS13** | Crater Island | Stansbury (25.8-24.3 ka) | 41.09 | -113.73 | 1365 |
| **SIS13** | Silver Island Range | Stansbury (25.8-24.3 ka) | 40.79 | -113.95 | 1363 |
| **CIB1** | Crater Island | Bonneville (~18 ka) | 41.07 | -113.79 | 1553 |
| **SIB5** | Silver Island Range | Bonneville (~18 ka) | 40.83 | -113.91 | 1541 |
| **SIP2** | Silver Island Range | Provo (18-14.5 ka BP) | 40.99 | -113.83 | 1474 |
| **SIP 16** | Silver Island Range | Provo (18-14.5 ka BP) | 40.83 | -113.90 | 1476 |
| **CIP3** | Crater Island Range calcite cement | Provo (18-14.5 ka BP) | 41.07 | -113.80 | 1468 |
| **CIP17** | Crater Island Range | Provo (18-14.5 ka BP) | 41.11 | -113.77 | 1478 |
| **CIP25** | Crater Island Range | Provo (18-14.5 ka BP) | 41.08 | -113.73 | 1472 |

**Table 4: Standards measured**

| Standard | Type | $\delta^{13}C$ | $\delta^{18}O$ | $\Delta_{47}$ |
|---|---|---|---|---|
| | | ‰ VPDB | ‰ VPDB | ‰ ARF |
| TVO3 | Carbonate | 2.8 | -8.2 | 0.713 |
| Carmel Chalk | Carbonate | -2.1 | -4.4 | 0.697 |
| Carrera Marble | Carbonate | 2.1 | -1.9 | 0.395 |
| Veinstrom-01 | Carbonate | -6.1 | -12.9 | 0.730 |
| ETH-1 | Carbonate | - | - | 0.288 |
| ETH-2 | Carbonate | - | - | 0.297 |
| ETH-3 | Carbonate | - | - | 0.716 |
| ETH-4 | Carbonate | - | - | 0.566 |
| Bonedry Tank $CO_2$ | 25°C gas breakseal | - | - | 25°C equilibration |
| Bonedry Tank $CO_2$ | 1000°C gas breakseal | - | - | Stochastic |
| Evap DI + Carrera Marble $CO_2$ | 25°C gas breakseal | - | - | 25°C equilibration |
| Evap DI + Carrera Marble $CO_2$ | 1000°C gas breakseal | - | - | Stochastic |

**Table 5: Air temperature transfer functions**

| Water T Interval | Air T Interval | Equation | $R^2$ | 1 s.e. | Source |
|---|---|---|---|---|---|
| April - June | Mean Annual Avg. | MAAT (°C)=−0.0097×$T_W^2$+1.379$T_W$−8.23 | 0.94 | 2.12 | Hren and Sheldon, 2012 |
| April - October | Mean Annual Avg. | MAAT (°C)=−0.0146×$T_W^2$+1.753$T_W$−16.079 | 0.95 | 1.89 | Hren and Sheldon, 2012 |
| June - August | Mean Annual Avg. | MAAT (°C)=−0.0055×$T_W^2$+1.476$T_W$−18.915 | 0.90 | 2.69 | Hren and Sheldon, 2012 |
| Mean Annual Avg. | Mean Annual Avg. | MAAT (°C)=−0.0318×$T_W^2$+2.195$T_W$−12.607 | 0.96 | 1.62 | Hren and Sheldon, 2012 |
| May - September | Mean Annual Avg. | MAAT (°C)=−0.00895×$T_W^2$+1.58$T_W$−17.4 | 0.92 | 2.34 | This study |
| Warmest Month | Mean Annual Avg. | MAAT (°C)=1.360×$T_W$-21.18 | 0.87 | 2.97 | This study |
| April - June | April - June | AMJAT (°C)=−0.0065×$T_W^2$+1.104$T_W$−0.258 | 0.94 | 1.74 | This study |
| May - September | May - September | MSAT (°C)=−0.00667×$T_W^2$+1.179$T_W$−1.432 | 0.91 | 1.63 | This study |
| April - October | April - October | AOAT (°C)=−0.0103×$T_W^2$+1.353$T_W$−3.875 | 0.95 | 1.49 | This study |
| June - August | June - August | JJAAT (°C)=−0.0053×$T_W^2$+1.078$T_W$+0.560 | 0.89 | 1.85 | This study |
| Warmest Month | Warmest Month | WMAT (°C)=0.8645×$T_W$+2.340 | 0.85 | 2.03 | This study |

# Table 6: Analytical runs

| Sample I.D. | Sample Type | Total Runs | Total Analyses | $\delta^{13}C$ ‰ VPDB | | $\delta^{18}O_{mineral}$ ‰ VPDB | | $\Delta_{47}$ ‰ ARF | T - Lake °C | $\delta^{18}O_{water}$ ‰ VSMOW | *Site Averages* $\Delta_{47}$ ‰ ARF | T - Lake °C | $\delta^{18}O_{water}$ ‰ VSMOW |
|---|---|---|---|---|---|---|---|---|---|---|---|---|---|
| ***Stansbury Gulch - Gastopod - Stansbury Oscillation*** | | | | | | ***Age Range: 25.3 - 24.5 ka BP (Currey, 1983)*** | | | | | | | |
| SG1-P-5,7 | Pyrgulopsis | 1 | 8 | 2.5 | ± 0.003 | -4.1 | ± 0.010 | 0.726 | 16.1 | -5.6 | 0.744 ± 0.005 | 11.9 ± 1.0 | -6.6 ± 0.2 |
| SG1-P-9,10 | Pyrgulopsis | 1 | 8 | 1.4 | ± 0.003 | -4.2 | ± 0.014 | 0.734 | 14.2 | -6.1 | | | |
| SG1-P-11,13,14 | Pyrgulopsis | 1 | 8 | 1.3 | ± 0.002 | -4.2 | ± 0.007 | 0.747 | 11.4 | -6.7 | | | |
| SG1-P-4,18 | Pyrgulopsis | 1 | 8 | 2.2 | ± 0.034 | -4.4 | ± 0.013 | 0.751 | 10.5 | -7.1 | | | |
| SG1-P-16,19 | Pyrgulopsis | 1 | 8 | 1.3 | ± 0.002 | -4.1 | ± 0.012 | 0.742 | 12.4 | -6.4 | | | |
| SG1-P-15,17 | Pyrgulopsis | 1 | 8 | 2.6 | ± 0.024 | -4.2 | ± 0.020 | 0.759 | 8.8 | -7.3 | | | |
| SG1-P-22,23 | Pyrgulopsis | 1 | 8 | 1.7 | ± 0.004 | -4.4 | ± 0.009 | 0.734 | 14.2 | -6.3 | | | |
| SG1-P-25,29,38 | Pyrgulopsis | 1 | 9 | 1.1 | ± 0.004 | -4.3 | ± 0.013 | 0.763 | 7.9 | -7.6 | | | |
| **Mean** | | | | **1.7** | | **-4.2** | | **0.744** | **11.9** | **-6.6** | | | |
| **1 S.E.** | | | | **0.2** | | **0.0** | | **0.005** | **1.0** | **0.2** | | | |
| ***Highway 30 Gravel Pit - Gastopod - Transgressive*** | | | | | | ***Age Range: 23.4 - 22.5 ka BP (Hydrograph in Miller et al., 2013)*** | | | | | | | |
| 30GP-S-1 | Stagnicola | 2 | 16 | -0.8 | ± 0.002 | -4.1 | ± 0.005 | 0.737 | 13.4 | -6.2 | 0.743 ± 0.006 | 12.3 ± 1.3 | -6.1 ± 0.3 |
| 30GP1-S-2 | Stagnicola | 1 | 8 | -0.9 | ± 0.005 | -4.1 | ± 0.010 | 0.739 | 13.1 | -6.2 | | | |
| 30GP1-S-3 | Stagnicola | 1 | 8 | -2.2 | ± 0.005 | -3.3 | ± 0.010 | 0.732 | 14.7 | -5.0 | | | |
| 30GP1-S-1114A | Stagnicola | 1 | 9 | 0.1 | ± 0.005 | -3.9 | ± 0.019 | 0.739 | 13.1 | -6.1 | | | |
| 30GP1-S-1114B | Stagnicola | 1 | 9 | 0.4 | ± 0.005 | -3.4 | ± 0.013 | 0.767 | 7.1 | -6.8 | | | |
| **Mean** | | | | **-0.7** | | **-3.8** | | **0.743** | **12.3** | **-6.1** | | | |
| **1 S.E.** | | | | **0.5** | | **0.2** | | **0.006** | **1.3** | **0.3** | | | |
| ***Pilot Valley - Gastopod - Transgressive*** | | | | | | ***Age Range: 22.9 - 22.8 ka BP (Hydrograph in Miller et al., 2013)*** | | | | | | | |
| PV1-S-1 | Stagnicola | 1 | 8 | -1.3 | ± 0.004 | -3.6 | ± 0.009 | 0.745 | 11.7 | -6.0 | 0.748 ± 0.004 | 11.1 ± 0.8 | -6.2 ± 0.2 |
| PV1-S-2 | Stagnicola | 1 | 8 | -1.4 | ± 0.012 | -3.5 | ± 0.039 | 0.732 | 14.7 | -5.2 | | | |
| PV1-S-3 | Stagnicola | 3 | 24 | -0.5 | ± 0.011 | -3.9 | ± 0.010 | 0.736 | 13.7 | -5.9 | | | |
| PV1-S-4 | Stagnicola | 1 | 8 | -0.2 | ± 0.007 | -4.0 | ± 0.016 | 0.753 | 10.1 | -6.7 | | | |
| PV1-S-5 | Stagnicola | 2 | 16 | -1.0 | ± 0.005 | -3.3 | ± 0.010 | 0.749 | 11.0 | -5.8 | | | |
| PV1-S-6 | Stagnicola | 2 | 16 | -1.5 | ± 0.005 | -3.5 | ± 0.006 | 0.757 | 9.2 | -6.5 | | | |
| PV1-S-7 | Stagnicola | 1 | 8 | -1.6 | ± 0.002 | -3.5 | ± 0.007 | 0.759 | 8.8 | -6.6 | | | |
| PV1-S-8 | Stagnicola | 2 | 16 | -1.0 | ± 0.003 | -4.0 | ± 0.006 | 0.757 | 9.3 | -6.9 | | | |
| **Mean** | | | | **-1.1** | | **-3.6** | | **0.748** | **11.1** | **-6.2** | | | |
| **1 S.E.** | | | | **0.2** | | **0.1** | | **0.004** | **0.8** | **0.2** | | | |
| ***Ferber Wash - Gastopod - Transgressive*** | | | | | | ***Age Range: 23.2 - 22.6 ka BP (Hydrograph in Miller et al., 2013)*** | | | | | | | |
| FW1-S-2 | Stagnicola | 1 | 8 | -1.9 | ± 0.008 | -3.3 | ± 0.011 | 0.757 | 9.1 | -6.3 | 0.746 ± 0.005 | 11.6 ± 1.0 | -5.7 ± 0.2 |
| FW1-S-4 | Stagnicola | 3 | 24 | -0.6 | ± 0.003 | -3.5 | ± 0.006 | 0.735 | 14.0 | -5.4 | | | |
| FW1-S-5 | Stagnicola | 2 | 16 | -1.3 | ± 0.006 | -3.1 | ± 0.013 | 0.738 | 13.2 | -5.2 | | | |
| FW1-S-6 | Stagnicola | 1 | 8 | 0.1 | ± 0.003 | -3.4 | ± 0.007 | 0.757 | 9.2 | -6.3 | | | |
| FW1-S-7 | Stagnicola | 3 | 24 | -1.4 | ± 0.004 | -3.1 | ± 0.009 | 0.742 | 12.5 | -5.4 | | | |
| **Mean** | | | | **-1.0** | | **-3.3** | | **0.746** | **11.6** | **-5.7** | | | |
| **1 S.E.** | | | | **0.3** | | **0.1** | | **0.005** | **1.0** | **0.2** | | | |
| FW1-P-A | Pyrgulopsis | 1 | 8 | -0.7 | ± 0.005 | -3.5 | ± 0.018 | 0.745 | 11.8 | -5.9 | 0.744 ± 0.008 | 12.0 ± 1.8 | -5.9 ± 0.4 |
| FW1- P- 3,4 | Pyrgulopsis | 1 | 8 | -1.5 | ± 0.008 | -3.5 | ± 0.008 | 0.743 | 12.2 | -5.9 | | | |
| FW1 -P-7 | Pyrgulopsis | 1 | 8 | -0.3 | ± 0.073 | -3.7 | ± 0.123 | 0.716 | 18.4 | -4.7 | | | |
| FWP1-P-5,11 | Pyrgulopsis | 1 | 8 | 0.2 | ± 0.007 | -3.5 | ± 0.014 | 0.740 | 12.8 | -5.7 | | | |
| FW1-P-4,5 | Pyrgulopsis | 1 | 8 | -0.7 | ± 0.002 | -3.2 | ± 0.004 | 0.743 | 12.2 | -5.5 | | | |
| FWI-P-12,13 | Pyrgulopsis | 1 | 8 | 0.3 | ± 0.005 | -3.9 | ± 0.012 | 0.779 | 4.5 | -8.0 | | | |
| **Mean** | | | | **-0.5** | | **-3.6** | | **0.744** | **12.0** | **-5.9** | | | |
| **1 S.E.** | | | | **0.3** | | **0.1** | | **0.008** | **1.8** | **0.4** | | | |

| Sample I.D. | Sample Type | Total Runs | Total Analyses | $\delta^{13}C$ ‰ VPDB | | $\delta^{18}O_{mineral}$ ‰ VPDB | | $\Delta_{47}$ ‰ ARF | T - Lake °C | $\delta^{18}O_{water}$ ‰ VSMOW | *Site Averages* $\Delta_{47}$ ‰ ARF | T - Lake °C | $\delta^{18}O_{water}$ ‰ VSMOW |
|---|---|---|---|---|---|---|---|---|---|---|---|---|---|
| ***Great Stone Face Gastopod - Transgressive*** | | | | ***Age Range: 22.8 - 21.9 ka BP (Hydrograph in Miller et al., 2013)*** | | | | | | | | | |
| GSF1-S-3 | Stagnicola | 1 | 8 | 0.9 | ± 0.005 | -3.8 | ± 0.011 | 0.735 | 14.0 | -5.8 | 0.720 ± 0.007 | 17.5 ± 1.5 | -4.9 ± 0.4 |
| GSF1-S-5 | Stagnicola | 1 | 8 | 0.7 | ± 0.004 | -3.6 | ± 0.010 | 0.708 | 20.3 | -4.2 | | | |
| GSF1-S-6 | Stagnicola | 1 | 8 | 0.2 | ± 0.004 | -3.6 | ± 0.009 | 0.719 | 17.7 | -4.7 | | | |
| GSF1-S-8 | Stagnicola | 1 | 8 | 0.0 | ± 0.018 | -4.1 | ± 0.010 | 0.744 | 12.1 | -6.4 | | | |
| GSF1-S-10 | Stagnicola | 2 | 16 | 0.3 | ± 0.031 | -3.7 | ± 0.010 | 0.703 | 21.6 | -4.1 | | | |
| GSF1-S-1114B | Stagnicola | 1 | 9 | -0.9 | ± 0.005 | -3.7 | ± 0.015 | 0.713 | 19.1 | -4.6 | | | |
| **Mean** | | | | **0.2** | | **-3.7** | | **0.720** | **17.5** | **-4.9** | | | |
| **1 S.E.** | | | | **0.3** | | **0.1** | | **0.007** | **1.5** | **0.4** | | | |
| ***DMAD Reservoir - Gastropod - Transgressive*** | | | | ***Age Range: 23.4 - 22.5 ka BP (Hydrograph in Miller et al., 2013)*** | | | | | | | | | |
| OC5A-P-3 | Pyrgulopsis | 1 | 8 | -0.4 | ± 0.001 | -4.5 | ± 0.005 | 0.750 | 10.6 | -7.1 | 0.755 ± 0.005 | 9.6 ± 1.0 | -7.2 ± 0.2 |
| OC5A-P-6 | Pyrgulopsis | 1 | 8 | -0.3 | ± 0.004 | -4.1 | ± 0.007 | 0.751 | 10.5 | -6.8 | | | |
| OC5A-P-7 | Pyrgulopsis | 1 | 8 | 0.7 | ± 0.002 | -4.3 | ± 0.001 | 0.764 | 7.6 | -7.6 | | | |
| **Mean** | | | | **0.0** | | **-4.3** | | **0.755** | **9.6** | **-7.2** | | | |
| **1 S.E.** | | | | **0.3** | | **0.1** | | **0.005** | **1.0** | **0.2** | | | |
| ***LRSW3 - Gastropod - Transgressive*** | | | | ***Age Range: 23 ka BP (Hydrograph in Miller et al., 2013)*** | | | | | | | | | |
| LRSW3-S-1 | Stagnicola | 4 | 32 | -0.7 | ± 0.004 | -2.6 | ± 0.011 | 0.721 | 17.1 | -3.8 | 0.725 ± 0.004 | 16.4 ± 0.9 | -5.6 ± 0.3 |
| LRSW3-S-2 | Stagnicola | 1 | 8 | -1.1 | ± 0.006 | -3.9 | ± 0.012 | 0.712 | 19.3 | -4.7 | | | |
| LRSW3-S-3 | Stagnicola | 2 | 17 | -0.8 | ± 0.005 | -4.2 | ± 0.012 | 0.744 | 12.0 | -6.6 | | | |
| LRSW3-S-5 | Stagnicola | 2 | 16 | -0.8 | ± 0.005 | -4.0 | ± 0.008 | 0.708 | 20.3 | -4.6 | | | |
| LRSW3-S-6 | Stagnicola | 1 | 8 | -0.1 | ± 0.005 | -4.2 | ± 0.009 | 0.715 | 18.6 | -5.1 | | | |
| LRSW3-S-1114C | Stagnicola | 1 | 9 | -0.9 | ± 0.006 | -4.3 | ± 0.015 | 0.730 | 15.2 | -6.0 | | | |
| LRSW3-S-1114-d,e | Stagnicola | 1 | 9 | -1.9 | ± 0.006 | -4.6 | ± 0.015 | 0.721 | 17.1 | -5.8 | | | |
| LRSW3-S-1114-f,g | Stagnicola | 1 | 9 | 0.0 | ± 0.004 | -4.6 | ± 0.019 | 0.738 | 13.3 | -6.7 | | | |
| LRSW3-1114-h,i | Stagnicola | 1 | 9 | -1.0 | ± 0.007 | -4.9 | ± 0.013 | 0.732 | 14.6 | -6.7 | | | |
| **Mean** | | | | **-0.8** | | **-4.1** | | **0.725** | **16.4** | **-5.6** | | | |
| **1 S.E.** | | | | **0.2** | | **0.2** | | **0.004** | **0.9** | **0.3** | | | |
| ***Highway 30 Gravel Pit - Transgressive*** | | | | ***Age: slightly younger than 23.4 ka BP (Hydrograph in Miller et al., 2013)*** | | | | | | | | | |
| 30GP2-M-1 | Marl | 2 | 17 | 1.8 | ± 0.006 | -7.9 | ± 0.017 | 0.746 | 17.1 | -8.4 | 0.714 ± 0.011 | 25.0 ± 2.6 | -7.0 ± 0.5 |
| 30GP2-M-4 | Marl | 3 | 24 | 1.4 | ± 0.004 | -8.0 | ± 0.011 | 0.701 | 28.3 | -6.3 | | | |
| 30GP2-M-5 | Marl | 4 | 33 | 1.4 | ± 0.004 | -8.3 | ± 0.007 | 0.705 | 27.2 | -6.8 | | | |
| 30GP2-M-328 | Marl | 1 | 9 | 1.8 | ± 0.005 | -8.1 | ± 0.013 | 0.704 | 27.4 | -6.5 | | | |
| **Mean** | | | | **1.6** | | **-8.1** | | **0.714** | **25.0** | **-7.0** | | | |
| **1 S.E.** | | | | **0.1** | | **0.1** | | **0.011** | **2.6** | **0.5** | | | |
| ***Pilot Valley - Marl - Transgressive*** | | | | ***Age: slightly younger than 22.9 ka BP (Hydrograph in Miller et al., 2013)*** | | | | | | | | | |
| PV2-M-1 | Marl | 1 | 8 | 2.6 | ± 0.004 | -7.1 | ± 0.008 | 0.739 | 18.6 | -7.3 | 0.735 ± 0.005 | 19.7 ± 1.3 | -6.8 ± 0.4 |
| PV2-M-3 | Marl | 3 | 24 | 2.7 | ± 0.005 | -6.6 | ± 0.008 | 0.739 | 18.6 | -6.8 | | | |
| PV2-M-4 | Marl | 2 | 16 | 2.1 | ± 0.004 | -7.3 | ± 0.006 | 0.742 | 17.9 | -7.6 | | | |
| PV2-M-5 | Marl | 1 | 8 | 3.0 | ± 0.002 | -6.6 | ± 0.009 | 0.720 | 23.5 | -5.7 | | | |
| **Mean** | | | | **2.6** | | **-6.9** | | **0.735** | **19.7** | **-6.8** | | | |
| **1 S.E.** | | | | **0.2** | | **0.2** | | **0.005** | **1.3** | **0.4** | | | |
| ***Ferber Wash - Marl - Transgressive*** | | | | ***Age: slightly younger than 23.2 ka BP (Hydrograph in Miller et al., 2013)*** | | | | | | | | | |
| FW2-M-1 | Marl | 1 | 8 | 2.2 | ± 0.013 | -6.3 | ± 0.013 | 0.743 | 17.8 | -6.6 | 0.732 ± 0.007 | 20.6 ± 1.7 | -5.3 ± 0.5 |
| FW2-M-3 | Marl | 1 | 8 | 3.5 | ± 0.004 | -5.7 | ± 0.004 | 0.724 | 22.4 | -5.2 | | | |
| FW2-M-4 | Marl | 2 | 16 | 3.8 | ± 0.006 | -5.5 | ± 0.006 | 0.716 | 24.3 | -4.5 | | | |
| FW2-M-5 | Marl | 1 | 8 | 4.8 | ± 0.005 | -4.5 | ± 0.005 | 0.743 | 17.7 | -4.9 | | | |
| **Mean** | | | | **3.6** | | **-5.5** | | **0.732** | **20.6** | **-5.3** | | | |
| **1 S.E.** | | | | **0.5** | | **0.4** | | **0.007** | **1.7** | **0.5** | | | |

| Sample I.D. | Sample Type | Total Runs | Total Analyses | $\delta^{13}C$ ‰ VPDB | | $\delta^{18}O_{mineral}$ ‰ VPDB | | $\Delta_{47}$ ‰ ARF | T - Lake °C | $\delta^{18}O_{water}$ ‰ VSMOW | *Site Averages* $\Delta_{47}$ ‰ ARF | *Site Averages* T - Lake °C | *Site Averages* $\delta^{18}O_{water}$ ‰ VSMOW |
|---|---|---|---|---|---|---|---|---|---|---|---|---|---|
| ***Great Stone Face - Marl - Transgressive*** | | | | ***Age: slightly younger than 22.8 ka BP (Hydrograph in Miller et al., 2013)*** | | | | | | | | | |
| GSF2-M-1 | Marl | 3 | 24 | 4.3 | ± 0.003 | -4.5 | ± 0.005 | 0.707 | 26.7 | -3.0 | 0.718 ± 0.007 | 24.0 ± 1.7 | -3.6 ± 0.4 |
| GSF2-M-2 | Marl | 2 | 16 | 4.3 | ± 0.006 | -4.4 | ± 0.015 | 0.695 | 29.9 | -2.3 | | | |
| GSF2-M-3 | Marl | 3 | 24 | 4.3 | ± 0.003 | -4.5 | ± 0.009 | 0.724 | 22.3 | -3.9 | | | |
| GSF2-M-4 | Marl | 1 | 8 | 4.3 | ± 0.003 | -4.3 | ± 0.007 | 0.739 | 18.7 | -4.5 | | | |
| GSF2-M-5 | Marl | 4 | 32 | 4.1 | ± 0.003 | -4.5 | ± 0.004 | 0.710 | 26.1 | -3.2 | | | |
| GSF2-M-6 | Marl | 1 | 8 | 4.1 | ± 0.002 | -4.6 | ± 0.005 | 0.733 | 20.2 | -4.4 | | | |
| **Mean** | | | | **4.2** | | **-4.5** | | **0.718** | **24.0** | **-3.6** | | | |
| **1 S.E.** | | | | **0.0** | | **0.0** | | **0.007** | **1.7** | **0.4** | | | |
| ***DMAD Reservoir - Marl - Transgressive*** | | | | ***Age: slightly younger than 23.4 ka BP (Hydrograph in Miller et al., 2013)*** | | | | | | | | | |
| OC-5B-M-1 | Marl | 2 | 16 | 2.6 | ± 0.003 | -4.4 | ± 0.011 | 0.733 | 20.2 | -4.2 | 0.703 ± 0.029 | 28.0 ± 7.8 | -2.7 ± 1.5 |
| OC-5B-M-2 | Marl | 2 | 17 | 2.4 | ± 0.003 | -4.5 | ± 0.010 | 0.674 | 35.8 | -1.2 | | | |
| **Mean** | | | | **2.5** | | **-4.4** | | **0.703** | **28.0** | **-2.7** | | | |
| **1 S.E.** | | | | **0.1** | | **0.0** | | **0.029** | **7.8** | **1.5** | | | |
| ***LRSW3 - Marl - Transgressive*** | | | | ***Age: slightly younger than 23 ka BP (Hydrograph in Miller et al., 2013)*** | | | | | | | | | |
| LRSW3-M-AB | Marl | 1 | 8 | 0.6 | ± 0.005 | -5.1 | ± 0.013 | 0.700 | 28.7 | -3.3 | 0.715 ± 0.009 | 24.8 ± 2.3 | -4.0 ± 0.4 |
| LRSW3-M-D | Marl | 1 | 8 | 0.4 | ± 0.005 | -5.0 | ± 0.013 | 0.730 | 20.8 | -4.7 | | | |
| LRSW3-M-328 | Marl | 1 | 9 | 0.0 | ± 0.006 | -5.1 | ± 0.015 | 0.715 | 24.8 | -4.0 | | | |
| **Mean** | | | | **0.3** | | **-5.1** | | **0.715** | **24.8** | **-4.0** | | | |
| **1 S.E.** | | | | **0.2** | | **0.1** | | **0.009** | **2.3** | **0.4** | | | |
| ***Pilot Valley - Tufa - Stansbury Oscillation*** | | | | ***Age Range: 25.8 - 24.5 ka BP (Hydrograph in Miller et al., 2013)*** | | | | | | | | | |
| CIS3 | Tufa | 3 | 27 | 5.5 | ± 0.005 | -2.9 | ± 0.016 | 0.752 | 11.5 | -4.6 | 0.742 ± 0.005 | 13.9 ± 1.4 | -4.4 ± 0.3 |
| CIS7 | Tufa | 4 | 36 | 5.1 | ± 0.006 | -3.8 | ± 0.015 | 0.731 | 16.9 | -4.4 | | | |
| CIS13 | Tufa | 4 | 36 | 5.6 | ± 0.007 | -2.7 | ± 0.018 | 0.736 | 15.6 | -3.5 | | | |
| SIS13 | Tufa | 3 | 27 | 5.2 | ± 0.005 | -3.5 | ± 0.013 | 0.751 | 11.8 | -5.1 | | | |
| **Mean** | | | | **5.4** | | **-3.2** | | **0.74** | **13.9** | **-4.4** | | | |
| **1 S.E.** | | | | **0.1** | | **0.3** | | **0.005** | **1.4** | **0.3** | | | |
| ***Pilot Valley - Tufa - Bonneville Shoreline*** | | | | ***Age Range: 18.4 - 17.4 ka BP (Hydrograph in Miller et al., 2013)*** | | | | | | | | | |
| CIB1 | Tufa | 4 | 36 | 4.3 | ± 0.005 | -3.6 | ± 0.014 | 0.757 | 10.3 | -5.6 | 0.746 ± 0.011 | 13.0 ± 2.7 | -4.8 ± 0.8 |
| SIB5 | Tufa | 4 | 36 | 5.5 | ± 0.006 | -3.2 | ± 0.015 | 0.735 | 15.7 | -4.0 | | | |
| **Mean** | | | | **4.9** | | **-3.4** | | **0.746** | **13.0** | **-4.8** | | | |
| **1 S.E.** | | | | **0.6** | | **0.2** | | **0.011** | **2.7** | **0.8** | | | |
| ***Pilot Valley - Tufa - Provo Shoreline*** | | | | ***Age Range: 17.4 - 14.5 ka BP (Hydrograph in Miller et al., 2013)*** | | | | | | | | | |
| CIP3 | Tufa | 4 | 36 | 3.8 | ± 0.006 | -4.3 | ± 0.015 | 0.739 | 14.7 | -5.3 | 0.745 ± 0.003 | 13.3 ± 0.9 | -5.3 ± 0.3 |
| CIP17 | Tufa | 1 | 9 | 4.0 | ± 0.006 | -4.2 | ± 0.017 | 0.734 | 16.0 | -5.0 | | | |
| CIP25 | Tufa | 3 | 27 | 4.0 | ± 0.005 | -4.2 | ± 0.014 | 0.750 | 12.0 | -5.8 | | | |
| SIP2 | Tufa | 4 | 36 | 5.6 | ± 0.006 | -2.9 | ± 0.012 | 0.748 | 12.5 | -4.4 | | | |
| SIP16 | Tufa | 3 | 27 | 3.6 | ± 0.005 | -4.4 | ± 0.013 | 0.752 | 11.6 | -6.2 | | | |
| **Mean** | | | | **4.2** | | **-3.7** | | **0.750** | **12.0** | **-5.3** | | | |
| **1 S.E.** | | | | **0.4** | | **0.8** | | **0.002** | **0.5** | **0.9** | | | |

**Table 7: Gastropod annual air temperature reconstruction**

| | Water T (°C) | | Seasonal surface water temperature to Mean Annual Air Temperature transfer functions (°C) | | | | | | | | | | | |
|---|---|---|---|---|---|---|---|---|---|---|---|---|---|---|
| **Sample** | **T-$\Delta_{47}$** | **1 s.e.** | **AMJ** | **1 s.e.** | **JJA** | **1 s.e.** | **MJJAS** | **1 s.e.** | **A-O** | **1 s.e.** | **Mean Ann. Lake T** | **1 s.e.** | **Warm Month** | **1 s.e.** |
| **SG-P** | 11.9 | 1 | 6.9 | 1.1 | -2.1 | 1.3 | 0.2 | 1.4 | 2.8 | 1.4 | 9.1 | 1.4 | -4.9 | 1.4 |
| | | | | | | | | | | | | | | |
| **30 GP1-S** | 12.3 | 1.3 | 7.3 | 1.5 | -1.6 | 1.8 | 0.7 | 1.8 | 3.3 | 1.8 | 9.6 | 1.8 | -4.5 | 1.8 |
| **PV1-S** | 11.1 | 0.8 | 5.8 | 0.9 | -3.3 | 1 | -1 | 1.1 | 1.5 | 1.1 | 7.8 | 1.1 | -6.1 | 1.1 |
| **FW1-S** | 11.6 | 1 | 6.5 | 1.2 | -2.5 | 1.4 | -0.3 | 1.4 | 2.3 | 1.4 | 8.6 | 1.5 | -5.4 | 1.4 |
| **FW1-P** | 12 | 1.8 | 6.9 | 2 | -2 | 2.4 | 0.2 | 2.4 | 2.8 | 2.5 | 9.1 | 2.5 | -4.9 | 2.4 |
| | | | | | | | | | | | | | | |
| **GSF1-S** | 17.5 | 1.5 | 12.9 | 1.6 | 5.2 | 1.9 | 7.5 | 1.9 | 10.1 | 1.8 | 16 | 1.6 | 2.6 | 2.1 |
| **LRSW3-S** | 16.4 | 0.9 | 11.8 | 1 | 3.8 | 1.2 | 6.1 | 1.2 | 8.7 | 1.2 | 14.8 | 1.1 | 1.1 | 1.3 |
| | | | | | | | | | | | | | | |
| **Bonneville Basin LGM** | 11.7 | 0.3 | 6.6 | 0.6 | -2.4 | 0.6 | -0.1 | 0.7 | 2.5 | 0.7 | 8.8 | 0.8 | -5.2 | 0.6 |
| | | | | | | | | | | | | | | |
| **Sevier Basin LGM** | 16.9 | 0.5 | 12.3 | 0.8 | 4.5 | 1 | 6.8 | 1 | 9.4 | 0.9 | 15.4 | 0.8 | 1.8 | 1 |
| | | | | | | | | | | | | | | |
| **All Gastropods - LGM** | 13.5 | 2.7 | 8.5 | 3 | -0.1 | 3.6 | 2.2 | 3.6 | 4.8 | 3.6 | 11 | 3.5 | -2.9 | 3.7 |

**1. Reconstructions reflect assumptions of unique intervals of growth for gastropods. These values are used to calculate Mean Annual Air Temperature using transfer functions (Hren and Sheldon, 2012). For gastropods, the most applicable transfer function is MJJAS water temperature to Mean Annual Air Temperature.**

**Table 8: Gastropod annual air temperature reconstruction: LGM minus modern**

| | Water T (°C) | | LGM Mean Annual Air Temperature Minus Modern (°C) | | | | | | | | | | | |
|---|---|---|---|---|---|---|---|---|---|---|---|---|---|---|
| **Sample** | **T-$\Delta_{47}$** | **1 s.e.** | **AMJ** | **1 s.e.** | **JJA** | **1 s.e.** | **MJJAS** | **1 s.e.** | **A-O** | **1 s.e.** | **Mean Ann. Lake T** | **1 s.e.** | **Warm Month** | **1 s.e.** |
| | | | ***MAAT Depression - Gastropod*** | | | | | | | | | | | |
| **SG-P** | 11.9 | 1 | -3.7 | 1.1 | -12.6 | 1.3 | -10.4 | 1.4 | -7.8 | 1.4 | -1.5 | 1.4 | -15.5 | 1.4 |
| | | | | | | | | | | | | | | |
| **30 GP1-S** | 12.3 | 1.3 | -1.4 | 1.5 | -10.3 | 1.8 | -8 | 1.8 | -5.4 | 1.8 | 0.9 | 1.8 | -13.2 | 1.8 |
| **PV1-S** | 11.1 | 0.8 | -2.9 | 0.9 | -12 | 1 | -9.7 | 1.1 | -7.2 | 1.1 | -0.9 | 1.1 | -14.8 | 1.1 |
| **FW1-S** | 11.6 | 1 | -3 | 1.2 | -12 | 1.4 | -9.8 | 1.4 | -7.2 | 1.4 | -0.9 | 1.5 | -14.9 | 1.4 |
| **FW1-P** | 12 | 1.8 | -2.6 | 2 | -11.5 | 2.4 | -9.3 | 2.4 | -6.7 | 2.5 | -0.4 | 2.5 | -14.4 | 2.4 |
| | | | | | | | | | | | | | | |
| **GSF1-S** | 17.5 | 1.5 | 2.9 | 1.6 | -4.8 | 1.9 | -2.5 | 1.9 | 0.1 | 1.8 | 6 | 1.6 | -7.4 | 2.1 |
| **LRSW3-S** | 16.4 | 0.9 | 1.6 | 1 | -6.4 | 1.2 | -4.1 | 1.2 | -1.5 | 1.2 | 4.6 | 1.1 | -9.1 | 1.3 |
| | | | | | | | | | | | | | | |
| **Bonneville Basin LGM** | 11.7 | 0.3 | -2.5 | 0.7 | -11.5 | 0.6 | -9.2 | 0.8 | -6.6 | 0.8 | -0.3 | 0.8 | -14.3 | 0.6 |
| | | | | | | | | | | | | | | |
| **Sevier Basin LGM** | 16.9 | 0.5 | 2.2 | 0.9 | -5.6 | 1.1 | -3.3 | 1.1 | -0.7 | 1.1 | 5.3 | 1 | -8.3 | 1.2 |
| | | | | | | | | | | | | | | |
| **All Gastropods - LGM** | 13.5 | 2.7 | -0.9 | 2.5 | -9.5 | 3.1 | -7.2 | 3.1 | -4.6 | 3.2 | 1.6 | 3 | -12.3 | 3.2 |

**1. Reconstructions reflect assumptions of unique intervals of growth for gastropods. These values are used to calculate seasonal air temperature using transfer functions developed from the Hren and Sheldon (2012) dataset. For gastropods, the most applicable transfer function is MJJAS water temperature to MJJAS air temperature.**

**2. 1971-2000 climate normals from the PRISM Climate Group were used to calculate temperature depression at study sites.**

**Table 9: Gastropod seasonal air temperature reconstruction**

| | Water T (°C) | | Seasonal surface water temperature to Seasonal Air Temperature transfer functions (°C) | | | | | | | | | |
|---|---|---|---|---|---|---|---|---|---|---|---|---|
| **Sample** | **T-$\Delta_{47}$** | **1 s.e.** | **AMJ** | **1 s.e.** | **JJA** | **1 s.e.** | **MJJAS** | **1 s.e.** | **A-O** | **1 s.e.** | **Warm Month** | **1 s.e.** |
| | | | ***Seasonal Air Temperature - Gastropod*** | | | | | | | | | |
| **SG-P** | 11.9 | 1 | 12 | 0.9 | 12.7 | 1 | 11.7 | 1 | 10.8 | 1.1 | 12.7 | 0.9 |
| | | | | | | | | | | | | |
| **30 GP1-S** | 12.3 | 1.3 | 12.3 | 1.2 | 13 | 1.2 | 12 | 1.3 | 11.2 | 1.4 | 13 | 1.1 |
| **PV1-S** | 11.1 | 0.8 | 11.2 | 0.7 | 11.8 | 0.7 | 10.8 | 0.8 | 9.8 | 0.9 | 11.9 | 0.7 |
| **FW1-S** | 11.6 | 1 | 11.7 | 1 | 12.4 | 1 | 11.4 | 1 | 10.4 | 1.1 | 12.4 | 0.9 |
| **FW1-P** | 12 | 1.8 | 12 | 1.7 | 12.7 | 1.7 | 11.7 | 1.8 | 10.9 | 2 | 12.7 | 1.6 |
| | | | | | | | | | | | | |
| **GSF1-S** | 17.5 | 1.5 | 17 | 1.3 | 17.8 | 1.3 | 17.1 | 1.4 | 16.6 | 1.5 | 17.4 | 1.3 |
| **LRSW3-S** | 16.4 | 0.9 | 16.1 | 0.8 | 16.8 | 0.8 | 16.1 | 0.9 | 15.5 | 0.9 | 16.5 | 0.8 |
| | | | | | | | | | | | | |
| **Bonneville Basin LGM** | 11.7 | 0.3 | 11.8 | 0.5 | 12.5 | 0.4 | 11.5 | 0.5 | 10.6 | 0.6 | 12.5 | 0.5 |
| | | | | | | | | | | | | |
| **Sevier Basin LGM** | 16.9 | 0.5 | 16.6 | 0.7 | 17.3 | 0.7 | 16.6 | 0.7 | 16.1 | 0.8 | 17 | 0.6 |
| | | | | | | | | | | | | |
| **All Gastropods - LGM** | 13.5 | 2.7 | 13.4 | 2.5 | 14.1 | 2.5 | 13.2 | 2.7 | 12.4 | 2.9 | 14 | 2.4 |

**1. Reconstructions reflect assumptions of unique intervals of growth for gastropods. These values are used to calculate seasonal air temperature using transfer functions developed from the Hren and Sheldon (2012) dataset. For gastropods, the most applicable transfer function is MJJAS water temperature to MJJAS air temperature.**

**2. 1971-2000 climate normals from the PRISM Climate Group were used to calculate temperature depression at**

**Table 10: Gastropod seasonal air temperature reconstruction: LGM minus modern**

| | Water T (°C) | | Seasonal Air Temperature minus Modern Seasonal Air Temperature (°C) | | | | | | | | | |
|---|---|---|---|---|---|---|---|---|---|---|---|---|
| **Sample** | **T-$\Delta_{47}$** | **1 s.e.** | **AMJ** | **1 s.e.** | **JJA** | **1 s.e.** | **MJJAS** | **1 s.e.** | **A-O** | **1 s.e.** | **Warm Month** | **1 s.e.** |
| | | | ***Seasonal Air Temperature - Gastropod*** | | | | | | | | | |
| **SG-P** | 11.9 | 1 | -2.5 | 0.9 | -10 | 1 | -8.4 | 1 | -6.4 | 1.1 | -11.8 | 0.9 |
| | | | | | | | | | | | | |
| **30 GP1-S** | 12.3 | 1.3 | -0.7 | 1.2 | -7.8 | 1.2 | -6.2 | 1.3 | -4.3 | 1.4 | -9.5 | 1.1 |
| **PV1-S** | 11.1 | 0.8 | -1.8 | 0.7 | -8.8 | 0.7 | -7.3 | 0.8 | -5.5 | 0.9 | -10.5 | 0.7 |
| **FW1-S** | 11.6 | 1 | -2 | 1 | -9.2 | 1 | -7.7 | 1 | -5.8 | 1.1 | -11 | 0.9 |
| **FW1-P** | 12 | 1.8 | -1.6 | 1.7 | -8.9 | 1.7 | -7.3 | 1.8 | -5.3 | 2 | -10.7 | 1.6 |
| | | | | | | | | | | | | |
| **GSF1-S** | 17.5 | 1.5 | 2.7 | 1.3 | -4.4 | 1.3 | -2.5 | 1.4 | -0.2 | 1.5 | -6.5 | 1.3 |
| **LRSW3-S** | 16.4 | 0.9 | 1.5 | 0.8 | -5.7 | 0.8 | -3.7 | 0.9 | -1.5 | 0.9 | -7.8 | 0.8 |
| | | | | | | | | | | | | |
| **Bonneville Basin LGM** | 11.7 | 0.3 | -1.5 | 0.6 | -8.7 | 0.4 | -7.1 | 0.6 | -5.2 | 0.6 | -10.4 | 0.6 |
| | | | | | | | | | | | | |
| **Sevier Basin LGM** | 16.9 | 0.5 | 2.1 | 0.8 | -5.1 | 0.9 | -3.1 | 0.9 | -0.8 | 0.9 | -7.2 | 0.9 |
| | | | | | | | | | | | | |
| **All Gastropods - LGM** | 13.5 | 2.7 | -0.3 | 1.9 | -7.5 | 2 | -5.8 | 2.2 | -3.8 | 2.4 | -9.3 | 1.8 |

**1. Reconstructions reflect assumptions of unique intervals of growth for gastropods. These values were used to calculate seasonal air temperature using transfer functions developed from the Hren and Sheldon (2012) dataset. For gastropods, the most applicable transfer function is MJJAS water temperature to MJJAS average air temperature.**

**2. 1971-2000 climate normals from the PRISM Climate Group were used to calculate temperature depression at study sites.**

**Table 11: Marl annual air temperature reconstruction**

| | Water T (°C) | | Seasonal surface water temperature to Mean Annual Air Temperature transfer functions (°C) | | | | | | | | | | | |
|---|---|---|---|---|---|---|---|---|---|---|---|---|---|---|
| **Sample** | **T-$\Delta_{47}$** | **1 s.e.** | **AMJ** | **1 s.e.** | **JJA** | **1 s.e.** | **MJJAS** | **1 s.e.** | **A-O** | **1 s.e.** | **Mean Ann. Lake T** | **1 s.e.** | **Warm Month** | **1 s.e.** |
| | | | ***MAAT - Marl*** | | | | | | | | | | | |
| **30 GP2-M** | 25 | 2.6 | 20.2 | 2.3 | 14.5 | 3.1 | 16.5 | 2.9 | 18.6 | 2.6 | 22.4 | 1.4 | 12.8 | 3.6 |
| **PV2-M** | 19.7 | 1.3 | 15.1 | 1.3 | 8 | 1.6 | 10.2 | 1.6 | 12.7 | 1.5 | 18.2 | 1.2 | 5.5 | 1.8 |
| **FW2-M** | 20.6 | 1.7 | 16 | 1.6 | 9.1 | 2.1 | 11.3 | 2 | 13.8 | 1.9 | 19.1 | 1.4 | 6.8 | 2.3 |
| | | | | | | | | | | | | | | |
| **GSF2-M** | 24 | 1.7 | 19.3 | 1.6 | 13.3 | 2.1 | 15.3 | 2 | 17.6 | 1.8 | 21.7 | 1.1 | 11.4 | 2.4 |
| **LRSW3-M** | 24.8 | 2.3 | 20 | 2 | 14.3 | 2.7 | 16.2 | 2.5 | 18.4 | 2.3 | 22.2 | 1.3 | 12.5 | 3.1 |
| | | | | | | | | | | | | | | |
| **Bonneville Basin - site avg** | 21.7 | 1.6 | 17.1 | 1.6 | 10.5 | 2 | 12.7 | 1.9 | 15 | 1.8 | 19.9 | 1.3 | 8.4 | 2.2 |
| | | | | | | | | | | | | | | |
| **Sevier Basin - site avg** | 24.4 | 0.4 | 19.6 | 0.4 | 13.8 | 0.5 | 15.8 | 0.5 | 18 | 0.4 | 22 | 0.3 | 12 | 0.5 |
| | | | | | | | | | | | | | | |
| **All Marl - LGM** | 22.8 | 0.5 | 18.1 | 0.4 | 11.8 | 0.6 | 13.9 | 0.5 | 16.2 | 0.4 | 20.7 | 0.1 | 9.8 | 0.7 |

**1. Reconstructions reflect assumptions of unique intervals of growth for marl. These values are used to calculate Mean Annual Air Temperature using transfer functions (Hren and Sheldon, 2012). For marl, the most applicable transfer function is warmest month water temperature to Mean Annual Air Temperature.**

**Table 12: Marl annual air temperature reconstruction: LGM minus modern**

| | Water T (°C) | | LGM Mean Annual Air Temperature Minus Modern (°C) | | | | | | | | | | | |
|---|---|---|---|---|---|---|---|---|---|---|---|---|---|---|
| **Sample** | **T-$\Delta_{47}$** | **1 s.e.** | **AMJ** | **1 s.e.** | **JJA** | **1 s.e.** | **MJJAS** | **1 s.e.** | **A-O** | **1 s.e.** | **Mean Ann. Lake T** | **1 s.e.** | **Warm Month** | **1 s.e.** |
| | | | ***MAAT Depression - Marl*** | | | | | | | | | | | |
| **30 GP2-M** | 25 | 2.6 | 11.5 | 2.3 | 5.8 | 3.1 | 7.8 | 2.9 | 9.9 | 2.6 | 13.7 | 1.4 | 4.1 | 3.6 |
| **PV2-M** | 19.7 | 1.3 | 6.4 | 1.3 | -0.7 | 1.6 | 1.5 | 1.6 | 4 | 1.5 | 9.5 | 1.2 | -3.2 | 1.8 |
| **FW2-M** | 20.6 | 1.7 | 6.5 | 1.6 | -0.4 | 2.1 | 1.8 | 2 | 4.3 | 1.9 | 9.6 | 1.4 | -2.7 | 2.3 |
| | | | | | | | | | | | | | | |
| **GSF2-M** | 24 | 1.7 | 9.3 | 1.6 | 3.3 | 2.1 | 5.3 | 2 | 7.6 | 1.8 | 11.7 | 1.1 | 1.4 | 2.4 |
| **LRSW3-M** | 24.8 | 2.3 | 9.8 | 2 | 4.1 | 2.7 | 6 | 2.5 | 8.2 | 2.3 | 12 | 1.3 | 2.3 | 3.1 |
| | | | | | | | | | | | | | | |
| **Bonneville Basin - site avg** | 21.7 | 1.6 | 8.1 | 1.7 | 1.6 | 2.1 | 3.7 | 2 | 6.1 | 1.9 | 10.9 | 1.4 | -0.6 | 2.3 |
| | | | | | | | | | | | | | | |
| **Sevier Basin - site avg** | 24.4 | 0.4 | 9.5 | 0.3 | 3.7 | 0.4 | 5.7 | 0.4 | 7.9 | 0.3 | 11.9 | 0.2 | 1.9 | 0.4 |
| | | | | | | | | | | | | | | |
| **All Marl - LGM** | 22.8 | 0.5 | 8.7 | 0.4 | 2.4 | 0.6 | 4.5 | 0.5 | 6.8 | 0.4 | 11.3 | 0.1 | 0.4 | 0.7 |

**1. Reconstructions reflect assumptions of unique intervals of growth for marl. These values are used to calculate annual air temperature using transfer functions developed from the Hren and Sheldon (2012) dataset. For marl, the most applicable transfer function is warmest month water temperature to warmest month air temperature.**

**2. 1971-2000 climate normals from the PRISM Climate Group were used to calculate temperature depression at study sites.**

**Table 13: Marl seasonal air temperature reconstruction**

| | Water T (°C) | | Seasonal surface water temperature to Seasonal Air Temperature transfer functions (°C) | | | | | | | | | |
|---|---|---|---|---|---|---|---|---|---|---|---|---|
| **Sample** | **T-$\Delta_{47}$** | **1 s.e.** | **AMJ** | **1 s.e.** | **JJA** | **1 s.e.** | **MJJAS** | **1 s.e.** | **A-O** | **1 s.e.** | **Warm Month** | **1 s.e.** |
| | | | ***Seasonal Air Temperature - Marl*** | | | | | | | | | |
| **30 GP2-M** | 25 | 2.6 | 23.3 | 2 | 24.2 | 2.1 | 23.9 | 2.2 | 23.5 | 2.1 | 23.9 | 2.3 |
| **PV2-M** | 19.7 | 1.3 | 18.9 | 1.1 | 19.7 | 1.1 | 19.2 | 1.2 | 18.7 | 1.2 | 19.3 | 1.1 |
| **FW2-M** | 20.6 | 1.7 | 19.7 | 1.4 | 20.5 | 1.4 | 20 | 1.5 | 19.6 | 1.5 | 20.1 | 1.4 |
| | | | | | | | | | | | | |
| **GSF2-M** | 24 | 1.7 | 22.5 | 1.4 | 23.4 | 1.4 | 23 | 1.5 | 22.6 | 1.5 | 23.1 | 1.5 |
| **LRSW3-M** | 24.8 | 2.3 | 23.1 | 1.8 | 24 | 1.8 | 23.7 | 1.9 | 23.3 | 1.9 | 23.7 | 2 |
| | | | | | | | | | | | | |
| **Bonneville Basin - site avg** | 21.7 | 1.6 | 20.6 | 1.3 | 21.5 | 1.4 | 21 | 1.4 | 20.6 | 1.5 | 21.1 | 1.4 |
| | | | | | | | | | | | | |
| **Sevier Basin - site avg** | 24.4 | 0.4 | 22.8 | 0.3 | 23.7 | 0.3 | 23.3 | 0.3 | 23 | 0.3 | 23.4 | 0.3 |
| | | | | | | | | | | | | |
| **All Marl - LGM** | 22.8 | 0.5 | 21.5 | 0.4 | 22.3 | 0.4 | 21.9 | 0.4 | 21.6 | 0.4 | 22 | 0.5 |

**1. Reconstructions reflect assumptions of unique intervals of growth for marl. These values are used to calculate seasonal air temperature using transfer functions developed from the Hren and Sheldon (2012) dataset. For marl, the most applicable transfer function is warmest month water temperature to warmest month air temperature.**

**2. 1971-2000 climate normals from the PRISM Climate Group were used to calculate temperature depression at**

**Table 14: Marl seasonal air temperature reconstruction: LGM minus modern**

| | Water T (°C) | | Seasonal Air Temperature minus Modern Seasonal Air Temperature (°C) | | | | | | | | | |
|---|---|---|---|---|---|---|---|---|---|---|---|---|
| **Sample** | **T-$\Delta_{47}$** | **1 s.e.** | **AMJ** | **1 s.e.** | **JJA** | **1 s.e.** | **MJJAS** | **1 s.e.** | **A-O** | **1 s.e.** | **Warm Month** | **1 s.e.** |
| | | | ***Seasonal Air Temperature - Marl*** | | | | | | | | | |
| **30 GP2-M** | 25 | 2.6 | 10.3 | 2 | 3.4 | 2.1 | 5.7 | 2.2 | 8 | 2.1 | 1.4 | 2.3 |
| **PV2-M** | 19.7 | 1.3 | 6 | 1.1 | -0.9 | 1.1 | 1.1 | 1.2 | 3.4 | 1.2 | -3 | 1.1 |
| **FW2-M** | 20.6 | 1.7 | 6.1 | 1.4 | -1.1 | 1.4 | 1 | 1.5 | 3.4 | 1.5 | -3.3 | 1.4 |
| | | | | | | | | | | | | |
| **GSF2-M** | 24 | 1.7 | 8.1 | 1.4 | 1.2 | 1.4 | 3.4 | 1.5 | 5.8 | 1.5 | -0.9 | 1.5 |
| **LRSW3-M** | 24.8 | 2.3 | 8.5 | 1.8 | 1.5 | 1.8 | 3.8 | 1.9 | 6.3 | 1.9 | -0.6 | 2 |
| | | | | | | | | | | | | |
| **Bonneville Basin - site avg** | 21.7 | 1.6 | 7.4 | 1.4 | 0.5 | 1.5 | 2.6 | 1.5 | 4.9 | 1.5 | -1.6 | 1.5 |
| | | | | | | | | | | | | |
| **Sevier Basin - site avg** | 24.4 | 0.4 | 8.3 | 0.2 | 1.3 | 0.2 | 3.6 | 0.2 | 6.1 | 0.2 | -0.7 | 0.2 |
| | | | | | | | | | | | | |
| **All Marl - LGM** | 22.8 | 0.5 | 7.8 | 0.4 | 0.8 | 0.4 | 3 | 0.4 | 5.4 | 0.4 | -1.3 | 0.5 |

**1. Reconstructions reflect assumptions of unique intervals of growth for marl. These values are used to calculate seasonal air temperature using transfer functions developed from the Hren and Sheldon (2012) dataset. For marl, the most applicable transfer function is warmest month water temperature to warmest month air temperature.**

**2. 1971-2000 climate normals from the PRISM Climate Group were used to calculate temperature depression at study sites.**

**Table 15: Tufa annual air temperature**

| | Water T (°C) | | Seasonal surface water temperature to Mean Annual Air Temperature transfer functions (°C) | | | | | | | | | | | |
|---|---|---|---|---|---|---|---|---|---|---|---|---|---|---|
| **Sample** | **T-$\Delta_{47}$** | **1 s.e.** | **AMJ** | **1 s.e.** | **JJA** | **1 s.e.** | **MJJAS** | **1 s.e.** | **A-O** | **1 s.e.** | **Mean Ann. Lake T** | **1 s.e.** | **Warm Month** | **1 s.e.** |
| | | | ***MAAT - Tufa*** | | | | | | | | | | | |
| **CIS3** | 11.6 | 3.5 | 6.5 | 4.1 | -2.5 | 4.7 | -0.3 | 4.7 | 2.3 | 4.8 | 8.6 | 4.7 | -5.4 | 4.8 |
| **CIS7** | 17 | 2.6 | 12.4 | 2.7 | 4.6 | 3.3 | 6.8 | 3.2 | 9.5 | 3.1 | 15.5 | 2.6 | 1.9 | 3.5 |
| **CIS13** | 15.7 | 1.9 | 11 | 2 | 2.9 | 2.4 | 5.2 | 2.4 | 7.8 | 2.4 | 14 | 2.1 | 0.1 | 2.5 |
| **SIS13** | 11.9 | 3.2 | 6.8 | 3.7 | -2.2 | 4.2 | 0.1 | 4.3 | 2.7 | 4.3 | 9 | 4.3 | -5 | 4.3 |
| | | | | | | | | | | | | | | |
| **CIB1** | 10.4 | 2.4 | 5 | 2.8 | -4.2 | 3.2 | -2 | 3.2 | 0.5 | 3.3 | 6.7 | 3.4 | -7.1 | 3.2 |
| **SIB5** | 15.8 | 3 | 11.2 | 3.3 | 3.1 | 3.9 | 5.4 | 3.9 | 8 | 3.8 | 14.2 | 3.3 | 0.3 | 4.1 |
| | | | | | | | | | | | | | | |
| **CIP3** | 14.8 | 2.5 | 10.1 | 2.7 | 1.7 | 3.2 | 4 | 3.2 | 6.7 | 3.2 | 12.9 | 2.9 | -1.1 | 3.4 |
| **CIP17** | 16 | 3.5 | 11.4 | 3.7 | 3.3 | 4.4 | 5.6 | 4.4 | 8.3 | 4.3 | 14.4 | 3.7 | 0.6 | 4.7 |
| **CIP25** | 12 | 2.4 | 6.9 | 2.7 | -2 | 3.1 | 0.3 | 3.2 | 2.9 | 3.2 | 9.2 | 3.2 | -4.8 | 3.2 |
| **SIP2** | 12.6 | 2.6 | 7.6 | 2.9 | -1.2 | 3.4 | 1.1 | 3.5 | 3.7 | 3.5 | 10 | 3.4 | -4.1 | 3.5 |
| **SIP16** | 11.6 | 1.7 | 6.5 | 2 | -2.5 | 2.3 | -0.3 | 2.3 | 2.3 | 2.4 | 8.6 | 2.4 | -5.4 | 2.3 |
| | | | | | | | | | | | | | | |
| **Stansbury Tufa** | 14 | 2.7 | 9.2 | 3 | 0.7 | 3.6 | 2.9 | 3.6 | 5.6 | 3.6 | 11.7 | 3.5 | -2.1 | 3.7 |
| **Bonneville Tufa** | 13.1 | 3.9 | 8.1 | 4.4 | -0.6 | 5.2 | 1.7 | 5.2 | 4.3 | 5.3 | 10.4 | 5.3 | -3.4 | 5.3 |
| **Provo Tufa** | 13.4 | 1.9 | 8.5 | 2.1 | -0.1 | 2.5 | 2.1 | 2.6 | 4.8 | 2.6 | 11 | 2.5 | -2.9 | 2.6 |

**1. Reconstructions reflect assumptions of unique intervals of growth for tufa. These values are used to calculate Mean Annual Air Temperature using transfer functions (Hren and Sheldon, 2012). For tufa, the most applicable transfer function is JJA water temperature to Mean Annual Air Temperature.**

**Table 17: Tufa seasonal air temperature reconstruction**

| | Water T (°C) | | Seasonal surface water temperature to Seasonal Air Temperature transfer functions (°C) | | | | | | | | | |
|---|---|---|---|---|---|---|---|---|---|---|---|---|
| **Sample** | **T-$\Delta_{47}$** | **1 s.e.** | **AMJ** | **1 s.e.** | **JJA** | **1 s.e.** | **MJJAS** | **1 s.e.** | **A-O** | **1 s.e.** | **Warm Month** | **1 s.e.** |
| | | | ***Seasonal Air Temperature - Tufa*** | | | | | | | | | |
| **CIS3** | 11.6 | 3.5 | 11.7 | 3.3 | 12.3 | 3.3 | 11.3 | 3.5 | 10.4 | 3.8 | 12.4 | 3.1 |
| **CIS7** | 17 | 2.6 | 16.6 | 2.2 | 17.3 | 2.3 | 16.7 | 2.4 | 16.1 | 2.5 | 17 | 2.2 |
| **CIS13** | 15.7 | 1.9 | 15.4 | 1.7 | 16.2 | 1.7 | 15.4 | 1.8 | 14.8 | 1.9 | 15.9 | 1.6 |
| **SIS13** | 11.9 | 3.2 | 11.9 | 3 | 12.6 | 3 | 11.6 | 3.2 | 10.7 | 3.4 | 12.6 | 2.7 |
| | | | | | | | | | | | | |
| **CIB1** | 10.4 | 2.4 | 10.5 | 2.2 | 11.2 | 2.3 | 10.1 | 2.4 | 9 | 2.6 | 11.3 | 2 |
| **SIB5** | 15.8 | 3 | 15.6 | 2.7 | 16.3 | 2.7 | 15.6 | 2.9 | 15 | 3 | 16 | 2.6 |
| | | | | | | | | | | | | |
| **CIP3** | 14.8 | 2.5 | 14.7 | 2.2 | 15.4 | 2.3 | 14.6 | 2.4 | 13.9 | 2.5 | 15.1 | 2.2 |
| **CIP17** | 16 | 3.5 | 15.8 | 3 | 16.5 | 3.1 | 15.8 | 3.3 | 15.2 | 3.4 | 16.2 | 3 |
| **CIP25** | 12 | 2.4 | 12.1 | 2.2 | 12.7 | 2.2 | 11.8 | 2.4 | 10.9 | 2.6 | 12.7 | 2 |
| **SIP2** | 12.6 | 2.6 | 12.6 | 2.4 | 13.3 | 2.4 | 12.3 | 2.6 | 11.5 | 2.8 | 13.2 | 2.2 |
| **SIP16** | 11.6 | 1.7 | 11.7 | 1.6 | 12.4 | 1.6 | 11.3 | 1.7 | 10.4 | 1.9 | 12.4 | 1.5 |
| | | | | | | | | | | | | |
| **Stansbury Tufa** | 14 | 2.7 | 13.9 | 2.5 | 14.6 | 2.5 | 13.8 | 2.7 | 13 | 2.9 | 14.5 | 2.3 |
| **Bonneville Tufa** | 13.1 | 3.9 | 13 | 3.6 | 13.7 | 3.6 | 12.8 | 3.9 | 12 | 4.2 | 13.7 | 3.3 |
| **Provo Tufa** | 13.4 | 1.9 | 13.4 | 1.8 | 14 | 1.8 | 13.2 | 1.9 | 12.4 | 2.1 | 13.9 | 1.7 |

**1. Reconstructions reflect assumptions of unique intervals of growth for tufa. These values are used to calculate seasonal air temperature using transfer functions developed from the Hren and Sheldon (2012) dataset. For tufa, the most applicable transfer function is JJA water temperature to JJA air temperature.**

**2. 1971-2000 climate normals from the PRISM Climate Group were used to calculate temperature depression at sites.**

**Table 16: Tufa annual air temperature reconstruction: LGM minus modern**

| | Water T (°C) | | LGM Mean Annual Air Temperature Minus Modern (°C) | | | | | | | | | | | |
|---|---|---|---|---|---|---|---|---|---|---|---|---|---|---|
| **Sample** | **T-$\Delta_{47}$** | **1 s.e.** | **AMJ** | **1 s.e.** | **JJA** | **1 s.e.** | **MJJAS** | **1 s.e.** | **A-O** | **1 s.e.** | **Mean Ann. Lake T** | **1 s.e.** | **Warm Month** | **1 s.e.** |
| | | | ***MAAT Depression - Tufa*** | | | | | | | | | | | |
| **CIS3** | 11.6 | 3.5 | -3.7 | 4.1 | -12.7 | 4.7 | -10.5 | 4.7 | -7.9 | 4.8 | -1.6 | 4.7 | -15.6 | 4.8 |
| **CIS7** | 17 | 2.6 | 2.2 | 2.7 | -5.6 | 3.3 | -3.3 | 3.2 | -0.7 | 3.1 | 5.3 | 2.6 | -8.3 | 3.5 |
| **CIS13** | 15.7 | 1.9 | 0.8 | 2 | -7.3 | 2.4 | -5 | 2.4 | -2.4 | 2.4 | 3.8 | 2.1 | -10 | 2.5 |
| **SIS13** | 11.9 | 3.2 | -3.4 | 3.7 | -12.3 | 4.2 | -10.1 | 4.3 | -7.5 | 4.3 | -1.2 | 4.3 | -15.2 | 4.3 |
| | | | | | | | | | | | | | | |
| **CIB1** | 10.4 | 2.4 | -5.2 | 2.8 | -14.4 | 3.2 | -12.2 | 3.2 | -9.7 | 3.3 | -3.4 | 3.4 | -17.3 | 3.2 |
| **SIB5** | 15.8 | 3 | 1 | 3.3 | -7.1 | 3.9 | -4.8 | 3.9 | -2.2 | 3.8 | 4 | 3.3 | -9.8 | 4.1 |
| | | | | | | | | | | | | | | |
| **CIP3** | 14.8 | 2.5 | -0.1 | 2.7 | -8.4 | 3.2 | -6.1 | 3.2 | -3.5 | 3.2 | 2.7 | 2.9 | -11.2 | 3.4 |
| **CIP17** | 16 | 3.5 | 1.2 | 3.7 | -6.8 | 4.4 | -4.5 | 4.4 | -1.9 | 4.3 | 4.3 | 3.7 | -9.5 | 4.7 |
| **CIP25** | 12 | 2.4 | -3.2 | 2.7 | -12.1 | 3.1 | -9.9 | 3.2 | -7.3 | 3.2 | -1 | 3.2 | -15 | 3.2 |
| **SIP2** | 12.6 | 2.6 | -2.6 | 2.9 | -11.4 | 3.4 | -9.1 | 3.5 | -6.5 | 3.5 | -0.2 | 3.4 | -14.2 | 3.5 |
| **SIP16** | 11.6 | 1.7 | -3.7 | 2 | -12.7 | 2.3 | -10.4 | 2.3 | -7.9 | 2.4 | -1.6 | 2.4 | -15.6 | 2.3 |
| | | | | | | | | | | | | | | |
| **Stansbury Tufa** | 14 | 2.7 | -1 | 3 | -9.5 | 3.6 | -7.2 | 3.6 | -4.6 | 3.6 | 1.6 | 3.5 | -12.3 | 3.7 |
| **Bonneville Tufa** | 13.1 | 3.9 | -2.1 | 4.4 | -10.7 | 5.2 | -8.5 | 5.2 | -5.9 | 5.3 | 0.3 | 5.3 | -13.5 | 5.3 |
| **Provo Tufa** | 13.4 | 1.9 | -1.7 | 2.1 | -10.3 | 2.5 | -8 | 2.6 | -5.4 | 2.6 | 0.8 | 2.5 | -13.1 | 2.6 |

**1. Reconstructions reflect assumptions of unique intervals of growth for tufa. These values are used to calculate annual air temperature using transfer functions developed from the Hren and Sheldon (2012) dataset. For tufa, the most applicable transfer function is JJA water temperature to JJA air temperature.**

**2. 1971-2000 climate normals from the PRISM Climate Group were used to calculate temperature depression at study sites.**

**Table 18: Tufa seasonal air temperature reconstruction: LGM minus modern**

| | Water T (°C) | | Seasonal surface water temperature to Seasonal Air Temperature transfer functions (°C) | | | | | | | | | |
|---|---|---|---|---|---|---|---|---|---|---|---|---|
| **Sample** | **T-$\Delta_{47}$** | **1 s.e.** | **AMJ** | **1 s.e.** | **JJA** | **1 s.e.** | **MJJAS** | **1 s.e.** | **A-O** | **1 s.e.** | **Warm Month** | **1 s.e.** |
| | | | ***Seasonal Air Temperature - Tufa*** | | | | | | | | | |
| **CIS3** | 11.6 | 3.5 | -3.0 | 3.3 | -10.2 | 3.3 | -8.7 | 3.5 | -6.7 | 3.8 | -12.2 | 3.1 |
| **CIS7** | 17.0 | 2.6 | 2.0 | 2.2 | -5.2 | 2.3 | -3.4 | 2.4 | -1.0 | 2.5 | -7.5 | 2.2 |
| **CIS13** | 15.7 | 1.9 | 0.8 | 1.7 | -6.4 | 1.7 | -4.6 | 1.8 | -2.3 | 1.9 | -8.7 | 1.6 |
| **SIS13** | 11.9 | 3.2 | -2.7 | 3.0 | -10.0 | 3.0 | -8.4 | 3.2 | -6.4 | 3.4 | -12.0 | 2.7 |
| | | | | | | | | | | | | |
| **CIB1** | 10.4 | 2.4 | -4.2 | 2.2 | -11.4 | 2.3 | -9.9 | 2.4 | -8.1 | 2.6 | -13.3 | 2.0 |
| **SIB5** | 15.8 | 3.0 | 1.0 | 2.7 | -6.3 | 2.7 | -4.5 | 2.9 | -2.2 | 3.0 | -8.5 | 2.6 |
| | | | | | | | | | | | | |
| **CIP3** | 14.8 | 2.5 | 0.0 | 2.2 | -7.2 | 2.3 | -5.5 | 2.4 | -3.2 | 2.5 | -9.4 | 2.2 |
| **CIP17** | 16.0 | 3.5 | 1.1 | 3.0 | -6.1 | 3.1 | -4.2 | 3.3 | -1.9 | 3.4 | -8.3 | 3.0 |
| **CIP25** | 12.0 | 2.4 | -2.6 | 2.2 | -9.8 | 2.2 | -8.2 | 2.4 | -6.2 | 2.6 | -11.8 | 2.0 |
| **SIP2** | 12.6 | 2.6 | -2.0 | 2.4 | -9.3 | 2.4 | -7.7 | 2.6 | -5.6 | 2.8 | -11.3 | 2.2 |
| **SIP16** | 11.6 | 1.7 | -3.0 | 1.6 | -10.2 | 1.6 | -8.7 | 1.7 | -6.7 | 1.9 | -12.2 | 1.5 |
| | | | | | | | | | | | | |
| **Stansbury Tufa** | 14.0 | 2.7 | -0.7 | 2.5 | -8.0 | 2.5 | -6.3 | 2.7 | -4.1 | 2.9 | -10.1 | 2.3 |
| **Bonneville Tufa** | 13.1 | 3.9 | -1.6 | 3.6 | -8.8 | 3.6 | -7.2 | 3.9 | -5.1 | 4.2 | -10.9 | 3.3 |
| **Provo Tufa** | 13.4 | 1.9 | -1.3 | 1.8 | -8.5 | 1.8 | -6.9 | 1.9 | -4.7 | 2.1 | -10.6 | 1.7 |

**1. Reconstructions reflect assumptions of unique intervals of growth for tufa. These values are used to calculate seasonal air temperature using transfer functions developed from the Hren and Sheldon (2012) dataset. For tufa, the most applicable transfer function is JJA water temperature to JJA air temperature.**

**2. 1971-2000 climate normals from the PRISM Climate Group were used to calculate temperature depression at sites.**

**Table 19: Seasonal evaporation reconstruction – Gastropods – Linacre, 1993**

| *Gastropod Evaporation Reconstruction* | **MJJAS Air T** | **Error** | **Evaporation at Stansbury LL, 1350 m** | **Error** | **Evaporation at LGM LL, 1450 m** | **Error** |
|---|---|---|---|---|---|---|
| **Sample** | | | **MJJAS mm/day** | | **MJJAS mm/day** | |
| | | | | | | |
| **SG-P** | 11.7 | 1.0 | 5.65 | 0.50 | 5.85 | 0.47 |
| | | | | | | |
| **30 GP1-S** | 12.0 | 1.3 | 5.87 | 0.67 | 6.12 | 0.59 |
| **PV1-S** | 10.8 | 0.8 | 5.28 | 0.37 | 5.62 | 0.20 |
| **FW1-S** | 11.4 | 1.0 | 5.46 | 0.50 | 5.77 | 0.36 |
| **FW1-P** | 11.7 | 1.8 | 5.62 | 0.89 | 5.90 | 0.79 |
| | | | | | | |
| **GSF1-S** | 17.1 | 1.5 | 7.89 | 0.84 | 8.07 | 0.85 |
| **LRSW3-S** | 16.1 | 0.9 | 7.39 | 0.50 | 7.57 | 0.51 |
| | | | | | | |
| **Bonneville Basin - Gastropod Avg. LGM** | 11.5 | 0.5 | 5.56 | 0.25 | 5.85 | 0.21 |
| | | | | | | |
| **Sevier Basin - Gastropod Avg. LGM** | 16.6 | 0.7 | 7.64 | 0.35 | 7.82 | 0.36 |
| | | | | | | |
| **All Gastropods LGM** | 13.19 | 2.70 | 6.25 | 1.10 | 6.51 | 1.04 |

**Table 20: Seasonal LGM gastropod evaporation estimates – relative to modern**

| *Gastropod Evaporation Reconstruction* | **Evaporation at LGM LL, 1450 m** | **Error** | **Modern Evaporation** | **LGM minus Modern** | **Fraction of modern** |
|---|---|---|---|---|---|
| **Sample** | (mm/day) | | (mm/day) | (mm/day) | |
| | | | | | |
| **SG-P** | 5.85 | 0.47 | 10.13 | -4.28 | 0.58 |
| | | | | | |
| **30 GP1-S** | 6.12 | 0.59 | 9.05 | -2.93 | 0.68 |
| **PV1-S** | 5.62 | 0.20 | 9.24 | -3.62 | 0.61 |
| **FW1-S** | 5.77 | 0.36 | 9.62 | -3.86 | 0.60 |
| **FW1-P** | 5.90 | 0.79 | 9.62 | -3.73 | 0.61 |
| | | | | | |
| **GSF1-S** | 8.07 | 0.85 | 9.75 | -1.68 | 0.83 |
| **LRSW3-S** | 7.57 | 0.51 | 10.05 | -2.48 | 0.75 |
| | | | | | |
| **Bonneville Basin - Gastropod Avg. LGM** | 5.85 | 0.21 | 9.38 | -3.53 | 0.62 |
| | | | | | |
| **Sevier Basin - Gastropod Avg. LGM** | 7.82 | 0.36 | 9.90 | -2.08 | 0.79 |
| | | | | | |
| **All Gastropods LGM** | 6.51 | 1.04 | 9.55 | -3.05 | 0.68 |

**Table 21: Annual evaporation reconstruction – Gastropods from seasonal – Linacre, 1993**

| *Gastropod Evaporation Reconstruction* | **MJJAS Water T** | **Error** | **Evaporation at LGM LL, 1450 m** | **Error** | **Evaporation at LGM LL, 1450 m** | **Error** |
|---|---|---|---|---|---|---|
| **Sample** | | | **(m/yr)** | | **(mm/day)** | |
| | | | | | | |
| **30 GP1-S** | 12.0 | 1.3 | 1.31 | 0.13 | 3.59 | 0.35 |
| **PV1-S** | 10.8 | 0.8 | 1.20 | 0.04 | 3.30 | 0.12 |
| **FW1-S** | 11.4 | 1.0 | 1.23 | 0.08 | 3.38 | 0.21 |
| **FW1-P** | 11.7 | 1.8 | 1.26 | 0.17 | 3.46 | 0.46 |
| | | | | | | |
| **GSF1-S** | 17.1 | 1.5 | 1.73 | 0.18 | 4.74 | 0.50 |
| **LRSW3-S** | 16.1 | 0.9 | 1.62 | 0.11 | 4.44 | 0.30 |
| | | | | | | |
| **Bonneville Basin - Gastropod Avg. LGM** | 11.5 | 0.5 | 1.25 | 0.05 | 3.43 | 0.12 |
| | | | | | | |
| **Sevier Basin - Gastropod Avg. LGM** | 16.6 | 0.7 | 1.67 | 0.08 | 4.59 | 0.21 |
| | | | | | | |
| **All Gastropods LGM** | 13.19 | 2.70 | 1.39 | 0.22 | 3.82 | 0.61 |

**Table 22: Annual LGM gastropod evaporation estimates relative to modern**

| *Gastropod Evaporation Reconstruction* | **Evaporation at LGM LL, 1450 m** | **Error** | **Modern ann rate** | **LGM minus Modern difference** | **fraction of modern** |
|---|---|---|---|---|---|
| **Sample** | **(mm/day)** | **Error** | **(mm/day)** | **(mm/day)** | |
| | | | | | |
| **30 GP1-S** | 3.59 | 0.35 | 5.20 | -1.61 | 0.69 |
| **PV1-S** | 3.30 | 0.12 | 5.33 | -2.03 | 0.62 |
| **FW1-S** | 3.38 | 0.21 | 5.65 | -2.26 | 0.60 |
| **FW1-P** | 3.46 | 0.46 | 5.65 | -2.19 | 0.61 |
| | | | | | |
| **GSF1-S** | 4.74 | 0.50 | 5.73 | -1.00 | 0.83 |
| **LRSW3-S** | 4.44 | 0.30 | 5.93 | -1.49 | 0.75 |
| | | | | | |
| **Bonneville Basin - Gastropod Avg. LGM** | 3.43 | 0.12 | 5.46 | -2.02 | 0.63 |
| | | | | | |
| **Sevier Basin - Gastropod Avg. LGM** | 4.59 | 0.21 | 5.83 | -1.24 | 0.79 |
| | | | | | |
| **All Gastropods LGM** | 3.82 | 0.61 | 5.58 | -1.76 | 0.68 |

**Table 23: Precipitation reconstruction – Matsubara and Howard, 2009**

| | | | Multiplicative model | | | Additive model | | |
|---|---|---|---|---|---|---|---|---|
| **Site** | **Transfer Function Used** | **P-Modern (mm/day)** | **Precip. (mm/day)** | **Error** | **Minus Present** | **Precip. (mm/day)** | **Error** | **Minus Present** |
| **Bonneville Basin Gastropod at LGM** | **MJJAS** | 0.56 | 0.20 | 0.10 | -0.36 | 0.05 | 0.16 | -0.51 |
| **Sevier Subbasin Gastropod at LGM** | **MJJAS** | 0.60 | 0.92 | 0.22 | 0.32 | 1.19 | 0.26 | 0.59 |
| **All Gastropod at LGM** | **MJJAS** | 0.57 | 0.44 | 0.39 | -0.13 | 0.43 | 0.61 | -0.14 |
| **Stansbury Gulch Gastropod - pre-LGM** | **MJJAS** | 1.04 | 0.14 | 0.14 | -0.90 | 0.33 | 0.14 | -0.72 |

**Table 24: Proxy comparison to clumped isotope results at Lake Bonneville**

| Region | Δ MAAT (°C)[1] | ΔP[2] | ΔE[3] | Analysis | Reference |
|---|---|---|---|---|---|
| **Bonneville Basin** | **-9.2 ± 0.8** | **0.75** | **0.60 – 0.69** | **Clumped isotope - gastropod** | **This study** |
| **Sevier Subbasin** | **-3.1 ± 1.1** | **0.75** | **0.75 – 0.83** | **Clumped isotope - gastropod** | **This study** |
| **Pilot Valley Subbasin** | **-9.5 ± 3.6 to -10.3 ± 2.5** | - | **0.47 – 0.61** | **Clumped isotope - tufa** | **This study** |
| Bonneville Basin | -7.9 ± 0.9 | 0.9 | 0.7 | GCM (LGM minus Pre-Industrial) | PMIP3 Ensemble Mean[4] |
| Sevier Subbasin | -7.6 ± 0.7 | 1.0 | 0.7 | GCM (LGM minus Pre-Industrial) | PMIP3 Ensemble Mean[4] |
| Lake Bonneville | -13.0 | 1.2 to 1.3 | - | Sediment Yield Rate | Lemons et al., 1996 |
| Bonneville Basin | -6 to -7 | - | - | Floral and faunal assays of fossil packrat middens | Madsen et al., 2001 |
| Lake Bonneville | −10 ± 3 | - | 0.12 | Amino acid racemization in lacustrine gastropods and ostracods | Kaufman, 2003 |
| Lake Bonneville | -6 to -9 | - | - | Amino acid racemization in lacustrine gastropods and ostracods | McCoy 1987 |
| Lake Bonneville | -13 | 1.0 | - | GCM and RCM | Hostetler et al., 1994 |
| Grays Lake, ID - Snake River Plain | -7 to -10 | - | - | Lake core pollen record | Beiswenger, 1991 |
| Southwest USA | -10 to -11 | 0.8 to 0.9 | 0.5 | Tree lines, pollen | Galloway, 1970 |
| Bonneville and Lahontan Region | -0.2 to -5.8 | 1.0 to 2.0 | 0.4 to 1.0 | Physical lake basin models | Matsubara and Howard, 2009 |
| Great Basin | -7.0 | 1.0 | - | Nivation landform morphology | Dohrenwend, 1984 |
| Great Basin | -2.5 to -3 | 1.5 to 2.0 | - | Hydrologic balance model | Antevs, 1952 |
| Great Basin | -10 | 1.7 | 0.55 to 0.90 | Hydrologic balance model | Smith and Street-Perrot, 1983 |

1. **Change in mean annual air temperature is reported as the difference from the modern value for proxy data.**
2. **Change in precipitation is reported as a fraction of the modern value for proxy data.**
3. **Change in evaporation is reported as a fraction of the value for proxy data.**
4. **PMIP3 LGM outputs were compared to modeled pre-Industrial control values.**

**Table 25: Modern river discharge Lake Bonneville**

| | Modern Discharge ($m^3$/sec) | Source |
|---|---|---|
| Bear River | 68.0 | USGS stn 10126000 |
| Logan Canyon | 18.4 | Jewell et al., 2010 |
| Blacksmith Fork | 8.2 | Jewell et al., 2010 |
| Emigration Creek | 1.1 | Jewell et al., 2010 |
| Parleys Canyon | 3.2 | Jewell et al., 2010 |
| Mill Creek | 1.0 | Jewell et al., 2010 |
| Big Cottonwood Creek | 6.4 | Jewell et al., 2010 |
| Little Cottonwood Creek | 7.2 | Jewell et al., 2010 |
| American Fork | 5.5 | Jewell et al., 2010 |
| Jordan River | 15.0 | USGS stn 10171000 |
| Provo River | 22.6 | Jewell et al., 2010 |
| Hobble Creek | 4.4 | Jewell et al., 2010 |
| Spanish Fork | 15.2 | Jewell et al., 2010 |
| Beaver River | 1.0 | USGS stn 10234500 |
| Sevier River | 24.0 | Jewell et al., 2010 |
| **Total:** | **201.2** | |

**Table 26: Modern climate data at study sites**

| | Air temperature (°C) | | | | | P | E |
|---|---|---|---|---|---|---|---|
| | **JJA** | **MJJAS** | **A-O** | **Warmest Month** | **Mean Annual** | **(mm/day)** | **(mm/day)** |
| SG-P | 22.7 | 20.1 | 17.2 | 24.5 | 10.5 | 1.04 | 4.7 |
| | | | | | | | |
| 30 GP | 20.8 | 18.2 | 15.5 | 22.5 | 8.7 | 0.57 | 5.2 |
| PV1 | 20.6 | 18.1 | 15.3 | 22.4 | 8.7 | 0.55 | 5.3 |
| FW1 | 21.6 | 19.0 | 16.2 | 23.4 | 9.5 | 0.55 | 5.6 |
| Pilot Valley Tufa | 22.6 | 20.0 | 17.1 | 24.6 | 10.2 | 0.55 | 5.7 |
| | | | | | | 0.00 | |
| GSF1 | 22.2 | 19.6 | 16.8 | 24.0 | 10.0 | 0.64 | 5.7 |
| LRSW3 | 22.5 | 19.8 | 17.0 | 24.3 | 10.2 | 0.56 | 5.9 |

**Table 27: Modern precipitation $\delta^{18}O_{water}$**

| | | Sampling Elevation (‰ VSMOW) | | Bonneville Level - 1550m (‰ VSMOW) | |
|---|---|---|---|---|---|
| **Site** | **Elev.** | **$\delta^{18}O$ Weighted Ann. Mean** | **95% CI** | **$\delta^{18}O$ Weighted Ann. Mean** | **95% CI** |
| 30GP | 1438 | -13.5 | 0.4 | -13.7 | 0.4 |
| SG | 1362 | -13.2 | 0.5 | -13.6 | 0.5 |
| PV | 1465 | -13.4 | 0.4 | -13.5 | 0.3 |
| FW | 1453 | -13.2 | 0.4 | -13.3 | 0.4 |
| GSF | 1449 | -12.8 | 0.5 | -13.0 | 0.5 |
| OC5 | 1434 | -12.9 | 0.6 | -13.1 | 0.6 |
| LRSW3 | 1402 | -12.6 | 0.4 | -12.9 | 0.3 |

**Sources**: Bowen, G. J. (2014) The Online Isotopes in Precipitation Calculator, version 2.2.; Bowen G. J. and Revenaugh J. (2003) Interpolating the isotopic composition of modern meteoric precipitation. Water Resources Research 39(10), 1299, doi:10.129/2003WR002086. (for annual average values)

**Table 28: Lake calibration locality information**

| Site / sample | Lat. | Long. | Elev. (m) | Open or closed | Source | Type | System Type | Mineral |
|---|---|---|---|---|---|---|---|---|
| Microbialite - North Arm Great Salt Lake | 41.4 | -112.7 | 1280 | Closed | This Study | Microbialite | Lake | calcite |
| Ooid - North Arm Great Salt Lake (Spiral Jetty) | 41.4 | -112.7 | 1281 | Closed | This Study | Ooid | Lake | calcite |
| Microbialite - Great Salt Lake South Arm | 41.0 | -112.2 | 1280 | Closed | This Study | Microbialite | Lake | calcite |
| Ooid - Great Salt Lake South Arm (Antelope Island) | 41.0 | -112.2 | 1282 | Closed | This Study | Ooid | Lake | calcite |
| Walker Lake | 38.7 | -118.8 | 1190 | Closed | Petryshyn et al., 2012 | Tufa Tower | Lake | calcite |
| Pavilion Lake | 50.9 | -121.7 | 823 | Closed | Petryshyn et al., 2015 | Microbialite | Lake | calcite |
| Kelly Lake | 51.0 | -121.8 | 1070 | Closed | Petryshyn et al., 2015 | Microbialite | Lake | calcite |
| Lago Sarmiento | -51.0 | -72.7 | 77 | Closed | This study | Bioherm | Lake | calcite |
| Laguna Pozuelos | -22.4 | -66.0 | 3600 | Closed | This study | Micrite | Lake | calcite |
| Zaca Lake - 2015 Runs | 34.8 | -120.0 | 730 | Closed | This study | Micrite | Lake | calcite |
| Mar Chiquita | -30.8 | -62.5 | 68 | Closed | This study | Micrite | Lake | calcite |
| Lake Tanganyika - North Burundi Coast | -6.2 | -330.4 | 773 | Open | This study | Gastropod - Spekia Zonata | Lake | aragonite |
| Utah Spring (Clear Lake) | 39.1 | -112.6 | 1401 | Closed | This study | Gastropod | Lake | aragonite |
| Lake Mead | 36.3 | -114.4 | 372 | Open | Huntington et al., 2010 | Lake edge precipitate | Lake | calcite |
| Mono Lake tufa | 37.6 | -119.0 | 1899 | Closed | Huntington et al., 2010 | Tufa | Lake | calcite |
| Lake Crowley | 37.6 | -118.7 | 2058 | Open | Huntington et al., 2010 | Micrite | Lake | calcite |
| Blue (Eagle) Lake | 39.8 | -106.8 | 2552 | - | Huntington et al., 2010 | Core-top | Lake | calcite |
| Emerald Lake | 39.1 | -111.5 | 3093 | - | Huntington et al., 2010 | Core-top | Lake | calcite |
| South Grizzy Creek Lake | 39.7 | -107.3 | 3242 | - | Huntington et al., 2010 | Core-top | Lake | calcite |
| Tso Nag | 31.6 | 82.3 | 4810 | - | Huntington et al., 2014 | Gastropod - Lymnaeid | Lake | aragonite |

| Site / sample | Lat. | Long. | Elev. (m) | Open or closed | Source | Type | System Type | Mineral |
|---|---|---|---|---|---|---|---|---|
| Zhongba Interdune Pool | 29.7 | 84.2 | 4570 | - | Huntington et al., 2014 | Gastropod - Lymnaeid | Interdune pool | aragonite |
| Tsangpo - Creek Margin | 29.6 | 84.9 | 4580 | - | Huntington et al., 2014 | Gastropod - Radix sp. | Creek | aragonite |
| Lake Towuti Gastropod | -2.8 | 121.5 | 293 | Open | This study | Gastropod | Lake | aragonite |
| Nimgun Lake (DK93-07) | 59.6 | -160.8 | 320 | Closed | This study | Gastropod | Lake | aragonite |
| Surprise Valley | 41.5 | -120.1 | 1363.5 | Closed | This study | Evaporite crust | Lake | likely calcite |
| Vail Lake | 33.5 | -117.0 | 432 | Open | This study | Bivalve - Corbicula | Reservoir | aragonite |
| Bacalar | 18.7 | -88.4 | 2 |  | This study | microbialite | Lake | calcite |
| Laguna La Salada (LS1) | 23.4 | -101.1 | 2035 | Dry Lake | This study | micrite | Dry Lake | calcite |
| Laguna La Salada (LS2) | 23.4 | -101.1 | 2035 | Dry Lake | This study | micrite | Dry Lake | calcite |
| Laguna Las Cruces | 22.7 | -100.1 | 2106 | Dry Lake | This study | micrite | Dry Lake | calcite |
| Laguna El Potosi (EP2) | 24.8 | -99.7 | 2164 | Dry Lake | This study | micrite | Dry Lake | calcite |
| Laguna El Potosi (EP1) | 24.8 | -99.7 | 2164 | Dry Lake | This study | micrite | Dry Lake | calcite |
| Colorado River Near Yuma, AZ | 32.7 | -114.7 | 38 | River | This study | Bivalve - Corbicula | River | aragonite |
| Oak Creek Near Sedona, AZ | 34.8 | -111.8 | 1207 | River | This study | Bivalve - Corbicula | River | aragonite |
| Springs at Left Fork Santa Clara River | 37.4 | -113.5 | 2123 | Springs | This study | Gastropod | Spring | aragonite |
| Painter Spring | 39.2 | -113.4 | 1633 | Springs | This study | Gastropod - Pyrgulopsis | Spring | aragonite |

**Table 29: Lake calibration data for regressions**

| Sample | $\Delta_{47}$ ARF [1] | 1 s.e. | No. of samples | No. of runs | Water T (°C) | Water T Error | Water T Source |
|---|---|---|---|---|---|---|---|
| Microbialite - North Arm Great Salt Lake | 0.709 | 0.012 | 1 | 3 | 24.4 | 0.4 | USGS stn 10010100 Nr Saline UT |
| Ooid - North Arm Great Salt Lake (Spiral Jetty) | 0.719 | 0.014 | 1 | 8 | 24.4 | 0.4 | USGS stn 10010100 Nr Saline UT |
| Microbialite - Great Salt Lake South Arm | 0.714 | 0.012 | 1 | 3 | 24.1 | 0.5 | USGS stn 6 mi W of Antelope Island |
| Ooid - Great Salt Lake South Arm (Antelope Island) | 0.717 | 0.018 | 1 | 8 | 24.1 | 0.5 | USGS stn 6 mi W of Antelope Island |
| Walker Lake Tufa Tower Sample 1 | 0.697 | 0.011 | 1 | 2 | 24 | 4 | Beutal et al., 2001; Yuan, 2006; Petryshyn et al., 2015 |
| Walker Lake Tufa Tower Sample 2 | 0.696 | 0.005 | 1 | 2 | 24 | 4 | Beutal et al., 2001; Yuan, 2006; Petryshyn et al., 2015 |
| Walker Lake Tufa Tower Sample 3 | 0.698 | 0.009 | 1 | 2 | 24 | 4 | Beutal et al., 2001; Yuan, 2006; Petryshyn et al., 2015 |
| Pavilion Lake Microbialite | 0.732 | 0.008 | 1 | 3 | 19 | 2 | Petryshyn et al., 2015 |
| Kelly Lake Microbialite | 0.731 | 0.007 | 1 | 3 | 17 | 2 | Petryshyn et al., 2015 |
| Lago Sarmiento | 0.738 | 0.008 | 1 | 5 | 12.2 | 2 | Solari et al., 2010 |
| Laguna Pozuelos | 0.763 | 0.012 | 1 | 3 | 14.6 | 2 | Ferraro et al., 2004 |

| Sample | $\Delta_{47}$ ARF [1] | 1 s.e. | No. of samples | No. of runs | Water T (°C) | Water T Error | Water T Source |
|---|---|---|---|---|---|---|---|
| Zaca Lake - 2015 Runs | 0.701 | 0.004 | 2 | 3 | 19 | 2 | Feakins et al., 2014 (0-3 m depth) |
| Mar Chiquita | 0.761 | 0.005 | 3 | - | 14 | 2 | Reati et al., 1997 |
| Tanganyika (86-RJ-71) | 0.699 | 0.004 | 1 | 3 | 26.9 | 2 | Dettman et al., 2005; Hren and Sheldon, 2012 - 2 stations |
| Tanganyika (86-RJ-71) | 0.68 | 0.006 | 1 | 2 | 26.9 | 2 | Dettman et al., 2005; Hren and Sheldon, 2012 - 2 stations |
| Tanganyika (85-AC-53) | 0.691 | 0.008 | 1 | 1 | 26.9 | 2 | Dettman et al., 2005; Hren and Sheldon, 2012 - 2 stations |
| Tanganyika Cohen Gastropod | 0.665 | 0.036 | 1 | 3 | 26.9 | 2 | Dettman et al., 2005; Hren and Sheldon, 2012 - 2 stations |
| 19.5 North Burundi Coast - Cohen LS1 | 0.689 | 0.016 | 2 | 6 | 26.9 | 2 | Dettman et al., 2005; Hren and Sheldon, 2012 - 2 stations |
| 19.5 North Burundi Coast - Cohen SZ1 | 0.684 | 0.012 | 2 | 4 | 26.9 | 2 | Dettman et al., 2005; Hren and Sheldon, 2012 - 2 stations |
| Utah Spring (Clear Lake) | 0.76 | 0.012 | 1 | 1 | 15 | 3 | Hovingh, – field data |

| Sample | $\Delta_{47}$ ARF [1] | 1 s.e. | No. of samples | No. of runs | Water T (°C) | Water T Error | Water T Source |
|---|---|---|---|---|---|---|---|
| Utah Spring (Clear Lake) | 0.742 | 0.015 | 1 | 5 | 15 | 3 | Hovingh,– field data |
| Lake Mead | 0.709 | 0.002 | 3 | - | 24.2 | 3 | Hren and Sheldon, 2012 (April - Oct) |
| Mono Lake tufa | 0.735 | 0.006 | 3 | - | 19.5 | 3 | Fig. 5 May-Oct (Huntington et al., 2010) |
| Lake Crowley | 0.734 | 0.017 | 3 | - | 18 | 3 | Fig. 5 May-Oct (Huntington et al., 2010) |
| Blue (Eagle) Lake | 0.755 | 0.016 | 4 | - | 16 | 3 | Fig. 5 May-Oct (Huntington et al., 2010) |
| Emerald Lake | 0.775 | 0.012 | 4 | - | 12 | 3 | Fig. 5 May-Oct (Huntington et al., 2010) |
| South Grizzy Creek Lake | 0.772 | 0.023 | 3 | - | 11 | 3 | Fig. 5 May-Oct (Huntington et al., 2010) |
| Tso Nag | 0.721 | 0.01 | 1 | - | 15 | 4 | Huntington et al., 2014 |
| Zhongba Interdune Pool | 0.711 | 0.011 | 1 | - | 15 | 2 | Huntington et al., 2014 |
| Tsangpo - Creek Margin | 0.721 | 0.01 | 1 | - | 15 | 2 | Huntington et al., 2014 |
| Lake Towuti Gastropod | 0.656 | 0.006 | 3 | 14 | 29 | 1 | Tierney and Russell, 2009 |
| Nimgun Lake (DK93-07) | 0.763 | 0.013 | 7 | 10 | 8 | 3 | Lake Temps in Togiak Refuge (MacDonald, 1996) |

| Sample | $\Delta_{47}$ ARF [1] | 1 s.e. | No. of samples | No. of runs | Water T (°C) | Water T Error | Water T Source |
|---|---|---|---|---|---|---|---|
| Laguna Bacalar Microbialite | 0.685 | 0.005 | 11 | 11 | 26.3 | 2 | www.lagunabacalarinstitute.com |
| Laguna La Salada (LS1) | 0.734 | 0.006 | 1 | 2 | 23.6 | 3 | Priyadarsi et al., 2014 |
| Laguna La Salada (LS2) | 0.734 | 0.015 | 1 | 2 | 23.6 | 3 | Priyadarsi et al., 2014 |
| Laguna Las Cruces | 0.747 | 0.006 | 1 | 4 | 23.2 | 3 | Priyadarsi et al., 2013 |
| Laguna El Potosi (EP2) | 0.705 | 0.008 | 1 | 4 | 23.6 | 3 | http://atlasclimatico.unam.mx/atlas/ |
| Laguna El Potosi (EP1) | 0.702 | 0.002 | 1 | 2 | 23.6 | 3 | http://atlasclimatico.unam.mx/atlas/ |
| Springs at Left Fork Santa Clara River - Gastropod | 0.732 | 0.009 | 1 | 3 | 13 | 3 | USGS Surface Water Monitoring Program - 9409100 |
| Painter Spring Gastropod | 0.744 | 0.005 | 1 | 3 | 12.5 | 3 | USGS Technical Publication No. 56 |

**1. Samples from Huntington et al., 2010, 2014 were corrected to reflect an acid digestion fractionation factor of 0.092 per mille, following Henkes and Passey, 2013. All samples run at UCLA were digested at 90°C and corrected using the 0.092 fractionation factor.**

## 10.0 APPENDIX

## APPENDIX A: GEOLOGIC SETTING

Lake Bonneville was comprised of two major basin units, and numerous smaller subbasins. The largest unit is the Bonneville Basin, which includes the modern Great Salt Lake. The floor of the Bonneville Basin is characterized by shallow gradients. The Bear River delivers the majority of water to the Bonneville Basin. The initiation of the Bear River flow beginning at 50 ka BP increased the water budget in the Bonneville Basin by at least 30 percent (Link et al., 1999). This in part may explain why the lacustrine episode during MIS 2 reached a larger extent than previous lake cycles (MIS 6, MIS 12, MIS 16). The smaller Sevier Basin is the southern component of the lake. The Sevier and Beaver Rivers are the principal drainages feeding the Sevier Basin.

### Tephrochronology

In addition to radiocarbon, volcanic ashes provide a robust correlative tool at Bonneville (Fig. A1). The Hansel Valley Eruption, (31.3 ka BP) dispersed a basaltic ash that coincides with the onset of transgression (Oviatt and Nash, 1989; Oviatt et al., 1992). In the northern half of the Bonneville Basin, transgression has been further constrained with Thiokol basaltic ash, erupted at 26.5 ka BP. The Pony Express ash (circa 20 ka BP) erupted during the LGM (Oviatt et al., 1994), and the Pahvant ash occurs within 15 meters of the lake highstand (Oviatt and Nash, 1989; Oviatt et al., 1994). During the Provo phase of the lake, the Tabernacle Hill Basalt erupted into Black Rock Desert shortly after the Bonneville Flood. The Mazama Ash (c. 7.6 ka) is also well represented in the basin (Oviatt and Nash, 1989). Ash is often distinct in outcrop and is useful for orienting oneself in the field.


**Figure A1**: The Pahvant Butte ash within Bonneville marl at the Great Stone Face field site. Pahvant Butte erupted when Lake Bonneville was within 15 m of its highstand.

**Overview of Sequences prior to Bonneville**

The record for the systems preceding Lake Bonneville is sparse, as lake sediments are reworked extensively during interlacustral periods (Scott et al., 1983; Machete et al., 1992; Oviatt et al., 1999; Balch et al., 2005). In the 1970 Burmester core from the Great Salt Lake, Eardley et al. (1973) originally identified ~28 lacustrine parasequences covering ~780 ka. More recent investigations (Oviatt et al., 1999) consolidate these into 4, which correspond with cold

periods in the marine record (OIS 2, 6, 12, 16).

**Cutler Dam (**60 ka BP)

**Little Valley Lake** (~150 ka BP)

**Pokes Point Lake** (417 +/- 55 ka BP)

**Lava Creek Lake** (~620 ka BP)

Debbie Balch and Andy Cohen at the University of Arizona drilled a new core in 2000, using the Glad-800 rig. A continuous core drilled to a depth of 121 m below the lake core records 280 ka of lake history. This record begins at OIS 8.4: 280 – 230 ka BP, where shallow marshes and saline to hypersaline lake conditions are prevalent. From ~230,000 – 86,000 years BP, the general trend is for continuous saline to hypersaline conditions. High salinity over this time is implied by abundant evaporites (including gypsum and halite), interbedded with carbonate muds, and few brine shrimp fossils, and an absence of ostracodes and mollusks. The Little Valley cycle at OIS 6 (170,000 +/- 20,000 years BP) contains freshwater ostracodes, and is a brief exception to the more typical saline conditions. The Little Valley cycle, is followed by an evaporite unit. There may have been no water in the basin for much of OIS 5. The Cutler Dam (minor) transgression at OIS 4 (60 +/- 6 ka BP), is defined by a brief interval of low frequency ostracodes. The Cutler Dam Lake appears to have been brackish and relatively shallow.

**The Bonneville Cycle**

The initial onset of transgression was not uniform across the subbasins of Bonneville, due to local variations in hydrology. Prior to 32 ka BP, ephemeral saline lakes were present in

the Great Salt Lake subbasin of Bonneville (Balch et al., 2005).

**Stansbury Level (1,370 m AMSL)**

The Stansbury Shoreline (1,370 m elevation) was briefly established 1-2 times during the transgressive phase. A fall in lake level of 30-50m, between 25.8 and 24.5 ka BP, defines the Stansbury Oscillatory period (Oviatt et al., 1992; Oviatt, 1997). The Stansbury Oscillation correlates with Heinrich Event 2, although it is not clear whether lake levels dropped synchronously with ice rafting in the North Atlantic or slightly out of phase. In outcrop, falling lake events during the Stansbury Oscillation are manifest as gravel wedges between clay and marl. The existence of a teleconnection with the North Atlantic is further supported regionally, where montane glaciers in the Wasatch and Uinta Mountains, east of the Bonneville Basin, also retreated and advanced contemporaneously with the lake (Clark and Bartlein, 1995).

In outcrop, falling lake events during the Stansbury are manifest as gravel wedges between clay and marl, emplaced when the lake was deeper (Gilbert, 1890; McCoy, 1987; Oviatt et al., 1994b). Gilbert (1890) documented an outcrop of yellow clay and white marl separated by gravel wedge ~60 km NW of Leamington, UT as the Stansbury interval.

**Bonneville Shoreline (1,550 m AMSL)**

Following the Stansbury period, the lake experienced a prolonged transgression up to the Bonneville shoreline, 1,550 m elevation (Oviatt, 1997; Oviatt et al., 1999). Lake levels rose at approximately 60m/ka during this interval (Oviatt et al., 1992). Three oscillations have been defined during the post-Stansbury transgressive period. They occur from 22.8 to 22.0 ka BP,

21.3 to 20.2 ka BP, and 19.7 to 19.0 ka BP (Oviatt et al., 1992; Godsey et al., 2011; Miller et al., 2011). Oscillations during the transgressive interval, when the lake was hydrologically closed, indicate intervals of diminished moisture (Precipitation-Evaporation). Shortly after the LGM, the lake began to overflow at an alluvial dam at the northern margin, near Red Rock Pass, in Southern Idaho (Jarrett and Malde, 1987; Janecke and Oaks, 2011). The development of an outlet prevented lake levels from rising above 1,550 meters. The highstand was extremely short in duration, and terminated with the Bonneville Flood at 18 ka BP.

**Bonneville Flood (18 ka)**

Lake levels abruptly dropped ~100 m after an alluvial dam was breached at Zenda pass in S. Idaho (Currey, 1982; Jarrett and Malde, 1987; Oviatt et al., 1992; O'Connor, 1993). During the flood, the average discharge rate is estimated to have been between 793,000 and 1,020,000 cubic meters per second (Jarrett and Malde, 1999). Approximately 4,700 cubic kilometers of water was released from the lake. The flood was short-lived: < 1 year, possibly less than 1 mo (Malde, 1968). After the flood the outlet shifted from Zenda to Red Rock Pass. There appears to be a correlation between the failure of the alluvial dam at Zenda and movement along the Riverdale Fault nearby. However, it is not clear whether movement along the fault induced the flood, or occurred after, as a result of unloading at the hanging wall (Janecke and Oaks, 2011).

**Provo Shoreline (1,450 m AMSL)**

The lake remained hydrologically open throughout the Provo Phase (Oviatt, 1997; Benson et al., 2011). The Provo Shoreline is typically the most well developed geomorphic feature in the Bonneville and Sevier Basins (Miller et al., 2013). Sack (1999) questions the

relative age of the Provo shoreline, and favors a rapid recession of lake levels following the Bonneville Flood. She argues that Provo landforms appear artificially large because sediments of Provo age lie atop Bonneville sediments, and in many cases the division between the two is not distinct. Although there is some disagreement on the duration of the Provo shoreline, recent chronostratigraphic work indicates rapid recession by 14.5 ka BP (Miller et al., 2013). The floral record indicates that the Provo climate may have been wetter and/or warmer than the full glacial regime (Madsen et al., 2001). However, because open system conditions define both the Bonneville and Provo intervals it is difficult to compare hydrologic input from geomorphology alone.

**Post-Provo Recession**

Closed basin conditions were permanently established after lake levels dropped below the Provo threshold (Miller et al., 2013; Oviatt, 2015). The Post-Provo recession roughly correlates with the termination of H1 (Oviatt, 1997). During the final recession, the higher elevation Sevier Basin became hydrologically disconnected from the Bonneville Basin. As the lake dropped, the Sevier River cut downwards through the Bonneville highstand delta and reworked sediments (Oviatt et al., 1994). Lake levels continued to drop steadily, but temporarily rose to the Gilbert shore during the Younger Dryas (Oviatt et al., 1992; Oviatt et al., 2005; Oviatt, 2014a). During the Holocene, lake levels dropped below the Gilbert level and typically remained at the modern Great Salt Lake shore at 1,280 meters. Periodically, the lake may have dried almost entirely, as mud crack structures occur below the bed of the Great Salt Lake (Balch et al, 2005). From 4.5 to 3 ka BP, a shift in the dominant flora from desert scrub to pine and sage suggests a shortlived cooling trend (Madsen et al, 2001).

## APPENDIX B: MODERN CLIMATE

### Air Temperature at Study Sites

Modern Mean Annual Air Temperatures (MAAT) at sites evaluated in this study range from 8.7 to 10.5°C. Summer air temperatures over the June through August (JJA) interval range from 20.8 to 22.7°C. Average annual precipitation at sites ranges from 205 to 380 mm. May is the wettest month, accounting for 11 to 14 percent of annual precipitation at sites. For this study, climate normals from the 1971 to 2000 period of record were evaluated. Stansbury Gulch is an outlier in both respects. This site is on the eastern side of the Bonneville Basin and receives 380 mm of annual precipitation, which is significantly greater than the mean value of 220 mm for all other sites. Orographic forcing from the Wasatch Mountains accounts for greater precipitation delivery on the eastern side of the Basin.

### Oxygen Isotope Values in Waters at Study Sites

Oxygen isotope measurements of surface water and precipitation provide context for local and regional scale hydrologic processes, including evaporation trends within watersheds (Coplen and Kendall, 2000; Bowen and Ravenaugh, 2003). For further definition of stable isotope notation, refer to Methodology. The mean oxygen isotope value for modern annual precipitation across sites is -13.1‰ V-SMOW, with values ranging from -13.5 to -12.6‰ V-SMOW (Bowen, 2014; Bowen and Ravenaugh, 2003). When site elevations are normalized to the Bonneville lake level of 1550m AMSL, the mean precipitation $\delta^{18}O$ value across all sites is -13.3‰, and ranges from -13.7 to -12.9‰ V-SMOW (Bowen, 2014; Bowen and Ravenaugh, 2003). Precipitation during the December through February interval (DJF) is the most depleted with respect to $^{18}O$, with a mean value of -16.6 ‰ across all sites, normalized at

1550 m elevation. Summer precipitation is the most enriched, with an average $\delta^{18}O$ value of -9.8‰ across all sites, normalized to 1550m.

**Oxygen Isotopes in Modern Rivers**

River input accounts for much of the water budget in the modern Great Salt Lake, and likely exhibited a strong forcing on lake levels during the LGM. Rivers across the region derive water from snowmelt in the Wasatch and Uinta Mountains along the eastern margin of the basin. At the modern Great Salt Lake, the principal inflow is sourced from the Bear and Weber Rivers. At its mouth near Corinne (Fig. B1), Bear River water exhibits mean $\delta^{18}O$ of -15.0 ‰ V-SMOW, with values for discharge ranging between -16.4 and -13.3‰ (Coplen and Kendall, 2000). Average $\delta^{18}O$ in the Weber River (Fig. B1) at Plain City, near its terminus, is -15.9‰, and ranges between -16.4 and -14.9‰ (Coplen and Kendall, 2000). In the Sevier Subbasin, the Sevier River exhibits mean $\delta^{18}O$ of -13.3‰, and ranges between -13.9 and -12.5‰ (Coplen and Kendall, 2000). Weighted annual precipitation $\delta^{18}O$ for study sites in the Sevier Basin is -12.8‰, while the average at study sites within the Bonneville Basin is -13.3‰ (Bowen, 2014; Bowen and Ravenaugh, 2003). Rivers derive water from snowmelt at high elevations that is more depleted with respect to $^{18}O$, which accounts in part for the offset from precipitation at sites.

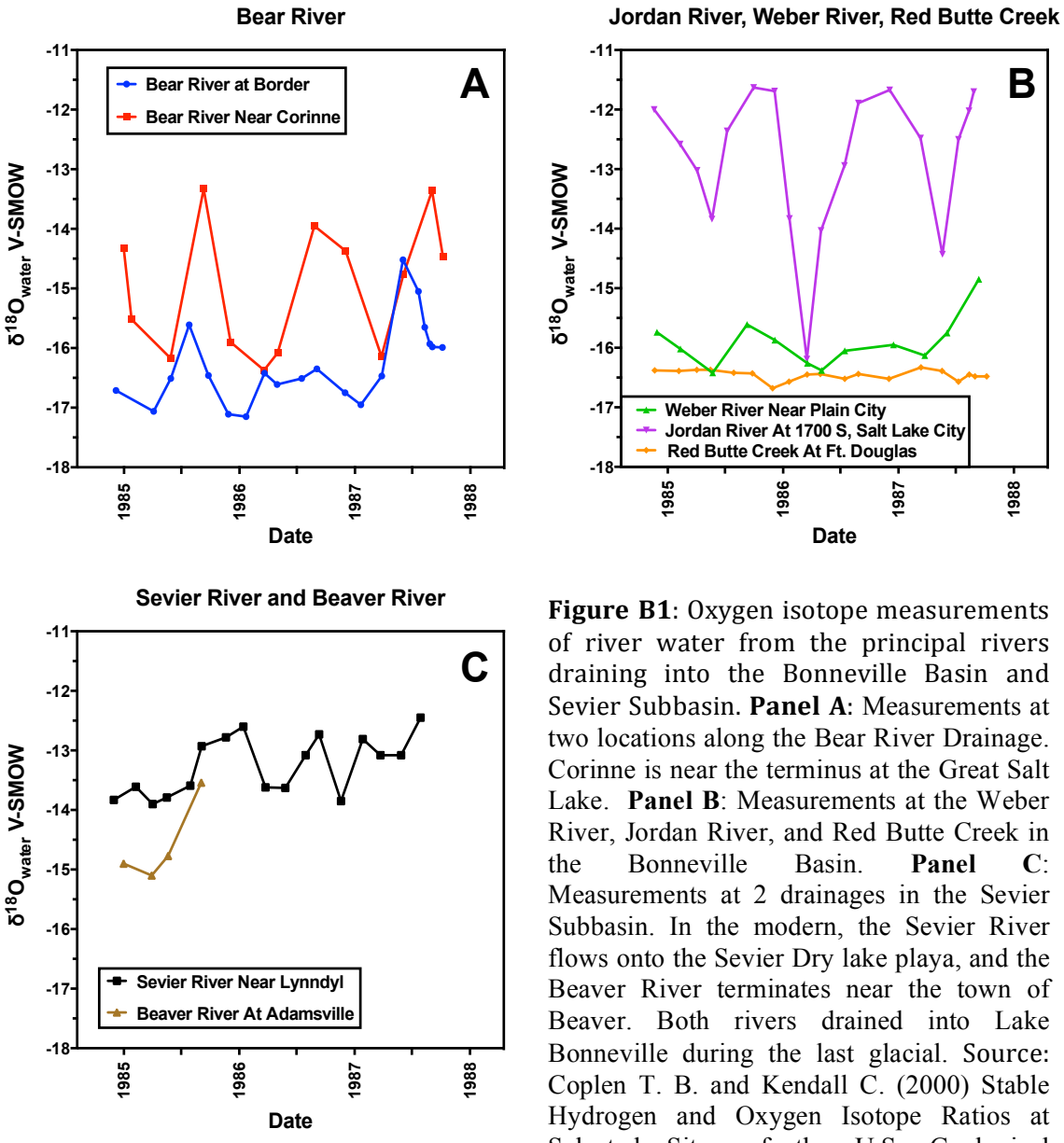


**Figure B1**: Oxygen isotope measurements of river water from the principal rivers draining into the Bonneville Basin and Sevier Subbasin. **Panel A**: Measurements at two locations along the Bear River Drainage. Corinne is near the terminus at the Great Salt Lake. **Panel B**: Measurements at the Weber River, Jordan River, and Red Butte Creek in the Bonneville Basin. **Panel C**: Measurements at 2 drainages in the Sevier Subbasin. In the modern, the Sevier River flows onto the Sevier Dry lake playa, and the Beaver River terminates near the town of Beaver. Both rivers drained into Lake Bonneville during the last glacial. Source: Coplen T. B. and Kendall C. (2000) Stable Hydrogen and Oxygen Isotope Ratios at Selected Sites of the U.S. Geological Survey's NASQAN and Benchmark Surface Water Networks, OFR 00-160

## Oxygen Isotope Chemistry of the Great Salt Lake

The average $\delta^{18}O$ of the Great Salt Lake varies as a function of river inflow, precipitation, and evaporation (Pedone, 2002). Evaporative enrichment accounts for the

significant offset between precipitation, runoff, and lake water $\delta^{18}O$ values (Pedone, 2002). From 1979 and 1982, the oxygen isotope value of the South Arm of the Great Salt Lake ranged between -2.6 and -3.6‰, while the North Arm ranged between -1.1 and -2.9‰ (Pedone, 2002). The lake underwent significant expansion from 1982 until 1986. During this time, surface waters in the South Arm exhibited $\delta^{18}O$ values ranging from -2.9 to -10.1‰, while North Arm surface waters were -2.0 to -5.6‰ (Pedone, 2002). From 1993 to 1996, $\delta^{18}O$ values in the South Arm returned to a pretransgressive state, with South Arm values ranging between -2 and -6‰, and North Arm values, ranging between 0 and -2‰ (Pedone, 2002). The lake annually undergoes evaporative enrichment of $^{18}O$ relative to $^{16}O$ during the summer. $\delta^{18}O$ is lowest in spring, when rivers deliver isotopically depleted snowmelt (Pedone, 2002).

## APPENDIX C: CLIMATE MODEL OUTPUTS

In this study, clumped isotope based reconstructions of temperature, evaporation, and precipitation were directly compared to PMIP3 models. However, the gridded pre-Industrial values utilized in the PMIP3 models differ from observed modern climate in many cases. Thus, the magnitude of change in these parameters relative to modern for clumped isotopes, and pre-Industrial control values for models, was also considered. In many cases, the difference between a given LGM climate reconstruction and control value is a more directly comparable benchmark by which to compare, and evaluate, the performance of individual models against proxy data. Figures C2 and C3 graphically represent Paleoclimate Modeling Intercomparison Project Phase 3 (PMIP3) pre-Industrial control values and modern climate parameters for the Bonneville Basin and Sevier Subbasin.

### List of Figures

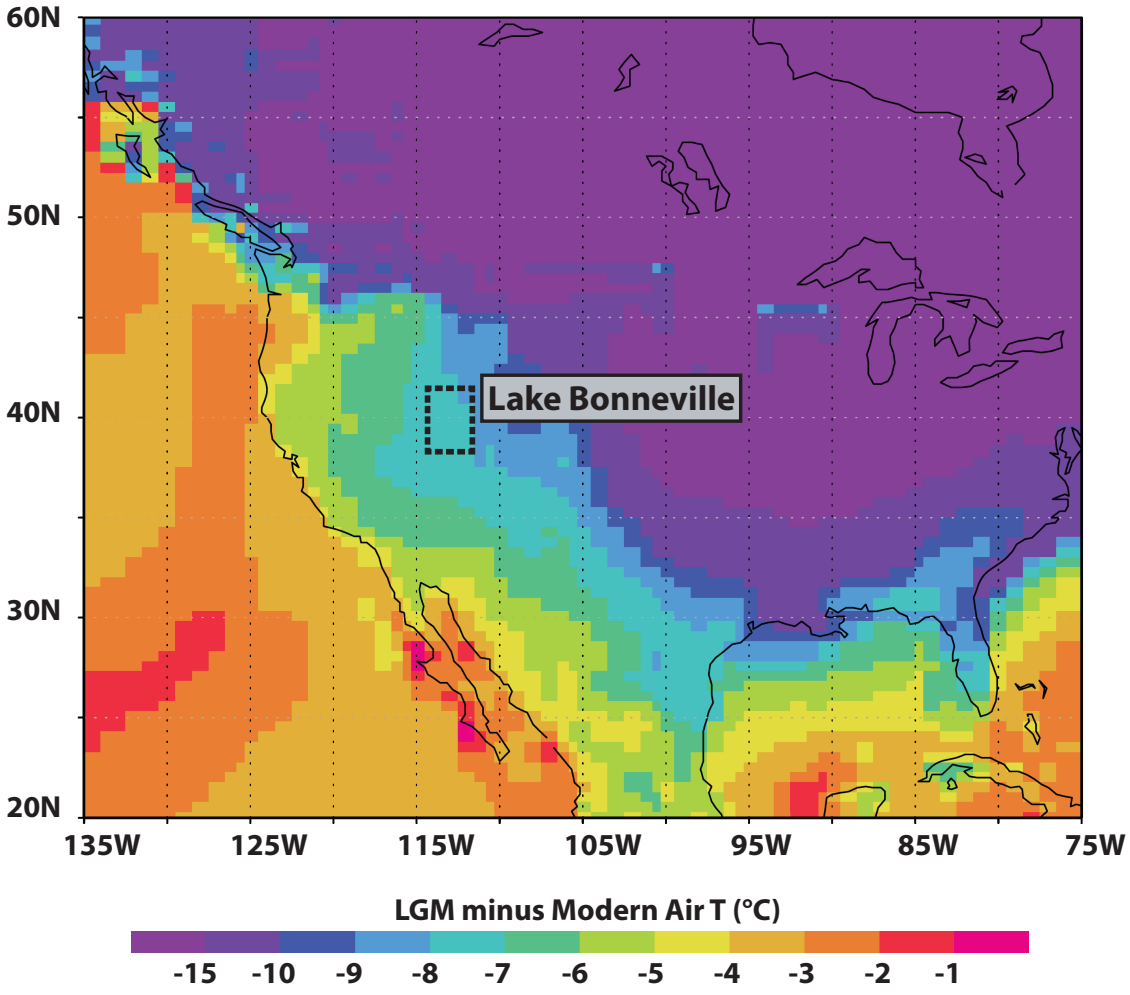


**Figure C1**: ***The LMDZ climate model indicates that air temperatures were depressed by 7-8°C below modern at Bonneville during the LGM.*** The gastropod clumped isotope reconstruction of annual air temperature at Lake Bonneville indicates 9-10°C of temperature depression. The model output shown here is considered preliminary at this time (Risi, 2014).

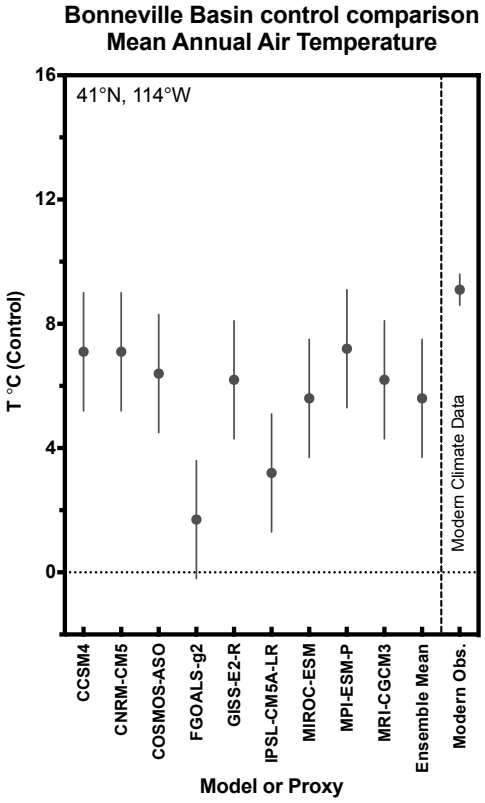


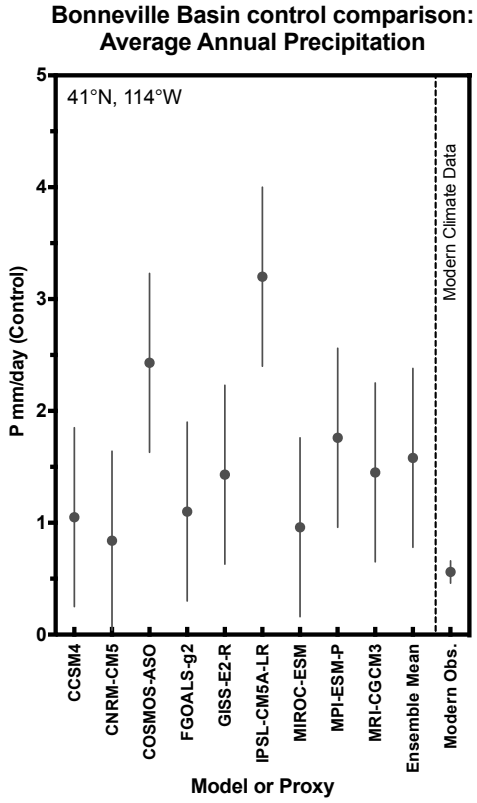


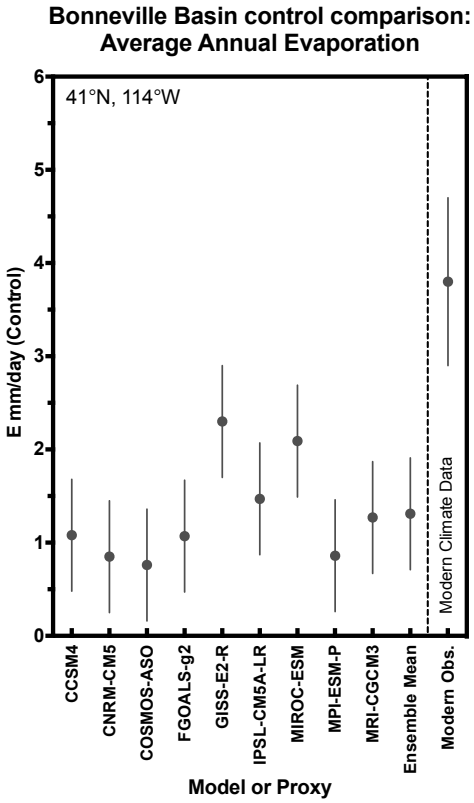


**Figure C2**: Bonneville Basin PMIP3 pre-industrial control values compared to modern climate parameters.

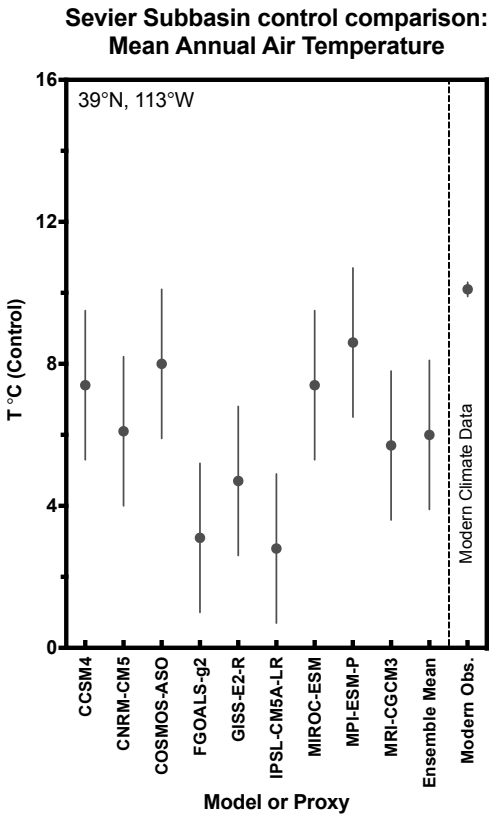


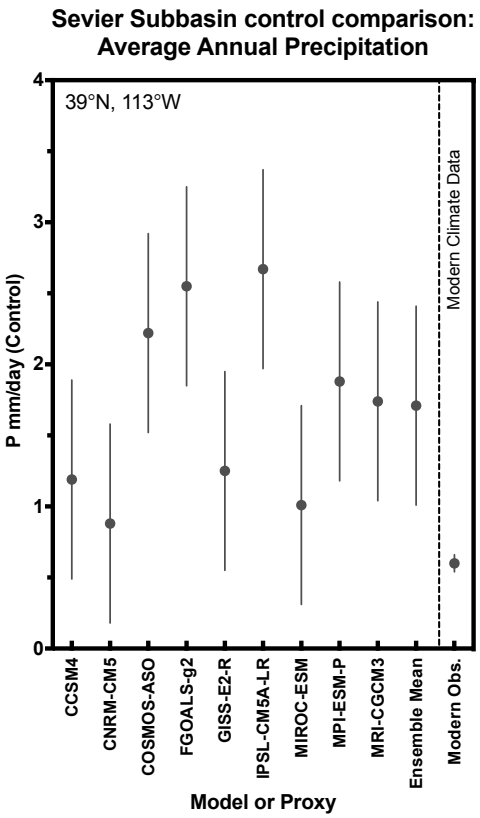


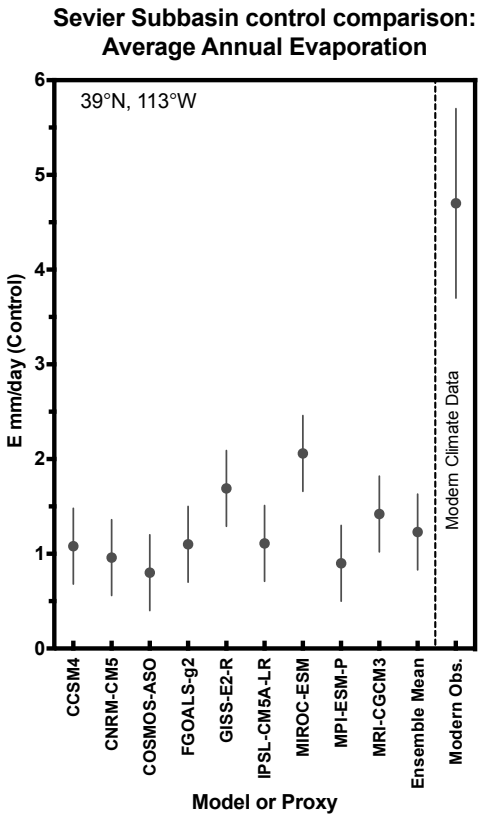


**Figure C3**: Sevier Subbasin PMIP3 pre-industrial control values compared to modern climate parameters.

## APPENDIX D: WATER BUDGET CALCULATIONS

### Water budget reconstruction

The water budget in a lake basin is comprised of hydrologic input and output components (Mifflin and Wheat, 1979). These variables are defined below:

$$\Delta S = A_L P_L - A_L E_L + RO - S_o \pm GW$$

($\Delta S$) = change in storage ($m^3/yr$)

($A_L$) = Area of lake

(RO) = Runoff ($m^3/yr$)

($P_L$) = precipitation (m/yr)

($E_L$) = evaporation (m/yr)

($S_I$) = Stream inflow ($m^3/yr$)

($S_O$) = Stream inflow ($m^3/yr$)

(GW) = Groundwater flux in, or out, of the lake ($m^3/yr$)

During the transgressive phase of lake Bonneville, the lake was a closed basin system. Therefore, outflow ($S_O$) stream outflow is zero. Groundwater inputs are difficult to quantify (Oviatt, 2015), but estimates at the modern Great Salt Lake indicate a contribution of approximately 3% (USGS, 1990). This value has not been constrained for Lake Bonneville. Estimates for stream inflow at Lake Bonneville are presented in previous work, based upon geomorphic study of fluvial deposits (Lemons et al., 1996). A refined hydrologic budget equation is provided below that can be used to solve for precipitation over Lake Bonneville:

$$\Delta S = A_L P_L - A_L E_L + S_I$$

Here, evaporation is the only water loss component of significance. A positive change in storage results from increases in precipitation over the lake, and surface runoff, relative to evaporation. The effective precipitation over the lake (P – E), plus runoff from the basin (Si) determines the magnitude by which ΔS will be positive or negative.

Evaporation estimates from LGM gastropod samples were applied to estimate the amount of precipitation over the lake required to maintain steady shorelines at 1,450 m AMSL, the average lake level during the LGM. Balancing water loss with precipitation and river input, generates a first order estimate of the influx of water required to maintain a stable shoreline. River input and precipitation were assumed to increase or decrease over the lake by equal percentages. The requisite precipitation to balance evaporation was also considered at modern river discharge rates, 1.3 times modern (Lemons, 1997), and double modern (Jewell, 2010). These analyses suggest that moisture input would have been 2.7 to 3.7 times modern levels. These values are higher than expected. This approach underestimates, or does not adequately consider, all the relevant hydrologic variables, including groundwater input and overland flow into the lake.

This type of reconstruction should be interpreted with caution. The evaporation/runoff balance model presented here oversimplifies the Bonneville system in several key ways. First, groundwater flux is not considered. In the modern era, groundwater comprises approximately 3 percent of the Great Salt Lake water budget (USGS), but may have represented a larger component of the lake water budget during the LGM. Other hydrologic components of the lake system that are not specifically quantified include: direct overland flow into the lake, seasonal

bias in moisture delivery, the role of snow/ice melt from regional glaciers on the spring-summer runoff regime, and spatial variations in precipitation and evaporation across the basin. Evaporation may have been reduced by ice cover during the fall and winter time. The eastern margin, which abuts the Wasatch Mountains, is 30 to 70 percent wetter than the western shore, where samples were collected for this study (PRISM, 2014). If a similar E-W precipitation gradient were maintained during the LGM, the selection of modern precipitation data for a reference point would also influence hydrologic budget results.

## APPENDIX E: CLUMPED ISOTOPE LAKE CALIBRATION

The following contains regression figures, and site profiles for the clumped isotope lake calibration utilized in this thesis. Clumped isotope values were compared to calcification temperatures at modern lakes, springs, and rivers in North America, South America, Africa, Tibet, and Indonesia. Samples evaluated include: biogenic carbonate, micrite, microbialite, and tufa (Figure E1). Regressions are presented in figures E2-E10. Tables 28-29 include water temperature, clumped isotope ($\Delta_{47}$) results, and lake basin hydrographic data used to generate calibrations.

### List of figures



### List of tables

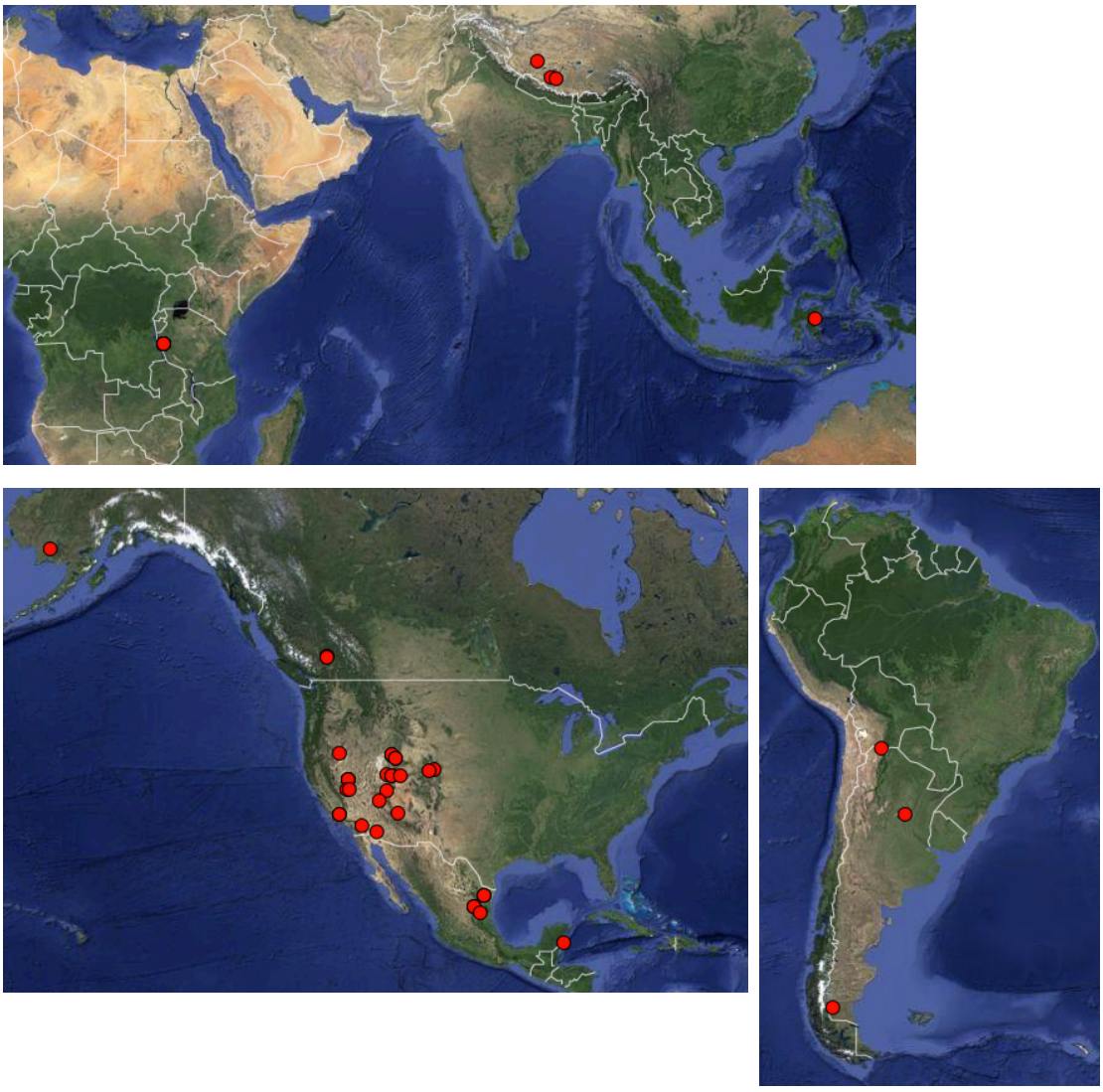

**Figure E1:** ***Site coverage for clumped isotope lake calibration is geographically extensive, and includes aragonitic and calcitic carbonate phases.*** Biogenic shells include: unionid bivalves, lymnaeid gastropods, hydrobiid gastropods. Biologically mediated and abiotic carbonates include: microbialites, tufa, micrite, playa evaporites. Sites include: freshwater lakes, closed basin saline lakes, spring-fed lakes, playas, and rivers.

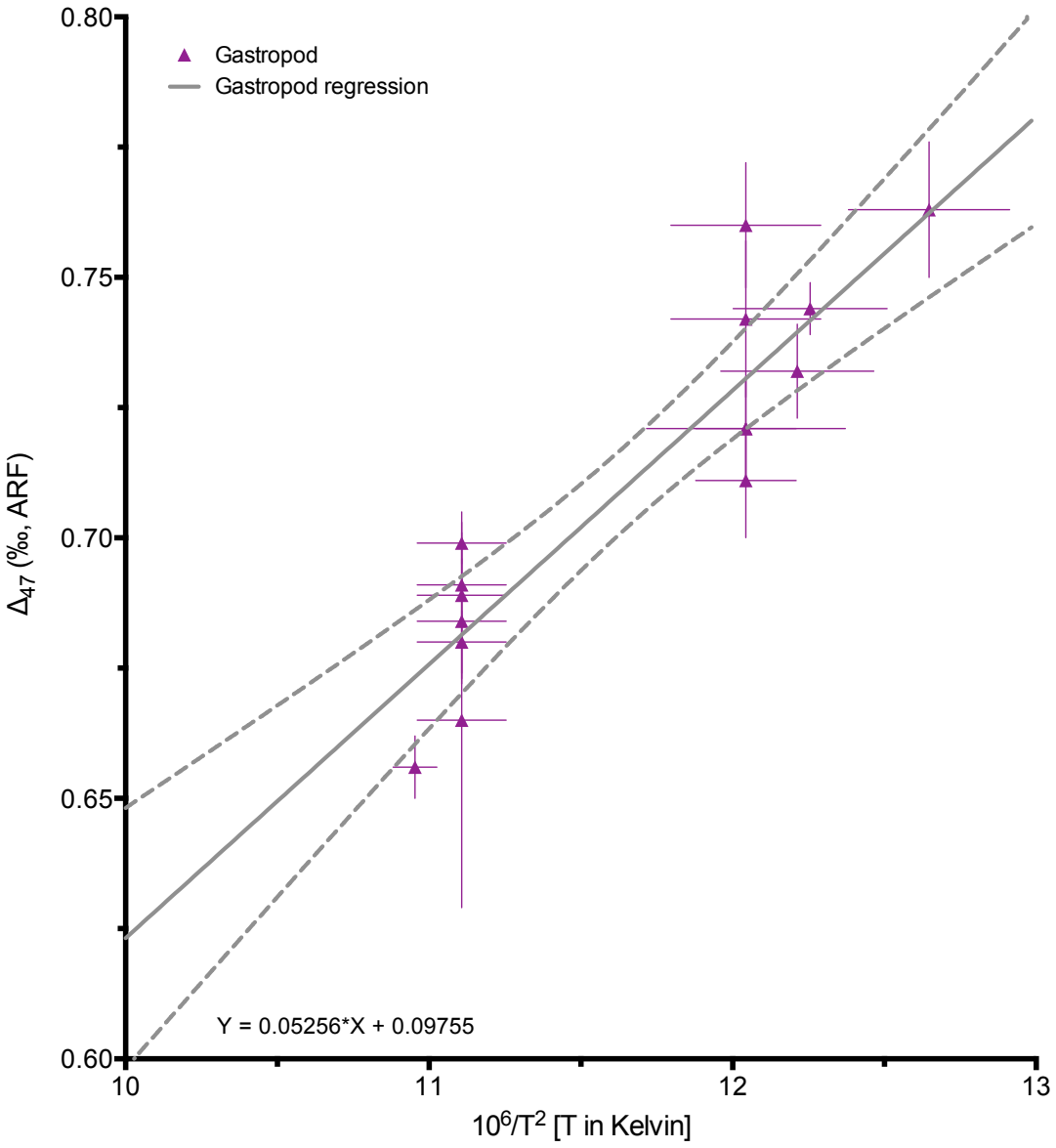


**Figure E2**: ***Lake calibration regression for modern gastropods***. The water temperature, $\Delta_{47}$ clumped isotope temperature, and locality information are provided in Tables 4-5. The gastropod regression includes a compilation of data from the Tripati Lab at UCLA and the Eiler Lab at the California Institute of Technology (Huntington et al., 2014; this study). All sample $\Delta_{47}$ data was calculated on the Absolute Reference (Dennis et al., 2011). For samples that underwent acid digestion at 90 °C, a correction term of 0.092 was added to the $\Delta_{47}$ value (Henkes et al., 2013). Uncertainties of individual samples are reported with 1 s.e. The uncertainty of the calibration line is reported with a 95% confidence band. Regression statistics: $R^2$ = 0.83, n = 15 samples, p value < 0.0001. The Celsius temperature range displayed above is 4.2 – 43 °C.

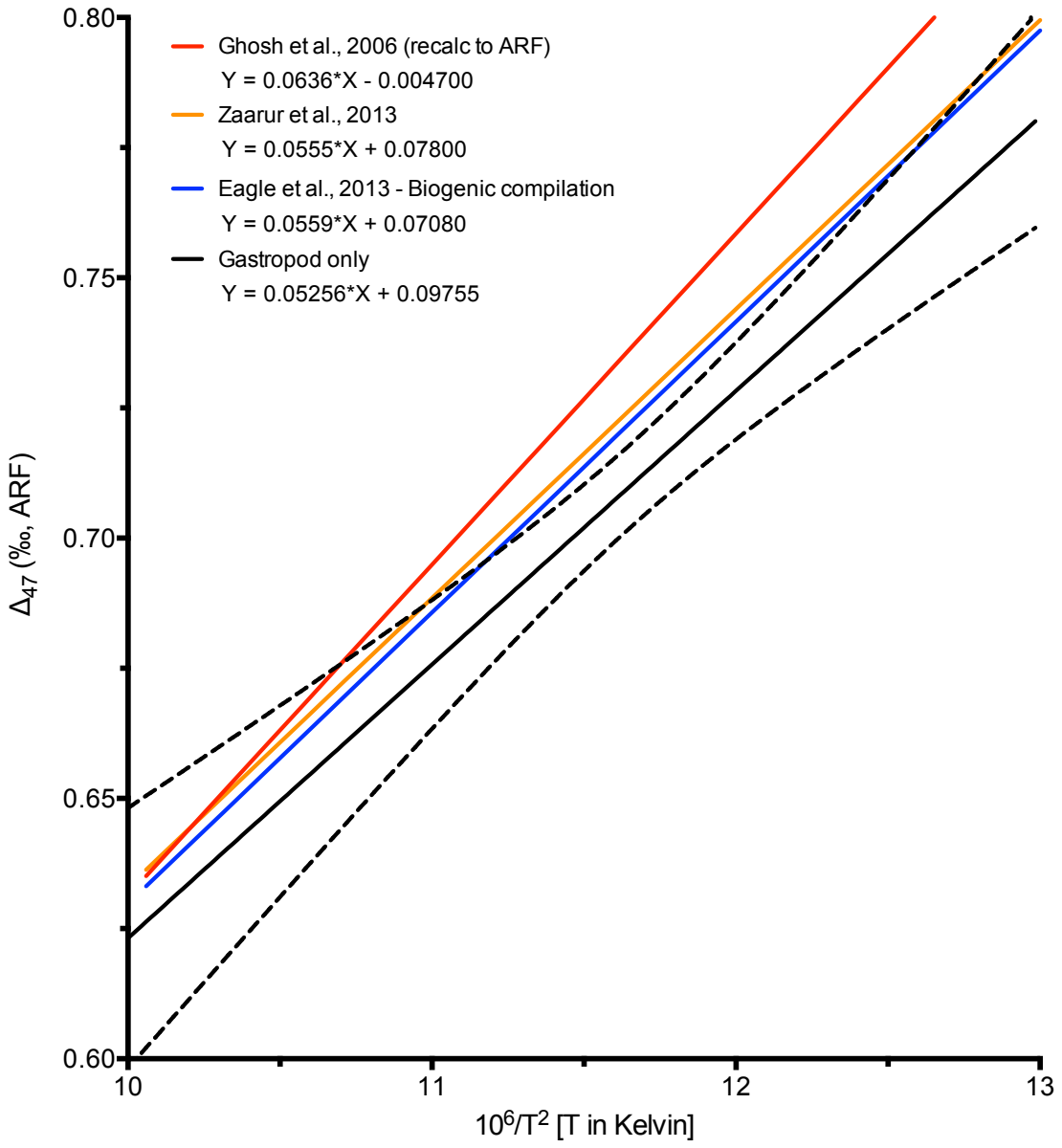


**Figure E3**: ***Lake gastropod calibration compared with published steep slope clumped isotope calibrations***. The water temperature, $\Delta_{47}$ clumped isotope temperature, and locality information are provided in Tables 4-5. The gastropod regression includes a compilation of data from the Tripati Lab at UCLA and the Eiler Lab at the California Institute of Technology (Huntington et al., 2014; this study). All sample $\Delta_{47}$ data was calculated on the Absolute Reference (Dennis et al., 2011). For samples that underwent acid digestion at 90 °C, a correction term of 0.092 was added to the $\Delta_{47}$ value (Henkes et al., 2013). The uncertainty of the calibration line is reported with a 95% confidence band. Regression statistics: $R^2$ = 0.83, n = 15 samples, p value < 0.0001. The Celsius temperature range displayed above is 4.2 – 43 °C.

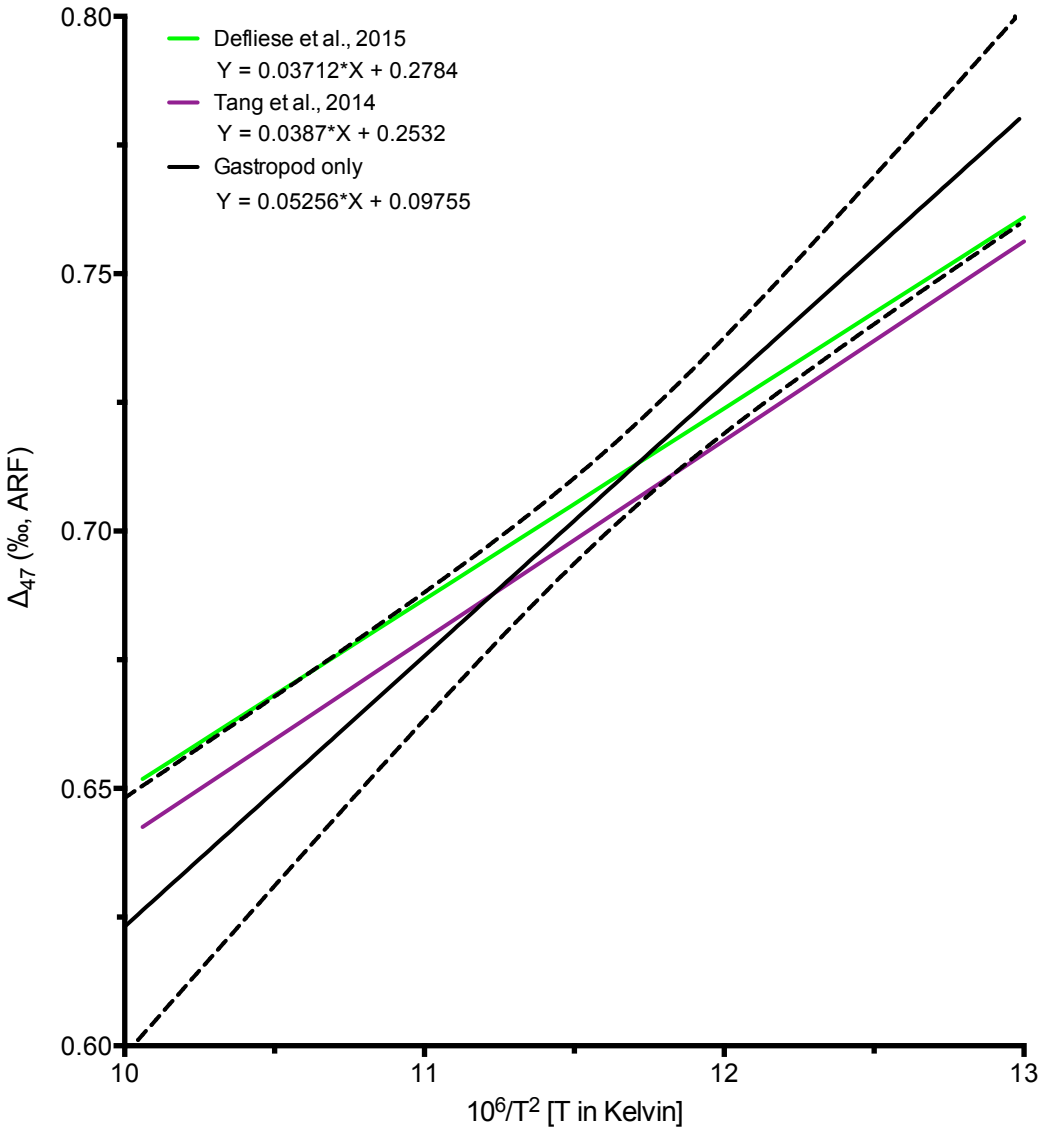


**Figure E4**: ***Lake gastropod calibration compared with published shallow slope clumped isotope calibrations.*** The water temperature, $\Delta_{47}$ clumped isotope temperature, and locality information are provided in Tables 4-5. The gastropod regression includes a compilation of data from the Tripati Lab at UCLA and the Eiler Lab at the California Institute of Technology (Huntington et al., 2014; this study). All sample $\Delta_{47}$ data was calculated on the Absolute Reference (Dennis et al., 2011). For samples that underwent acid digestion at 90 °C, a correction term of 0.092 was added to the $\Delta_{47}$ value (Henkes et al., 2013). The uncertainty of the calibration line is reported with a 95% confidence band. Regression statistics: $R^2$ = 0.83, n = 15 samples, p value < 0.0001. The Celsius temperature range displayed above is 4.2 – 43 °C.

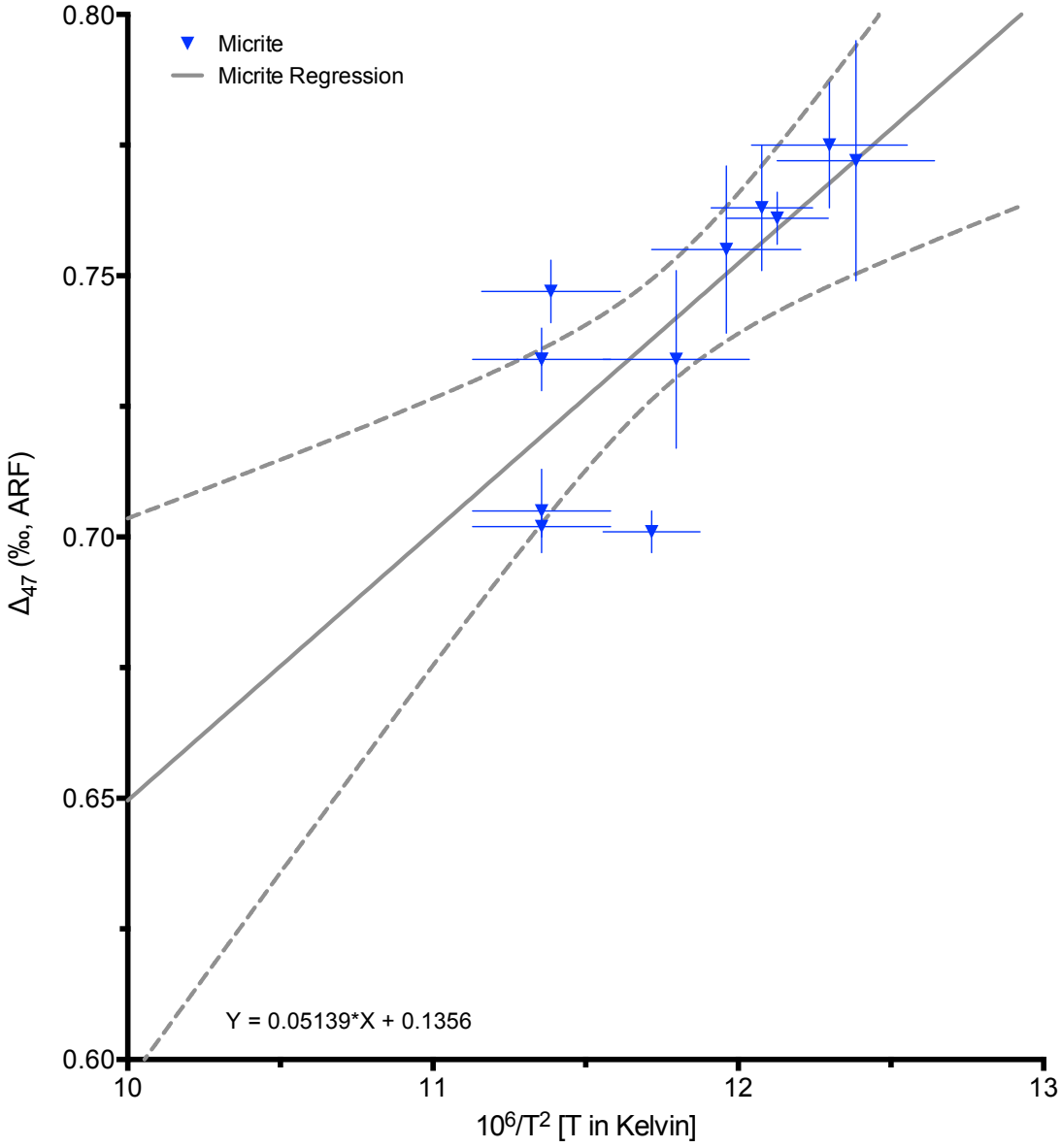


**Figure E5**: ***Lake calibration regression for modern micrite***. The water temperature, $\Delta_{47}$ clumped isotope temperature, and locality information are provided in Tables 4-5. The micrite regression includes a compilation of data from the Tripati Lab at UCLA and the Eiler Lab at the California Institute of Technology (Huntington et al., 2010; this study). All sample $\Delta_{47}$ data was calculated on the Absolute Reference (Dennis et al., 2011). For samples that underwent acid digestion at 90 °C, a correction term of 0.092 was added to the $\Delta_{47}$ value (Henkes et al., 2013). Uncertainties of individual samples are reported with 1 s.e. The uncertainty of the calibration line is reported with a 95% confidence band. Regression statistics: $R^2$ = 0.59, n = 12 samples, p value = 0.0033. The Celsius temperature range displayed above is 4.2 – 43 °C.

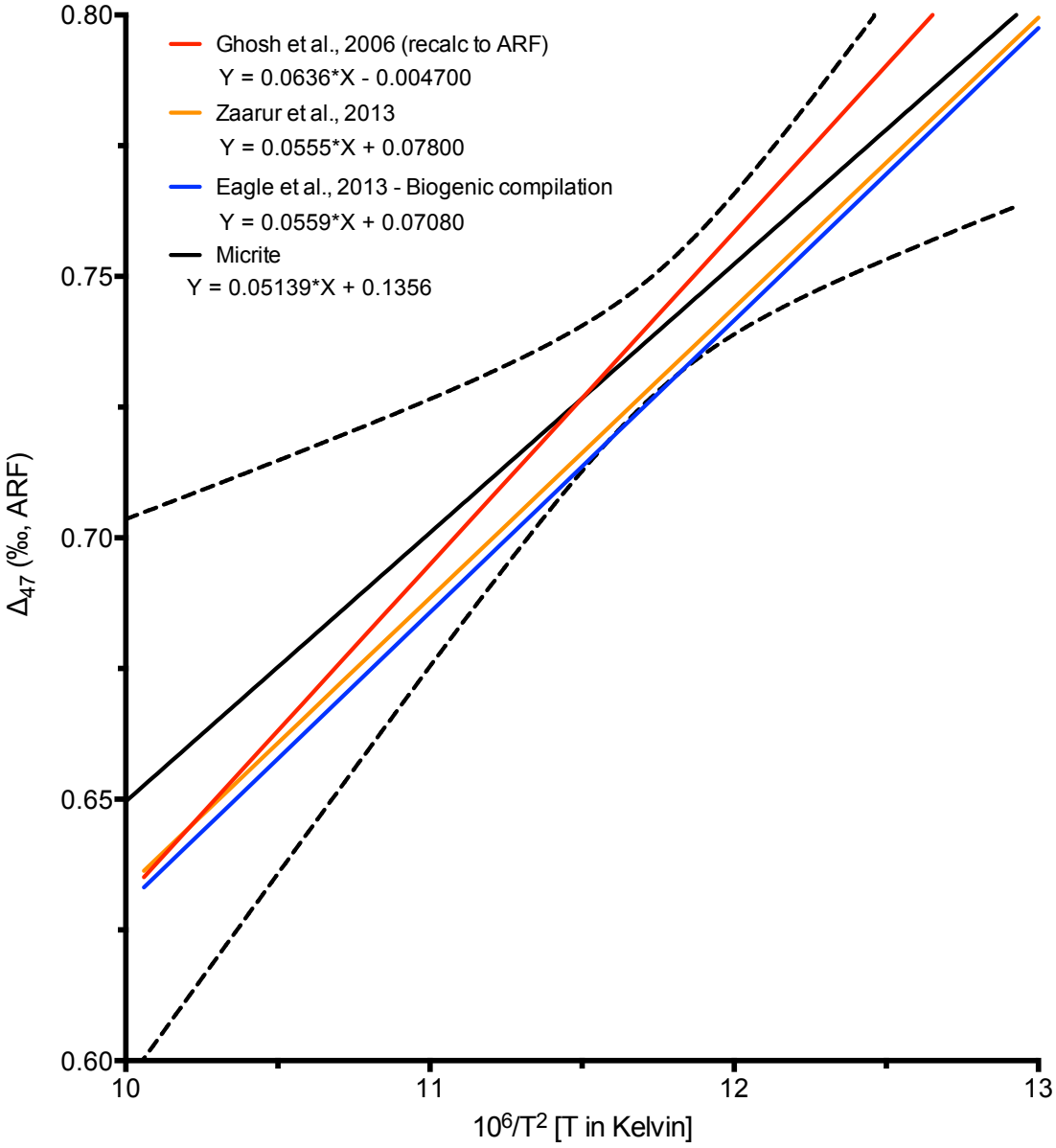


**Figure E6**: ***Modern micrite calibration compared with published steep slope clumped isotope calibrations***. The water temperature, $\Delta_{47}$ clumped isotope temperature, and locality information are provided in Tables 4-5. The micrite regression includes a compilation of data from the Tripati Lab at UCLA and the Eiler Lab at the California Institute of Technology (Huntington et al., 2010; this study). All sample $\Delta_{47}$ data was calculated on the Absolute Reference (Dennis et al., 2011). For samples that underwent acid digestion at 90 °C, a correction term of 0.092 was added to the $\Delta_{47}$ value (Henkes et al., 2013). The uncertainty of the calibration line is reported with a 95% confidence band. Regression statistics: $R^2$ = 0.59, n = 12 samples, p value = 0.0033. The Celsius temperature range displayed above is 4.2 – 43 °C.

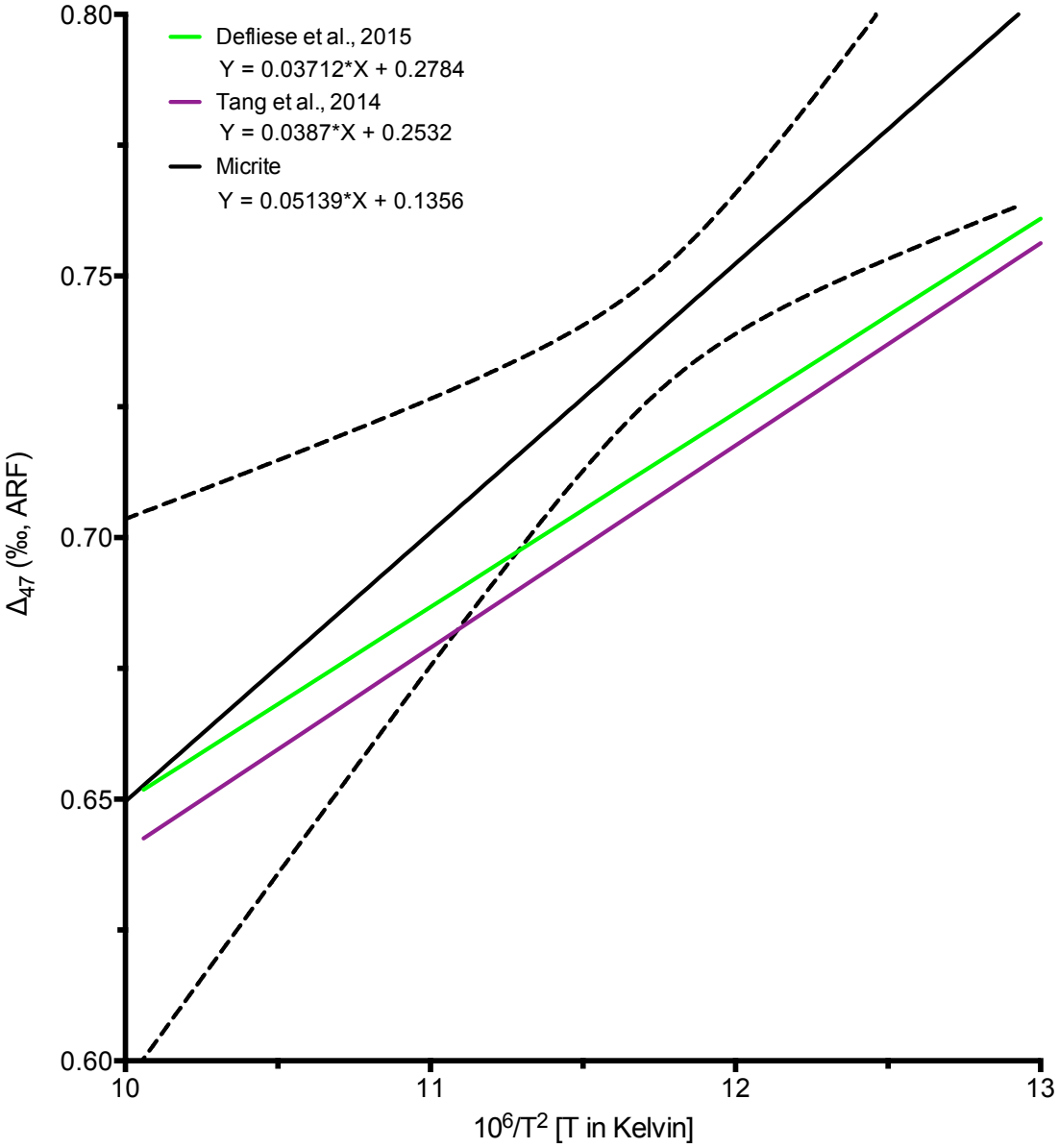


**Figure E7**: ***Modern micrite calibration compared with published shallow slope clumped isotope calibrations***. The water temperature, $\Delta_{47}$ clumped isotope temperature, and locality information are provided in Tables 4-5. The micrite regression includes a compilation of data from the Tripati Lab at UCLA and the Eiler Lab at the California Institute of Technology (Huntington et al., 2010; this study). All sample $\Delta_{47}$ data was calculated on the Absolute Reference (Dennis et al., 2011). For samples that underwent acid digestion at 90 °C, a correction term of 0.092 was added to the $\Delta_{47}$ value (Henkes et al., 2013). The uncertainty of the calibration line is reported with a 95% confidence band. Regression statistics: $R^2$ = 0.59, n = 12 samples, p value = 0.0033. The Celsius temperature range displayed above is 4.2 – 43 °C.

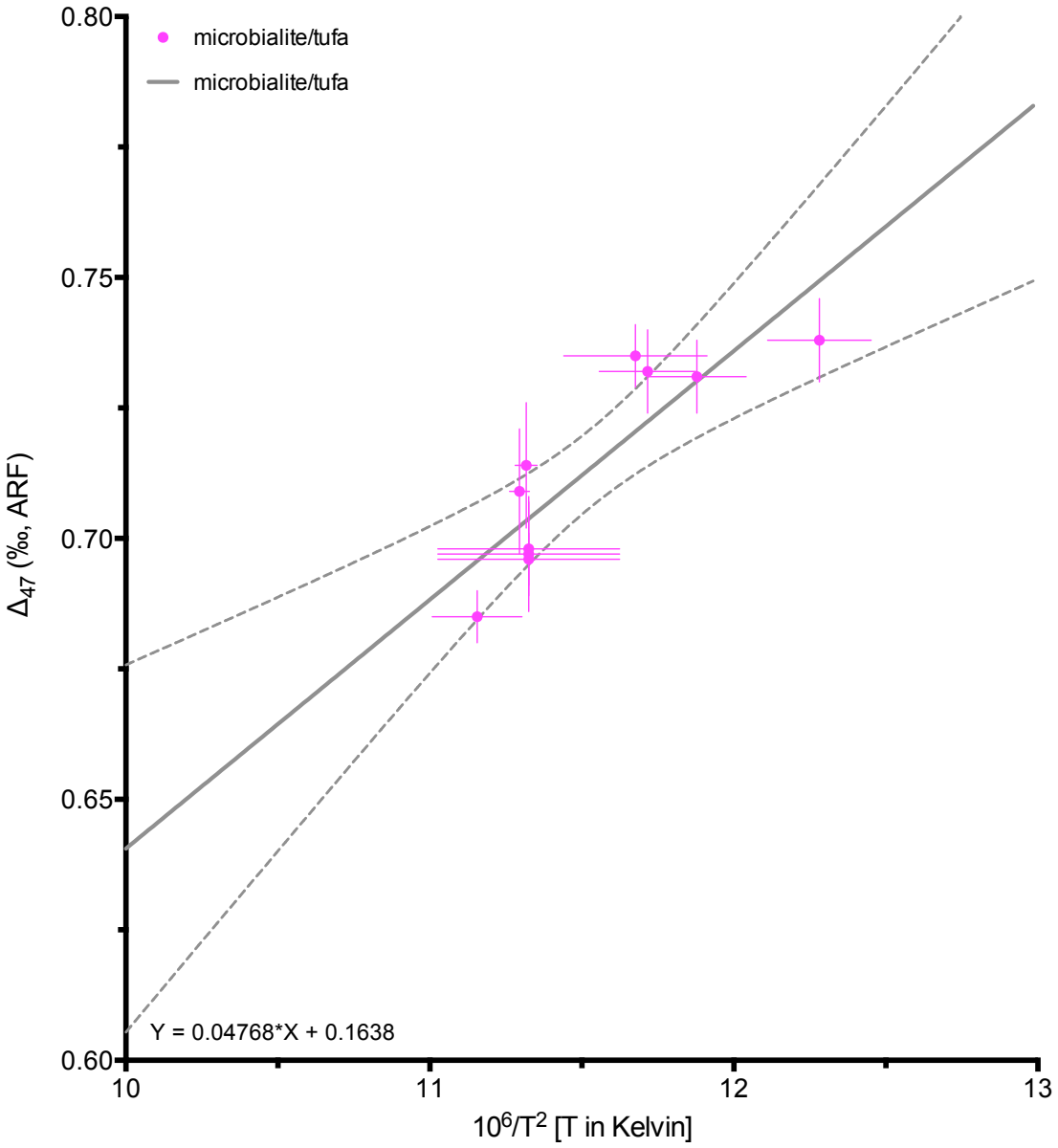


**Figure E8**: ***Lake calibration regression for modern microbialite and tufa***. The water temperature, $\Delta_{47}$ clumped isotope temperature, and locality information are provided in Tables 4-5. The microbialite / tufa regression includes a compilation of data from the Tripati Lab at UCLA and the Eiler Lab at the California Institute of Technology (Huntington et al., 2010; this study). All sample $\Delta_{47}$ data was calculated on the Absolute Reference (Dennis et al., 2011). For samples that underwent acid digestion at 90 °C, a correction term of 0.092 was added to the $\Delta_{47}$ value (Henkes et al., 2013). Uncertainties of individual samples are reported with 1 s.e. The uncertainty of the calibration line is reported with a 95% confidence band. Regression statistics: $R^2$ = 0.75, n = 10 samples, p value = 0.0012. The Celsius temperature range displayed above is 4.2 – 43 °C.

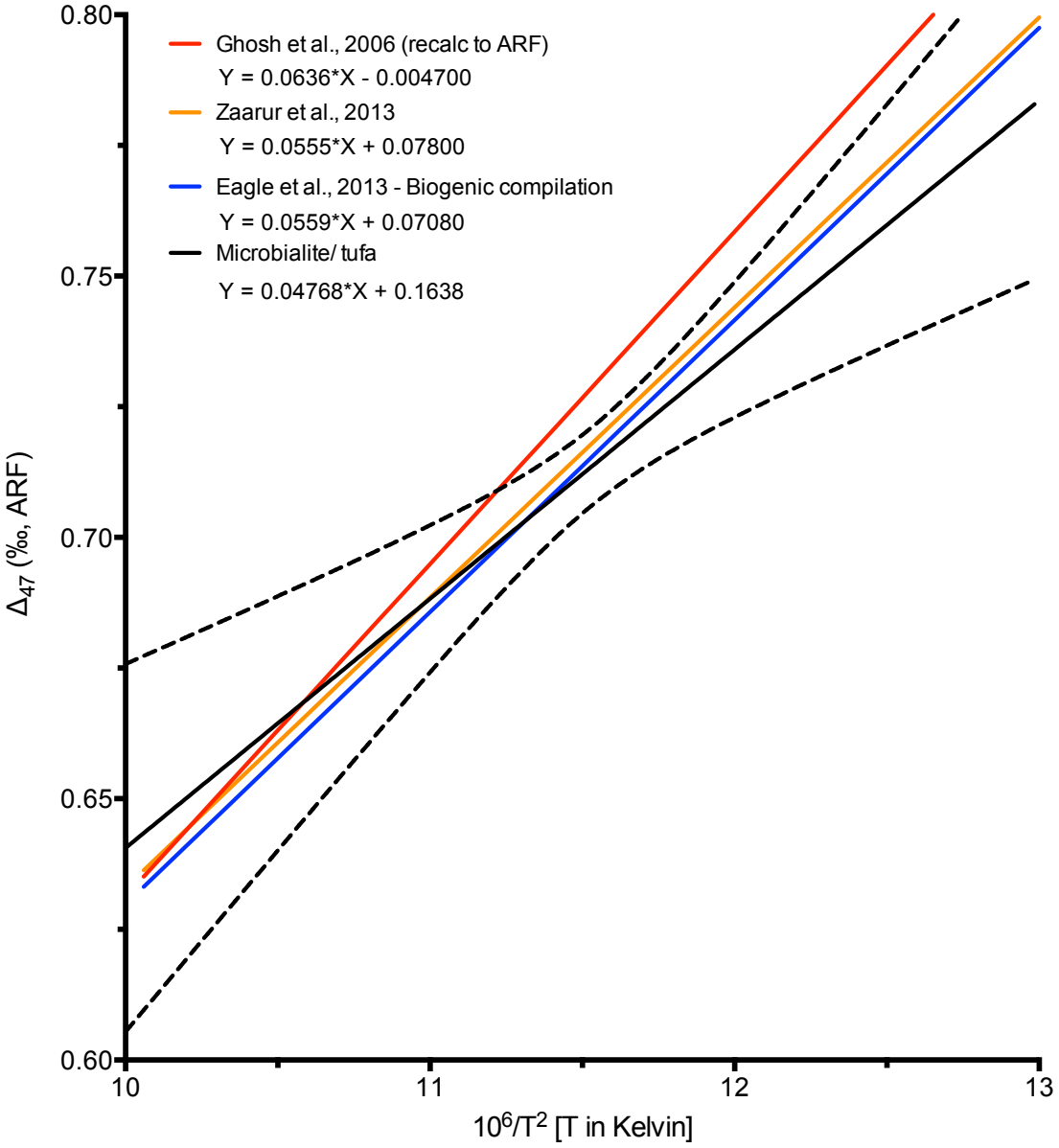


**Figure E9**: ***Modern microbialite and tufa calibration compared with published steep slope clumped isotope calibrations***. The water temperature, $\Delta_{47}$ clumped isotope temperature, and locality information are provided in Tables 4-5. The microbialite / tufa regression includes a compilation of data from the Tripati Lab at UCLA and the Eiler Lab at the California Institute of Technology (Huntington et al., 2010; this study). All sample $\Delta_{47}$ data was calculated on the Absolute Reference (Dennis et al., 2011). For samples that underwent acid digestion at 90 °C, a correction term of 0.092 was added to the $\Delta_{47}$ value (Henkes et al., 2013). Uncertainties of individual samples are reported with 1 s.e. The uncertainty of the calibration line is reported with a 95% confidence band. Regression statistics: $R^2$ = 0.75, n = 10 samples, p value = 0.0012. The Celsius temperature range displayed above is 4.2 – 43 °C.

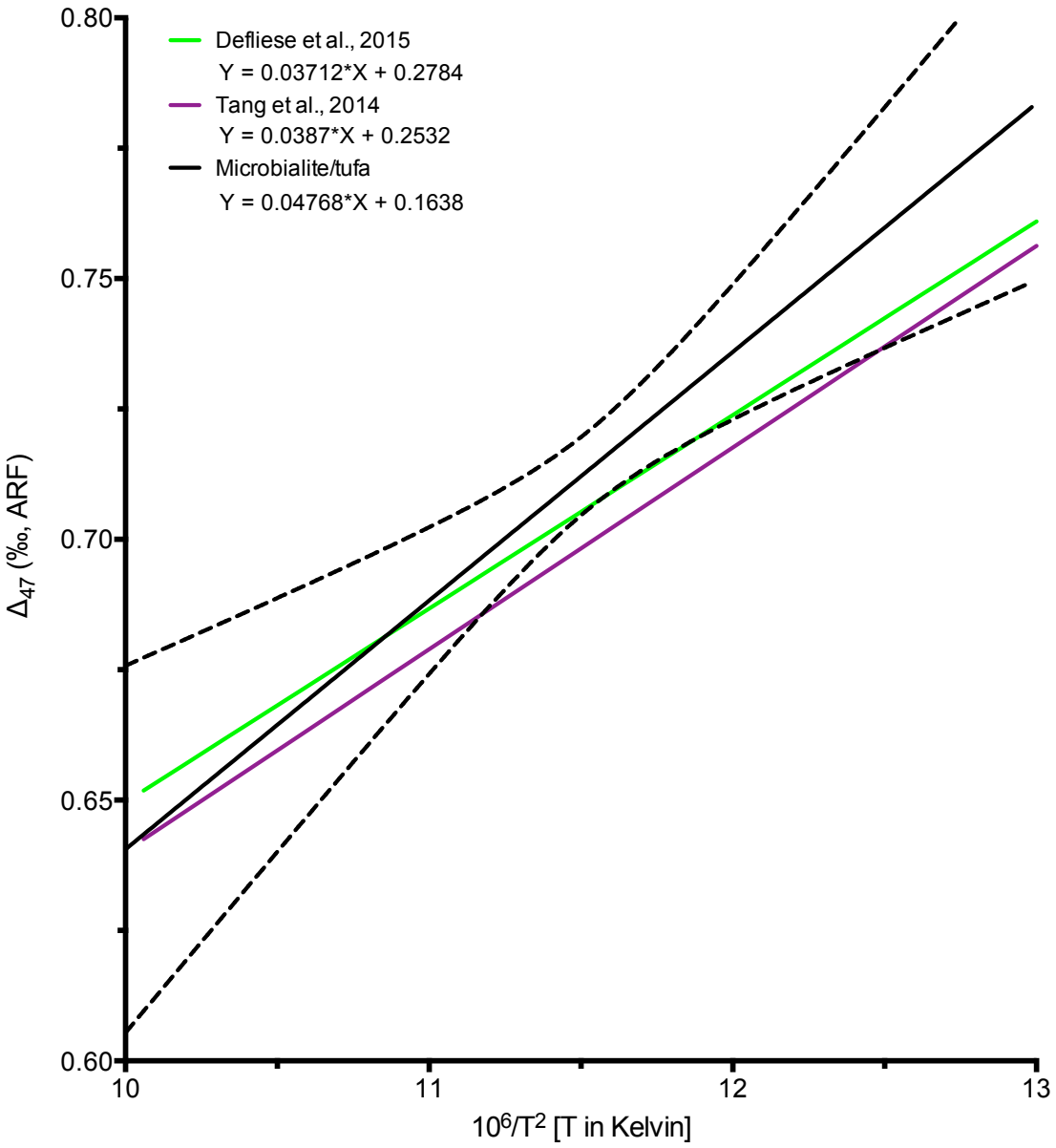


**Figure E10**: ***Modern microbialite and tufa calibration compared with published shallow slope clumped isotope calibrations***. The water temperature, $\Delta_{47}$ clumped isotope temperature, and locality information are provided in Tables 4-5. The microbialite / tufa regression includes a compilation of data from the Tripati Lab at UCLA and the Eiler Lab at the California Institute of Technology (Huntington et al., 2010; this study). All sample $\Delta_{47}$ data was calculated on the Absolute Reference (Dennis et al., 2011). For samples that underwent acid digestion at 90 °C, a correction term of 0.092 was added to the $\Delta_{47}$ value (Henkes et al., 2013). Uncertainties of individual samples are reported with 1 s.e. The uncertainty of the calibration line is reported with a 95% confidence band. Regression statistics: $R^2 = 0.75$, n = 10 samples, p value = 0.0012. The Celsius temperature range displayed above is 4.2 – 43 °C.

**North American Lake Sites**

**The Great Salt Lake (coordinates: 41.44º, -112.67º; elevation: 1280 m AMSL):** remnant of Lake Bonneville, situated in the northeastern region of the Bonneville Basin. The principal inflow is from the Bear, Weber, and Jordan Rivers. The lake is subdivided into two arms by a railroad causeway. The North Arm is more evaporated. Salinity ranges from 5 to 27 percent. Approximately 200-500 mm of rain falls over the lake basin annually. Mean average air temperatures over the South Arm approach 11.3 ºC, and summer water temperatures may reach 25-26ºC (Crosman and Horel, 2009). In this study, microbialite and ooid carbonates were evaluated from sites in both the North Arm at Spiral Jetty and the South Arm at Antelope Island.

**Walker Lake (coordinates: 38.7º, -118.8º; elevation: 1190 m AMSL):** remnant of Lake Lahontan, situated in the western Great Basin. Annual precipitation is 121 mm/yr (PRISM). Summer air temperatures reach 24ºC, while mean annual air temperature over the lake is 12-13ºC (PRISM). The maximum water depth is 33 m and the mean depth is 20 m (Petryshyn et al., 2015). Runoff from the Sierra Nevada Mountains provides the majority of recharge, which has diminished over the last century, following the onset of agricultural diversion in 1915 (Newton and Grossman, 1988).

**Mono Lake (coordinates: 37.94º, -119.03º; elevation: 1899 m):** closed basin lake, within the Mono Basin, north of the Long Valley/ Owens Valley region of Eastern California. The lake is saline today, but waters were fresh during the LGM, when the lake was more expansive. Lake volume varies as a function of both climate and amount of agricultural diversion of tributaries. The modern annual precipitation over the lake is 285 mm. Air temperatures are 18.0ºC in the summer (PRISM), and 8.6ºC annually (Hren and Sheldon, 2012). Water

temperatures are 10.8ºC in the summer (JJA) and 9.9ºC in the spring-autumn (Hren and Sheldon, 2012).

**Blue Lake (coordinates: 39.75º, -106.8º; elevation: 2552 m AMSL):** high elevation lake in Colorado, 100 km west of Denver. Lake surface area is 0.0115 $km^2$, and the catchment area is 2.24 $km^2$. Mean annual air temperatures are 4.5ºC. Mean summer water temperature is 6.2 ºC. Annual precipitation is 512.5 mm. (Polissar and Freeman, 2010). Huntington et al. (2010) report clumped isotope measurements of coretop lake sediment at this site.

**Emerald Lake** (coordinates: 39.07ºN, -111.5ºW; elevation: 3093 m AMSL): small high elevation lake on the Wasatch Plateau in central Utah. The summer surface water temperatures are ~1.6 ºC. Mean air temperatures are 2ºC. Average annual precipitation is 845.8 mm. The water depth is 9 m (Morris et al., 2012). The lake surface area is 0.0338 $km^2$, while the watershed area is 0.367 $km^2$ (Polissar and Freeman, 2010). Huntington et al. (2010) report clumped isotope measurements of coretop lake sediment at this site.

**Grizzly Creek Lake (coordinates: 39.69º, -107.3º; 3242 m AMSL):** small **(**0.0534-$km^2$) high altitude lake, located 140 km west of Denver. The catchment area is 0.855-$km^2$. Groundwater is a significant component of the water budget (Polissar and Freeman, 2010). Annual precipitation is 1032.1 mm. Mean annual air temperature is 0.9 ºC. Summer water temperatures are 2.3ºC. Huntington et al. (2010) report clumped isotope measurements of coretop lake sediment at this site.

**Zaca Lake (**coordinates: 34.79, -120.04; elevation: 730 m AMSL): small (0.07 $km^2$) lake in southern California. The watershed area is 9 $km^2$. The average depth is 9.6 m, and the maximum depth is 13 m. The lake is recharged by overland flow and groundwater (Feakins et al., 2014). Micritic carbonate was analyzed in this study.

**Utah Springs:** gastropods were collected at Spring Lake in the Clear Lake Waterfowl Management Area, the Left Fork of the Santa Clara River, and Painter Spring in the Tule Valley. Water temperatures at collection sites ranged from 10-15ºC (USGS).

**Pavilion Lake (coordinates: 50.86º, -121.70º; elevation: 823 m AMSL):** freshwater, oligotrophic system situated in Marble Canyon (Lim et al., 2009), a limestone valley in the Canadian Rockies. The Marble Range, which forms the lake catchment, is comprised of limestone, argillite, chert, and lava flows, with a cap of quaternary alluvium (Renaut, 1990). Maximum lake depth is ~65 m and total area is 4.58 $km^2$ (Laval et al., 2000). Mean summer water surface temperatures are 20ºC (Petryshyn et al., 2015). Annual rainfall is ~200 mm (Lim et al., 2009), and surface inflow is sourced from Pavilion Creek, however, groundwater is the primary source of recharge (Laval et al., in review). Lakewater pH is 8.3 (Lim et al., 2009). Petryshyn et al. (2015) report clumped isotope measurements of microbialite associated calcite at two lakes in the Canadian Rocky Mountains. These results are applied to the microbialite/ tufa clumped isotope calibration line presented in this thesis.

**Kelly Lake (coordinates: 50.01º, -121.80º; elevation: 1,070 m AMSL)**, is sixteen kilometers to the north of Pavilion Lake, within the Marble Range (Lim et al., 2011). A marl bench encircles the lake, extending from 0.5 m below the water surface to 20 m above (Ferris et al., 1997). The surface area is 0.46 $km^2$, and the maximum depth is 40 m. Mean pH of lakewater is 8.0 (Ferris et al., 1997). Hydrologic inputs include groundwater and precipitation, 300-400 mm/yr (Renaut, 1990). Summer lake surface temperatures are approximately 17 ºC (Ferris et al., 1997). Petryshyn et al. (2015) report clumped isotope measurements of microbialite associated calcite at two lakes in the Canadian Rocky Mountains. These results are applied to the microbialite/ tufa clumped isotope calibration line presented in this thesis.

**Nimgun Lake (coordinates: 59.56º, -160.77º; elevation: 320 m AMSL):** located in the Togiak Wildlife Management Area in SE Alaska. Summer water temperatures range from 6.1 to 9.6ºC. Aragonitic gastropods were contributed by Darrell Kaufman (NAU) from this site.

**Central Mexican dry lakes:** late Holocene coretop samples of micrite were evaluated from three modern dry lakes in North-Central Mexico. Samples were provided by Priyadarsi Roy at the following sites:

**Lago Las Cruces (coordinates: 22.65º, -100.12º; elevation: 2,106 m AMSL)**

**La Salada (coordinates: 23.43º, -101.13º; elevation: 2,035 m AMSL)**

**El Potosi (coordinates: 24.83º, -99.69º; elevation: 2164 m AMSL).**

Carbonate content in samples ranges from 10 to 60 percent. Water temperature at the time of carbonate formation was estimated from regional air temperature. Wide (2 stdev) ranges of uncertainty were assigned to water temperatures in order to reflect the significant uncertainty associated with carbonate growth temperatures at these sites.

**Bacalar (coordinates: 18.68º, -88.38º; elevation: 2 m AMSL):** microbialite was collected from Lake Bacalar, located in the southern Yucatan Peninsula in Mexico. Mean water temperature at Bacalar is 26.3ºC, and ranges from 20.7 to 31.8ºC. Freshwater thrombolite and stromatolite growths are abundant throughout the lake (Castro-Contreras et al., 2014).

**South America**

**Lago Sarmiento (coordinates: -51.047º, -72.743º; elevation: 77 m AMSL):** closed basin lake in southern Patagonia. The principal inflow is sourced from Laguna Verde. The maximum water depth is 312 m. Annual precipitation is 639 mm. Mean pH ranges from 8.3-8.7 (Solari et al., 2010). Air temperatures range from -1ºC in the winter to 13.8ºC in the summer, while mean annual air temperature at this lake is 7ºC. Water temperatures experience a smaller

annual range from 6.2ºC in the winter to 12.2ºC in the summer (Solari et al., 2010). In this study, clumped isotope measurements were carried out on carbonates from a living bioherm deposit at the lake.

**Laguna Pozuelos (coordinates: -22.352º, -66º; elevation: 3600 m AMSL):** endorheic basin lake in Northwest Argentina. The catchment lithology is comprised of sedimentary sequences (claystones, sandstones, marl limestones, conglomerates) interbedded with volcanic materials (Bonaventura et al., 1995). The area of the lake is 70 $km^2$. The majority of inflow is sourced from the Santa Catalina and Cincel Rivers. Annual precipitation over the lake basin is 350 mm (Bonaventura et al., 1995). The lake is shallow, with a maximum depth of less than 0.5 m during typical years. Depth may increase during wetter years. Mean air temperatures in the basin are below 9 ºC, approaching 3.5 ºC in the winter and 13 ºC in the summer. Salinity may reach 20717 mg $L^{-1}$ (Bonaventura et al., 1995). In August of 2001, water temperature was 15 ºC and pH was 6.5 (Ferrero et al., 2004). The calcification temperature of micritic carbonate from the lake was evaluated in this study.

**Mar Chiquita (coordinates: -30.75º, -62.5º; elevation: 68 m AMSL):** large closed basin lake, located in the Paraná-Plata Basin in Northern Argentina. The surface area of the lake has varied historically, from less than 2000 to 6000 $km^2$ (Troin et al., 2010). Water depth is shallow, ranging from a mean depth of 3.70 to maximum depth of 8.60 m (Reati et al., 1996). The catchment area is 37570 $km^2$, and is bounded on the east by the Bordo de Los Altos fault (Reati et al., 1996; Troin et al., 2010). Inflow is derived from both groundwater and several rivers, including the Rio Dulce from the north, and the Rios Xanaes and Suquía from the southwest (Troin et al., 2010). Annual precipitation varies from 0.8 and 1.3 m. Mean annual air temperatures are around 19 ºC. Surface water temperatures range from 14 to 29ºC over the

course of the year (Reati et al., 1996; Troin et al., 2010). Salinity values range from 27 to 360 g /L, as a function of both moisture delivery, and evaporative loss (Troin et al., 2010).

**Africa and Asia**

**Lake Tanganyika (coordinates: -3.396º, -29.136º; elevation: 773 m AMSL):** large freshwater N-S trending lake in central Africa bordered by the Democratic Republic of the Congo, Burundi, and Zambia. The mean depth of the lake is 570 m, while the maximum depth is 1470 m. Lake area is 32900 $km^2$ (Coulter, 1963). The mean annual air temperature varies across the lakes from 24.0ºC at the north end to 23.1ºC at the south end (Hren & Sheldon, 2010). Roughly two-thirds of recharge is pluvial rain, while the remainder is sourced from the Malagarazi and Ruzizi rivers, and many other smaller rivers. The Lukuga River (at the eastern margin) is the principal outlet (Coulter 1963; Crul 1997). pH ranges from 8.4 to 9.1 (Crul, 1997). Andy Cohen (U. of Arizona) contributed gastropod samples (Larigeria and Spekia) collected on the Burundi Coast at 0-1 m water depth, Water temperature was 25.5ºC at the time of collection.

**Lake Towuti (coordinates: -2.75º, 121.53º; elevation: 293 m AMSL):** open basin lake in Indonesia. The surface area is 561 $km^2$. Water depth is 200 m. Aragonitic gastropods were collected from the lake. Climate is warm and humid, with mean annual precipitation at ~3 m/yr. Water temperature associated with gastropod growth is 29ºC (Tierney and Russell, 2009).

**Zhada Basin Gastropods (coordinates: 29.6º to 31.6º N, 82.3º to 84.1ºE; elevation: 4570 to 4810 m AMSL):** clumped isotope temperatures were reported from modern Lymnaeid gastropods collected in the Zhada Basin, as part of a paleoaltimetry study on the Tibetan Plateau (Huntington et al., 2014). Samples were collected from Tso Nag Lake, as well as an interdune

pool, and creek margin. Sample materials were analyzed in the Eiler Lab at the California Institute of Technology.

## 11.0 CITATIONS


Anadon, P., Cabrera, L.L., Kelts, K., 2009. Lacustrine Facies Analysis (Special Publication 13 of the IAS). John Wiley & Sons.

Antevs, E., 1948. The Great Basin, with Emphasis on Glacial and Postglacial Times: Climatic Changes and Pre white Man. III. University of Utah.

Ashfaq, M., Bowling, L.C., Cherkauer, K., Pal, J.S., Diffenbaugh, N.S., 2010. Influence of climate model biases and daily-scale temperature and precipitation events on hydrological impacts assessment: A case study of the United States. J. Geophys. Res. Atmospheres 115, D14116. doi:10.1029/2009JD012965

Balch, D.P., Cohen, A.S., Schnurrenberger, D.W., Haskell, B.J., Valero Garces, B.L., Beck, J.W., Cheng, H., Edwards, R.L., 2005. Ecosystem and paleohydrological response to Quaternary climate change in the Bonneville Basin, Utah. Palaeogeogr. Palaeoclimatol. Palaeoecol. 221, 99–122. doi:10.1016/j.palaeo.2005.01.013

Baskin, R., 2008. Hydrology of Great Salt Lake: History, Water Balance, Conditions, Lake Dynamics.

Bedford, D., 2005. Utah's Great Salt Lake: A Complex Environmental-Societal System*. Geogr. Rev. 95, 73–96. doi:10.1111/j.1931-0846.2005.tb00192.x

Benson, L.V., Lund, S.P., Smoot, J.P., Rhode, D.E., Spencer, R.J., Verosub, K.L., Louderback, L.A., Johnson, C.A., Rye, R.O., Negrini, R.M., 2011. The rise and fall of Lake Bonneville between 45 and 10.5 ka. Quat. Int., PACLIM: Proceedings of the 24th Pacific Climate Workshop, 2009 235, 57–69. doi:10.1016/j.quaint.2010.12.014

Bonaventura, S.M., Tecchi, R., Vignale, D., 1995. The vegetation of the Puna Belt at laguna de

Pozuelos Biosphere Reserve in northwest Argentina. Vegetatio 119, 23–31. doi:10.1007/BF00047368

Bowen, G. J., 2014. The Online Isotopes in Precipitation Calculator, version 2.2.

Bowen G. J. and Revenaugh J. (2003) Interpolating the isotopic composition of modern meteoric precipitation. Water Resources Research 39(10), 1299, doi:10.129/2003WR002086.

Broughton, J.M., Madsen, D.B., Quade, J., 2000. Fish Remains from Homestead Cave and Lake Levels of the Past 13,000 Years in the Bonneville Basin. Quat. Res. 53, 392–401. doi:10.1006/qres.2000.2133

Castro-Contreras, S.I., Gingras, M.K., Pecoits, E., Aubet, N.R., Petrash, D., Castro-Contreras, S.M., Dick, G., Planavsky, N., Konhauser, K.O., 2014. Textural and Geochemical Features of Freshwater Microbialites from Laguna Bacalar, Quintana Roo, Mexico. PALAIOS 29, 192–209. doi:10.2110/palo.2013.063

Clark, P.U., Bartlein, P.J., 1995. Correlation of late Pleistocene glaciation in the western United States with North Atlantic Heinrich events. Geology 23, 483–486. doi:10.1130/0091-7613(1995)023<0483:COLPGI>2.3.CO;2

Coulter, G., W., 1963. Hydrological Changes in Relation to Biological Production in Southern Lake Tanganyika. Limnol. Oceanogr. 8, 463–477. doi:10.4319/lo.1963.8.4.0463

Crosman, E.T., Horel, J.D., 2009. MODIS-derived surface temperature of the Great Salt Lake. Remote Sensing of Environment 113, 73–81. doi:10.1016/j.rse.2008.08.013

Crul, R. C., 1997. Limnology and Hydrology of Lakes Tanganyika and Malawi: Comprehensive and Comparative Study of Great Lakes: UNESCO/IHP-IV Project M-5.1. Unesco.

Csank, A.Z., Tripati, A.K., Patterson, W.P., Eagle, R.A., Rybczynski, N., Ballantyne, A.P., Eiler, J.M., 2011. Estimates of Arctic land surface temperatures during the early Pliocene from two novel proxies. Earth Planet. Sci. Lett. 304, 291–299. doi:10.1016/j.epsl.2011.02.030

Currey, D.R., 1990. Quaternary palaeolakes in the evolution of semidesert basins, with special emphasis on Lake Bonneville and the Great Basin, U.S.A. Palaeogeogr. Palaeoclimatol. Palaeoecol., Paleoenvironments of Aid Lands 76, 189–214. doi:10.1016/0031-0182(90)90113-L

Currey, D.R., 1982. Lake Bonneville-Selected features of relevance to neotectonic analysis. US Geol. Surv. Open-File Rep. 82.

Defliese, W.F., Hren, M.T., Lohmann, K.C., 2015. Compositional and temperature effects of phosphoric acid fractionation on Δ47 analysis and implications for discrepant calibrations. Chem. Geol. 396, 51–60. doi:10.1016/j.chemgeo.2014.12.018

Dennis, K.J., Affek, H.P., Passey, B.H., Schrag, D.P., Eiler, J.M., 2011. Defining an absolute reference frame for "clumped" isotope studies of CO2. Geochim. Cosmochim. Acta 75, 7117–7131. doi:10.1016/j.gca.2011.09.025

Dennis, K.J., Schrag, D.P., 2010. Clumped isotope thermometry of carbonatites as an indicator of diagenetic alteration. Geochim. Cosmochim. Acta 74, 4110–4122. doi:10.1016/j.gca.2010.04.005

Denniston, R.F., Asmerom, Y., Polyak, V., Dorale, J.A., Carpenter, S.J., Trodick, C., Hoye, B., González, L.A., 2007. Synchronous millennial-scale climatic changes in the Great Basin and the North Atlantic during the last interglacial. Geology 35, 619–622. doi:10.1130/G23445A.1

Dettman, D.L., Reische, A.K., Lohmann, K.C., 1999. Controls on the stable isotope composition of seasonal growth bands in aragonitic fresh-water bivalves (unionidae). Geochim. Cosmochim. Acta 63, 1049–1057. doi:10.1016/S0016-7037(99)00020-4

Duston, N.M., Owen, R.M., Wilkinson, B.H., 1986. Water chemistry and sedimentological observations in littlefield lake, michigan: Implications for lacustrine marl deposition. Environ. Geol. Water Sci. 8, 229–236. doi:10.1007/BF02524950

Eagle, R.A., Eiler, J.M., Tripati, A.K., Ries, J.B., Freitas, P.S., Hiebenthal, C., Wanamaker, A.D., Taviani, M., Elliot, M., Marenssi, S., Nakamura, K., Ramirez, P., Roy, K., 2013. The influence of temperature and seawater carbonate saturation state on bond ordering in bivalve mollusks. Biogeosciences 10, 4591–4606. doi:10.5194/bg-10-4591-2013

Eagle, R.A., Risi, C., Mitchell, J.L., Eiler, J.M., Seibt, U., Neelin, J.D., Li, G., Tripati, A.K., 2013. High regional climate sensitivity over continental China constrained by glacial-recent changes in temperature and the hydrological cycle. PNAS 110, 8813–8818. doi:10.1073/pnas.1213366110

Eardley, A.J., Shuey, R.T., Gvosdetsky, V., Nash, W.P., Picard, M.D., Grey, D.C., Kukla, G.J., 1973. Lake Cycles in the Bonneville Basin, Utah. Geol. Soc. Am. Bull. 84, 211–216. doi:10.1130/0016-7606(1973)84<211:LCITBB>2.0.CO;2

Eiler, J.M., 2007. “Clumped-isotope” geochemistry—The study of naturally-occurring, multiply-substituted isotopologues. Earth Planet. Sci. Lett. 262, 309–327. doi:10.1016/j.epsl.2007.08.020

Epstein, S., Buchsbaum, R., Lowenstam, H.A., Urey, H.C., 1953. Revised Carbonate-Water Isotopic Temperature Scale. Geological Society of America Bulletin 64, 1315–1326. doi:10.1130/0016-7606(1953)64[1315:RCITS]2.0.CO;2

Feakins, S.J., Kirby, M.E., Cheetham, M.I., Ibarra, Y., Zimmerman, S.R.H., 2014. Fluctuation in leaf wax D/H ratio from a southern California lake records significant variability in isotopes in precipitation during the late Holocene. Organic Geochemistry 66, 48–59. doi:10.1016/j.orggeochem.2013.10.015

Felton, A., Jewell, P.W., Chan, M., Currey, D., 2006. Controls of Tufa Development in Pleistocene Lake Bonneville, Utah. J. Geol. 114, 377–389. doi:10.1086/501218

Ferrero, M., Farías, M. E., & Siñeriz, F., 2004. Preliminary characterization of microbial communities in High Altitude Wetlands of Northwestern Argentina by determining terminal restriction fragment length polymorphisms. Revista Latinoamericana de Microbiologia, 46(3), 72-80.

Ferris, F. G., Thompson, J. B., & Beveridge, T. J., 1997. Modern freshwater microbialites from Kelly Lake, British Columbia, Canada. Palaios, 213-219.

Ghosh, P., Adkins, J., Affek, H., Balta, B., Guo, W., Schauble, E.A., Schrag, D., Eiler, J.M., 2006. 13C–18O bonds in carbonate minerals: A new kind of paleothermometer. Geochimica et Cosmochimica Acta 70, 1439–1456. doi:10.1016/j.gca.2005.11.014

Gilbert, K.G., 1890. U.S. Geological Survey Professional Paper. U.S. Government Printing Office.

Godsey, H.S., Currey, D.R., Chan, M.A., 2005. New evidence for an extended occupation of the Provo shoreline and implications for regional climate change, Pleistocene Lake Bonneville, Utah, USA. Quat. Res. 63, 212–223. doi:10.1016/j.yqres.2005.01.002

Godsey, H.S., Oviatt, C.G., Miller, D.M., Chan, M.A., 2011. Stratigraphy and chronology of offshore to nearshore deposits associated with the Provo shoreline, Pleistocene Lake

Bonneville, Utah. Palaeogeogr. Palaeoclimatol. Palaeoecol. 310, 442–450. doi:10.1016/j.palaeo.2011.08.005

Guo, W., Mosenfelder, J.L., Goddard III, W.A., Eiler, J.M., 2009. Isotopic fractionations associated with phosphoric acid digestion of carbonate minerals: Insights from first-principles theoretical modeling and clumped isotope measurements. Geochim. Cosmochim. Acta 73, 7203–7225. doi:10.1016/j.gca.2009.05.071

Hart, W.S., Quade, J., Madsen, D.B., Kaufman, D.S., Oviatt, C.G., 2004a. The 87Sr/86Sr ratios of lacustrine carbonates and lake-level history of the Bonneville paleolake system. Geol. Soc. Am. Bull. 116, 1107–1119. doi:10.1130/B25330.1

Hart, W.S., Quade, J., Madsen, D.B., Kaufman, D.S., Oviatt, C.G., 2004b. The 87Sr/86Sr ratios of lacustrine carbonates and lake-level history of the Bonneville paleolake system. Geol. Soc. Am. Bull. 116, 1107–1119. doi:10.1130/B25330.1

Henkes, G.A., Passey, B.H., Wanamaker Jr., A.D., Grossman, E.L., Ambrose Jr., W.G., Carroll, M.L., 2013. Carbonate clumped isotope compositions of modern marine mollusk and brachiopod shells. Geochimica et Cosmochimica Acta 106, 307–325. doi:10.1016/j.gca.2012.12.020

Hershler, R., & Sada, D. W., 2002. Biogeography of Great Basin aquatic snails of the genus Pyrgulopsis. Smithsonian Contributions to the Earth Sciences, 33(2002), 255-276.

Hershler, R., Liu, H.-P., Sada, D.W., 2007. Origin and diversification of the soldier meadow springsnails (Hydrobiidae: Pyrgulopsis), a species flock in the northwestern Great Basin, United States. J. Molluscan Stud. 73, 167–183. doi:10.1093/mollus/eym014

Hill, P.S., Tripati, A.K., Schauble, E.A., 2014. Theoretical constraints on the effects of pH, salinity, and temperature on clumped isotope signatures of dissolved inorganic carbon

species and precipitating carbonate minerals. Geochim. Cosmochim. Acta 125, 610–652. doi:10.1016/j.gca.2013.06.018

Hodell, D.A., Schelske, C.L., Fahnenstiel, G.L., Robbins, L.L., 1998. Biologically induced calcite and its isotopic composition in Lake Ontario. Limnol. Oceanogr. 43, 187–199. doi:10.4319/lo.1998.43.2.0187

Horton, Travis, Defliese, William, Tripati, Aradhna, Oze, Christopher, 2015. Evaporation induced $\delta^{18}O$ and $\delta^{13}C$ enrichment in lake systems: a global perspective on hydrologic balance effects on terrestrial stable isotopic proxy records. Quaternary Science Reviews. Submitted Manuscript.

Horel, John, 2015. Monitoring the Great Salt Lake. Retrieved from http://home.chpc.utah.edu/~u0035056/jhorel/seminar_lake.html.

Hostetler, S.W., Giorgi, F., Bates, G.T., Bartlein, P.J., 1994. Lake-Atmosphere Feedbacks Associated with Paleolakes Bonneville and Lahontan. Science 263, 665–668. doi:10.1126/science.263.5147.665

Hren, M.T., Sheldon, N.D., 2012. Temporal variations in lake water temperature: Paleoenvironmental implications of lake carbonate δ18O and temperature records. Earth and Planetary Science Letters 337–338, 77–84. doi:10.1016/j.epsl.2012.05.019

Huntington, K.W., Saylor, J., Quade, J., Hudson, A.M., 2015. High late Miocene–Pliocene elevation of the Zhada Basin, southwestern Tibetan Plateau, from carbonate clumped isotope thermometry. Geol. Soc. Am. Bull. 127, 181–199. doi:10.1130/B31000.1

Huntington, K.W., Wernicke, B.P., Eiler, J.M., 2010. Influence of climate change and uplift on Colorado Plateau paleotemperatures from carbonate clumped isotope thermometry. Tectonics 29. doi:10.1029/2009TC002449

Ibarra, D.E., Egger, A.E., Weaver, K.L., Harris, C.R., Maher, K., 2014. Rise and fall of late Pleistocene pluvial lakes in response to reduced evaporation and precipitation: Evidence from Lake Surprise, California. Geol. Soc. Am. Bull. B31014.1. doi:10.1130/B31014.1

Janecke, S.U., Oaks, R.Q., 2011. Reinterpreted history of latest Pleistocene Lake Bonneville: Geologic setting of threshold failure, Bonneville flood, deltas of the Bear River, and outlets for two Provo shorelines, southeastern Idaho, USA. Field Guid. 21, 195–222. doi:10.1130/2011.0021(09)

Jarrett, R.D., Malde, H.E., 1987. Paleodischarge of the late Pleistocene Bonneville Flood, Snake River, Idaho, computed from new evidence. Geol. Soc. Am. Bull. 99, 127–134. doi:10.1130/0016-7606(1987)99<127:POTLPB>2.0.CO;2

Jewell, P.W., 2007. Morphology and paleoclimatic significance of Pleistocene Lake Bonneville spits. Quaternary Research 68, 421–430. doi:10.1016/j.yqres.2007.07.004

Jewell, P.W., 2010. River incision, circulation, and wind regime of Pleistocene Lake Bonneville, USA. Palaeogeography, Palaeoclimatology, Palaeoecology 293, 41–50. doi:10.1016/j.palaeo.2010.04.028

Jones, M.D., Roberts, C.N., Leng, M.J., 2007. Quantifying climatic change through the last glacial–interglacial transition based on lake isotope palaeohydrology from central Turkey. Quaternary Research, Reconstructing past environments from remnants of human occupation and sedimentary archives in western Eurasia 67, 463–473. doi:10.1016/j.yqres.2007.01.004

Kele, Sándor et al., 2014. Calibration of the conventional carbonate water and ‘clumped isotope’ thermometer on calcitic and aragonitic travertines and calcareous tufas in the 5-95 ºC temperature range. 4th Int. WS on Clumped Isotopes.

Kaufman, D.S., 2003. Amino acid paleothermometry of Quaternary ostracodes from the Bonneville Basin, Utah. Quat. Sci. Rev. 22, 899–914. doi:10.1016/S0277-3791(03)00006-4

Kelts, K., Hsü, K.J., 1978. Freshwater Carbonate Sedimentation, in: Lerman, A. (Ed.), Lakes. Springer New York, pp. 295–323.

Kim, S.-T., O'Neil, J.R., 1997. Equilibrium and nonequilibrium oxygen isotope effects in synthetic carbonates. Geochim. Cosmochim. Acta 61, 3461–3475. doi:10.1016/S0016-7037(97)00169-5

Kim, S.-T., O'Neil, J.R., Hillaire-Marcel, C., Mucci, A., 2007. Oxygen isotope fractionation between synthetic aragonite and water: Influence of temperature and Mg2+ concentration. Geochimica et Cosmochimica Acta 71, 4704–4715. doi:10.1016/j.gca.2007.04.019

Lechler, A.R., Niemi, N.A., Hren, M.T., Lohmann, K.C., 2013. Paleoelevation estimates for the northern and central proto–Basin and Range from carbonate clumped isotope thermometry. Tectonics 32, 295–316. doi:10.1002/tect.20016

Lim, D.S.S., Laval, B.E., Slater, G., Antoniades, D., Forrest, A.L., Pike, W., Pieters, R., Saffari, M., Reid, D., Schulze-Makuch, D., Andersen, D., McKay, C.P., 2009. Limnology of Pavilion Lake, B. C., Canada – Characterization of a microbialite forming environment. Fundamental and Applied Limnology / Archiv f??r Hydrobiologie 173, 329–351. doi:10.1127/1863-9135/2009/0173-0329

Link, P. K., Kaufman, D. S., & Thackray, G. D., 1999. Field guide to Pleistocene lakes

Thatcher and Bonneville and the Bonneville flood, southeastern Idaho. Guidebook to the geology of eastern Idaho, 251-266.

Linacre, E.T., 1993. Data-sparse estimation of lake evaporation, using a simplified Penman equation. Agricultural and Forest Meteorology 64, 237–256. doi:10.1016/0168-1923(93)90031-C

Louderback, L.A., Rhode, D.E., 2009. 15,000 Years of vegetation change in the Bonneville basin: the Blue Lake pollen record. Quat. Sci. Rev. 28, 308–326. doi:10.1016/j.quascirev.2008.09.027

Lyle, M., Heusser, L., Ravelo, C., Yamamoto, M., Barron, J., Diffenbaugh, N.S., Herbert, T., Andreasen, D., 2012. Out of the Tropics: The Pacific, Great Basin Lakes, and Late Pleistocene Water Cycle in the Western United States. Science 337, 1629–1633. doi:10.1126/science.1218390

Lysne, Steven and Koetsier, Peter, 2006. Experimental Studies on Habitat Preference and Tolerances of Three Species of Snails from the Snake River of Southern Idaho. American Malacological Bulletin, 21(1-2), 77-85.

Lysne, S.J., Riley, L.A., Clark, W.H., 2007. The Life History, Ecology, and Distribution of the Jackson Lake Springsnail (Pyrgulopsis robusta Walker 1908). J. Freshw. Ecol. 22, 647–653. doi:10.1080/02705060.2007.9664825

Madsen, D.B., Rhode, D., Grayson, D.K., Broughton, J.M., Livingston, S.D., Hunt, J., Quade, J., Schmitt, D.N., Shaver III, M.W., 2001. Late Quaternary environmental change in the Bonneville basin, western USA. Palaeogeogr. Palaeoclimatol. Palaeoecol. 167, 243–271. doi:10.1016/S0031-0182(00)00240-6

Matsubara, Y., Howard, A.D., 2009. A spatially explicit model of runoff, evaporation, and lake extent: Application to modern and late Pleistocene lakes in the Great Basin region, western United States. Water Resour. Res. 45, W06425. doi:10.1029/2007WR005953

McCoy, W.D., 1987. Quaternary aminostratigraphy of the Bonneville Basin, western United States. Geol. Soc. Am. Bull. 98, 99–112. doi:10.1130/0016-7606(1987)98<99:QAOTBB>2.0.CO;2

McGee, D., Quade, J., Edwards, R.L., Broecker, W.S., Cheng, H., Reiners, P.W., Evenson, N., 2012. Lacustrine cave carbonates: Novel archives of paleohydrologic change in the Bonneville Basin (Utah, USA). Earth Planet. Sci. Lett. 351–352, 182–194. doi:10.1016/j.epsl.2012.07.019

Menking, K.M., Anderson, R.Y., Shafike, N.G., Syed, K.H., Allen, B.D., 2004. Wetter or colder during the Last Glacial Maximum? Revisiting the pluvial lake question in southwestern North America. Quat. Res. 62, 280–288. doi:10.1016/j.yqres.2004.07.005

Mifflin, M. D., & Wheat, M. M., 1979. Pluvial lakes and estimated pluvial climates of Nevada. Mackay School of Mines, University of Nevada.

Miller, D.M., Oviatt, C.G., Mcgeehin, J.P., 2013. Stratigraphy and chronology of Provo shoreline deposits and lake-level implications, Late Pleistocene Lake Bonneville, eastern Great Basin, USA. Boreas 42, 342–361. doi:10.1111/j.1502-3885.2012.00297.x

Mock, C.J., Bartlein, P.J., 1995. Spatial Variability of Late-Quaternary Paleoclimates in the Western United States. Quat. Res. 44, 425–433. doi:10.1006/qres.1995.1087

Morris, J.L., Brunelle, A., 2012. Pollen accumulation in lake sediments during historic spruce beetle disturbances in subalpine forests of southern Utah, USA. The Holocene 22, 961–974. doi:10.1177/0959683612437870

Munroe, J.S., Laabs, B.J.C., Shakun, J.D., Singer, B.S., Mickelson, D.M., Refsnider, K.A., Caffee, M.W., 2006. Latest Pleistocene advance of alpine glaciers in the southwestern Uinta Mountains, Utah, USA: Evidence for the influence of local moisture sources. Geology 34, 841–844. doi:10.1130/G22681.1

Munroe, J.S., Laabs, B.J.C., 2013. Temporal correspondence between pluvial lake highstands in the southwestern US and Heinrich Event 1. J. Quaternary Sci. 28, 49–58. doi:10.1002/jqs.2586

Nelson, S.T., Wood, M.J., Mayo, A.L., Tingey, D.G., Eggett, D., 2005. Shoreline tufa and tufaglomerate from Pleistocene Lake Bonneville, Utah, USA: stable isotopic and mineralogical records of lake conditions, processes, and climate. J. Quat. Sci. 20, 3–19. doi:10.1002/jqs.889

Newton, M. S., & Grossman, E. L., 1988. Late Quaternary chronology of tufa deposits, Walker Lake, Nevada. The Journal of Geology, 417-433.

O'Connor, J.E., 1993. Hydrology, Hydraulics, and Geomorphology of the Bonneville Flood. Geol. Soc. Am. Spec. Pap. 274, 1–84. doi:10.1130/SPE274-p1

Olander, H., Birks, H.J.B., Korhola, A., Blom, T., 1999. An expanded calibration model for inferring lakewater and air temperatures from fossil chironomid assemblages in northern Fennoscandia. The Holocene 9, 279–294. doi:10.1191/095968399677918040

Oliver, George V. and William R. Bosworth III. 1999. Rare, imperiled, and recently extinct or extirpated mollusks of Utah[:] a literature review. Publication number 99-29. Utah Division of Wildlife Resources, Salt Lake City. 230 pp.

Oster, J.L., Ibarra, D.E., Winnick, M.J., Maher, K., 2015. Steering of westerly storms over

western North America at the Last Glacial Maximum. Nat. Geosci. 8, 201–205. doi:10.1038/ngeo2365

Oviatt, C.G., 1988. Late Pleistocene and Holocene lake fluctuations in the Sevier Lake basin, Utah, USA. J. Paleolimnol. 1, 9–21. doi:10.1007/BF00202190

Oviatt, C.G., 1997. Lake Bonneville fluctuations and global climate change. Geology 25, 155–158. doi:10.1130/0091-7613(1997)025<0155:LBFAGC>2.3.CO;2

Oviatt, C. G., 2014. The Gilbert episode in the Great Salt Lake basin, Utah. Utah Geological Survey.

Oviatt, C., 2014. THE IMPORTANCE OF GROUNDWATER IN LAKE BONNEVILLE HISTORY. Presented at the 2014 GSA Annual Meeting in Vancouver, British Columbia, GSA, Vancouver, BC.

Oviatt, C.G., 2015. Chronology of Lake Bonneville, 30,000 to 10,000 yr B.P. Quaternary Science Reviews 110, 166–171. doi:10.1016/j.quascirev.2014.12.016

Oviatt, C.G., Thompson, R.S., Kaufman, D.S., Bright, J., Forester, R.M., 1999. Reinterpretation of the Burmester Core, Bonneville Basin, Utah. Quaternary Research 52, 180–184. doi:10.1006/qres.1999.2058

Oviatt, C.G., Currey, D.R., Sack, D., 1992. Radiocarbon chronology of Lake Bonneville, Eastern Great Basin, USA. Palaeogeogr. Palaeoclimatol. Palaeoecol. 99, 225–241. doi:10.1016/0031-0182(92)90017-Y

Oviatt, C.G., Habiger, G.D., Hay, J.E., 1994a. Variation in the composition of Lake Bonneville marl: a potential key to lake-level fluctuations and paleoclimate. J. Paleolimnol. 11, 19–30. doi:10.1007/BF00683268

Oviatt, C.G., Habiger, G.D., Hay, J.E., 1994b. Variation in the composition of Lake Bonneville marl: a potential key to lake-level fluctuations and paleoclimate. J. Paleolimnol. 11, 19–30. doi:10.1007/BF00683268

Oviatt, C.G., Madsen, D.B., Schmitt, D.N., 2003. Late Pleistocene and early Holocene rivers and wetlands in the Bonneville basin of western North America. Quat. Res. 60, 200–210. doi:10.1016/S0033-5894(03)00084-X

Oviatt, C.G., Mccoy, W.D., Nash, W.P., 1994c. Sequence stratigraphy of lacustrine deposits: A Quaternary example from the Bonneville basin, Utah. Geol. Soc. Am. Bull. 106, 133–144. doi:10.1130/0016-7606(1994)106<0133:SSOLDA>2.3.CO;2

Oviatt, C.G., Miller, D.M., McGeehin, J.P., Zachary, C., Mahan, S., 2005. The Younger Dryas phase of Great Salt Lake, Utah, USA. Palaeogeogr. Palaeoclimatol. Palaeoecol. 219, 263–284. doi:10.1016/j.palaeo.2004.12.029

Oviatt, C.G., Nash, W.P., 1989. Late Pleistocene basaltic ash and volcanic eruptions in the Bonneville basin, Utah. Geol. Soc. Am. Bull. 101, 292–303. doi:10.1130/0016-7606(1989)101<0292:LPBAAV>2.3.CO;2

Oviatt, C.G., Thompson, R.S., Kaufman, D.S., Bright, J., Forester, R.M., 1999. Reinterpretation of the Burmester Core, Bonneville Basin, Utah. Quat. Res. 52, 180–184. doi:10.1006/qres.1999.2058

Pedone, V., 2002. Oxygen-isotope composition of the Great Salt Lake, 1979 to 1996, in JW Gwynn (ed.), Great Salt Lake: an overview of change. Utah Geological Survey.

Pedone, V., 2004. PALEOHYDROLOGY OF LAKE BONNEVILLE DETERMINED BY MINERALOGY AND C, O, AND SR ISOTOPE COMPOSITIONS OF AUTHIGENIC CARBONATES.

Petryshyn, V.A., Lim, D., Laval, B.L., Brady, A., Slater, G., Tripati, A.K., 2015. Reconstruction of limnology and microbialite formation conditions from carbonate clumped isotope thermometry. Geobiology 13, 53–67. doi:10.1111/gbi.12121

Platt, N.H., Wright, V.P., 1991. Lacustrine carbonates: facies models, facies distributions and hydrocarbon aspects. 1991.

Polissar, P.J., Freeman, K.H., 2010. Effects of aridity and vegetation on plant-wax δD in modern lake sediments. Geochimica et Cosmochimica Acta 74, 5785–5797. doi:10.1016/j.gca.2010.06.018

Powers, L., Werne, J.P., Vanderwoude, A.J., Sinninghe Damsté, J.S., Hopmans, E.C., Schouten, S., 2010. Applicability and calibration of the TEX86 paleothermometer in lakes. Org. Geochem. 41, 404–413. doi:10.1016/j.orggeochem.2009.11.009

PRISM Climate Group, 2014, Oregon State University, http://prism.oregonstate.edy.

Reheis, M.C., Adams, K.D., Oviatt, C.G., Bacon, S.N., 2014a. Pluvial lakes in the Great Basin of the western United States—a view from the outcrop. Quat. Sci. Rev. 97, 33–57. doi:10.1016/j.quascirev.2014.04.012

Renaut, R.W., 1990. Recent carbonate sedimentation and brine evolution in the saline lake basins of the Cariboo Plateau, British Columbia, Canada. Hydrobiologia 197, 67–81. doi:10.1007/BF00026939

Reati, G. J., Florín, M., Fernández, G. J., & Montes, C. (1996). The Laguna de Mar Chiquita (Córdoba, Argentina): a little known, secularly fluctuating, saline lake. International Journal of Salt Lake Research, 5(3), 187-219.

Robertson, D.M., Ragotzkie, R.A., 1990. Changes in the thermal structure of moderate to large sized lakes in response to changes in air temperature. Aquat. Sci. 52, 360–380. doi:10.1007/BF00879763

Sack, D., 1999. The Composite Nature of the Provo Level of Lake Bonneville, Great Basin, Western North America. Quat. Res. 52, 316–327. doi:10.1006/qres.1999.2081

Schauble, E.A., Ghosh, P., Eiler, J.M., 2006. Preferential formation of 13C–18O bonds in carbonate minerals, estimated using first-principles lattice dynamics. Geochimica et Cosmochimica Acta 70, 2510–2529. doi:10.1016/j.gca.2006.02.011

Schleser, G.H., Helle, G., Lücke, A., Vos, H., 1999. Isotope signals as climate proxies: the role of transfer functions in the study of terrestrial archives. Quat. Sci. Rev. 18, 927–943. doi:10.1016/S0277-3791(99)00006-2

Schultze-Lam, S., Schultze-Lam, S., Beveridge, T.J., Des Marais, D.J., 1997. Whiting events: Biogenic origin due to the photosynthetic activity of cyanobacterial picoplankton. Limnol. Oceanogr. 42, 133–141. doi:10.4319/lo.1997.42.1.0133

Smol, J.P., 1992. Paleolimnology: an important tool for effective ecosystem management. J. Aquat. Ecosyst. Health 1, 49–58. doi:10.1007/BF00044408

Shanahan, T.M., Pigati, J.S., Dettman, D.L., Quade, J., 2005. Isotopic variability in the aragonite shells of freshwater gastropods living in springs with nearly constant temperature and isotopic composition. Geochimica et Cosmochimica Acta 69, 3949–3966. doi:10.1016/j.gca.2005.03.049

Solari, M.A., Hervé, F., Le Roux, J.P., Airo, A., Sial, A.N., 2010. Paleoclimatic significance of

lacustrine microbialites: A stable isotope case study of two lakes at Torres del Paine, southern Chile. Palaeogeography, Palaeoclimatology, Palaeoecology 297, 70–82. doi:10.1016/j.palaeo.2010.07.016

Street-Perrott, F.A., Harrison, S.P., 1984. Temporal Variations in Lake Levels Since 30,000 YR BP—An Index of the Global Hydrological Cycle, in: Hansen, J.E., Takahashi, T. (Eds.), Climate Processes and Climate Sensitivity. American Geophysical Union, pp. 118–129.

Swart, P.K., Burns, S.J., Leder, J.J., 1991. Fractionation of the stable isotopes of oxygen and carbon in carbon dioxide during the reaction of calcite with phosphoric acid as a function of temperature and technique. Chem. Geol. Isot. Geosci. Sect. 86, 89–96. doi:10.1016/0168-9622(91)90055-2

Talbot, M.R., 1990. A review of the palaeohydrological interpretation of carbon and oxygen isotopic ratios in primary lacustrine carbonates. Chem. Geol. Isot. Geosci. Sect. 80, 261–279. doi:10.1016/0168-9622(90)90009-2

Tang, J., Dietzel, M., Fernandez, A., Tripati, A.K., Rosenheim, B.E., 2014. Evaluation of kinetic effects on clumped isotope fractionation (Δ47) during inorganic calcite precipitation. Geochim. Cosmochim. Acta 134, 120–136. doi:10.1016/j.gca.2014.03.005

Thompson, R.S., Mead, J.I., 1982. Late Quaternary environments and biogeography in the Great Basin. Quaternary Research 17, 39–55. doi:10.1016/0033-5894(82)90044-8

Tierney, J.E., Russell, J.M., 2009. Distributions of branched GDGTs in a tropical lake system: Implications for lacustrine application of the MBT/CBT paleoproxy. Organic Geochemistry 40, 1032–1036. doi:10.1016/j.orggeochem.2009.04.014

Tripati, A.K., Eagle, R.A., Thiagarajan, N., Gagnon, A.C., Bauch, H., Halloran, P.R., Eiler, J.M.,

2010. 13C–18O isotope signatures and “clumped isotope” thermometry in foraminifera and coccoliths. Geochimica et Cosmochimica Acta 74, 5697–5717. doi:10.1016/j.gca.2010.07.006

Tripati, A.K., Sahany, S., Pittman, D., Eagle, R.A., Neelin, J.D., Mitchell, J.L., Beaufort, L., 2014. Modern and glacial tropical snowlines controlled by sea surface temperature and atmospheric mixing. Nature Geosci 7, 205–209. doi:10.1038/ngeo2082

Troin, M., Vallet-Coulomb, C., Sylvestre, F., Piovano, E., 2010. Hydrological modelling of a closed lake (Laguna Mar Chiquita, Argentina) in the context of 20th century climatic changes. Journal of Hydrology 393, 233–244. doi:10.1016/j.jhydrol.2010.08.019

Urey, H.C., Lowenstam, H.A., Epstein, S., McKINNEY, C.R., 1951. Measurement of Paleotemperatures and Temperatures of the Upper Cretaceous of England, Denmark, and the Southeastern United States. Geological Society of America Bulletin 62, 399–416. doi:10.1130/0016-7606(1951)62[399:MOPATO]2.0.CO;2

U.S. Geological Survey, 2014. National Water Information System data available on the World Wide Web (Water Data for the Nation), URL [http://waterdata.usgs.gov/nwis/]

Vaughn, C. M. (1953). Effects of temperature on hatching and growth of Lymnaea stagnalis appressa Say. American Midland Naturalist, 49, 214-228.

Vasconcelos, C., McKenzie, J.A., Warthmann, R., Bernasconi, S.M., 2005. Calibration of the $\delta^{18}O$ paleothermometer for dolomite precipitated in microbial cultures and natural environments. Geology 33, 317–320. doi:10.1130/G20992.1

Wacker, U., Fiebig, J., Schoene, B.R., 2013. Clumped isotope analysis of carbonates: comparison of two different acid digestion techniques. Rapid Commun. Mass Spectrom. 27, 1631–1642. doi:10.1002/rcm.6609

Wagner, J.D.M., Cole, J.E., Beck, J.W., Patchett, P.J., Henderson, G.M., Barnett, H.R., 2010. Moisture variability in the southwestern United States linked to abrupt glacial climate change. Nat. Geosci. 3, 110–113. doi:10.1038/ngeo707

Yu, S.-Y., Shen, J., Colman, S.M., 2008. Modeling the Radiocarbon Reservoir Effect in Lacustrine Systems. Radiocarbon 49, 1241–1254. doi:10.2458/azu_js_rc.49.3016

Yu, Z., Wright Jr., H.E., 2001. Response of interior North America to abrupt climate oscillations in the North Atlantic region during the last deglaciation. Earth-Sci. Rev. 52, 333–369. doi:10.1016/S0012-8252(00)00032-5

Zaarur, S., Affek, H.P., Brandon, M.T., 2013. A revised calibration of the clumped isotope thermometer. Earth Planet. Sci. Lett. 382, 47–57. doi:10.1016/j.epsl.2013.07.026